

Die approbierte Originalversion dieser Dissertation ist an der Hauptbibliothek der Technischen Universität Wien aufgestellt (<http://www.ub.tuwien.ac.at>).

The approved original version of this thesis is available at the main library of the Vienna University of Technology (<http://www.ub.tuwien.ac.at/englweb/>).



TECHNISCHE  
UNIVERSITÄT  
WIEN  
Vienna University of Technology



## DISSERTATION

### **Quantitative (phospho)-Proteomics identifies a Novel Role for Hedgehog in Reprogramming Adipocyte Energy Metabolism**

Ausgeführt zum Zwecke der Erlangung des akademischen Grades eines Doktors der  
Naturwissenschaften

Unter der Leitung von  
Univ. Prof. DI Dr. techn. Peter Christian Kubicek

Institut 166  
Institut für Verfahrenstechnik Umwelttechnik und Technische Biowissenschaften

Eingereicht an der Technischen Universität Wien  
Fakultät für Technische Chemie

von

Martina Bayer  
Matrikelnummer 0626160  
Portnergasse 15/4/16, A-1220 Wien

Wien, Juni 2011

Auch darf nicht geleugnet werden, dass wir persönlich einem Buch gar manchen Fehler verzeihen, indem wir uns durch dessen Entdeckung geschmeichelt fühlen.

nach Johann W. von Goethe

## ABSTRACT

Hedgehog (HH) signaling plays a fundamental role in developmental processes conserved from flies to humans, whereas aberrant HH reactivation has been linked to multiple cancer types. Recent data from our laboratory identified (i) a key role for HH in inhibiting white but not brown adipocyte differentiation in vitro and in vivo, and (ii) that this inhibitory HH effect on white fat cell differentiation can be blocked by the activated T-cell cytokine interferon-gamma (IFN- $\gamma$ ). However, no studies have so far addressed the impact of HH on mature adipocytes and no data at all are available on HH induced (phospho)-proteomic changes. Therefore, we set out to address both aspects and made use of quantitative proteomic approaches to identify for the first time new HH targets and mechanisms in mature adipocytes.

We performed 2D-PAGE and quantitative label-free 1D-GeLC/MSMS with (i) phospho-protein enriched samples; and (ii) cytoplasmic fractions to gain unbiased insight into rapid phosphorylation and lasting expression changes, respectively. Western blots were performed to validate results. Cellular metabolites were measured by ELISA.

Phospho-protein-specific 1D- and 2D-gels revealed a highly reproducible phosphorylation of pyruvate dehydrogenase (PDH) E1 alpha in HH treated samples. In line with this data we observed a significant up-regulation of PDH-kinase in the cytoplasmic fraction. Furthermore, the glycolytic key enzymes phosphofructokinase (PFK) and pyruvate kinase M2 (PKM2) were significantly altered in HH treated samples, leading to a shift towards lactate production. Pathway analyses identified major changes in glycolysis and mitochondrial function (OXPHOS, TCA cycle). Of note, increased NAD<sup>+</sup>/NADH and NADP<sup>+</sup>/NADPH ratios further reflected HH induced metabolic reprogramming.

In summary, our unbiased (phospho)-proteomic screen identified HH as a hitherto unknown regulator of cellular energy metabolism, leading to increased glucose turnover and lactate production.

## ZUSAMMENFASSUNG

Der sogenannte Hedgehog Signaltransduktionsweg (HH-STW) spielt eine essentielle Rolle in Entwicklungsprozessen von der Fruchtfliege bis hin zum Mensch. Eine unzureichende Funktion des HH-STW führt zu schweren Missbildungen, wobei eine Überreaktion mit Tumorentstehung in Verbindung steht.

Rezente Daten unserer Forschungsarbeiten bestätigten (i) eine Schlüsselfunktion des HH-STW in der Inhibierung der Differenzierung weißer, aber nicht brauner Fettzellen sowohl in vitro als auch in vivo und (ii) dass diese hemmende Wirkung durch das aktivierte T-Zellen Zytokin Interferon-gamma (IFN- $\gamma$ ) blockiert wird. Interessanterweise hat sich bis dato keine Studie damit befasst, den HH-STW in reifen Fettzellen zu untersuchen. Auch sind keine relevanten (phospho)-proteomischen Daten vorhanden. Somit setzten wir uns das Ziel, als erste Forschungsgruppe weltweit, neue Mechanismen des HH-STW auf reife Fettzellen, mit Hilfe quantitativer proteomischer Methoden zu erfassen.

2D-PAGE und quantitative label-free 1D-GeLC/MSMS mit (i) angereicherten Phosphoproteinen und (ii) der zytoplasmatischen Fraktion reifer Adipozyten wurde angewandt. Ziel war es, Änderungen in (De)-Phosphorylierungen beziehungsweise des Expressionsmusters in Hedgehog (HH) stimulierten Fettzellen zu detektieren. Western blot Analysen, sowie ELISA Messungen zellulärer Metaboliten untermauerten diese Ergebnisse.

Phosphoprotein-spezifische 1D- und 2D-Gele identifizierten eine hoch reproduzierbare Phosphorylierung der Pyruvate Dehydrogenase (PDH) E1 alpha in HH stimulierten Adipozyten. Passend dazu, war die zugehörige PDH Kinase überexprimiert in der zytoplasmatischen Fraktion reifer Fettzellen anzutreffen. Die glykolytischen Schlüsselenzyme Phosphofruktokinase (PFK) und Pyruvat Kinase M2 (PKM2) waren ebenfalls signifikant verändert in HH behandelten Proben. Diese Änderungen zeigten einen Glukosefluss in Richtung erhöhter Laktatproduktion. Detailuntersuchungen bestätigten Änderungen der Glykolyse und der mitochondrialen Funktion (TCA Zyklus, OXPHOS) und zeigten auch erhöhte  $\text{NAD}^+/\text{NADH}$  und  $\text{NADP}^+/\text{NADPH}$  Ratios.

Schlussendlich ermittelten diese (phospho)-proteomischen Daten den HH-STW als einen unbekanntem Regulator des Energiestoffwechsels, der zu einem erhöhten Glucosedurchsatz und Laktatproduktion führt.

## **ACKNOWLEDGEMENTS**

First of all I would like to thank Harald Esterbauer for his excellent work as a supervisor. I am especially grateful for his support and guidance during my PhD studies.

Next I wish to thank Christian Kubicek for his great work as co-supervisor at the Technical University of Vienna.

My thanks also go to Christopher Gerner and his group, Goran Mitulovic' and Andrew Pospisilik and his group for their excellent support throughout the whole project and their constructive criticism and advice.

I am thankful to all my colleagues, especially to Maria Ozsvar, Stefanie Tauber and mainly to Sabine Amann for their constant encouragement, ideas, support and motivation.

Finally, I would like to express my deepest appreciation to Salvatore Palma and my family, who has always encouraged me to follow my career goals and interests. Thank you for your enormous support.

# TABLE OF CONTENTS

<b>1.</b>	<b>STATE OF THE ART .....</b>	<b>1</b>
<b>1.1.</b>	<b>The hedgehog signaling pathway .....</b>	<b>1</b>
1.1.1.	The hedgehog protein family.....	2
1.1.2.	The hedgehog signaling components .....	3
1.1.3.	Hedgehog processing, secretion and transduction.....	5
1.1.4.	Mammalian hedgehog at the primary cilium.....	6
1.1.5.	Hedgehog signaling regulation in drosophila.....	7
1.1.6.	Small-molecule modulators of hedgehog signaling .....	8
1.1.7.	Hedgehog signaling and its role in adipogenesis.....	8
<b>1.2.</b>	<b>Obesity and its related disorders.....</b>	<b>9</b>
1.2.1.	Adipose tissue.....	10
1.2.2.	Obesity and metabolic disorders.....	10
1.2.3.	Adipogenesis .....	11
<b>2.</b>	<b>PROBLEM DEFINITION AND OBJECTIVE.....</b>	<b>12</b>
<b>3.</b>	<b>MATERIAL AND METHODS.....</b>	<b>14</b>
<b>3.1.</b>	<b>Cell culture .....</b>	<b>14</b>
3.1.1.	Reagents and solutions .....	14
3.1.2.	Procedure .....	14
<b>3.2.</b>	<b>Sample preparation .....</b>	<b>16</b>
3.2.1.	Reagents and solutions .....	16
3.2.2.	Procedure .....	18
3.2.2.1.	Phospho-proteomics .....	18
3.2.2.2.	Expression-profile .....	19
3.2.2.3.	Western blot samples.....	19
<b>3.3.</b>	<b>Proteomic analysis .....</b>	<b>20</b>
3.3.1.	2D-PAGE .....	20
3.3.1.1.	Reagents and solutions .....	20
3.3.1.2.	Procedure.....	22
3.3.2.	1D-GeLC/MSMS .....	24
3.3.2.1.	Reagents and solutions .....	24
3.3.2.2.	Procedure.....	25
3.3.3.	Mass spectrometry analysis.....	26
3.3.3.1.	Reagents and solutions .....	26
3.3.3.2.	Procedure.....	28

<b>3.4. Western blot .....</b>	<b>31</b>
3.4.1. Reagents and solutions .....	31
3.4.2. Procedure .....	33
<b>3.5. Quantitative real time PCR .....</b>	<b>35</b>
3.5.1. Reagents and solutions .....	35
3.5.2. Procedure .....	35
<b>3.6. Kinexus – antibody microarray .....</b>	<b>37</b>
3.6.1. Procedure .....	37
<b>3.7. BioAssay Systems EnzymChrom™ .....</b>	<b>38</b>
<b>3.8. Enzymatic determination of glucose and lactate .....</b>	<b>40</b>
<b>4. RESULTS .....</b>	<b>43</b>
<b>4.1. Quantitative phospho-protein identification of HH treated adipocytes .....</b>	<b>44</b>
4.1.1. Depth and coverage of the 3T3-L1 adipocyte phospho-proteome .....	45
4.1.2. Phospho-protein-specific 2D- and 1D-gels revealed phosphorylation of pyruvate dehydrogenase E1 alpha in HH treated samples .....	47
4.1.3. In-depth analysis of the 1D-phospho-proteome identified major changes in adipocyte energy metabolism .....	50
<b>4.2. Quantitative proteomics of HH signaling in mature adipocytes .....</b>	<b>56</b>
4.2.1. Depth and coverage of the 3T3-L1 adipocyte proteome .....	57
4.2.2. In-depth analysis of 1D-adipocyte-proteome identified major changes in glycolysis and mitochondrial function .....	68
<b>4.3. Kinexus – antibody microarray .....</b>	<b>77</b>
<b>4.4. Validation of HH triggered reprogramming of cellular energy metabolism ...</b>	<b>78</b>
<b>5. DISCUSSION AND CONCLUSION.....</b>	<b>81</b>
<b>6. REFERENCES.....</b>	<b>90</b>
<b>7. SUPPLEMENT.....</b>	<b>94</b>
<b>7.1. Curriculum Vitae.....</b>	<b>94</b>
<b>7.2. Papers .....</b>	<b>96</b>

## TABLE OF FIGURES

**Figure 1:** Current model of hedgehog processing, secretion and transduction

**Figure 2:** Hedgehog signaling at the primary cilium

**Figure 3:** 3T3-L1 adipocyte differentiation

**Figure 4:** Schematic outline of the phospho-protein-specific proteomics approach

**Figure 5:** Phospho-2D-gel

**Figure 6:** Phospho-proteome dataset

**Figure 7:** Pyruvate dehydrogenase complex

**Figure 8:** Phosphorylation of PDHA1 in HH treated samples identified by 2D-PAGE

**Figure 9:** Phosphorylation of PDHA1 in HH treated samples identified by 1D- GeLC/MSMS and verified by Scaffold

**Figure 10:** Pie charts illustrating metabolic pathways of phospho-protein-specific 1D-gels

**Figure 11:** Pie charts illustrating signaling pathways of phospho-protein-specific 1D-gels

**Figure 12:** Pie charts and bar charts illustrating GO terms of phospho-protein-specific 1D-gels

**Figure 13:** Schematic workflow of expression proteome

**Figure 14:** 2D-gel of adipocytes

**Figure 15:** Quantitative Venn diagrams visualize the outcome of the cytoplasmic-proteome approach

**Figure 16:** Spectrum of (non)-phosphorylated PDHA1

**Figure 17:** Pie charts illustrating metabolic pathways of expression-proteomics

**Figure 18:** Pie charts illustrating signaling pathways of expression-proteomics

**Figure 19:** Map of cellular energy metabolism and its main reactions

**Figure 20:** Pie charts illustrating GO terms of expression-proteomics

**Figure 21:** Schematic cartoon of insulin signaling

**Figure 22:** Validation of hedgehog triggered reprogramming of cellular energy metabolism

**Figure 23:** Cellular metabolites in SAG treated 3T3-L1 adipocytes

**Figure 24:** Schematic illustration of aerobic glycolysis (Warburg effect)

**Figure 25:** Current working model of HH stimulated adipocytes



## TABLE OF TABLES

**Table 1:** Cutoff points proposed by a WHO expert committee for the classification of overweight

**Table 2:** Isoelectric focusing setting

**Table 3:** Pyruvate dehydrogenase E1a modification sites

**Table 4:** Metabolic pathway analysis of phospho-protein enriched adipocytes

**Table 5:** Signaling pathway analysis of phospho-protein enriched adipocytes

**Table 6:** Phospho-protein list of selected pathways

**Table 7:** Proteins identified by 2D-PAGE

**Table 8:** Proteins up-regulated by the 1D-GeLC/MSMS approach

**Table 9:** Proteins down-regulated by the 1D-GeLC/MSMS approach

**Table 10:** Metabolic Pathway analysis of cytoplasmic adipocytes

**Table 11:** Signaling Pathway analysis of cytoplasmic adipocytes

**Table 12:** Mitochondrial proteins revealed by GO analysis

**Table 13:** Regulation of mitochondrial proteins revealed by GO analysis

**Table 14:** Examples of phospho-proteins identified by Kinexus, a Systems Proteomic Company

## LIST OF ABBREVIATIONS

1D-	One dimensional
1D-GeLC/MSMS	1D-gel liquid chromatography/ tandem mass spectrometry
1D-PAGE	1D-polyacrylamide gel electrophoresis
2D-	Two dimensional
2D-PAGE	2D-polyacrylamide gel electrophoresis
A	Acetylation
aa	Amino acid
AA	Acrylamide
ACN	Acetonitrile
ADP	Adenosindiphosphat
AKT1	Protein-serine kinase B alpha
APS	Ammonium persulfate
ATP	Adenosintriphosphat
BAT	Brown adipose tissue
BCA	Bicinchoninic acid assay
bME	2- Mercaptoethanol
BMI	Body mass index
BOC	Brother of CDO
boi	Brother of iHog
BPB	Bromphenolblue
C/EBP	CCAAT/enhancer binding protein
CDO	Cell-adhesion molecule-related, down-regulated by oncogenes
CHAPS	3-[(3-cholamido-propyl) dimethyl-ammonio]-1-propanesulfonate
ci	Cubitus interruptus
CKI	Casein kinase I
cos2	Costal-2
CS	Calf Serum
Ctr	Control
ddH <sub>2</sub> O	Water double distilled
DEX	Dexamethasone
DHH	Desert hedgehog
DISP	Dispatched
DMEM	Dulbecco's Modified Eagle's Medium
DTT	1,4-Dithio-D,L threitol high purity
EDTA	Ethylene diamine tetra acetic acid
EGTA	Ethylene glycol tetra acetic acid
ELISA	Enzyme-linked immunosorbent assay
ESI	Electro spray ionization
FA	Fatty acid
FBP	Fructose 1,6-bisphosphate
FBS	Fetal bovine serum
FDR	False discovery rate
FFA(s)	Free fatty acid(s)
FU	Fused, mammals
Fu	Fused, drosophila
GANT	GLI antagonist
GAS1	Glycophosphatidylinositol (GPI)-linked protein

GLI	Glioma-associated
GLI3R	Gli3 repressor
GLIA	GLI activator
GLUT4	Glucose transporter 4
GO	Gene ontology
GPCR	G-protein coupled receptors
G <sub>s,i,q,12</sub>	G-protein
GSK3 $\beta$	Glycogen synthase kinase 3 $\beta$
HH	Hedgehog
HHIP	HH-binding protein
HI	Heat inactivated
HP	Hypotonic extraction buffer
HRP	HorseRadish Peroxidase
IAA	Iodacetamide
IBMX	Isobutylmethylxanthine
IEF	Isoelectric focusing
IFN- $\gamma$	Interferon-gamma
IFT	Intraflagellar transport
IHH	Indian hedgehog
iHog	Interference hedgehog
IPG	Immobilized pH gradient
IPI db	International protein index database
IR	Insulin receptor
IRS1	Insulin receptor substrate 1
LC	Liquid chromatography
LP	Lipoprotein
m/z	Mass-to-charge ratio
MALDI	Matrix-assisted laser-desorption ionization
MAPK	Mitogen-activated protein kinase
MS	Mass Spectrometry
MSMS	Tandem mass spectrometry
NAD <sup>+</sup>	Oxidized nicotinamide adenine dinucleotide
NADH	Reduced nicotinamide adenine dinucleotide
NADP <sup>+</sup>	Oxidized nicotinamide adenine dinucleotide phosphate
NADPH	Reduced nicotinamide adenine dinucleotide phosphate
OXPHOS	Oxidative phosphorylation
P	Phosphorylation
PBS	Phosphate buffered saline
PC	Primary cilium
PDA	1,4-Bis (acryloyl) piperazine
PDH	Pyruvate dehydrogenase
PDHA1	Pyruvate dehydrogenase E1 alpha
PDHC	PDH complex
PDK	Pyruvate dehydrogenase kinase
PEP	Phosphoenolpyruvate
PFK1	Phosphofructokinase-1
PI3K	Phosphatidylinositol 3-kinase
PK	Pyruvate kinase
PKA	Protein Kinase A
PKM1	PK isozyme M1

PKM2	PK isozyme M2
PMSF	Phenylmethylsulfonyl fluoride
PPAR $\gamma$	Peroxisome proliferator-activated receptor gamma
PTCH	Patched, mammals
ptc	Patched, drosophila
PTX	Bordetella pertussis toxin
PVDF	Polyvinylidene fluoride
Q-RT-PCR	Quantitative real time PCR
RecSHH	Recombinant Mouse Sonic hedgehog
RuBPS	Ruthenium II tris (bathophenanthroline disulfonate)
S	Serine
SAG	Smoothened agonist
SANT1	Smoothened antagonist 1
SDS	Sodium dodecyl sulfate
SDS-PAGE	Sodiumdodecylsulfate-polyacrylamide gel electrophoresis
SEM	Standard error of mean
SHH	Sonic hedgehog
SHH-N	Shh N-terminal fragment
SHH-Np	Shh N-terminal fragment, palmitolyated
SMO	Smoothened, mammals
smo	Smoothened, drosophila
SUFU	Suppressor of FU, mammals
su(fu)	Suppressor of fU, drosophila
T	Threonine
T2D	Type 2 diabetes
TBS-T	TBS/Tween 20
TCA cycle	Tricaroxylic acid cycle
TEMED	N,N,N',N'-Tetramethylethylendiamine
TF(s)	Transcriptions factor(s)
TM	Transmembrane
TZD	Thiazolidinedione
VAMP	Vesicle-associated membrane protein
WAT	White adipose tissue
WB	Western blot
WHO	World Health Organization
Y	Tyrosine

# 1. STATE OF THE ART

The hedgehog (HH) family of secreted signaling proteins plays a central role in multiple developmental processes conserved from flies to humans. Studies of HH over the past 30 years have documented diverse functions ranging from a key role during embryogenesis and organogenesis. It controls cell growth, survival and fate and functions as a regulator of proliferation, differentiation, pattern formation and in stem cells renewal [6-8]. Aberrant activation has been linked to multiple types of human cancer and leads to tumorigenesis [9-11], whereas constitutive repression of the pathway leads to developmental disorders, like limb- and organ malformations [6, 8].

The origin of the name hedgehog derives from the short and “spiked” phenotype of the cuticle of the HH mutant *Drosophila* larvae. This phenotype has been discovered by Nusslein-Volhard and Wieschaus (1980) in their famous screen for mutations that impair the development of the fruit fly larval body plan, which hence has been honored with the Nobel price [6-8]. Several studies identified an anti-adipogenic role of HH in inhibiting adipocyte differentiation. Already a one-hour stimulation was shown to be sufficient to significantly reduce adipocyte markers, up-regulate preadipocyte markers and therefore tremendously affect fat mass [12-14]. Since obesity is considered the new epidemic of the 21<sup>st</sup> century and represents a major risk factor for numerous chronic diseases like diabetes, heart disorders, hypertension, stroke and certain forms of cancer, it is representing one of the greatest social, medical and economic challenges today [12]. Interestingly, several studies and our findings highlight HH signaling as a potential therapeutic target to treat obesity and its related disorders [9, 13, 14].

## 1.1. The hedgehog signaling pathway

The expression of different HH isoforms is tightly controlled by highly complex and divergent transcriptional enhancers [7]. The mechanisms for subsequent HH processing and secretion appear to be conserved in evolution and are likely to apply to all HH isoforms, including a wide range of invertebrates, *Drosophila melanogaster* (fruit fly), *Diadema antillarum* (sea urchin) and vertebrates, *Mus musculus* (mouse), *Gallus gallus* (chicken) as well as humans [8]. Briefly, binding of HH proteins to its transmembrane receptor Patched (PTCH), relieves the normal repression of a second transmembrane

protein Smoothed (SMO) allowing the signal to be conveyed to the nucleus by the *ci/GLI* (Cubitus interruptus/Glioma-associated) family of transcriptions factors (TFs) affecting expression of specific target genes [6-8, 10, 15].

### **1.1.1. The hedgehog protein family**

HH proteins act as morphogens controlling multiple different developmental processes. Signaling can be direct or indirect, over a short or long range in a time- and dose-dependent manner. Therefore changing of concentration and/or duration of HH seems to significantly influence intracellular signaling. Generally induced genes are involved in positive and negative feedback mechanisms and include *GLI1*, *PTCH* and *HIP* [8]. On the other hand HH proteins act as mitogens regulating cell proliferation or as inducing factors controlling the form of a developing organ [6].

As aforementioned, the components and mechanisms involved in hedgehog signaling seem to be largely conserved from flies to humans. However, unlike the fruit fly, which has a single HH gene, duplication events in the vertebrate genome have resulted in the generation of three genes named Desert hedgehog (*DHH*), Indian hedgehog (*IHH*) and Sonic hedgehog (*SHH*). *IHH* and *SHH* are more closely related to each other than to *DHH*, which in turn is most closely related to *Drosophila* hedgehog [6-8, 15].

*DHH* expression is largely restricted to gonads, including sertoli cells of testis and granulosa cells of ovaries. *DHH* deficient male mice are infertile due to complete loss of mature sperm [8]. Furthermore, it is found to be expressed in Schwann cells and is essential for the structural and functional integrity of peripheral nerves [16].

*IHH* is known to be expressed in a limited number of tissues, including primitive endoderm, gut and early hypertrophic chondrocytes in the growth plates of bones. About 50% of *IHH*<sup>-/-</sup> embryos die during early embryogenesis due to poor formation of yolk-sac vasculature [8].

*SHH* represents the most broadly expressed mammalian HH protein and the most actively investigated ligand. It is expressed in numerous cell types and is involved in many biological processes such as development of limbs, skeleton, central nervous system and

lung. Deletion of SHH causes limb malformation, absence of vertebrae and most of the ribs, defects in ventral neural tube and failure of lung branching [8]. Furthermore SHH protein regulates adult stem/progenitor cell behavior. Human SHH protein shows a similarity of 92.4% in the amino acid sequence with its murine homolog [10].

Of note, all HH proteins undergo co- and posttranslational modifications, including auto processing and lipid modification (see 1.1.3. Hedgehog processing, secretion and transduction).

### **1.1.2. The hedgehog signaling components**

Dispatched (DISP) is a twelve pass transmembrane (TM) transporter-like protein and is required in HH-producing cells to transport lipid-modified HH protein to the extracellular space. Therefore, loss of DISP function leads to accumulation of HH in the producing cell and decreases target gene expression in responding cells [6, 7, 10, 15]. The three vertebrate HH family proteins are released by a set of human dispatched homologues, DISP1, DISP2 and DISP3. In contrast mice show two dispatched homologues, mDISPA and mDISPB [17].

PTCH is a twelve pass transmembrane protein and functions as a signaling receptor. In vertebrates two PTCH isoforms exist, named PTCH1 and PTCH2. PTCH1, which is the better characterized one, shows 54% sequence homology with PTCH2. Both bind to all HH family proteins with similar affinity but differ in the potency to induce a response. It is generally accepted that most signaling events seem to involve PTCH1. Binding of HH to its receptor results in loss of PTCH activity and consequent activation of SMO [10]. PTCH is a target gene of the HH signaling and therefore inhibits signaling by a negative feedback loop [6, 7, 15].

SMO is a seven pass transmembrane protein and due to its structure often included in a sub-family of G-protein coupled receptors (GPCR) [11, 18]. Seven pass TM receptors are coupled to G-proteins ( $G_s$ ,  $G_i$ ,  $G_q$ ,  $G_{12}$ ). Their activation typically changes second messengers and activates a variety of lipid and protein kinases.  $G_i$  is required for SHH signaling in at least some vertebrate cells [18] and this effect can be inhibited by Bordetella pertussis toxin (PTX), a toxin which modifies most  $G_i$  proteins and blocks the interaction

of G-proteins with its receptors. However the capacity of SMO to couple to G-proteins is still under investigation as controversial reports on this topic exists [19]. HH activates SMO by binding to and inactivating PTCH.

Other cell surface proteins which are able to bind HH proteins and negatively regulate the HH pathway are the HH-binding protein (HHIP) and glycosphosphatidylinositol (GPI)-linked protein (GAS1). Curiously, no identifiable homologs of HHIP or GAS1 are present in fruit flies. Additional molecules, which positively affect the pathway, are the single transmembrane protein cell-adhesion molecule-related, down-regulated by oncogenes (CDO) and Brother of CDO (BOC) and its drosophila homologs interference hedgehog (iHog) and Brother of iHog (boi) [6-8, 15].

The most obvious differences between drosophila and vertebrate HH signaling exist at the level of transcriptional control by the ci/GLI transcription factors [7]. These TF convey the signal from SMO to the nucleus affecting gene expression.

Ci is bi-functional and serves as both repressor and activator [20]. In mammals these opposing activities are distributed between three ci homologues, GLI1, GLI2 and GLI3. They all belong to the family of C2-H2 zinc finger domains and can specifically interact with DNA sequences encompassing a GACCACCCA motif found in target gene promoters [10]. GLI1 functions as a strong transcriptional activator and its expression is dependent on GLI2 and/or GLI3-mediated transcription so that GLI1 expression can be used as a convenient readout of the state of classical HH pathway activation [18]. GLI2 and GLI3 proteins contain both activator and repressor domains, whereas GLI2 functions principally as activator and GLI3 acts mainly as repressor of target gene expression [10].

Further intracellular components which are important for regulating HH transduction in drosophila include a kinesine-like protein, costal-2 (cos2). cos2 is a key negative regulator of the HH signaling downstream of smo [7]. It forms a so-called “HH signaling complex” with fused (fu), a protein serine-threonine kinase that acts positively on the HH pathway and several other serine-threonine kinases such as Protein kinase A (PKA), Casein kinase I (CKI) and Glycogen synthase kinase 3 $\beta$  (GSK3 $\beta$ ), to interact with ci and to regulate its activity and action [18]. Ci transcriptional activity is also negatively regulated through its binding to Suppressor of FU (SUFU) [8] [21]. FU, SUFU and the other kinases PKA, CKI



and GSK3 $\beta$  are homologous to the vertebrate signaling pathway. The exact role of the vertebrate *cos2* homologues, KIF7 and KIF27 has to be clarified [22].

### **1.1.3. Hedgehog processing, secretion and transduction**

One critical aspect of HH biology is its synthesis [15]. HH family proteins in both vertebrates and invertebrates are processed from a precursor protein (Figure 1). The human SHH ligand is synthesized from a 45 kDa precursor that undergoes an autocatalytic intramolecular cleavage at position 198 catalyzed by the C-terminal portion of the precursor. This reaction yields an ~19 kDa N-terminal fragment (SHH-N), which represents the mature and biologically active SHH form, and a 25 kDa C-terminal fragment, that has no other known function so far. During this reaction, cholesterol is coupled covalently to the C-terminus of SHH-N and the N-terminal signaling fragment is modified by palmitoylation (SHH-Np). These hydrophobic lipid modifications serve, at least in part, to localize SHH-Np to particular regions of the plasma membrane that are critical for proper HH trafficking and activity [10, 15].

HH proteins are secreted as monomers or lipoprotein (LP)-associated oligomers promoted by DISP and cell-surface heparan sulfate proteoglycans, shortly glypicans. Released HH ligands can act in autocrine and paracrine manners on producing and responsive cells localized near or at a distant localization of secreting cells. HH interacts with a complex of PTCH and CDO/BCO. CDO and BCO are the closest mammalian relatives of *Drosophila* iHog and boi and are cell-surface proteins which positively regulate the HH pathway. Together with HHIP and GAS1, which negatively affect the HH pathway, they regulate the range and level of HH signaling. Binding of SHH-N inactivates PTCH and therefore activates SMO. Active SMO signals to the cytoplasm, leading to activation of the *ci*/GLI TFs, which control the output of HH signaling [10, 15].

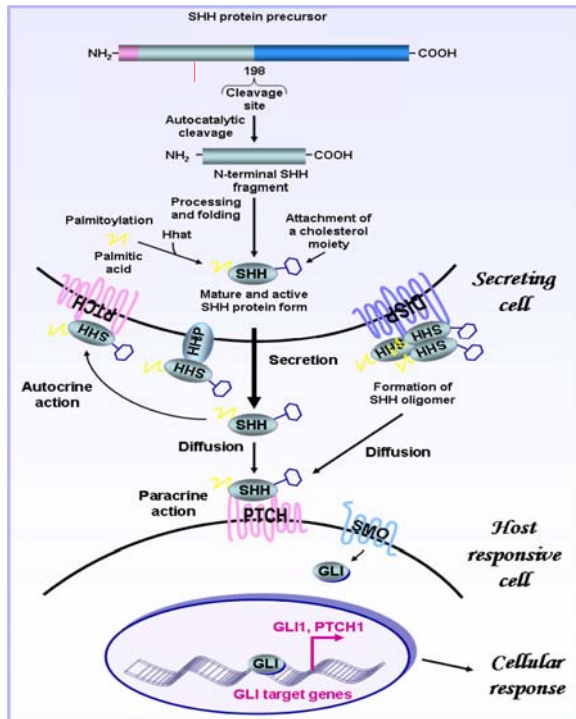


**Figure 1:** Current model of hedgehog processing, secretion and transduction; reviewed in Mimeault and Batra, 2010.

#### 1.1.4. Mammalian hedgehog at the primary cilium

A unique feature of vertebrate HH signaling is that primary cilia (PC) are essential for signal transduction. The PC is a tiny microtubule-based organelle observed on most vertebrate cells [21]. It serves as a sensory “antenna” for the detection of optical, mechanical and chemical signals. The function of PC is regulated by large protein complexes involved in intraflagellar transport (IFT) of proteins up and down the cilia. Interestingly mutations in components of the IFT apparatus impair HH signaling in mice [11].

Active PTCH receptor is localized at the base of the PC and prevents SMO localization to the PC. Moreover, all three GLI TFs as well as SUFU are colocalized at the tip of the cilium in the absence of the HH ligand [11, 23]. Binding of HH protein to its receptor PTCH results in a decreased number of PTCH molecules in the cilium, perhaps due to internalization from the plasma membrane and/or degradation [21]. This delocalization of PTCH from the PC recruits SMO to the cilium and inhibits proteolytic processing of GLI2 and GLI3 with subsequent induction of GLI1 transcription (GLI activator, GLIA) (Figure 2) [9, 10]. SUFU, the main negative regulator of mammalian HH signaling, is directly associated with GLI molecules and controls their nuclear translocation through an

intraflagellar transport. In the absence of HH, GLI2 and GLI3 are phosphorylated by PKA, GSK3 $\beta$  and CKI at the base of the cilium whereupon they are proteolytically processed and translocated to the nucleus and repress gene expression (GLI3 repressor, GLI3R) (Figure 2).

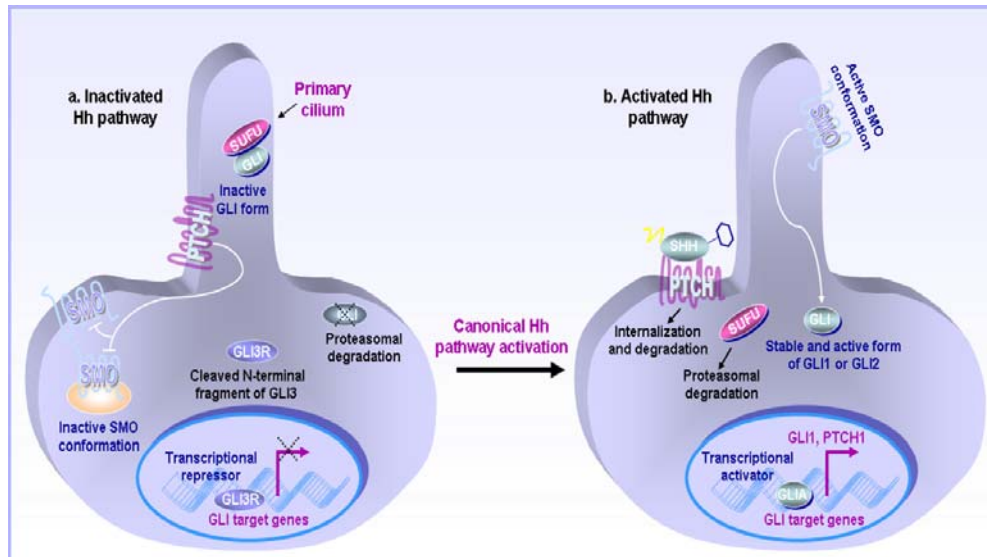


**Figure 2:** Hedgehog signaling at the primary cilium; reviewed in Mimeault and Batra, 2010. GLI3R, GLI3 repressor; GLIA, GLI1 activator

### 1.1.5. Hedgehog signaling regulation in drosophila

In both vertebrate and invertebrate HH signaling smoothed (*smo*, *drosophila*) is blocked by the receptor patched (*ptc*, *drosophila*) in the absence of HH proteins. In the presence of HH proteins *ptc* releases its inhibitory effect on *smo* and the signal can be conveyed via the *ci*/GLI TF to the nucleus. Cellular responsiveness to HH is regulated by the expression of these TF and differs between in- and vertebrates [8].

In fruit flies, active *smo* is hyperphosphorylated by PKA and CKI and acts through a protein complex containing *cos2*, *fu* and *ci* [7, 24]. *Fu*, a positive regulator of HH signaling, blocks the binding of *su(fu)* to *ci*. Therefore non-processed *ci* is able to enter the nucleus as transcriptional activator [7, 22]. In the absence of HH *smo* stays in an unphosphorylated state and *cos2* exerts a negative effect on HH signaling by recruiting the kinases PKA, CKI and GSK3 to hyperphosphorylate *ci* and mediating its proteolysis [24]. In the absence of HH pathway activity, this truncated form of *ci* enters the nucleus and represses target gene expression. Activation of the HH pathway blocks *ci* processing, allowing the full-length form to enter the nucleus.

### **1.1.6. Small-molecule modulators of hedgehog signaling**

There exist several synthetic and natural small-molecule modulators of the HH pathway [25]. The plant alkaloid cyclopamine was first identified as inhibitor, by binding directly SMO [21]. Other SHH signaling antagonists that bind to SMO are SANT1 (Smoothed Antagonist 1) and GDC-0449 [25]. The latter is currently tested in clinical trials on human basal cell carcinomas (BCCs). Agonists are purmorphamine [25] and SAG (Smoothed agonist) [26]. Antagonists acting at the level of GLI are GLI antagonist GANT58 and GANT61 [25].

### **1.1.7. Hedgehog signaling and its role in adipogenesis**

In 2000, first studies on HH signaling and its anti-adipogenic role were performed using murine mesenchymal cells [12, 27]. Mesenchymal stem cells are pluripotent cells that can differentiate into osteocytes, chondrocytes and adipocytes [28]. Activation of HH signaling in these cells promotes osteoblastic differentiation in correlation with the increase of PEF-1, a preadipocyte marker and a decrease of adipocyte markers [12, 27]. In 2004, a similar effect was reported in mesenchymal stem cells derived from human adipose tissue [12, 29]. HH is known as a crucial modulator of cell differentiation processes and its conserved anti-adipogenic role was first described by Suh et al in 2006 [14]. They found HH pathway components to be expressed in the fruit fly fat body as well as in mouse fat and their levels were regulated by adipogenesis and obesity. Expression levels of anti-adipogenic genes like GATA2, GATA3 and GILZ increase in presence of HH, as well as PEF-1 in 3T3-L1 cells. This data suggested that HH signaling acts upstream of peroxisome proliferator-activated receptor gamma (PPAR $\gamma$ ), the master regulator of adipogenesis, by inducing transcription factors as GATA2 to inhibit adipogenesis.

In 2010, we specified for the first time the anti-adipogenic role of HH protein in mammals [13]. In detail, genetic activation of HH signaling in vivo and in vitro blocks white but not brown adipocyte differentiation. White adipose tissue (WAT) stores excess calories as triglycerides and brown adipose tissue (BAT) burns lipids to generate heat and regulate body temperature. Fat specific SUFU knockout mice displayed an obvious lean phenotype due to a significant and global reduction of WAT. WAT fat pads revealed marked and significant reductions in adipocyte size and total number, whereas BAT showed no alterations in mass, size or number of adipocytes. Despite the marked differences in WAT

and body weight of SUFU knockout mice, there was no evidence of altered food intake or aberrant glucose tolerance and they showed normal regulation of energy expenditure. As previous studies indicated, we also observed a significant down-regulation of pro-adipogenic targets such as BMP2, BMP4, EGR2/KROX20, SFRP1 and SFRP2 and up-regulation of anti-adipogenic targets like NR2F2, GILZ, HES1 and NCOR2. We further demonstrated that endogenous GLI2 and GLI3 bind to multiple anti-adipogenic loci and implicate direct modulation of NCOR2 and NR2F2 in the dysregulation of adipogenesis, which confirmed the early anti-adipogenic action of HH signaling.

## 1.2. Obesity and its related disorders

The global epidemic of overweight and obesity - "globesity" - is rapidly becoming a major public health problem in many parts of the world. According to the World Health Organization (WHO) overweight and obesity are defined as a disease in which excess body fat has accumulated such that health may be adversely affected. Obesity is commonly defined as a body mass index (BMI, weight in kilograms divided by height in meters squared) of 30 kg/m<sup>2</sup> or higher (Table 1). The WHO currently estimates that at least 1.5 billion individuals worldwide are overweight. Almost one-third of these individuals are clinically obese, markedly raising their chances of cardiovascular disease, type 2 diabetes (T2D), certain forms of cancer, stroke and a decreased longevity. Unfortunately, obesity is also affecting children; as childhood obesity has tripled over the last 30 years. Importantly, in most countries nowadays more people die from the consequences of being overweight than underweight [30]. These run-away rates of obesity underscore the need for novel diagnostic tools and targeted therapies [13, 31].

BMI < 18,5	Underweight
BMI 18,5 – 24,9	Normal weight
BMI 25 – 29,9	Overweight
BMI 30 – 39,9	Obesity
BMI ≥ 40	Morbid obesity

**Table 2:** Cutoff points proposed by a WHO expert committee for the classification of overweight.

### **1.2.1. Adipose tissue**

Two types of adipose tissue are present in mammals: white adipose tissue (WAT) and brown adipose tissue (BAT). The differences in lipid content and mitochondrial abundance are the reasons for the color differences. As mentioned earlier WAT stores energy, i. e. excess calories, as lipid droplets in form of triglycerides [32]. Another key feature of WAT is the secretion of adipocyte-derived factors, known as adipokines (e. g. leptin, adiponectin). Thus, fat is a major endocrine organ and signaling tissue which interacts extensively with other organs to regulate whole-body metabolism, glucose and energy homeostasis, immune response, blood pressure control and bone mass [33, 34]. This adipokine networking system is altered in obese people, contributing to an impaired adipocyte metabolism. In contrast to WAT, BAT produces heat through uncoupling protein 1 (UCP-1) by uncoupling oxidative phosphorylation. BAT depots are difficult to find in human adults as its heat-producing-function is more essential in small mammals and newborn humans [35]. However, significant amounts of BAT have been recently identified also in adult humans [32, 35].

### **1.2.2. Obesity and metabolic disorders**

The obesity state was first described as “low-grade systemic inflammation” by Hotamisligil et al. in 1993 [32, 36]. In obese conditions, WAT becomes inflamed due to the excess consumption of calorie-rich food and its resulting cellular composition remodeling [30, 32]. The increase in adipocyte number (hyperplasia) and size (hypertrophy) as well as the marked infiltration with macrophages elevate the secretion of pro-inflammatory adipokines and cytokines and contribute to an aberrant adipocyte metabolism [32]. As a result higher rates of lipolysis and therefore also an increased release of free fatty acids (FFAs) is observed, which in turn results in increased hepatic gluconeogenesis and dyslipidaemia. Glucose and insulin action get out of control, reflected by raised circulating insulin levels and decreased skeletal muscle insulin sensitivity with reduced glucose uptake. Ultimately, this leads to peripheral insulin resistance, finally to pancreatic  $\beta$ -cell failure, and hence T2D. [3, 31, 37].

### 1.2.3. Adipogenesis

Adipocytes derive from multipotent mesenchymal stem cells, which have the capacity to differentiate into osteocytes, chondrocytes and adipocytes [38]. Adipogenesis is a precisely regulated process, where fibroblast-like preadipocytes differentiate into mature, lipid-laden adipocytes [39, 40]. The two principal adipogenic regulators are PPAR $\gamma$  and CCAAT/enhancer binding protein (C/EBP). PPAR $\gamma$  is considered as the master regulator of adipogenesis as it is sufficient and necessary for adipocyte differentiation [41]. There exists several additional proadipogenic (BMP-2/4, KROX20, SFRP-1/2) and antiadipogenic (GILZ, HES1, NCOR2, NR2F2) factors which increase and decrease with the level of adipogenesis respectively.

In vitro, 3T3-L1 cells, a common used preadipocyte cell line, have been fundamental to obesity and diabetes. Originally cells derived from Swiss mouse embryo tissue [42]. In vitro adipogenesis of these cells needs to be initiated. This induction mixture contains the adipogenic stimulants isobutylmethylxanthine (IBMX) and dexamethasone (DEX), which turn on PPAR $\gamma$  as well as insulin to facilitate glucose uptake and adipocyte differentiation. Thiazolidinediones which promote adipogenesis through binding to PPAR $\gamma$  enhance the differentiation capacity of the cell. During culturing it is important to maintain cells until they are fully confluent as this is require for growth arrest. Two days after the cells have been confluent differentiation is initiated with the induction cocktail. Small lipid droplets appear within 4-7 days after induction. Lipid accumulation continues throughout the first two weeks and finally, droplets fuse to a few big lipid droplets (Figure 3).

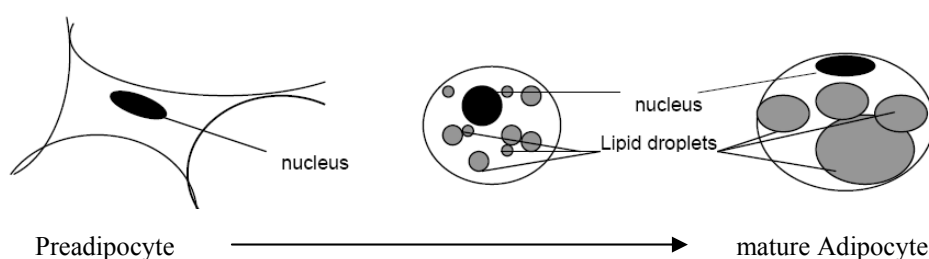


**Figure 3:** 3T3-L1 adipocyte differentiation (zenbio.com)

## 2. PROBLEM DEFINITION AND OBJECTIVE

Due to its dramatic increase, obesity is considered the new epidemic of the 21<sup>st</sup> century. Globally, there are more than 1.5 billion overweight adults and at least 500 million of them obese. Obesity is a major risk factor for numerous chronic diseases including diabetes, heart disease, hypertension stroke, and certain forms of cancer. Thus, obesity represents one of the greatest social, medical and economic challenges today.

HH is fundamental for developmental processes, while in adults activation of the HH pathway has been linked to several cancer types. Recent data from our laboratory first identified a key role for HH in inhibiting white but not brown adipocyte differentiation in vitro and in vivo [13]. Mice with a fat-specific HH activation showed almost complete loss of white adipose tissue, whereas development of brown adipose tissue was not affected. Despite the WAT-specific lipotrophy these mice exhibited normal glucose tolerance and insulin sensitivity. Interestingly, they revealed enhanced glucose uptake in the remaining white adipose tissue [13]. Furthermore, we described that this inhibitory HH effect on white fat cell differentiation can be blocked by the activated T-cell cytokine interferon-gamma (IFN- $\gamma$ ) [43]. Therefore, an antagonistic cross-talk between IFN- $\gamma$  and HH signaling exists in white adipose tissue [43].

Based on these observations we started a follow-up analysis to mechanistically elucidate the role of HH activation in mature adipocytes. Interestingly, no studies have so far addressed anything like that and no data at all are available on HH induced (phospho)-proteomic changes. Therefore, we set out to address both aspects and made use of quantitative proteomic approaches to identify for the first time new HH targets and mechanisms in mature adipocytes. The proteome describes the entire set of proteins expressed by a genome in a cell at a given time point under defined conditions. In order to understand the cellular and molecular mechanisms of HH on mature adipocytes we aimed to determine first the phosphoprotein enriched pattern and second the protein expression pattern to gain unbiased insight into rapid phosphorylation and lasting expression changes, respectively.

On the basis of our present results and new findings within this thesis work the HH pathway may be exploited as a novel treatment avenue for obesity and its related metabolic disorders.



This innovative objective was addressed by the following specific aims:

- (i) Delineation of the impact of HH on changes in the adipocyte phospho-proteome by 2D-PAGE and quantitative label-free 1D-GeLC/MSMS
- (ii) Exploration of the effect of HH on alterations in the cytoplasmic-proteome of adipocytes by 2D-PAGE and quantitative label-free 1D-GeLC/MSMS
- (iii) Functional characterization of promising candidates identified by MSMS to mechanistically elucidate the consequences of HH activation in mature adipocytes

### 3. MATERIAL AND METHODS

#### 3.1. Cell culture

##### 3.1.1. Reagents and solutions

Calf Serum (CS)	PAA
Dexamethasone (DEX)	Sigma
DMEM high glucose (4.5 g/L)	PAA
Fetal Bovine Serum HI (FBS)	PAA
Gentamicin 50 mg/mL	Gibco
Insulin	Sigma
3-isobutyl-1-methyloxanthine (IBMX)	Sigma
Methionine- and cysteine-free DMEM Medium	MP Biomedicals
PBS 1X	Sigma
Recombinant Mouse Sonic hedgehog (recSHH)	ProSpec
Smoothed Agonist (SAG)	Alexis
Tran35S-Label Metabolic Labeling Reagent 14mCi	MP Biomedicals
Troglitazone (TZD)	Sigma
Trypsin EDTA 1x 0.05%/0.02% in PBS	PAA

##### 3.1.2. Procedure

###### **Cell culture and adipocyte differentiation**

Murine 3T3-L1 preadipocytes (ATCC) were grown in DMEM containing 10% heat inactivated calf serum (CS) plus gentamicin in 5% CO<sub>2</sub> at 37°C. For adipocyte differentiation experiments, cells were grown to confluence in DMEM/ 10% CS. Two days after the cells reached confluence (day 0), they were induced to differentiate by changing the medium to DMEM containing 10% fetal bovine serum (FBS), 0.25 mM IBMX, 1 µM DEX, 1.74 µM insulin and 5 µM TZD. After 48 hours (day 2), the medium was replaced with DMEM supplemented with 10% FBS, 1.74 µM insulin and 5 µM TZD. After an additional 48 hours (day 4), insulin and TZD were withdrawn, and 80% medium was changed every second day with DMEM/10% FBS [13]. Differentiated cells were starved at day 9 for 18 hours in 1% BSA in DMEM and stimulated for 10 minutes (Phospho-Proteomics) and 48 hours (Expression-Profile) in DMEM plus 200 nM SAG. For Western

blot analysis differentiated cells were incubated for 2, 5, 10, 30 minutes and 48 hours with 200 nM SAG or 0.1-0.25 µg/mL recombinant SHH, respectively.

### **35S-Metabolic labeling**

Cells were routinely cultivated in DMEM supplemented with 10% CS and 10% FBS as described above. During the last 4 hours of 48 hours treatment, cells were incubated in methionine- and cysteine-free DMEM medium in the presence of 35S-labeled methionine and cysteine [44].

## 3.2. Sample preparation

### 3.2.1. Reagents and solutions

Aceton	Merck
Amberlite	Serva
3-[(3-cholamido-propyl) dimethyl-ammonio]-1-propanesulfonate	Gerbu
1,4-Dithio-D,L threitol high purity (DTT)	Gerbu
Cell Scraper	SPL Life Sciences
Ethylenediaminetetraacetic acid (EDTA)	Merck
Ethylene glycol tetra acetic acid (EGTA)	Merck
HEPES/NaOH pH 7.4, 1M	Sigma
25X Inhibitor Cocktail	Roche
Sodium chloride	Merck
Needles, 25G	BD Microlance
Nuclease Mix 100X	Amersham
Magnesium chloride	Merck
PhosphoProtein Purification Kit	Qiagen
PhosStop Phosphatase Inhibitor Cocktail Tablets	Roche
Phenylmethylsulfonyl fluoride (PMSF)	Sigma
Protease Inhibitors 100X	GE Healthcare
Single-use syringes 1 mL	Soft-Ject
Sodium dodecyl sulfate (SDS)	Sigma
Sodium deoxycholate	Sigma
Sucrose	Sigma
Thiourea	Sigma
Tran35S-Label Metabolic Labeling Reagent 14mCi	MP Biomedicals
Triton X-100	Sigma
Urea	Gerbu
Vivaspin™ sample concentrators 2	GE Healthcare
Water double distilled (ddH <sub>2</sub> O)	Mayrhofer

<b>Hypotonic extraction buffer (HP) <math>V_E = 100</math> mL</b>	
10 mM HEPES/NaOH pH 7.4; 1 M	1 mL
10 mM NaCl; 5 M	200 $\mu$ L
0.5 mM MgCl <sub>2</sub> ; 1 M	50 $\mu$ L
1 mM EGTA; 0.5 M	200 $\mu$ L

Store at 4°C

<b>HP-Mix (1mL / T150 flask)</b>	
25X Inhibitor Cocktail	1x IC
100 mM PMSF	1 mM PMSF

Prepare prior to use and keep on ice

<b>Isotonic solution (ISO) <math>V_E = 3</math> mL</b>	
0.25 M Sucrose; 2 M	1.25 mL
3 mM MgCl <sub>2</sub> ; 1 M	30 $\mu$ L
0.5% Triton X-100; 20%	175 $\mu$ L

Store 4 °C

<b>2 M Sucrose <math>V_E = 100</math> mL</b>	
2 M Sucrose	68.46 g
50 mM HEPES/NaOH pH 7.4; 1 M	5 mL
50 mM NaCl <sub>2</sub> ; 5 M	1 mL
5 mM MgCl <sub>2</sub> ; 1 M	500 $\mu$ L
1 mM EGTA; 0.5 M	200 $\mu$ L

Store 4°C

<b>Sample buffer stock <math>V_E = 10</math> mL</b>	
7 M Urea	4.2 g
2 M Thiourea	1.52 g
2% CHAPS	0.2 g
Amberlite	0.1 g

Filter and fill up to 10 mL, store 1 mL aliquots at -20°C

<b>Sample suffer <math>V_E = 1</math> mL</b>	
Sample buffer Stock	885 $\mu$ L
100 mM DTT; 1 M	100 $\mu$ L
0.2% Ampholytes 3.7-9.5; 40%	5 $\mu$ L
100X Protease Inhibitor	10 $\mu$ L
25X PhosStop	40 $\mu$ L
100X Nuclease Mix	10 $\mu$ L

Prepare freshly prior to use

<b>RIPA buffer V<sub>E</sub> = 250 mL</b>	
50 mM Tris-HCl pH 7.6; 1 M	12.5 mL
150 mM NaCl; 5 M	7.5 mL
1 mM EDTA; 0.5 M	0.5 mL
1% Triton X-100; 20%	12.5 mL
1% Sodium deoxycholate	2.5 g
0.1% SDS; 20%	1.25 mL

Add 1 mM PMSF and 1x IC prior to use, store at 4°C

### 3.2.2. Procedure

#### 3.2.2.1. Phospho-proteomics

Phosphoprotein enrichment was performed by affinity column purification of total adipocyte protein using a PhosphoProtein Purification Kit (Qiagen), according to the manufacturer's introduction. Briefly, cells, cultured in a 150 cm<sup>2</sup> flask, were washed twice with an ice cold HEPES based buffer on ice. Since a phosphate buffer for washing would interfere with binding of phosphorylated proteins to the column. Afterwards ~10<sup>7</sup> cells were resuspended in 5 mL lysis buffer containing protease- and phosphatase inhibitors and Benzonase Nuclease, provided by the manufacturer. Cell suspension was incubated on ice for 30-60 minutes with vortexing every 10 minutes. Subsequently cell lysates were centrifuged at 10.000 g and 4°C for 30 minutes (Allegra X-12R Centrifuge, Beckman Coulter). During centrifugation PhosphoProtein Purification Columns were prepared by detaching the top cap, breaking off the bottom closure, and allowing the storage buffer to flow out. 4 mL lysis buffer were applied to equilibrate the column. Supernatants were harvested and protein concentrations determined by using the Bradford assay (Bio-Rad). A final volume of 25 mL (i.e. approximately 2.5 mg protein) were poured into the upper reservoir of the column in two steps. The flow-through was collected and poured into the column for a second time to maximize binding of any phosphorylated protein in the sample. After this columns were washed once with 6 mL of lysis buffer and finally phosphoproteins were eluted five times with 500 µL of elution buffer, provided by the manufacturer.

Eluated fractions were combined concentrated and desalted, using Vivaspin™ sample concentrators (GE Healthcare) with a 10 kDa molecular weight cut-off according to the

instructions of the manufacturer. Protein concentration was determined using the Bradford or BCA (Pierce) method for proteins diluted in sample buffer or RIPA buffer, respectively.

#### 3.2.2.2. Expression-profile

Cells, culture in a 150 cm<sup>2</sup> flask, were washed twice with an ice cold 1X PBS on ice and scraped into 1 mL HP-Mix. Cells were allowed to swell on ice for 15 minutes. Then 150 µL ISO were added and mixed gently. Cells were disrupted by pushing them 10 times through a G25 (BD Microlance 3) needle. Intact nuclei and insoluble material were removed by centrifugation at 4000 g and 4°C for 10 minutes. Cytoplasmic proteins were precipitated with methanol-chloroform described by Wessel and Flügge [45]. Afterwards, protein samples were dissolved in Sample buffer for 2D polyacrylamide gel electrophoresis (2D-PAGE) or in RIPA buffer for 1D PAGE. Total protein concentration was determined by a Bradford assay and the BCA method, respectively.

For S35labeled cells, the same procedure was performed in an isotope laboratory according to the radioactive guidelines

#### 3.2.2.3. Western blot samples

Cells, cultured in 24 well plates, were washed twice with an ice cold 1X PBS on ice and scraped into 200 µL RIPA buffer containing 1X protease inhibitors and 1X PhosStop phosphatase inhibitor cocktail, snap frozen in liquid nitrogen and stored at -80°C over night. On the next day samples were shaken at 4°C for about an hour, centrifuged at 4°C at 16000 g for 30 minutes (Microfuge 22R Centrifuge, Beckman Coulter). 20 µg protein were mixed with Laemmli buffer and boiled at 95°C for 5 minutes.

### 3.3. Proteomic analysis

#### 3.3.1. 2D-PAGE

2D-PAGE is based upon two-dimensional separation of proteins. In the first dimension proteins are separated according to their charge by isoelectric focusing. In the second dimension proteins are separated based on their molecular mass by sodiumdodecylsulfate-(SDS)-PAGE. The gel was stained with a solution of Ruthenium II tris (bathophenanthroline disulfonate) (RuBPS) and obtained images were quantified and evaluated with Progenesis SameSpots. For further investigations gels were silver stained. Proteins of interest were picked, in-gel digested and analyzed by LC/MSMS. Within this so called gel-based proteomic approach, several samples can be handled and quantitatively compared in parallel.

##### 3.3.1.1. Reagents and solutions

Acetic Acid	Merck
Acrylamide (AA)	Gerbu
Agarose LM GQT	Gerbu
Albumin Standard, 2000 µg/mL	Pierce
Amberlite	Serva
Ammonium persulfate (APS)	Sigma
0.2% Ampholytes pH 3.7-9.5	Bio-Rad
1,4-Bis (acryloyl) piperazine (PDA)	Fluka
Bromphenolblue	Sigma
3-[(3-cholamido-propyl) dimethyl-ammonio]-1-propanesulfonate	Gerbu
1,4-Dithio-D,L threitol high purity (DTT)	Gerbu
Ettan™ Sample Preparation Kits and Reagents	GE Healthcare
Formic Acid	Merck
Glycerol 99.8%	Fluka
Glycine	Sigma
Iodacetamide (IAA)	Sigma
Nuclease Mix 100X	Amersham
PhosStop Phosphatase Inhibitor Cocktail Tablets	Roche
Plus One Mineral Oil Dry Strips Cover Fluid	GE Healthcare
Protease Inhibitors 100X	GE Healthcare



Protein assay dye-concentrate	Bio-Rad
Sodium dodecyl sulfate (SDS)	Gerbu
N,N,N',N'-Tetramethylethylenediamine (TEMED)	Sigma
Thiourea	Sigma
Tris	Gerbu
Urea	Gerbu

<b>Sample buffer stock <math>V_E = 10</math> mL</b>	
7 M Urea	4.2 g
2 M Thiourea	1.52 g
2% CHAPS	0.2 g
Amberlite	0.1 g

Filter and refill up to 10 mL, store 1 mL aliquots at  $-20^{\circ}\text{C}$

<b>Sample buffer <math>V_E = 1</math> mL</b>	
Sample suffer Stock	885 $\mu\text{L}$
100 mM DTT; 1 M	100 $\mu\text{L}$
0.2% Ampholytes 3.7-9.5; 40%	5 $\mu\text{L}$
100X Protease Inhibitor	10 $\mu\text{L}$
25X PhosStop	40 $\mu\text{L}$
100X Nuclease Mix	10 $\mu\text{L}$

Prepare freshly prior to use

<b>4x 18x16 cm gels: 1.5 mm thick, 12% AA/PDA; <math>V_E = 160</math> mL</b>	
12% AA/PDA; 30%	64 mL
400mM Tris-HCl pH 8.8; 2 M	32 mL
ddH <sub>2</sub> O	64 mL
0.05% APS; 10%	800 $\mu\text{L}$
TEMED	56 $\mu\text{L}$

Immediately pipette 2-propanol onto each casted gel.

<b>12x 26x22 cm gels: 1 mm thick. 12% AA/PDA; <math>V_E = 900</math> mL</b>	
12% AA/PDA; 30%	360 mL
400 mM Tris-HCl pH 8.8; 2 M	180 mL
ddH <sub>2</sub> O	360 mL
0.05 APS; 10%	4.5 mL
TEMED	390 $\mu\text{L}$

Immediately pipette 2-propanol onto each casted gel.

<b>10X Running buffer <math>V_E = 1000</math> mL</b>	
0.25 M Tris	30.3 g
2 M Glycine	150 g
1% SDS; 20%	50 mL

<b>Equilibration buffer <math>V_E = 200</math> mL</b>	
6 M Urea	72 g
0.05 Tris pH 8.8; 2 M	5 mL
2% SDS; 20%	20 mL
20% Glycerol; 99.8%	40 mL

Aliquots at  $-20^\circ\text{C}$

### 3.3.1.2. Procedure

Two different approaches were used to monitor HH induced changes in the adipocyte (phospho)-proteome. First, phospho-protein specific proteomics and second, expression-proteomics using the cytoplasmic fraction of adipocytes were used to perform 2D-gels.

#### **1<sup>st</sup> Dimension: passive rehydration and isoelectric focusing**

IPG strips were passively rehydrated with 50-100  $\mu\text{g}$  protein in 280  $\mu\text{L}$  using 17 cm strips pH 3-10 for phospho-proteomics and 400  $\mu\text{g}$  protein in 400  $\mu\text{L}$  using 24 cm strips pH 5-8 for the cytoplasmic protein expression profile. The appropriate volumes, mixed with bromphenolblue, were pipetted over the whole channel length of a tray. IPG strips were carefully placed into the tray, gel-side down, avoiding any air bubbles. After 15 minutes strips were overlaid with mineral oil and rehydrated for 16-20 hours. After passive rehydration the IPG strips were put with the gel side up into the ceramic bath filled with mineral oil. Filter paper pads were moistened with water and placed onto the strips in order to connect the electrodes. Isoelectric focusing (IEF) was performed in an Ettan IPGphor II system in a stepwise fashion (Table 2). After IEF, strips were put into the rehydration tray and sequentially equilibrated in Equilibration buffer with 100 mM DTT and 2.5% IAA for 10-15 minutes each.

**Table 2:** Isoelectric focusing settings

IEF steps	Phospho-Proteomics		Expression Profile	
	U [V]	Time [Vh]	U [V]	Time [Vh]
Gradient	500	1000	500	375
Step	500	2000	500	2250
Gradient	4500	12500	5000	19250
Step	4500	5400	5000	55000
Step	500	1000	500	1000

## 2<sup>nd</sup> Dimension

The 12% AA/PDA gels were casted the day before. For SDS-PAGE using the Ettan DALTwelve System, the IPG strips were washed in running buffer and placed on top of the gels and overlaid with 0.5% low-melting agarose. The gels were put into the electrophoresis-chambers and were run in running buffer at 5 W per gel for 30 minutes and then at 15 W per gel until the dye front completely ran off.

## Staining and image analysis

The gels were stained with a solution of RuBPS as described by Rabilloud et al [46]. Briefly, gels were fixed overnight in 50% methanol 10% acetic acid, washed twice with 20% methanol for 20 minutes, stained with a 400 nM solution of RuBPS in 20% methanol for 6-8 hours and destained in 50% methanol 7% acetic acid overnight. Fluorography scanning was performed with the FluorImager 595 (GE Healthcare, Fairfield, CT) at a resolution of 100  $\mu$ m. Non radioactive gels were stored in water at 4°C and silver-stained for spot picking. Radioactively labeled gels were dried using the slab gel dryer SE110 (Hoefer, San Francisco, CA), exposed to phosphor screens (Molecular Dynamics) and scanned using the Phosphorimager SI (Molecular Dynamics) at a resolution of 100  $\mu$ m as described by Haudek et al. [44, 47]. All 2D-gel data were independently reproduced three to five times. Detection, matching, background subtraction, normalization and quantitative comparison of 2D spots were accomplished using the Progenesis SameSpots software (Nonlinear Dynamics). Spots of interest were excised from a silver stained gel and subjected to in-gel digestion with trypsin as described below.

### 3.3.2. 1D-GeLC/MSMS

1D-PAGE approach is based on one-dimensional separation of proteins according to their molecular mass. Therefore, the 1D-gel contains bands and no spots, which are cut out of the gel and tryptically digested. All resulting peptides in one single band are separated by nano-flow liquid-chromatography (LC) and subsequently identified by tandem mass spectrometric (MSMS) analysis. The main advantage of this method is the high degree of automation of the analysis and the identification of much more proteins. However, in contrast to 2D-PAGE, 1D-GeLC/MSMS analysis is only a semi-quantitative method.

#### 3.3.2.1. Reagents and solutions

Acetone	Merck
Acetic Acid	JT. Baker
Acetonitrile LC/MS Chromasolv	Sigma
Acrylamide (AA)	Gerbu
Ammonium bicarbonate ( $\text{NH}_4\text{HCO}_3$ )	Sigma
Ammonium persulfate (APS)	Sigma
1,4-Bis (acryloyl) piperazine (PDA)	Fluka
Bromphenolblue	Sigma
1,4-Dithio-D,L threitol high purity (DTT)	Gerbu
Formaldehyde	Merck
Glycine	Gerbu
Protein assay dye-concentrate	Bio-Rad
Methanol	Sigma
Silver Nitrate ( $\text{AgNO}_3$ )	Sigma
Sodium dodecyl sulfate (SDS)	Gerbu
Sodium carbonate	Merck
Sodium Thiosulfate Pentahydrate ( $\text{Na}_2\text{S}_2\text{O}_3 \cdot 5\text{H}_2\text{O}$ )	Sigma
N,N,N',N'-Tetramethylethylenediamine (TEMED)	Sigma
Tris	Gerbu
Trypsin sequencing grade	Roche
Urea	Gerbu
Water double distilled (ddH <sub>2</sub> O)	Mayrhofer

<b>10X Running buffer V<sub>E</sub> =1000 mL</b>	
0.25 M Tris	30.3 g
2 M Glycine	150 g
1% SDS; 20%	50 mL

**2x 1.5 mm gels:**

<b>Bottom gel, 12%</b>	
30% AA/PDA	3 mL
2M Tris HCl pH 8.8	1.5 mL
20% SDS	38 $\mu$ L
ddH <sub>2</sub> O	3 mL
10% APS	34 $\mu$ L
TEMED	2.8 $\mu$ L

<b>Stacking gel, 6%</b>	
30% AA/PDA	2.4 mL
1M Tris HCl pH 6.8	2.3 mL
20% SDS	90 $\mu$ L
ddH <sub>2</sub> O	13.2 mL
10% APS	90 $\mu$ L
TEMED	18 $\mu$ L

2-3 cm high

3.3.2.2. Procedure

Phosphoproteins and proteins from cytoplasmic fractions of differentiated adipocytes were used for 1D-PAGE.

**1D-PAGE**

For 1D-GeLC/MSMS analysis enriched (phospho)-proteins in RIPA buffer (see 2. Sample Preparation) were mixed with Laemmli buffer and were loaded on a slab gel consisting of a 12% polyacrylamide separating gel and a 6% stacking gel. Electrophoresis was performed until the dye front ran approximately 2.5 cm into the separating gel. Gels were silver stained and 1D-PAGE lanes were cut into four gel slices for the phospho-proteomic approach and 10 gel slices for the protein expression method. Gel pieces were subsequently in-gel digested with trypsin as described in 3.3.3. Mass spectrometry analysis.

**MS-compatible silver stain**

After fixation, 2D-gels were washed with 50% methanol and double distilled water for 20 minutes each and sensitized 1 minute with 0.02% Na<sub>2</sub>S<sub>2</sub>O<sub>3</sub>. Sensitized gels were stained with ice-cold 0.1% AgNO<sub>3</sub> for 20 minutes, rinsed with double distilled water, and subsequently developed with 3% Na<sub>2</sub>CO<sub>3</sub>/0.05% formaldehyde as described by Mortz et al [48]. For 1D-gels washing for 10 minutes each and 30 seconds sensitizing was sufficient.

### 3.3.3. Mass spectrometry analysis

Mass Spectrometry (MS) is a technique characterizing molecules by measuring the masses of ions. The MS principle is to generate ions from either inorganic or organic compounds, to separate these ions by their mass-to-charge ratio ( $m/z$ ) and to detect them qualitatively and quantitatively by their respective  $m/z$  and abundance. MS consists of two principal components: an ion source and an ion detector.

Since proteins and peptides are large non-volatile molecules there are two major methods for generating gas-phase ions from them: matrix-assisted laser-desorption ionization (MALDI) and electro spray ionization (ESI). In our experiments we used ESI. The sample to be analyzed is dissolved in water with volatile organic compounds such as acetonitrile and subsequently dispersed by electrospray into a fine aerosol. Some of these fine droplets enter the inlet of the mass analyzer along a potential gradient, becoming desolvated which reduces them. They finally form multiple-charged ions which enter the high vacuum atmosphere of the spectrometer. Following the ESI source an ion trap is connected, which uses a combination of voltage and frequency fields to collect the ions. In the first step a quadrupole stabilizes the formed ions in the gas layer on an orbit depending on their  $m/z$ -relations. By tuning the quadrupole to different  $m/z$  values, and by recording the numbers of ions that pass through at each step, a spectrum is generated. In a second step, selected ions progress into the collision cell and collide with an inert gas like helium and are fragmented. Fragmented ions are scanned by the mass analyzer which gives their  $m/z$  spectrum. This spectrum can be used to directly deduce the sequence of the selected peptide.

#### 3.3.3.1. Reagents and solutions

Acetic Acid	JT. Baker
Acetonitrile LC/MS Chromasolv	Sigma
Ammonium bicarbonate	Sigma
1,4-Dithio-D,L threitol high purity (DTT)	Gerbu
Formic acid	Sigma
Iodacetamide (IAA)	Sigma
Methanol Chromasolv	Sigma
Potassium hexacyanoferrate ( $K_3Fe(CN)_6$ )	Sigma
Sodium thiosulfate ( $Na_2S_2O_3$ )	Sigma

Trypsin Sequencing Grade

Roche

<b>150 mM Potassium hexacyanoferrate <math>V_E = 10</math> mL</b>	
$K_3Fe(CN)_6$	0.4938 g

Store at 4°C

<b>500 mM Sodium thiosulfate <math>V_E = 10</math> mL</b>	
$Na_2S_2O_3$	1.2409 g

Store at 4°C

<b>Destaining solution</b>	
150 mM Potassium hexacyanoferrate	1 mL
500 mM Sodium thiosulfate	1 mL
ddH <sub>2</sub> O	8 mL

Prepare prior to use

<b>50 mM Ammonium bicarbonate (stock solution) <math>V_E = 50</math> mL</b>	
$NH_4HCO_3$	200 mg

Prepare prior to use

<b>10 mM DTT</b>	
10 $\mu$ L 1 M DTT/mL 50 mM $NH_4HCO_3$	

Prepare prior to use

<b>Iodacetamide</b>	
10.2 mg IAA/mL 50 mM $NH_4HCO_3$	

Prepare prior to use and protect from light

<b>Trypsin</b>	
0.1 $\mu$ g Trypsin/ $\mu$ L 1 mM HCl	

<b>Digestion buffer</b>	
0.15 $\mu$ L Trypsin/ $\mu$ L 50 mM $NH_4HCO_3$	

<b>Elution buffer</b>	
Acetonitrile	25 mL
Formic acid	1 mL
ddH <sub>2</sub> O	24 mL

### 3.3.3.2. Procedure

#### **Tryptic digest**

Stained gels were put on the Gel DOC 1000 White Light Source and spots of interest were excised manually from a 2D-gel. 1D-gels were cut into 4 to 10 gel slices per lane. Gel pieces were stored into a tube filled with 1% acetic acid until the in-gel digest with trypsin was performed.

Tryptic digestion was performed under a laminar flow and only Eppendorf tubes were used as described by Haudek et al. [44, 47]. The gel-pieces were destained with destaining solution and intensively washed with 50% methanol 10% acetic acid over night. The pH was neutralized with 50 mM  $\text{NH}_4\text{HCO}_3$ , and proteins were reduced with 10 mM DTT in 50 mM  $\text{NH}_4\text{HCO}_3$  at 56 °C for 30 minutes and alkylated with 50 mM IAA in 50 mM  $\text{NH}_4\text{HCO}_3$  in the dark for 20 minutes. Subsequently, gel-pieces were treated with acetonitrile (ACN) and dried in a vacuum centrifuge. Between each step, the tubes were shaken (Eppendorf thermomixer Comfort) at room temperature for 5-10 minutes. Dry gel-spots were treated with trypsin 0.1 mg/mL in 50 mM  $\text{NH}_4\text{HCO}_3$  on ice for 30 minutes, covered with 50 mM  $\text{NH}_4\text{HCO}_3$  and subsequently stored at 37°C overnight. Digested peptides were eluted by adding 5% formic acid 50% ACN. The supernatant was transferred into silicon coated tubes, and the elution procedure was repeated two times. Between each elution step the gel-pieces were ultrasonicated at 160 W for 10 minutes. Finally the peptide solution was concentrated in a vacuum centrifuge to a total volume of approximately 20  $\mu\text{L}$ .

#### **Protein identification and interpretation**

For mass spectrometry based protein identification, tryptic digests from spots of the phospho-proteomic approach were loaded on a Zorbax 300SB-C8 column (5  $\mu\text{m}$ , 0.3 mm, 5 mm) using the HPLC-Chip technology (Agilent, Palo Alto, CA) and separated by nanoflow LC (1100 Series LC system, Agilent), with a Zorbax 300SB-C18 (5  $\mu\text{m}$ , 75 mm, 150 mm) column at a flow rate of 250 nL/min using a gradient from 0.2% formic acid and 3% ACN to 0.2% formic acid and 45% ACN over 12 minutes. For 1D-GeLC/MSMS analysis peptides were loaded on a 40 nL Zorbax 300SB-C18 trapping column and separated by a 75  $\mu\text{m}$  x 150 mm Zorbax 300SB-C18 column at a flow rate of 400 nL/min, using a gradient from 0.2% formic acid and 3% ACN to 0.2% formic acid and 50% ACN



over 60 minutes. Peptide identification was accomplished by MSMS fragmentation analysis with an iontrap mass spectrometer (XCT-Ultra, Agilent) equipped with an orthogonal nanospray ion source [44, 47]. The MSMS data, including peak list generation and search engine, were interpreted by the Spectrum Mill MS Proteomics Workbench software (Version A.03.03, Agilent) allowing for two missed cleavages and searched against the SwissProt Database for murine proteins (Version 14.3 containing 20328 entries) allowing for precursor mass deviation of 1.5 Da, a product mass tolerance of 0.7 Da and a minimum matched peak intensity (% Scored Peak Intensity) of 70%. Carbamidomethylation of cysteines was set as fixed modification. No other modifications were considered here. To assess the reliability of the peptide scores, we performed searches against the corresponding reverse database. 6.0% positive hits were found with peptides scoring  $>9.0$ , while 0.2% positive hits were found with peptides scoring  $>13.0$ . Consequently, we set the threshold for protein identification scoring 14.0 or higher, resulting in a false discovery rate of 0.1%.

Mass spectrometry based protein identification of tryptic digests of the Expression proteomics approach were analyzed at the Max Planck Institute in Freiburg by Gerhard Mittler on an LTQ Orbitrap XL<sup>TM</sup> MS system (Thermo Fisher Scientific).

Peptides were separated on-line to the mass spectrometer by using an Agilent nano-HPLC 1200 system operated with two solvents (MS buffer A: 0.5% (v/v) acetic acid; MS buffer B: 0.5% (v/v) acetic acid, 80% (v/v) ACN). For each run 4  $\mu$ L sample volume was applied via the  $\mu$ WPS autosampler on to a home-made nano LC-column at a flow rate of 0.5  $\mu$ L/min. Depending on the sample complexity 120 or 140 min methods were run. For the 120 min method the sample was loaded at 2% MS buffer B for 22 minutes and eluted stepwise with several consecutive linear gradients over a period of 98 minutes. Details: flowrate 0.25  $\mu$ L/min, 22-25 min: 5% B, 25-90 min: 30% B, 90-100 min: 50% B, 100-109 min: 60% B, 109-115 min: 80% B, 116-120 min: 2% MS buffer B). Peptide raw files were processed into peak lists using the DTA SuperCharge program of the MSQuant software suite (version "2.0b1") [49]. In order to generate MASCOT .dat files peak lists were searched with MASCOT (version 2.2.02, Matrix Science) against IPI mouse database (version v3.62) which was concatenated with reversed copies of all sequences and supplemented with frequently observed contaminants (*e.g.* trypsin, human keratin, BSA). For all searches carbamidomethylated cysteines were set as a fixed modification. Three missed cleavages were allowed and a mass deviation of 0.5 Da was set as a maximum for MSMS peaks. For MS peaks the mass deviation was restricted to 5 ppm. Enzymatic

cleavage was restricted to trypsin allowing cleavage N-terminal to proline and between aspartic acid and proline (Trypsin/P +DP). The cleavage of the relatively weak DP peptide bond can be induced by TFA used during sample preparation.

All mass data were further processed with the Scaffold software tool (Version 3.0, Proteome Software, Portland, OR). First, to validate MSMS based peptide and protein identifications. Protein identifications were accepted if they contained at least 2 identified peptides. Proteins that contained similar peptides and could not be differentiated based on MSMS analysis alone were manually verified. Second, to quantitatively work out the samples by using the quantitative analysis setup of the Scaffold software. The applied fold-change test is a ratio of the spectral counts in one sample compared to the spectral counts in a second sample. Normalization and a minimum value of one were used for calculation and samples with a 1.5 fold-change were assessed as significantly altered. Finally the protein list was interpreted by Pathway Studio (Version 7.1, Ariadne Genomics, USA).

### 3.4. Western blot

PAGE refers to the use of a special matrix, polyacrylamide, for protein electrophoresis in order to separate them according to their sizes. Proteins separated by SDS-PAGE for analysis by Western blot, should be transferred immediately onto a support membrane such as polyvinylidene fluoride (PVDF). In order to identify the proteins on the membrane, protein-specific antibodies are incubated with the membrane and visualized using secondary antibodies conjugated to an enzyme (typically HorseRadish Peroxidase, HRP). Antibody reaction is detected and calculated by a chemoluminescence Imager.

#### 3.4.1. Reagents and solutions

30% Acrylamide/Bis Solution 29:1 (3.3% C)	Bio-Rad
Ammonium persulfate (APS)	Sigma
Bovine Serum Albumin, Fatty Acid Free (BSA)	PAA
Bromphenolblue (BPB)	Sigma
1,4-Dithio-D,L threitol high purity (DTT)	Gerbu
Glycerol 99.8%	Fluka
Glycine	Sigma
2- Mercaptoethanol (bME)	Sigma
Methanol Chromasolv	Sigma
PageRuler Plus Prestained Protein Ladder	Fermentas
PhosStop Phosphatase Inhibitor Cocktail Tablets	Roche
Protease Inhibitors 100X	GE Healthcare
Sodium dodecyl sulfate (SDS)	Gerbu
N,N,N',N'-Tetramethylethylenediamine (TEMED)	Sigma
SuperSignal West Femto Kit	Thermo Scientific
SuperSignal West Pico Kit	Thermo Scientific
Tris	Gerbu
Tween 20	Sigma

<b>4X Laemmli buffer V<sub>E</sub> = 9 mL</b>	
60 mM Tris pH 6.8; 1 M	2.4 mL
2% SDS	0.8 g
10% Glycerol	4 mL
0.0012% BPB; 0.1%	0.8 mL
100 mM DTT; 4 M	add prior to use

Store 1 mL aliquots at -20°C

<b>10X Running buffer V<sub>E</sub> = 1000 mL</b>	
0.25 M Tris	30.3 g
2 M Glycine	150 g
1% SDS; 20%	50 mL

<b>10X Transfer buffer V<sub>E</sub> = 1000 mL</b>	
0.25 M Tris	30.3 g
1.92 M Glycine	144.1 g

Add 10% Methanol to 1X solution and store at 4°C

<b>10X TBS pH 7.5 V<sub>E</sub> = 1000 mL</b>	
Tris	12.1 g
NaCl	87.6 g

Add 0.2% Tween 20 to 1X solution

<b>Stripping buffer V<sub>E</sub> = 100 mL</b>	
2% SDS; 20%	10 mL
100 mM bME	0.7 mL
65.2 mM Tris pH 6.8	6.25 mL

<b>Primary Antibody</b>	<b>3% BSA in TBS-T</b>	<b>Phosphosite</b>	<b>Company</b>	<b>Order number</b>
AKT1	1:5000	-	Cell signaling	4685
P-AKT1	1:1000	S <sup>473</sup>	Cell signaling	4058
P-GSK 3β	1:5000	S <sup>9</sup>	Cell signaling	9336
PDHE1α	1:5000	-	Cell signaling	3205
P-PDHE1α	1:50.000	S <sup>293</sup>	Abcam	ab77844
PDK1	1:5000	-	Cell signaling	3820
PKM2	1:10.000	-	Cell signaling	3198
PKM1	1:2000	-	Sigma	SAB4200094
P-PKM2	1:5000	Y <sup>105</sup>	Cell signaling	3827
β-Actin	1:10.000	-	Sigma	A5316

Secondary Antibody	3% BSA in TBS-T	Company	Order number
Anti rabbit	1:5000	Cell signaling	7074
Anti mouse	1:20.000	Cell signaling	7076

### 3.4.2. Procedure

#### SDS-Gel

Ingredients were added in the order indicated in the table below. The casting stand, -frame and glass plate sandwich with plastic combs from Bio-Rad were used. Gels were wrapped in a plastic foil together with a piece of wet paper and stored at 4°C for a few days or used immediately.

#### 2x 1 mm Bottom gel (10 mL)

Ingredient	8%	12%
30% AA/BIS	2.7 mL	4 mL
2 M Tris pH 8.8	1.9 mL	1.9 mL
20% SDS	50 µL	50 µL
ddH <sub>2</sub> O	5.3 mL	4 mL
10% APS	100 µL	100 µL
TEMED	10 µL	10 µL

#### 2x 1 mm Stacking gel (5 mL)

Ingredient	6%
30% AA/BIS	1.0 mL
1 M Tris pH 6.8	625 µL
20% SDS	25 µL
ddH <sub>2</sub> O	3.3 mL
10% APS	50 µL
TEMED	5 µL

#### SDS-PAGE

Protein samples stored at -20°C in Laemmli buffer were boiled for 5 minutes, spun down and placed on ice. Protein samples were loaded into the wells, gels were run at 60-100 V for 1-3 hours. The Bio-Rad Mini-PROTEAN Tetra System was used.

#### Protein transfer

PVDF membranes (GE Healthcare) were used for transfer. Due to its hydrophobic character membranes were rehydrated and dehydrated before and after use. PVDF membranes were soaked in 100% methanol for 30 seconds washed in distilled water for 2 minutes and equilibrated in transfer buffer for at least 5 minutes. Proteins were transferred at 4°C at constant voltage as follows: 10 minutes 20 V, 10 minutes 50 V and 1 hour 100 V.

**Immunodetection**

After the transfer was completed membranes were washed with double distilled water and blocked at room temperature in 5% BSA in TBS/Tween 20 (TBS-T) on a rotating platform for 2 hours. Blots were incubated at 4°C overnight with the optimal dilution of the primary antibody (see 3.4.1.). On the next day the primary antibody was removed, stored at -20°C and re-used a couple of times. Membranes were washed three times for 10 minutes in TBS-T with agitation and incubated with the secondary antibody at room temperature for one hour. The membrane was washed another time as mentioned above. For chemiluminescence-immunodetection, the membrane was incubated for approximately 3 minutes with the SuperSignal West Femto and Pico Kits (Pierce), respectively. Chemiluminescence signals were detected using the Bio-Rad Imager (ChemiDoc XRS Imager). Band densities were calculated using the Image Lab Software Version 3.0.1. (Bio-Rad).

### 3.5. Quantitative real time PCR

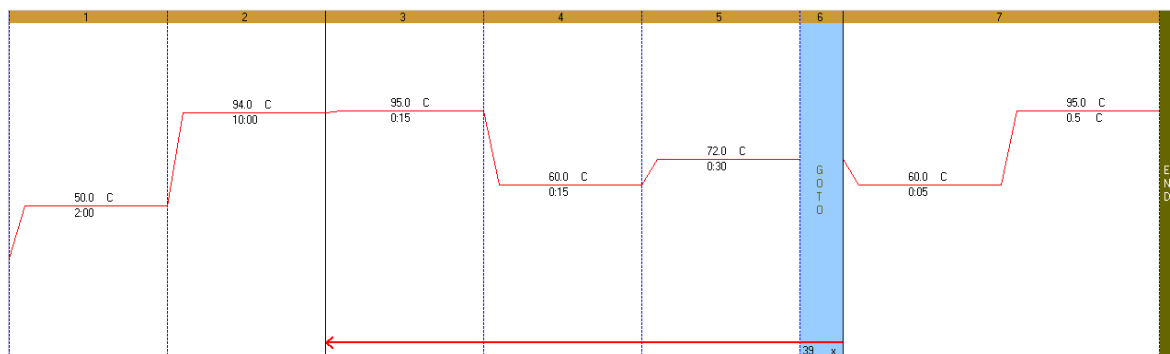
Quantitative real time PCR (Q-RT-PCR) was used to measure mRNA levels of respective target gens.

#### 3.5.1. Reagents and solutions

RNeasy Mini and Micro Isolation Kits	Qiagen
High Capacity cDNA Reverse Transcription Kit	Applied Biosystems
iQ SYBR Green Supermix	Bio-Rad

#### 3.5.2. Procedure

Total RNA was extracted from respective cells using the RNeasy Mini and Micro Isolation Kits according to the manufacturer's instructions. Isolated total RNA was reverse-transcribed into cDNA. Q-RT-PCR (C1000 Thermal Cycler CFX96™ Real Time System, Bio-Rad) reactions were performed using the iQ SYBR Green Supermix and the following settings.



Post-amplification melting curve analysis was performed to check for unspecific products and primer-only controls were included to ensure the absence of primer dimers. For normalization threshold cycles ( $C_t$ -values) of all replicate analyses were normalized to acidic ribosomal phosphoprotein P0 (Rplp0/36B4) within each sample to obtain sample-specific  $\Delta C_t$  values ( $= C_t$  gene of interest -  $C_t$  Rplp0). To compare the effect of various treatments with untreated controls,  $2^{-\Delta\Delta C_t}$  values were calculated to obtain fold expression levels, where  $\Delta\Delta C_t = (\Delta C_t \text{ treatment} - \Delta C_t \text{ control})$  [43]. Primers used are listed below.

<b>Gene Symbol</b>	<b>Alias</b>	<b>Species</b>		<b>Sequence (5'-3')</b>
GLI1	GLI1	mouse	forward	CGAGAGTGCCATGCCGCAGCAG
			reverse	TAGCAGCAACTGTCTAAATGATGCCA
Rplp0	Arp/36B4	mouse	forward	GCCAATAAGGTGCCAGCTGCTG
			reverse	GAGGTCTTCTCGGGTCCTAG



### **3.6. Kinexus – antibody**

Kinexus, a Systems Proteomics Company (<http://www.kinexus.ca>), offers different proteomics and bioinformatics services. The Kinex™ signal transduction protein profiling service utilizes unique antibody microarrays to track the differential binding of dye-labeled proteins in lysates prepared from cells and tissues. The Full Kinex™ Service we have chosen uses ~500 pan-specific antibodies and ~300 phospho-site-specific antibodies.

#### **3.6.1. Procedure**

Sample preparation was performed according to instructions. Briefly, adipocytes were washed twice with ice cold 1X PBS on ice and scraped into 200  $\mu$ L ice-cold lysis buffer (20 mM MOPS pH 7.0, 2 mM EGTA, 5 mM EDTA, 30 mM sodium fluoride, 60 mM  $\beta$ -glycerophosphate pH 7.2, 20 mM sodium pyrophosphate, 1 mM sodium orthovanadate, 1 mM PMSF, 3 mM benzamidine, 5  $\mu$ M pepstatin A, 10  $\mu$ M leupeptin, 1% Triton X-100, 1 mM DTT). Samples were sonicated and centrifuged to get rid of lipid droplets and DNA. Adipocyte samples stimulated with 200 nM SAG for 10-, 30 minutes and 48 hours were performed in triplicates. Equal amounts of each sample were mixed together and shipped on dry ice. Protein microarrays were performed and calculated by Kinexus.

### 3.7. BioAssay Systems EnzyChrom™

Measurements of  $\text{NADP}^+/\text{NADPH}$  and  $\text{NAD}^+/\text{NADH}$  ratios were done using the EnzyChrom™ Assay Kit according to the manufacturer's instructions. Datasheets listed below.

#### BioAssay Systems $\text{NADP}^+/\text{NADPH}$ ECNP006.pdf

### EnzyChrom™ $\text{NADP}^+/\text{NADPH}$ Assay Kit (ECNP-100)

#### Ultrasensitive Colorimetric Determination of $\text{NADP}^+/\text{NADPH}$ at 565 nm

#### DESCRIPTION

Pyridine nucleotides play an important role in metabolism and, thus, there is continual interest in monitoring their concentration levels. Quantitative determination of  $\text{NADP}^+/\text{NADPH}$  has applications in research pertaining to energy transformation and redox state of cells or tissue.

Simple, direct and automation-ready procedures for measuring  $\text{NADP}^+/\text{NADPH}$  concentration are very desirable. BioAssay Systems' EnzyChrom™  $\text{NADP}^+/\text{NADPH}$  assay kit is based on a glucose dehydrogenase cycling reaction, in which the formed NADPH reduces a formazan (MTT) reagent. The intensity of the reduced product color, measured at 565 nm, is proportionate to the  $\text{NADP}^+/\text{NADPH}$  concentration in the sample. This assay is highly specific for  $\text{NADP}^+/\text{NADPH}$  and is not interfered by  $\text{NAD}^+/\text{NADH}$ . Our assay is a convenient method to measure NADP, NADPH and their ratio.

#### APPLICATIONS

**Direct Assays:**  $\text{NADP}^+/\text{NADPH}$  concentrations and ratios in cell or tissue extracts.

#### KEY FEATURES

**Sensitive and accurate.** Detection limit 0.1  $\mu\text{M}$ , linearity up to 10  $\mu\text{M}$   $\text{NADP}^+/\text{NADPH}$  in 96-well plate assay.

**Convenient.** The procedure involves adding a single working reagent, and reading the optical density at time zero and 30 min at room temperature. No 37°C heater is required.

**High-throughput.** Can be readily automated as a high-throughput 96-well plate assay for thousands of samples per day.

#### KIT CONTENTS (100 tests in 96-well plates)

Assay Buffer: 10 mL      Glucose (1 M): 1.5 mL  
 MTT Solution: 1.5 mL      Enzyme Mix: 120  $\mu\text{L}$   
 NADP Standard: 0.5 mL 1 mM  
 $\text{NADP}^+/\text{NADPH}$  Extraction Buffers: each 12 mL

**Storage conditions.** Store all reagents at -20°C. Shelf life of at least 6 months (see expiry dates on labels).

**Precautions:** reagents are for research use only. Normal precautions for laboratory reagents should be exercised while using the reagents. Please refer to Material Safety Data Sheet for detailed information.

#### PROCEDURES

1. **Sample Preparation.** For tissues weigh ~20 mg tissue for each sample, wash with cold PBS. For cell samples, wash cells with cold PBS and pellet  $\sim 10^7$  cells for each sample. Homogenize samples (either tissue or cells) in a 1.5 mL eppendorf tube with either 100  $\mu\text{L}$  NADP extraction buffer for NADP determination or 100  $\mu\text{L}$  NADPH extraction buffer for NADPH determination. Heat extracts at 60°C for 5 min and then add 20  $\mu\text{L}$  Assay Buffer and 100  $\mu\text{L}$  of the opposite extraction buffer to neutralize the extracts. Briefly vortex and spin the samples down at 14,000 rpm for 5 min. Use supernatant for  $\text{NADP}^+/\text{NADPH}$  assays. Determination of both NADP and NADPH concentrations requires extractions from two separate samples.

2. **Calibration Curve.** Prepare 500  $\mu\text{L}$  10  $\mu\text{M}$  NADP Premix by mixing 5  $\mu\text{L}$  1 mM Standard and 495  $\mu\text{L}$  distilled water.

No	Premix + H <sub>2</sub> O	Vol ( $\mu\text{L}$ )	[NADP] ( $\mu\text{M}$ )
1	100 $\mu\text{L}$ + 0 $\mu\text{L}$	100	10
2	80 $\mu\text{L}$ + 20 $\mu\text{L}$	100	8
3	60 $\mu\text{L}$ + 40 $\mu\text{L}$	100	6
4	40 $\mu\text{L}$ + 60 $\mu\text{L}$	100	4
5	30 $\mu\text{L}$ + 70 $\mu\text{L}$	100	3
6	20 $\mu\text{L}$ + 80 $\mu\text{L}$	100	2
7	10 $\mu\text{L}$ + 90 $\mu\text{L}$	100	1
8	0 $\mu\text{L}$ + 100 $\mu\text{L}$	100	0

Dilute standard as shown in the Table. Transfer 40  $\mu\text{L}$  standards into wells of a clear bottom 96-well plate.

**Samples:** add 40  $\mu\text{L}$  sample per well in separate wells.

3. **Reagent Preparation.** For best results allow Enzyme to come to RT (15-30 min) before preparing the Working Reagent. For each well of reaction, prepare Working Reagent by mixing 60  $\mu\text{L}$  Assay Buffer, 1  $\mu\text{L}$  Enzyme Mix, 10  $\mu\text{L}$  Glucose and 14  $\mu\text{L}$  MTT. Fresh reconstitution is recommended.

4. **Reaction.** Add 80  $\mu\text{L}$  Working Reagent per well quickly. Tap plate to mix briefly and thoroughly.

5. Read optical density (OD<sub>565</sub>) for time "zero" at 565 nm (520-600nm) and OD<sub>30</sub> after a 30-min incubation at room temperature.

6. **Calculation.** Subtract OD<sub>30</sub> from OD<sub>0</sub> for the standard and sample wells. Use the  $\Delta\text{OD}$  values to determine sample  $\text{NADP}^+/\text{NADPH}$  concentration from the standard curve.

Note: If the sample  $\Delta\text{OD}$  values are higher than the  $\Delta\text{OD}$  value for the 10  $\mu\text{M}$  standard, dilute sample in distilled water and repeat this assay. Multiply the results by the dilution factor.

#### MATERIALS REQUIRED, BUT NOT PROVIDED

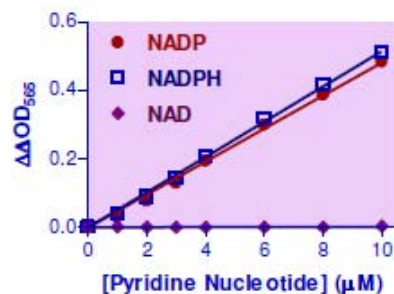
Pipetting (multi-channel) devices. Clear-bottom 96-well plates (e.g. Corning Costar) and plate reader.

#### GENERAL CONSIDERATIONS

1. At these concentrations, the standard curves for NADP and NADPH are identical. Since NADPH in solution is unstable, we provide only NADP as the standard.

2. This assay is based on an enzyme-catalyzed kinetic reaction. Addition of Working Reagent should be quick and mixing should be brief but thorough. Use of multi-channel pipettor is recommended.

3. The following substances interfere and should be avoided in sample preparation. EDTA (>0.5 mM), ascorbic acid, SDS (>0.2%), sodium azide, NP-40 (>1%) and Tween-20 (>1%).



Standard Curve in 96-well plate assay

#### PUBLICATIONS

1. Ding X et al (2009). Enhanced HtrA2/Omi expression in oxidative injury to retinal pigment epithelial cells and murine models of neurodegeneration. Invest Ophthalmol Vis Sci. 50(10):4957-66.

2. Tseng HC et al (2009). Metabolic engineering of Escherichia coli for enhanced production of (R)- and (S)-3-hydroxybutyrate. Appl Environ Microbiol. 75(10):3137-45.

3. Du J et al (2010). Mechanisms of ascorbate-induced cytotoxicity in pancreatic cancer. Clin Cancer Res. 16(2):509-20.



## EnzyChrom™ NAD<sup>+</sup>/NADH Assay Kit (E2ND-100)

### Ultrasensitive Colorimetric Determination of NAD<sup>+</sup>/NADH at 565 nm

#### DESCRIPTION

Pyridine nucleotides play an important role in metabolism and, thus, there is continual interest in monitoring their concentration levels. Quantitative determination of NAD<sup>+</sup>/NADH has applications in research pertaining to energy transformation and redox state of cells or tissue.

Simple, direct and automation-ready procedures for measuring NAD<sup>+</sup>/NADH concentration are very desirable. BioAssay Systems' EnzyChrom™ NAD<sup>+</sup>/NADH assay kit is based on a lactate dehydrogenase cycling reaction, in which the formed NADH reduces a formazan (MTT) reagent. The intensity of the reduced product color, measured at 565 nm, is proportionate to the NAD<sup>+</sup>/NADH concentration in the sample. This assay is highly specific for NAD<sup>+</sup>/NADH and with minimal interference (<1%) by NADP<sup>+</sup>/NADPH. Our assay is a convenient method to measure NAD, NADH and their ratio.

#### APPLICATIONS

**Direct Assays:** NAD<sup>+</sup>/NADH concentrations and ratios in cell or tissue extracts.

#### KEY FEATURES

**Sensitive and accurate.** Detection limit 0.05 μM, linearity up to 10 μM NAD<sup>+</sup>/NADH in 96-well plate assay.

**Convenient.** The procedure involves adding a single working reagent, and reading the optical density at time zero and 15 min at room temperature. No 37 °C heater is required.

**High-throughput.** Can be readily automated as a high-throughput 96-well plate assay for thousands of samples per day.

#### KIT CONTENTS (100 tests in 96-well plates)

**Assay Buffer:** 10 mL      **Lactate:** 1.5 mL  
**MTT Solution:** 1.5 mL      **Enzyme A:** 120 μL  
**NAD Standard:** 0.5 mL 1 mM      **Enzyme B:** 120 μL  
**NAD/NADH Extraction Buffers:** each 12 mL

**Storage conditions.** Store all reagents at -20 °C. Shelf life of at least 6 months after receipt.

**Precautions:** reagents are for research use only. Normal precautions for laboratory reagents should be exercised while using the reagents. Please refer to Material Safety Data Sheet for detailed information.

#### PROCEDURES

- Sample Preparation.** For tissues weigh ~20 mg tissue for each sample, wash with cold PBS. For cell samples, wash cells with cold PBS and pellet ~10<sup>6</sup> cells for each sample. Homogenize samples (either tissue or cells) in a 1.5 mL Eppendorf tube with either 100 μL NAD extraction buffer for NAD determination or 100 μL NADH extraction buffer for NADH determination. Heat extracts at 60 °C for 5 min and then add 20 μL Assay Buffer and 100 μL of the opposite extraction buffer to neutralize the extracts. Briefly vortex and spin the samples down at 14,000 rpm for 5 min. Use supernatant for NAD/NADH assays. Determination of both NAD and NADH concentrations requires extractions from two separate samples.
- Calibration Curve.** Prepare 500 μL 10 μM NAD Premix by mixing 5 μL 1 mM Standard and 495 μL distilled water. Dilute standard as follows.

No	Premix + H <sub>2</sub> O	Vol (μL)	[NAD] (μM)
1	100 μL + 0 μL	100	10
2	80 μL + 20 μL	100	8
3	60 μL + 40 μL	100	6
4	40 μL + 60 μL	100	4
5	30 μL + 70 μL	100	3
6	20 μL + 80 μL	100	2
7	10 μL + 90 μL	100	1
8	0 μL + 100 μL	100	0

Transfer 40 μL standards into wells of a clear flat-bottom 96-well plate.

**Samples.** Add 40 μL sample per well in separate wells.

- Reagent Preparation.** For each well of reaction, prepare Working Reagent by mixing 60 μL Assay Buffer, 1 μL Enzyme A, 1 μL Enzyme B, 14 μL Lactate and 14 μL MTT. Fresh reconstitution is recommended.
- Reaction.** Add 80 μL Working Reagent per well quickly. Tap plate to mix briefly and thoroughly.
- Read optical density (OD<sub>565</sub>)** for time "zero" at 565 nm (520-600nm) and OD<sub>15</sub> after a 15-min incubation at room temperature.
- Calculation.** Subtract OD<sub>0</sub> from OD<sub>15</sub> for the standard and sample wells. Use the ΔOD values to determine sample NAD/NADH concentration from the standard curve.

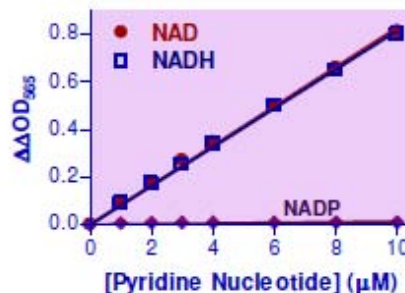
**Note:** If the sample ΔOD values are higher than the ΔOD value for the 10 μM standard, dilute sample in distilled water and repeat this assay. Multiply the results by the dilution factor.

#### MATERIALS REQUIRED, BUT NOT PROVIDED

Pipetting (multi-channel) devices. Clear-bottom 96-well plates (e.g. Corning Costar) and plate reader.

#### GENERAL CONSIDERATIONS

- At these concentrations, the standard curves for NAD and NADH are identical. Since NADH in solution is unstable, we provide only NAD as the standard.
- This assay is based on an enzyme-catalyzed kinetic reaction. Addition of Working Reagent should be quick and mixing should be brief but thorough. Use of multi-channel pipettor is recommended.
- The following substances interfere and should be avoided in sample preparation. EDTA (>0.5 mM), ascorbic acid, SDS (>0.2%), sodium azide, NP-40 (>1%) and Tween-20 (>1%).



Standard Curve in 96-well plate assay

#### LITERATURE

- Zhao, Z, Hu, X and Ross CW (1987). Comparison of Tissue Preparation Methods for Assay of Nicotinamide Coenzymes. *Plant Physiol.* 84: 987-988.
- Matsumura, H. and Miyachi S (1980). Cycling assay for nicotinamide adenine dinucleotides. *Methods Enzymol.* 69: 465-470.
- Vilcheze, C et al. (2005). Altered NADH/NAD<sup>+</sup> Ratio Mediates Coreistance to Isoniazid and Ethionamide in Mycobacteria. *Antimicrobial Agents and Chemotherapy.* 49(2): 708-720.

### 3.8. Enzymatic determination of glucose and lactate

Measurements of glucose and lactate were done using the Biomerieux Assay Kit according to the manufacturer's instructions. Datasheets listed below.

**REF 61 269 / 61 270** 07987 F - en - 201007

**Glucose RTU™** IVD

Enzymatic determination of glucose in human urine, serum and plasma.

---

**SUMMARY AND EXPLANATION (1)**

Glucose is the main source of energy for cells (glycolysis). It is supplied by food in the form of polysaccharides (starch, exogenous glycogen) or disaccharides (sucrose, lactose, maltose). They are hydrolysed during digestion into monosaccharides, including glucose.

In the liver and muscles, glucose is partially transformed into glycogen, a storage polymer. In case of increased energy needs, glycogenolysis and/or biosynthesis of glucose occurs (neoglucogenesis in the liver).

Glycemic homeostasis continuously provides energy to the cells. Glycemia regulation is complex and involves regulatory hepatic enzymes and hormones (insulin, thyroid hormone, glucagons, etc.) which ensure rapid adaptation.

Regulation of glycemia is related to that of other metabolisms such as proteins and fatty acids.

Under normal physiological conditions, glucose is not excreted in urine.

Apart from the screening for and monitoring of diabetic glucose is measured in cases of pancreatic, metabolic endocrine disorders. Fever and protein denaturation may also cause a decrease in glycaemia.

**PRINCIPLE**

Glucose is determined using the glucose oxidase peroxidase - chromogen sequence:

$$\text{Glucose} + \text{O}_2 \xrightarrow{\text{glucose oxidase}} \text{gluconic acid} + \text{H}_2\text{O}_2$$

The hydrogen peroxide formed is titrated according to the TRINDER reaction (2):

$$2\text{H}_2\text{O}_2 + \text{phenol} + 4\text{-aminoantipyrine} \xrightarrow{\text{peroxidase}} \text{quinoneimine} + 4\text{H}_2\text{O}$$

The colour intensity (quinoneimine), measured at 505 nm is proportional to the quantity of glucose in the sample.

---

**PRESENTATION AND CONTENT OF THE KIT**  
(Ref. 61 269 : 400 tests - Ref. 61 270 : 1000 tests)

Glucose RTU™ - Ref. 61 269 : 4 x 100 ml (liquid) - Ref. 61 270 : 4 x 250 ml (liquid)	Phosphate buffer pH 6.0 4-Aminoantipyrine Phenol TSA Peroxidase Glucose oxidase	225 mmol/l 0.3 mmol/l 0.5 mmol/l 5 mmol/l 2 300 U/l 2 10 000 U/l
--	--	---

1 package insert

---

**REAGENT AND MATERIAL REQUIRED BUT NOT PROVIDED**

**Reagent**  
Calimat (Ref. 62 321).

**Material**  
General laboratory equipment

**WARNINGS AND PRECAUTIONS**

- For *in vitro* diagnostic use only.
- For professional use only.
- Check that the reagents are intact before use.
- Do not use the reagents after the expiry date indicated on the box label.

**STORAGE CONDITIONS**

- Store the kit at 2-8°C.
- The reagent is stable until the expiry date indicated on the box label when stored in the recommended conditions.
- Do not freeze the reagent.
- The reagent is sensitive to freezing temperatures. Avoid contact with refrigerating surfaces.

**SPECIMENS**

**Specimen type (3, 4)**

- Serum or plasma collected in anticoagulant, antifibrinolytic agents: EDTA + sodium fluoride or lithium heparin + sodium fluoride.
- Preferably store on ice until centrifugation. Then centrifuge at a minimum of 1000 x g for 10 minutes soon as possible (maximum 1 hour after collection) into glycolysis.
- Preferably use plasma
- 24-hour urine samples, pure or diluted, if necessary, demineralised water

**Stability of serum and plasma (3, 4, 5, 6)**

- 48 hours at 18-25°C if separated from the erythrocyte leucocytes and platelets.
- 4 days at 2-8°C if separated from the erythrocyte leucocytes and platelets.
- 3 months at -25 - 6°C.

**Stability of urine (7)**

Store 24-hour urine samples in opaque vials at 2-8°C. Analyse without delay.

Glucose RTU™ 071017 F - en - 201607

---

**Relevant Interferents**

None of the following factors have been found to significantly influence this assay.

- hemolysis, after spiking samples with hemoglobin, up to 310 µmol/l (monomer).
- lipglycerides, up to 6 mmol/l.
- bilirubinemia, after spiking samples with bilirubin, up to 139 µmol/l.

However, it is recommended not to use samples that are visibly hemolyzed, lipemic or icteric and, if possible, to collect a new sample.

**QUALITY CONTROL**

- LYOTROL™ N (Ref. 62 373)
- LYOTROL™ P (Ref. 62 383)
- MONOTROL™ (Ref. 62 472)
- UNITROL™ (Ref. 62 453)

Perform a control for each series of tests to ensure validity. The value obtained must be within the acceptable range.

**Note**

It is the responsibility of the user to perform Quality Control in accordance with any local applicable regulations.

**LIMITATIONS OF THE METHOD**

In cases of very high hyperglycaemia (above 50 mmol/l), discoloration of the reaction medium can be observed visually and is revealed by an unstable absorbance during measurement. This phenomenon may produce a falsely low result. It is therefore necessary to perform the assay on the sample diluted 1/10 in a 9 g/l solution of NaCl.

**RANGE OF EXPECTED VALUES**

These figures are given as a guide; it is recommended that each laboratory establishes its own reference values from a rigorously selected population.

**Serum or plasma (1, 7)**

	mmol/l	g/l	mg/dl
Pregnant women	1.10 - 4.30	0.20 - 0.80	20 - 80
Neonates	1.70 - 3.30	0.31 - 0.59	31 - 60
Children	3.20 - 6.60	0.59 - 1.01	59 - 101
Women	4.10 - 6.50	0.74 - 1.08	74 - 108
Men	4.20 - 6.10	0.76 - 1.10	76 - 110

**Urine**

Under normal physiological conditions, glucose is not excreted in urine.

**PERFORMANCE (6)**

Studies performed using Glucose RTU™ reagent gave the following results.

The performance data presented were obtained using the procedure indicated in this package insert.

Any change or modification in the procedure may affect the results.

Performance data are given for information purposes only.

**Analytical detection limit**

The detection limit was determined using tests performed with demineralised water (mean ± 5 x standard deviation). The detection limit is less than or equal to 0.07 mmol/l (0.013 g/l or 1.26 mg/dl).

**Linearity**

The reagent is linear up to 22.2 mmol/l (4.00 g/l or 400 mg/dl).

---

**CALIBRATION**

Use Calimat (Ref. 62 321) multiparametric calibrator.

**INSTRUCTIONS FOR USE - MANUAL METHOD**

**Preparation of reagent**  
Ready-to-use reagent

**Stability after opening, in the original vial**

- 2 months at 2-8°C.
- 21 days at 20-26°C.

**Procedure:**

Wavelength: .....505 nm (492 to 556 nm)

Zero adjustment: .....reagent blank

	Reagent blank	Standard	Sample
Standard	-	10 µl	-
Sample	-	-	10 µl
Reagent	1 ml	1 ml	1 ml

Mix.

Perform photometry after incubation for:

- 10 minutes at 37°C.
- 20 minutes at 20-26°C.

**Colour intensity is stable:** ..... 1 hour at 20-25°C

**Calibration stability:** Perform a calibration for each series of tests.

**RESULTS AND INTERPRETATION**

Interpretation of the test results should be made taking into consideration the patient's history and, if necessary, the results of any other tests performed.

**Calculation**

$$\text{Sample concentration} = \frac{A_{\text{sample}}}{A_{\text{standard}}} \times n$$

n = concentration of standard

If urine samples are tested, and if necessary, multiply the result obtained by the dilution factor.

**CONVERSION FACTOR**

mmol/l x 0.180 = g/l g/l x 5.56 = mmol/l  
 mmol/l x 18 = mg/dl mg/dl x 0.056 = mmol/l

Glucose REF 61192 070873-en - 201007

**Precision**

**Intra-assay Precision**

Three serum samples were assayed in the same run

Level	n	Mean (mmol/l)	CV (%)
Level 1	20	2.50	2.01
Level 2	20	7.49	1.20
Level 3	20	17.00	1.16

Three urine samples were assayed in the same run

Level	n	Mean (mmol/l)	CV (%)
Level 1	20	1.21	3.45
Level 2	20	10.56	2.48
Level 3	20	31.50	2.15

**Inter-assay Precision**

Three serum samples were assayed in 20 different runs (1 run per day)

Level	n	Mean (mmol/l)	CV (%)
Level 1	20	1.85	3.01
Level 2	20	6.44	0.87
Level 3	20	19.80	1.17

**Correlation**

48 serum samples were assayed in comparison with a reagent on the market based on a hexokinase technique. The algebraic curve equation obtained is:  $y = 1.02x + 0.15$  (in mmol/l) with a correlation coefficient of 0.996.

**APPLICATIONS AVAILABLE ON REQUEST**

- Spectrophotometer applications (11867B)
- AU 600 / 640 / 2700 (13733A)
- HITACHI 704 (11899B)
- HITACHI 717 (11900C)
- HITACHI 911 (11901C)
- KONELAB 20 / 30 / 80 (12886B)
- MASCOIT PLUS / LISA (11902C)
- MEGA (12887B)
- MIRA S / MIRA PLUS (11903B)
- RA 1000 / XT (11904B)
- SELECTRA 2 HI / XL (11905C)
- Syndent<sup>®</sup> Lx / Dx (16140A)
- TARGA / FALCON 250 / BT 3000 plus (12888B)

**WASTE DISPOSAL**

- Discard reagents may be considered as non hazardous waste and disposed of accordingly.
- Dispose of all used reagents as well as any other contaminated disposable materials following procedures for infectious or potentially infectious products.

Both the kit and the reagents, REF 61000L and 61010C, are used, pending further regulatory instructions, according to 40800000 SA or one of its derivatives. Copy the name of the reagents to the property of the respective manufacturer.



biMérieux SA  
RCS LYON 673 620 300

60280 Marcy-Etoile / France  
Tel. 33 (0)4 78 87 20 00  
Fax 33 (0)4 78 87 20 00  
www.biomerieux.com



Printed in France

It is the responsibility of each laboratory to handle waste and effluents produced according to their type and degree of hazardness and to treat and dispose of them (or have them treated and disposed of) in accordance with any applicable regulations.

**LITERATURE REFERENCES**

1. GASPART E. - P-Glucose. Variations biologiques et valeurs de référence - In: SIEST G., HENNY and SCHLEB P. - *Interprétation des examens de laboratoire - Ed. Karger, 1991 - p. 205-223 - ISBN 3-8055-2756-X*
2. TRINDER P. - Determination of Glucose in Blood using Glucose Oxidase with an Alternative Oxygen Acceptor - *Ann Clin Biochem - 1958, vol. 6, n°24, p. 24-27*
3. STAHL M., JORGENSEN I., G. M. MYLTOFT, PETERSEN P. et al. - Optimization of preanalytical conditions and analysis of plasma glucose. 1. Impact of the new WHO and ADA recommendations on diagnosis of diabetes mellitus. - *Scand J Clin Lab Invest - 2001, vol. 61, p. 189-199*
4. FOUCHER S., RINA G., DESJEUUX C. et al. - Diabète de la glycémie avant centrifugation avec ou sans anticoagulant - *Ann Biol Clin - 2004, vol. 62, p. 691-694*
5. BOYANIGAN B. L., JR. and BLICK R. E. - Stability studies of twenty-four analytes in human plasma and serum. - *Clin Chem - 2002, vol. 48, n° 12, p. 2342-2347*
6. CHEVILLON I., LARROSE C., MOREAU N. et al. - Conservation des échantillons de sang avant analyse des paramètres biochimiques les plus courants. - *Ann Biol Clin - 1993, vol. 55, p. 200-204*
7. PRUDEN E. L., Mc PHERSON R. A., FURBERMAN S. A. - *Clinical guide to laboratory tests - Ed. 11E12, N.Y. / Saunders W.B. Company, 1995 - 3th ed. - Section 1 general clinical tests - p. 258-273 - ISBN 0-7216-5035-X*
8. VASSAULT A., GRAMMEYER D., NAUDIN C. et al. - Placome de validation d'échantillons (document 4) - *Ann Biol Clin - 1996, vol. 54, p. 100-105*

**INDEX OF SYMBOLS**

Symbol	Meaning
REF	Catalogue number
IVD	In Vitro Diagnostic Medical Device
	Manufacturer
	Temperature limitation
	Use by
LOT	Batch code
	Consult instructions for Use

**REF 61 192**

**Lactate PAP (Lact PAP)**

Enzymatic determination of L-lactate in human plasma and cerebrospinal fluid (CSF)

**SUMMARY AND EXPLANATION (1 - 5)**

Pyruvate plays an essential role in the metabolism of carbohydrates, lipids and proteins. If tissue oxygenation (hypoxia) is insufficient, pyruvate is metabolized into L-lactate. Most lactate acid is produced by glycolysis in white skeletal muscles, the brain, the skin, the renal medulla and erythrocytes. Lactatemia depends on the rate of lactate production in these tissues and its rate of metabolism. Approximately 65% of total basal lactate is transformed into glucose in the liver (gluconeogenesis); the rest is oxidized in red skeletal muscles and in the renal cortex.

Hyperlactatemia is defined as a mild to moderate (2-5 mmol/l) persistent increase in blood lactate concentration, without metabolic acidosis.

Lactic acidosis is characterized by persistently increased blood lactate levels (> 5 mmol/l) in association with metabolic acidosis.

Lactic acidosis may be either type A or B.

Type A is due to tissue hypoperfusion and is the most common type.

Type B is associated with defective oxygen utilization. It can be associated with intoxication (ethanol, methanol, salicylates), some type B lactic acidosis are inborn, while others are acquired (diabetes, renal or hepatic insufficiency, cancers).

An increase in lactatemia is observed:

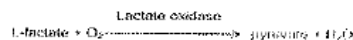
- each time the metabolism is oriented towards anaerobiosis, through a lack of oxygen: state of shock, severe hypoxia (carbon monoxide or cyanide poisoning, respiratory insufficiency), acute organ ischemia (myocardial infarction, acute aortic, crush syndrome), some complications of diabetes etc.

- following an increase in L-lactate production: certain tumors (hepatoma, lymphomas), certain drugs (antibiotic beta-lactams), certain drugs (antibiotic beta-lactams), some genetic diseases (type I glycogen storage diseases, errors in metabolism of fatty acid metabolism) after prolonged physical exertion.

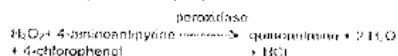
CSF L-lactate concentration varies in parallel with lactatemia. However, CSF L-lactate increases independently from lactatemia, in case of cerebrovascular accident, intracranial hemorrhage, bacterial meningitis, brain tumor, epilepsy, failure of metabolism affecting the central nervous system etc.

**PRINCIPLE**

Lactate PAP enables the determination of L-lactate by using the lactate oxidase - peroxidase - chromogen sequence:



The hydrogen peroxide formed is assayed according to a TRINDER type reaction (5, 7):



The intensity of the measured coloration (quinoneimine) is proportional to the quantity of L-lactate present in the sample.

**PRESENTATION AND CONTENT OF THE KIT (110 tests)**

Reagent	Quantity	Content	Quantity
Reagent 1 Standard	1 x 9 ml (liquid)	L-Lactate NaCl	3.00 mmol/l 1.99
Reagent 2 Buffer	2 x 70 ml (liquid)	PIPES buffer* (Piperazine 1,4-bis (2-ethanesulfonic acid)) pH 6.8 4-chlorophenol Surfactant NaCl	100 mmol/l 5.4 mmol/l 2.5g 1.99
Reagent 3 (reconstituted with R2)	11 x 10 ml (lyophilized)	Protein matrix (bovine) 4-aminobipyrine Peroxidase (POD) Lactate oxidase (LOD)	0.4 mmol/l 200 U/ml 250 U/ml 2.150 U/ml
11 white screw capsules			
1 package insert			

\* This reagent contains 1% PIPES. A Material Safety Data Sheet is available on request.

**MATERIAL REQUIRED BUT NOT PROVIDED**

General laboratory equipment

**WARNINGS AND PRECAUTIONS**

- For *in vitro* diagnostic use only.
- For professional use only.
- This kit contains products of animal origin. Certified knowledge of the origin and/or sanitary state of the animals does not totally guarantee the absence of transmissible pathogenic agents. It is therefore recommended that these products be treated as potentially infectious, and handled observing the usual safety precautions (do not ingest or inhale).
- Check that the reagents are intact before use.
- Do not use the reagent after the expiry date indicated on the label.
- The reagent contains sodium azide which can react with lead or copper plumbing to form explosive metal azides. If any liquid containing sodium azide is disposed of in the plumbing system, drains should be flushed with water to avoid build up.
- High quantities of lactate are present in sweat. Avoid touching pipette tips, caps and bottle tops and anything which could be in contact with the reagent.

**STORAGE CONDITIONS**

- Store the kit at 2-8°C
- All reagents are stable until the expiry date indicated on the box label when stored in the recommended conditions.

**SPECIMENS**

**Specimen type (1, 5)**

- Plasma collected in an antipolythytic-anticoagulant mixture sodium fluoride-EDTA, sodium fluoride-oxalate or heparin/lithium citrate.
- Certain precautions are necessary during collection, the patient must be resting, and if possible avoid using a tourniquet or limit venous stasis to 30 seconds.
- Centrifuge as soon as possible to separate the packed red cells from the plasma in order to limit glycolysis which leads to an increase in lactate concentration.

- Cerebrospinal Fluid

**Stability**

- Plasma (9)
  - 4 days at 2-8°C if separated from pellet
  - 3 months at -25 ± 5°C.
- CSF (2)
  - 24 hours at 2-8°C.
  - 3 hours at 20-25°C.
  - 1 month at -25 ± 5°C.

**Relevant Interferents (on plasma)**

None of the following factors have been found to significantly influence this assay.

- hemolysis, after spiking samples with hemoglobin, up to 124 µmol/l.
- triglycerides up to 5 mmol/l.
- bilirubinemia, after spiking samples with bilirubin, up to 293 µmol/l.

However, it is recommended not to use samples which are visibly hemolyzed, lipemic or icteric and, if possible, to collect a new sample.

Fifteen drugs were tested *in vitro*. No significant influence has been found when using normal therapeutic dosages. Only methyl-DOPA and ascorbic acid, at higher than normal dosages, lead to underestimation of lactate concentration.

**CALIBRATION**

- Use Calimat (Ref. 62 321): multiparametric calibrator, or
- Use Reagent 1 (Ref. 61 102).
  - Titer for Reagent 1: 3.00 mmol/l (270 mg/l or 27 mg/dl).
  - Aqueous solution prepared using 99% pure sodium L-lactate.

**INSTRUCTIONS FOR USE – MANUAL METHOD**

**Preparation of reagents**

- Open a bottle of Reagent 3 and discard the rubber cap.
- Reconstitute the contents of one vial of Reagent 3 with 10 ml of Reagent 2.
- Reseal the bottle with a white screw capsule from the plastic sachet.
- Mix gently by inverting the bottle.

**Stability in the original vial**

- 6 weeks at 2-8°C.
- 2 weeks at 20-25°C.

**Procedure**

Wavelength: ..... 505 nm (492 to 550 nm)  
 Zero adjustment: ..... reagent blank

	Reagent blank	Standard	Sample
Standard	-	10 µl	-
Sample	-	-	10 µl
Reconstituted Reagent 3	1 ml	1 ml	1 ml
Mix			
Perform photometry after incubation for 5 minutes at 20-25°C.			

For hyperlipidemic samples, it is recommended to prepare a sample blank by replacing reconstituted Reagent 3 with Reagent 2 as it is. Deduct the A of this sample blank from that obtained for the assay.

Colour intensity is stable: ..... 1 hour at 20-25°C

Calibration stability: Perform a calibration for each series of tests.

**RESULTS AND INTERPRETATION**

Interpretation of the test results should be made taking into consideration the patient's history and, if necessary, the results of any other tests performed.

**Calculation**

$$\text{Sample concentration} = \frac{A_{\text{sample}} \times x}{A_{\text{standard}}}$$

n = concentration of standard

**CONVERSION FACTOR**

$$\text{mmol/l} \times 90 = \text{mg/l} \quad \text{mg/l} \times 0.011 = \text{mmol/l}$$

$$\text{mmol/l} \times 9 = \text{mg/dl} \quad \text{mg/dl} \times 0.111 = \text{mmol/l}$$

**QUALITY CONTROL**

- LYOTROL™ N (Ref. 62 373)
- LYOTROL™ P (Ref. 62 383)

Perform a control for each series of tests to ensure validity. The value obtained must be within the acceptable range.

**Note**

It is the responsibility of the user to perform Quality Control in accordance with any local applicable regulations.

**RANGE OF EXPECTED VALUES (10)**

These figures are given as a guide, it is recommended that each laboratory establishes its own reference values from a rigorously selected population.

	mmol/l	mg/dl
Plasma		
• Venous blood	0.5 - 2.2	4.5 - 19.8
• Arterial blood	0.5 - 1.6	4.5 - 14.4
CSF	< 2.8	< 25.2

**PERFORMANCE (11)**

Studies performed using Lactate PAP reagent gave the following results.

The performance data presented were obtained using the procedure indicated in this package insert. Any change or modification in the procedure may affect the results.

Performance data are given for information purposes only.

**Analytical detection limit**

The detection limit was determined using tests performed with demineralized water (mean + 5 x standard deviation). The detection limit is less than or equal to 0.07 mmol/l (6.3 mg/l or 0.63 mg/dl).

**Linearity**

The reagent is linear up to 10 mmol/l (900 mg/dl or 90 mg/dl).

**Precision**

**Intra-assay precision**

Three serum samples were assayed in the same run.

	n	Mean (mmol/l)	CV (%)
Level 1	12	3.00	1.11
Level 2	12	7.02	1.08
Level 3	12	9.82	1.17

**Inter-assay precision**

Three plasma samples were assayed singly in 20 different runs (1 run per day).

	n	Mean (mmol/l)	CV (%)
Level 1	20	3.90	3.20
Level 2	20	6.91	1.90
Level 3	20	9.40	2.00

**Correlation**

26 plasma samples were assayed in comparison with a reagent on the market based on a UV technique. The alometric curve equation obtained is: y = 0.87 x + (in mmol/l) with a correlation coefficient of 1.000.

57 CSF samples were assayed in comparison with a reagent on the market based on a UV technique. The alometric curve equation obtained is: y = 1.02 x + 0.08 (in mmol/l) with a correlation coefficient of 0.995.

**APPLICATIONS AVAILABLE ON REQUEST**

- Spectrophotometer applications (12468B)
- AU 400 / 640 / 2700 (12810A)
- CX 5 / CX 7 / CX 9 (12823B)
- HITACHI 704 (12469C)
- HITACHI 717 (12470C)
- HITACHI 911 (12471C)
- KONELAB 20 / 30 / 60 (12824B)
- MASCOTT PLUS / LISA (12472C)
- MIRA S / MIRA PLUS (12473C)
- TARGA / FALCOR 250 / DT 3000 plus (12825B)

**WASTE DISPOSAL**

Dispose of used reagents as well as any contaminated disposable materials following procedures for infectious or potentially infectious products.

It is the responsibility of each laboratory to handle waste and effluents produced according to their nature and degree of hazardness and to treat and dispose of them (or have them treated and disposed of) in accordance with any applicable regulations.

## 4. RESULTS

For quantitative proteomics we utilized two methods. The first was 2D-PAGE analysis to enable quantitative comparison of 2D-gel patterns of control and HH treated samples. In the second set of experiments we performed quantitative label-free 1D-GeLC/MSMS analysis to (i) complement 2D-PAGE data and (ii) provide more comprehensive information on alterations in the phospho-proteome and protein expression in 3T3-L1 adipocytes exposed to SAG, a potent HH agonist.

Reversible phosphorylations of serine (S), threonine (T) and tyrosine (Y) residues are important post-translational modifications of proteins and key regulatory mechanisms in switching protein activity “on” or “off”. Many important cellular processes, such as signal transduction, metabolism, and carcinogenesis are controlled through reversible phosphorylation of proteins. Abnormally phosphorylated proteins have been associated with the pathology of a variety of disease states, including cancer [50] and diabetes [51]. Furthermore, several studies have characterized the role of specific phosphorylation events in the HH signaling pathway [24]. Consequently, we focused in our primary screen on phospho-proteins to gain more insight into the rapid “on-off-mechanisms” of HH treated adipocytes. In addition, the cytoplasmic-proteome was interrogated to obtain information on lasting expression changes. To reduce sample complexity and enhance the resolution of 2D-gels, cytoplasmic fractions instead of the whole cell lysates were analyzed. For better comparison, cytoplasmic proteins were also used for the 1D-GeLC/MSMS approach.



#### 4.1. Quantitative phospho-protein identification of HH treated adipocytes

The phospho-proteome was examined using the workflow depicted in Figure 4. Differentiated 3T3-L1 cells were stimulated with SAG, for 10 minutes and phospho-proteins were purified as described in Material and Methods. 1D- and 2D-gels were performed, spots of interest and bands were excised and subjected to in-gel tryptic digestion. Peptides were separated by nanoflow LC and identified by MSMS fragmentation analysis. MSMS data were interpreted by the SpectrumMill software and searched against the SwissProt database. Mass data were further processed with the Scaffold software tool to validate MSMS based peptide and protein identifications. Finally, the Scaffold generated protein list was interpreted by Pathway Studio.

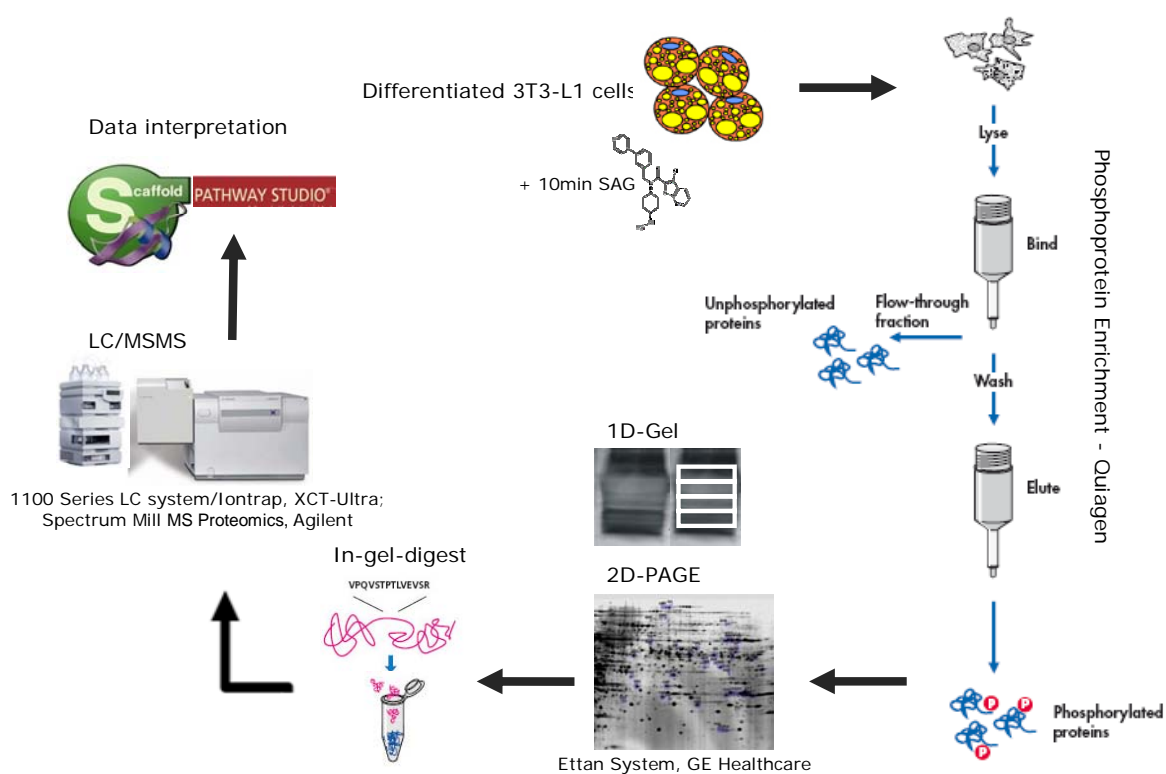


**Figure 4: Schematic outline of phospho-protein-specific proteomics approach**

Mature adipocytes were stimulated with SAG. Phospho-proteins were enriched via an antibody-based column and subjected 1D- and 2D-gels. Spots of interest and bands were in-gel digested, analyzed by LC/MSMS and interpreted by Scaffold and Pathway Studio.



#### 4.1.1. Depth and coverage of the 3T3-L1 adipocyte phospho-proteome

We detected in total 632 spots in three independent 2D-PAGE experiments. 50 spots of interest were identified by MSMS. 42 proteins of them were up-regulated in the HH treated sample (Figure 5A, B). Based on problems with spot picking and LC/MSMS identification no down regulated protein could be identified.

The 1D-GeLC/MSMS approach was done in triplicates and a total of 5153 spectra met the criteria for peptide validation (see 3.3.2.). More than 800 unique peptides (false discovery rate, FDR = 0.2%) corresponding to 255 distinct putative phospho- proteins (FDR = 0.1%) were identified. To access the reproducibility of our approach, Venn-diagrams illustrating the number of proteins identified in each replicate and the overlap between these triplicates are shown in Figure 6A. Control (Ctr) samples yielded 153 for Ctr-1, 151 for Ctr-2 and 136 proteins for Ctr-3, whereas 86 proteins were found in all three replicates. For the SAG treated samples 168 proteins were identified in SAG-1, 173 in SAG-2, in 154 SAG-3 and 113 proteins were found in all three replicates.

Quantitative evaluation of phospho-protein abundance using the number of MSMS spectra yielded 67 significantly regulated phospho-proteins in at least two out of three independent experiments. 45 phospho-proteins were up regulated and 22 were down regulated in the HH treated sample, showing a mean fold-change of  $\geq 1.5$  or  $\leq 0.66$ , respectively (Figure 6B). Comparative analysis revealed 30 proteins identified in both 1D- and 2D-gels, whereas 225 proteins were only identified by 1D-GeLC/MSMS analysis and 20 proteins by 2D-PAGE (Figure 6C).

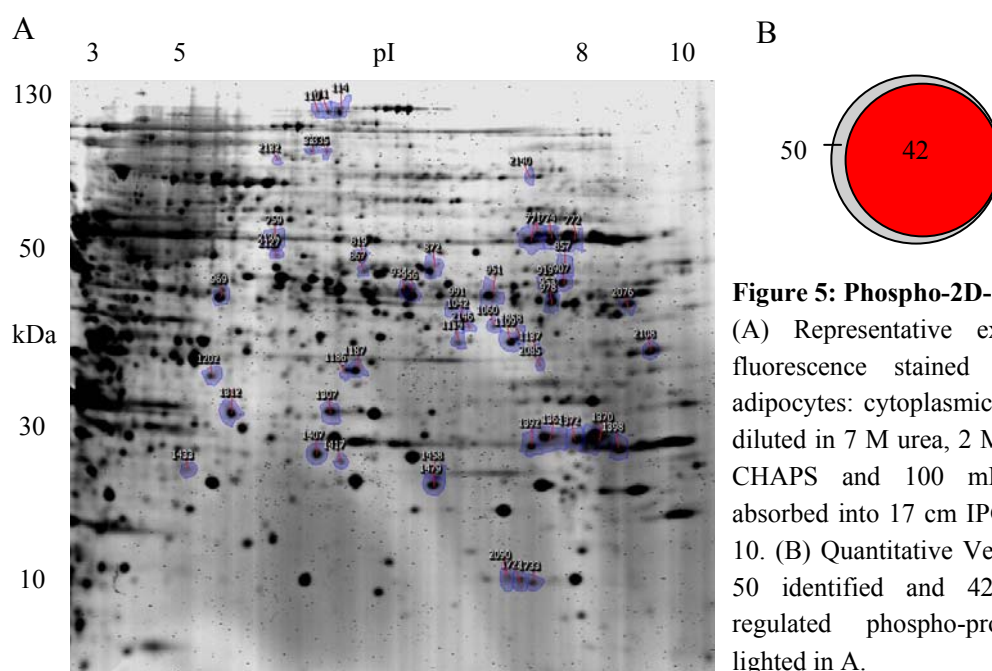


**Figure 5: Phospho-2D-gel**

(A) Representative example of a fluorescence stained 2D-gel from adipocytes: cytoplasmic proteins were diluted in 7 M urea, 2 M thiourea, 2% CHAPS and 100 mM DTT and absorbed into 17 cm IPG strips pH 3-10. (B) Quantitative Venn diagram of 50 identified and 42 significantly regulated phospho-proteins, highlighted in A.

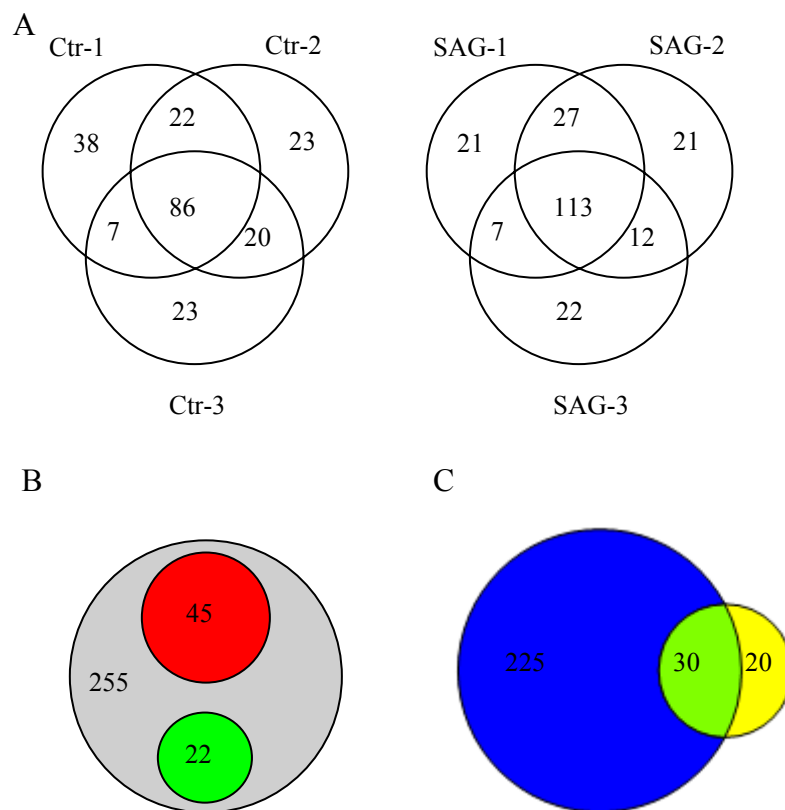


**Figure 6: Phospho-proteome dataset**

(A) Venn-diagrams illustrating the number of proteins identified in each replicate and the overlap between these triplicates for control (Ctr) and SAG treated samples. (B) Quantitative Venn diagram of 255 identified phospho-proteins by 1D-GeLC/MSMS, illustrating 45 up- and 22 down regulated proteins. (C) Quantitative Venn diagram illustrating comparative analysis of 30 proteins identified in both 1D- and 2D-gels, 225 proteins were only identified by 1D-GeLC/MSMS analysis and 20 proteins by 2D-PAGE.

#### 4.1.2. Phospho-protein-specific 2D- and 1D-gels revealed phosphorylation of pyruvate dehydrogenase E1 alpha in HH treated samples

Proteome profiling of HH treated adipocytes revealed a highly reproducible phosphorylation of pyruvate dehydrogenase (PDH) E1 alpha (PDHA1) with both 2D-PAGE (Figure 8) and 1D-GeLC/MSMS (Figure 9).

PDHA1, with a theoretical molecular weight of 43 kDa and an isoelectric point of 6.78-8.49, converts pyruvate to acetyl-CoA and links glycolysis with the TCA cycle (Figure 7). This reaction plays a crucial role in cellular energy metabolism. The activity of the PDH complex (PDHC) is tightly regulated by phosphorylation. Phosphorylation of one of three serine residues in the E1 subunit (S293, S300, and S232) by PDH kinase (PDK) inactivates PDHC, while dephosphorylation by PDH phosphatase restores its activity.

**Table 3: Pyruvate dehydrogenase E1 $\alpha$  modification sites**  
(De)-phosphorylation of at least one of three specific serine residues, represented in red, regulates the activity of the pyruvate dehydrogenase complex. p, phosphorylation; a, acetylation (phosphosite.org)

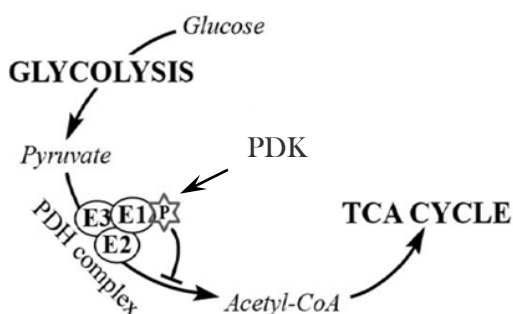


**Figure 7: Pyruvate dehydrogenase complex**  
PDHA1 links glycolysis with the TCA cycle. Its phosphorylation inhibits the conversion from pyruvate to acetyl-CoA. Deng, 2009, modified [1].

PDHA1 Sequence	
Modification	Mouse
K 77-a	TVRRMELkADQLYkQ
K 83-a	LkADQLYkQKIIRGF
Y 227	FICENNRyGMGtsVE
T 231-p	NNRYGMGtsVERAAA
S 232-p	NRYGMGtsVERAAAS
K 244-a	AASTDYYkRGDFIPG
Y 289-p	MELQTYRyHGHsMsD
S 293-p	TYRyHGHsMsDPGVs
S 295-p	RyHGHsMsDPGVsyR
S 300-p	sMsDPGVsyRTREEI
Y 301-p	MsDPGVsyRTREEIQ
S 314-p	IQEVRSKsDPIMLLk
K 321-a	sDPIMLLkDRMVNSN

Due to this multiple phosphorylation sites (Table 3) the 2D-gel shows three distinct spots, which may represent different phosphorylation sites and states, indicated by a slight shift in molecular weight and pH (Figure 8A, B). Phospho-protein abundance was determined by comparing fluorescence stained spot volumes (see 3.3.1.). A calculation revealed for all

PDHA1 spots and replicates a higher abundance in the HH treated sample (Figure 8C). Mean fold changes for PDHA1 Spot 1, 2 and 3 were 1.63, 1.98 and 1.51, respectively.

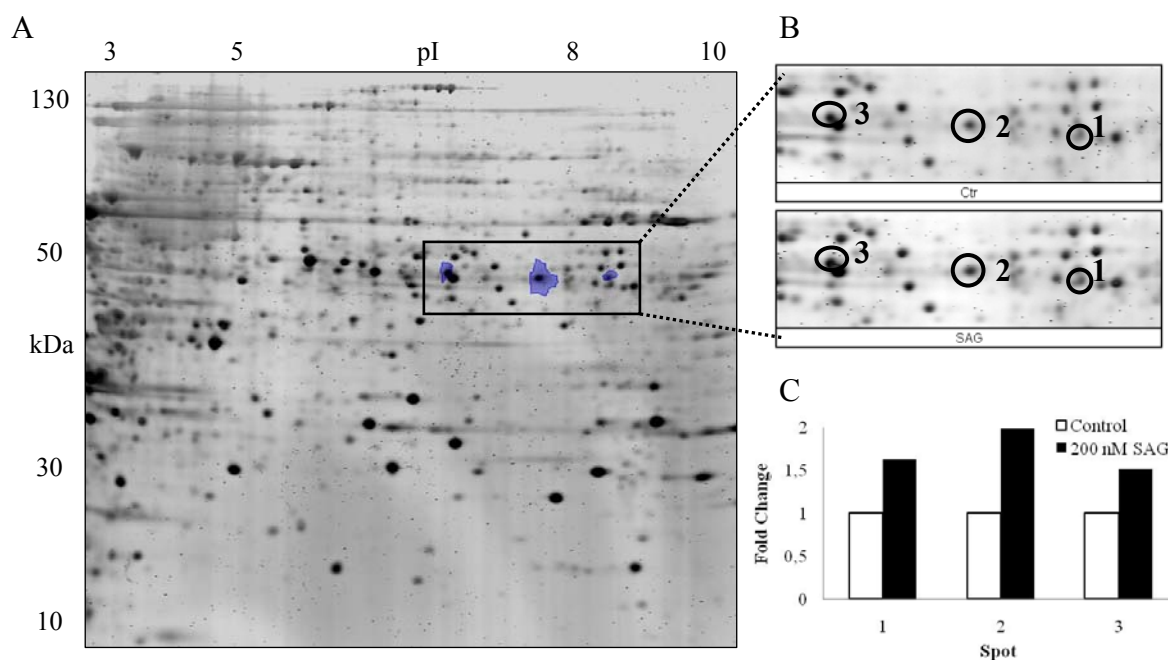


**Figure 8: Phosphorylation of PDHA1 in HH treated samples identified by 2D-PAGE**

(A) 2D-gel of phospho-proteins enriched from adipocytes treated with SAG, a potent HH agonist. (B) Spots of PDHA1 were identified by mass spectrometric analysis of tryptic digests and (C) quantitative phospho-protein abundance was calculated by Progenesis Same Spots.

In line with 2D-PAGE findings, the 1D-GeLC/MSMS approach identified phosphorylated PDHA1 in all replicates. Traditionally used spectral-counting as label-free quantification tool requires high-resolution mass spectrometry, especially for the detection of small changes in protein abundance. Possibly based on this insufficient identification by our MSMS only one replicate showed a significant alteration compared with its control sample (Figure 9A, B). The others displayed no or only a slight increase in SAG treated adipocytes. However protein identification probability was 100%, sequence coverage ranged from 12%-30% and identification of unique peptides ranged from 3-9 (Figure 9C).

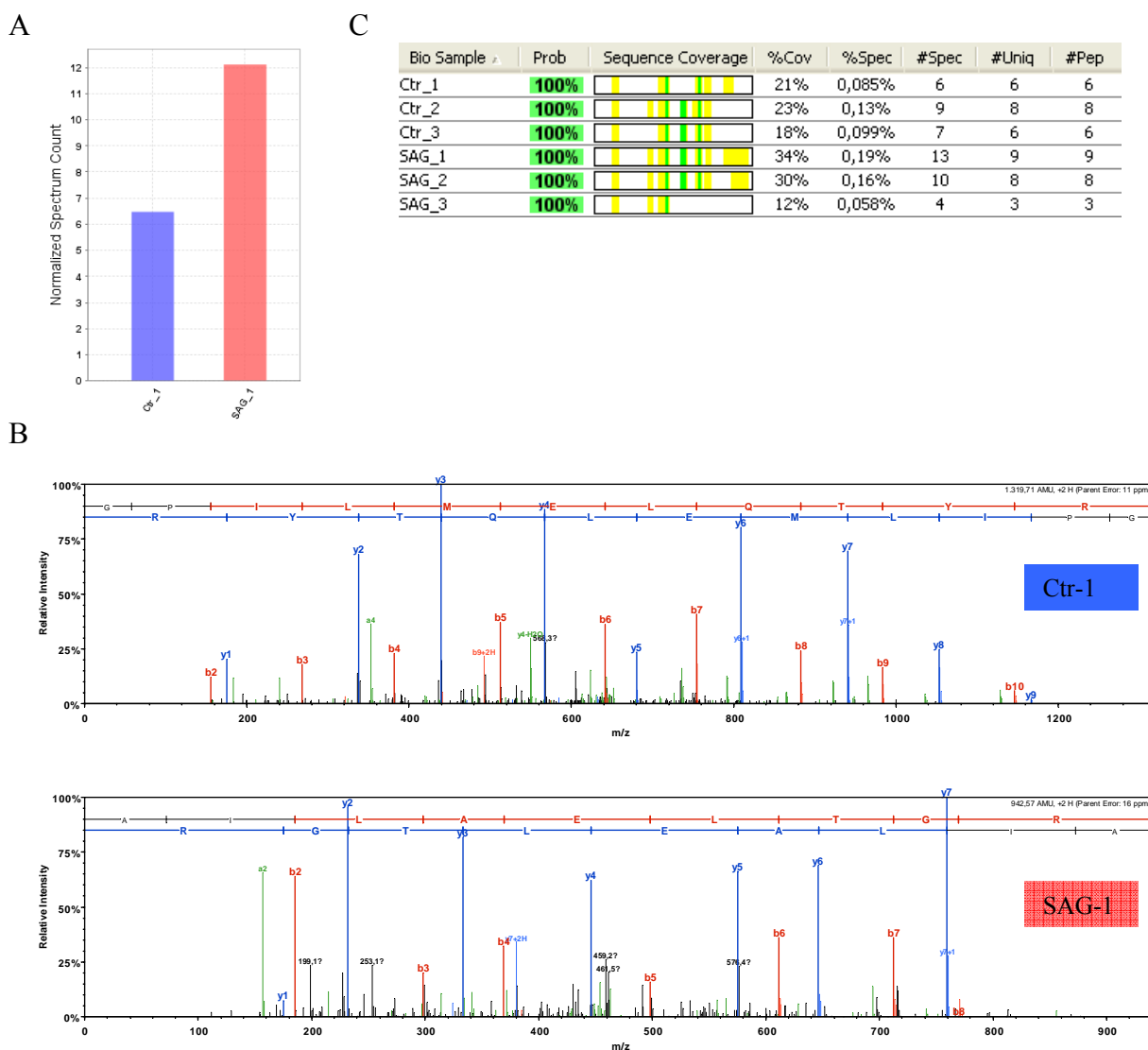


**Figure 9: Phosphorylation of PDHA1 in Hh treated samples identified by 1D-GeLC/MSMS and verified by Scaffold 3**

(A) Comparison of control (Ctr-1) and SAG treated (SAG-1) samples for phosphorylated PDHA1 abundance calculated by spectral-counting; (B) related MS spectra. (C) MS-based information on PDHA1 for all biological samples. Protein identification probability (Prob); Sequence coverage highlighted in yellow, green represents carbamidomethylation of cysteine; percentage of amino acids identified (%Cov); protein percentage of total spectra (%Spec); number of total spectra (#Spec); number of unique peptides spectra (#Uniq) and number of unique peptides (#Pep).

#### **4.1.3. In-depth analysis of the 1D-phospho-proteome identified major changes in adipocyte energy metabolism**

To enable in-depth analysis and easier interpretation of the dataset Pathway Studio and/or Scaffold were used for pathway analysis and categorization of protein functions. Annotated proteins were clustered according to metabolic and signaling pathways and Gene Ontology (GO) terms (Biological process, Cellular component and Molecular function). The statistical significance of over-represented or under-represented proteins in each category is indicated by the p-value ( $p \leq 0.05$ ) (Figure 10-12, 17, 18, 20 and Table 4, 5, 10-13).

Consistent with prior adipocyte-studies [5, 52], we found proteins involved in glucose metabolism, fatty acid oxidation and insulin signaling (Table 4, 5). As a direct proof of concept we identified HH signaling and the notch pathway as significantly present in our samples. Of note, a cross-talk between these two pathways is described in the literature [53, 54].

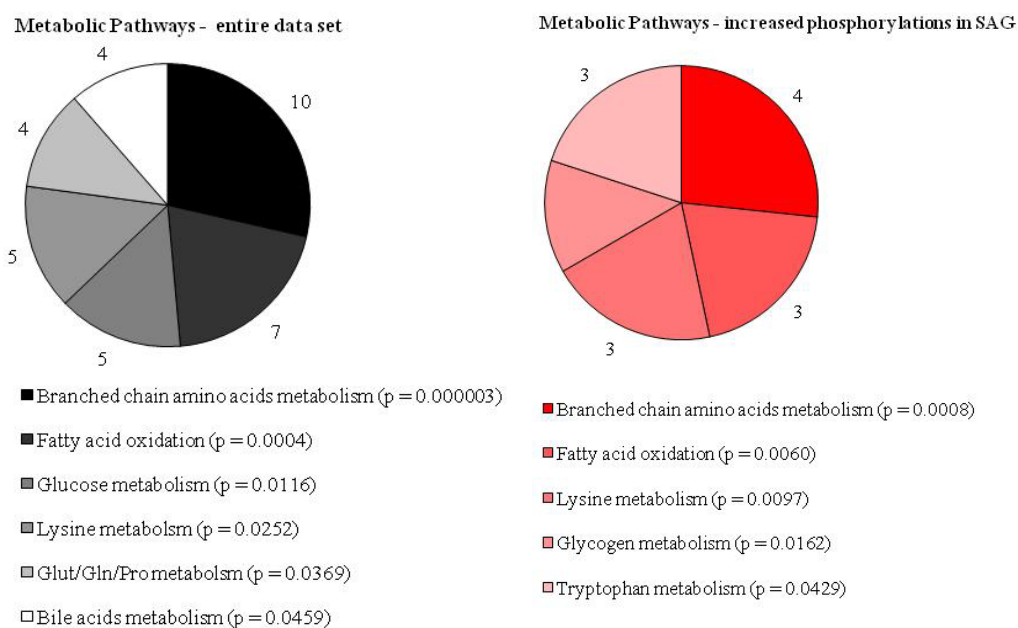
Interestingly, we found a strong impact of HH on cellular energy metabolism. Fatty acid (FA) oxidation ( $p = 0.0060$ ), glycogen metabolism ( $p = 0.0162$ ) and insulin signaling ( $p = 0.0001$ ) were significantly highlighted in the HH treated sample. For instance 3 (ACAT1, HADHA, ECHS1) out of 7 entities in fatty acid oxidation were differentially present in our phospho-proteomic studies.

Table 4 and 5 show all metabolic and signaling pathways significantly present (all p-values  $\leq 0.05$ ) in the phospho-protein enriched dataset. Pie charts illustrate related tables (Figure 10, 11). Phospho-proteins of selected pathways are listed in Table 6.

**Table 4: Metabolic pathway analysis of phospho-protein enriched adipocytes**

Metabolic Pathway - entire dataset	p-value	Entities	Gene Symbol
Branched chain aa metabolism	3.01E-06	10	ACAT1,OXCT1,ACADS,HADHA,ECHS1,HADHB,ACAA2,BCKDHA,BCKDHB,ACADSB
Fatty acid oxidation	0.0004	7	ACAT1,ACADS,HADHA,ECHS1,HADHB,ACAA2,ACADSB
Glucose metabolism	0.0116	5	GAPDH,TPI1,PGAM1,PDHA1,PDHB
Lysine metabolism	0.0252	5	ACAT1,HADHA,ECHS1,HADHB,ACAA2
Glut/Gln/Pro metabolism	0.0369	4	P4HB,EPRS,GLUD1,P4HA1
Bile acids metabolism	0.0459	4	ACAT1,HADHB,ACAA2,ACADSB

Metabolic Pathway - increased phosphorylation in SAG	p-value	Entities	Gene Symbol
Branched aa metabolism	0.0008	4	ACAT1,OXCT1,HADHA,ECHS1
Fatty acid oxidation	0.0060	3	ACAT1,HADHA,ECHS1
Lysine metabolism	0.0097	3	ACAT1,HADHA,ECHS1
Glycogen metabolism	0.0162	2	GYS1,PYGB
Tryptophan metabolism	0.0429	3	ACAT1,HADHA,ECHS1



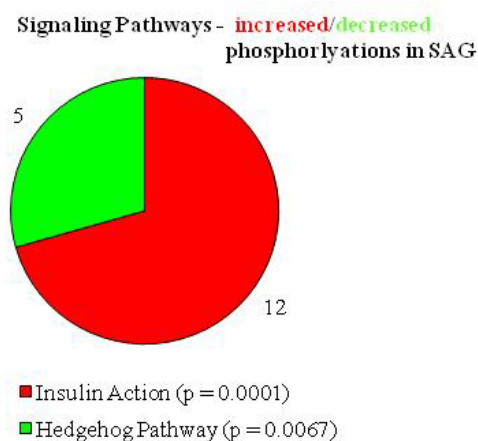
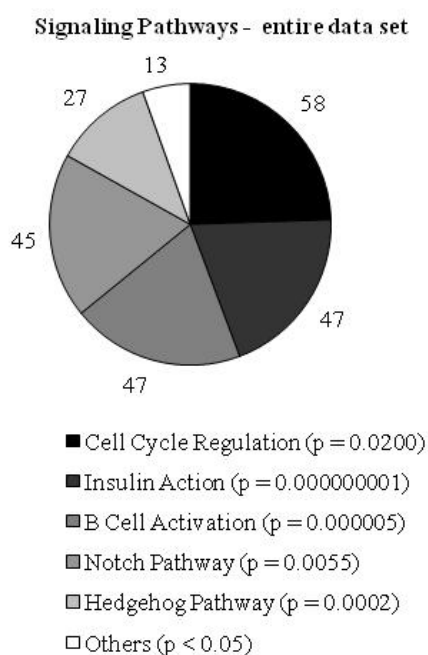
**Figure 10: Pie charts illustrating metabolic pathways of phospho-protein-specific 1D-gels**  
 Grey indicates the whole dataset without consideration of any changes. Red represents pathways with increased phosphorylation events in SAG treated adipocytes.

**Table 5: Signaling pathway analysis of phospho-protein enriched adipocytes**

Signaling Pathway - entire dataset	p-value	Entities	Gene Symbol
Cell Cycle Regulation	0.0200	58	TUBB2C,NUDT21,TUBB6,RPS6,EIF2S1,RPL22,LMNA,CBX3,NPM1, SNRPD1, TUBA1B,HNRNPKN,NCL,RANBP1,PRKACA,SFRS1,HMGB3,EEF2,HMGA2, NAP1L1,EIF4G1,PRKAR2B,PRKAR1A,MAGOH,ANP32A,RPL5,DDB1,PLCB1, HNRNPC,NUDC,DCTN1,CBX1,SKP1,EPRS,IPO7,RPS27A,ABCF1,IPO9,EIF3A, EIF3J,EEF1B2,PURA,RPLP2,EIF1AY,EEF1D,SFRS7,BTF3,NAP1L4,SUPT5H, EIF4G3,EEF1G,EIF2S2,TUBB2A,RPLP0,TUFM,RPLP1,TUBA1A,EIF3I, IDH3G,RPS6,EIF2S1,GAPDH,RPL22,LIPE,ACAT1,FABP4,HSPA8,PRKACA, IDH3A,ACACA,TPI1,EEF2,EIF4G1,ACLY,PRKAR2B,PRKAR1A,RPL5,GYS1, TALDO1,EPRS,RPS27A,ABCF1,ACADS,EIF3A,EIF3J,HADHA,EEF1B2,RPLP2, EIF1AY,EEF1D,PGAM1,SLC25A10,EIF4G3,EEF1G,EIF2S2,ECHS1,HADHB, RPLP0,TUFM,ACAA2,RPLP1,PDHA1,PDHB,ACADSB,EIF3I
Insulin Action	1.17E-09	47	MYH10,HSP90B1,HSP90AA1,RPS6,EIF2S1,HSPD1,RPL22,MSN,HSPA5,CFL1, HSPA8,CANX,HSPA9,MYH9,P4HB,EEF2,PDIA6,EIF4G1,HYOU1,TPM1, EIF3I CALM1,RPL5,DNAJA2,PLCB1,ST13,MYL6,DCLK1,CCT6A,SNAPIN,EPRS, RPS27A,CNN3,ABCF1,HSPA4,EIF3A,EIF3J,EEF1B2,RPLP2,EIF1AY,EEF1D, EIF4G3,EEF1G,EIF2S2,RPLP0,TUFM,RPLP1,
B Cell Activation	4.66E-06	47	PSMD11,TUBB2C,PTGES3,TUBB6,MYH10,GAPDH,LIPE,LMNA,MSN,ACAT1, UBA1,FABP4,CFL1,CBX3,TUBA1B,PPP1CA,TPI1,MYH9,HMGB3,HMGA2, NAP1L1,TPM1,NEDD4,PSMC2,CAND1,ANP32A,PSME1,UBE2H,NUDC,CBX1, CNN3,PSMC5,PSMD14,HADHA,PSMC6,NAP1L4,PGAM1,PSMC3,PSMC1,PSME2, TUBB2A,PSMC4,PDHA1,PDHB,TUBA1A
Notch Pathway	0.0055	45	PSMD11,PTGES3,UBA1,CBX3,PRKACA,HMGB3,HMGA2,NAP1L1,PRKAR2B, NEDD4,PSMC2,CAND1,PRKAR1A,ANP32A,PSME1,DDB1,UBE2H,CBX1, PSMC5,PSMD14,PURA,PSMC6,NAP1L4,PSMC3,PSMC1,PSME2,PSMC4
Hedgehog Pathway	0.0002	27	PRKACA,PRKAR2B,PRKAR1A,PLCB1
Others		4	

Signaling Pathway - increased phosphorylation in SAG	p-value	Entities	Gene Symbol
Insulin Action	0.0001	12	RPS6,EIF2S1,GAPDH,ACAT1,HSPA8,EEF2, ACLY,GYS1,HADHA,EIF1AY,ECHS1,HADHB

Signaling Pathway - decreased phosphorylation in SAG	p-value	Entities	Gene Symbol
Hedgehog	0.0067	5	HMGB3,NEDD4,UBE2H,PSME2,PSMC4

**Figure 11: Pie charts illustrating signaling pathways of phospho-protein-specific 1D-gels**

Grey indicates the whole dataset without consideration of any changes. Red represents pathways with increased and green with decreased phosphorylation events in SAG treated adipocytes.



**Table 6: Phospho-protein list of selected pathways**

<b>Fatty acid oxidation</b>				
<b>Swissprot</b>	<b>Protein Name</b>	<b>Gene symbol</b>	<b>1D-Gel</b>	<b>2D-Gel</b>
Q8BWT1	3-ketoacyl-CoA thiolase, mitochondrial	ACAA2	=	nd
Q07417	Short-chain specific acyl-CoA dehydrogenase	ACADS	=	+
Q9DBL1	Short/branched chain specific acyl-CoA dehydrogenase,	ACADSB	=	nd
Q8QZT1	Acetyl-CoA acetyltransferase	ACAT1	+	+
Q8BMS1	Trifunctional enzyme subunit alpha	HADHA	+	nd
Q99JY0	Trifunctional enzyme subunit beta	HADHB	+	+
Q8BH95	Enoyl-CoA hydratase	ECHS1	+	+
<b>Glucose metabolism</b>				
<b>Swissprot</b>	<b>Protein Name</b>	<b>Gene symbol</b>	<b>1D-Gel</b>	<b>2D-Gel</b>
P16858	Glyceraldehyde-3-phosphate dehydrogenase	GAPDH	+	+
P35486	Pyruvate dehydrogenase E1 component subunit alpha	PDHA1	=	+
Q9D051	Pyruvate dehydrogenase E1 component subunit beta	PDHB	=	nd
Q9DBJ1	Phosphoglycerate mutase 1	PGAM1	=	+
P17751	Triosephosphate isomerase	TPI1	=	nd
<b>Glycogen metabolism</b>				
<b>Swissprot</b>	<b>Protein Name</b>	<b>Gene symbol</b>	<b>1D-Gel</b>	<b>2D-Gel</b>
P54859	Glycogen [starch] synthase	GYS1	+	nd
Q8CI94	Glycogen phosphorylase	PYGB	+	nd
<b>Insulin Signaling</b>				
<b>Swissprot</b>	<b>Protein Name</b>	<b>Gene symbol</b>	<b>1D-Gel</b>	<b>2D-Gel</b>
Q6P542	ATP-binding cassette sub-family F member 1	ABCF1	=	nd
Q8BWT1	3-ketoacyl-CoA thiolase	ACAA2	=	nd
Q5SWU9	Acetyl-CoA carboxylase 1	ACACA	=	nd
Q07417	Short-chain specific acyl-CoA dehydrogenase	ACADS	=	nd
Q9DBL1	Short/branched chain specific acyl-CoA dehydrogenase	ACADSB	=	nd
Q8QZT1	Acetyl-CoA acetyltransferase	ACAT1	+	+
Q91V92	ATP-citrate synthase	ACLY	+	nd
Q8BH95	Enoyl-CoA hydratase	ECHS1	+	+
O70251	Elongation factor 1-beta	EEF1B2	=	nd
P57776	Elongation factor 1-delta	EEF1D	=	nd
Q9D8N0	Elongation factor 1-gamma	EEF1G	=	+
P58252	Elongation factor 2	EEF2	+	nd
Q8BH64	EH domain-containing protein 2	EIF1AY	+	nd
Q8BMJ3	Eukaryotic translation initiation factor 1A	EIF2S1	+	nd
Q6ZWX6	Eukaryotic translation initiation factor 2 subunit 1	EIF2S2	=	nd
Q99L45	Eukaryotic translation initiation factor 2 subunit 2	EIF3A	=	nd
Q9QZD9	Eukaryotic translation initiation factor 3 subunit I	EIF3I	=	nd
Q66JS6	Eukaryotic translation initiation factor 3 subunit J	EIF3J	=	nd
Q6NZJ6	Eukaryotic translation initiation factor 4 gamma 1	EIF4G1	=	nd
Q80XI3	Eukaryotic translation initiation factor 4 gamma 3	EIF4G3	=	nd
Q8CGC7	Bifunctional aminoacyl-tRNA synthetase	EPRS	=	nd
P04117	Fatty acid-binding protein	FABP4	=	nd
P16858	Glyceraldehyde-3-phosphate dehydrogenase	GAPDH	+	+
P54859	Glycogen [starch] synthase	GYS1	+	nd

Q8BMS1	Trifunctional enzyme subunit alpha	HADHA	+	nd
Q99JY0	Trifunctional enzyme subunit beta	HADHB	+	+
P63017	Heat shock cognate 71 kDa protein	HSPA8	+	nd
Q9D6R2	Isocitrate dehydrogenase [NAD] subunit alpha	IDH3A	=	nd
P70404	Isocitrate dehydrogenase [NAD] subunit gamma	IDH3G	=	nd
P54310	Hormone-sensitive lipase	LIPE	=	+
P35486	Pyruvate dehydrogenase E1 component subunit alpha	PDHA1	=	+
Q9D051	Pyruvate dehydrogenase E1 component subunit beta	PDHB	=	nd
Q9DBJ1	Phosphoglycerate mutase 1	PGAM1	=	+
P05132	cAMP-dependent protein kinase catalytic subunit	PRKACA	=	nd
Q9DBC7	cAMP-dependent protein kinase type I-alpha regulatory	PRKAR1A	=	nd
P31324	cAMP-dependent protein kinase type II-beta regulatory	PRKAR2B	=	nd
P67984	60S ribosomal protein L22	RPL22	=	nd
P14869	60S acidic ribosomal protein P0	RPLP0	=	nd
P47955	60S acidic ribosomal protein P1	RPLP1	=	nd
P99027	60S acidic ribosomal protein P2	RPLP2	+	nd
P62754	40S ribosomal protein S6	RPS6	=	nd
P62991	Ubiquitin	RPS27A	=	nd
Q9QZD8	Mitochondrial dicarboxylate carrier	SLC25A10	=	nd
Q93092	Transaldolase	TALDO1	=	+
P17751	Triosephosphate isomerase	TPI1	=	nd
Q8BFR5	Elongation factor Tu	TUFM	=	nd

=...no regulation; + phosphorylation up; nd...not detected

Benchmarking our results with the annotation of “Biological process” by Scaffold 3 ranked cellular process (184) and metabolic process (142) as top hits (Figure 12A). More in detail 9 (GAPDH, ACAT1, ACLY, OXCT1, PNPLA2, HADHA, ECHS1, HADHB, BCKDHA) out of 26 proteins defined as metabolic process were significantly enriched in the HH treated sample (Figure 12D). Lipid metabolic process (6 out of 16; ACLY, PNPLA2, HADHA, ECHS1, HADHB, ATP5B), and especially FA oxidation (3 out of 5; HADHA, ECHS1, HADHB) showed highly abundance too.

Categorical analysis based on “Cellular component” showed that majority of the proteins we identified were resident in intracellular organelles (182) and/or organelle parts (102) and in the cytoplasm (163) (Figure 12B). Of note mitochondria and its subcategories were significantly enriched in the HH treated sample (Figure 12E), indicating an impact of HH on mitochondrial function via phosphorylation changes. In line with the highly present component protein complex (10 [TUBB6, YWHAB, PSMA7, PSMD2, PSMC5, PSMD14, PSMB4, PSMC6, PSMC1, PSMB6] out of 38), the second greatest hit of “Molecular function”, binding (178) was significantly enriched too (Figure 12C).

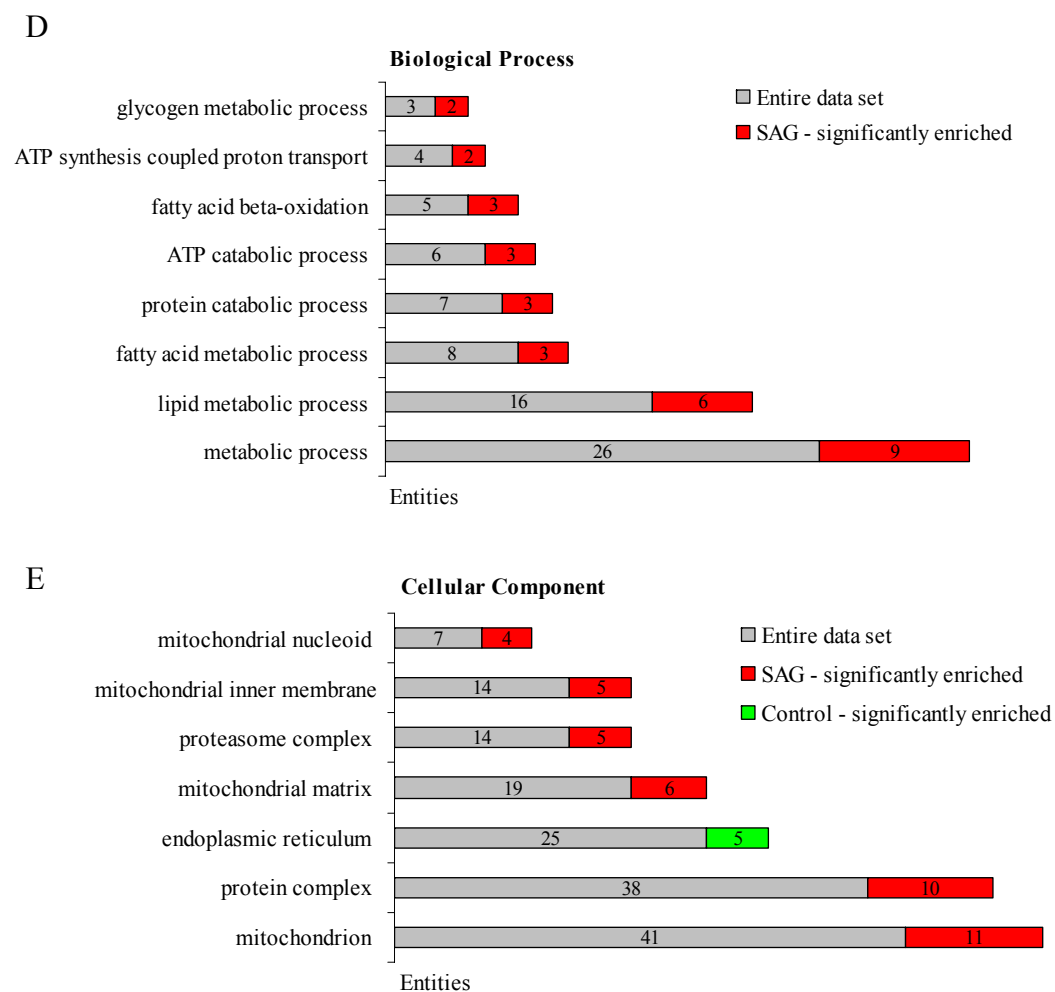
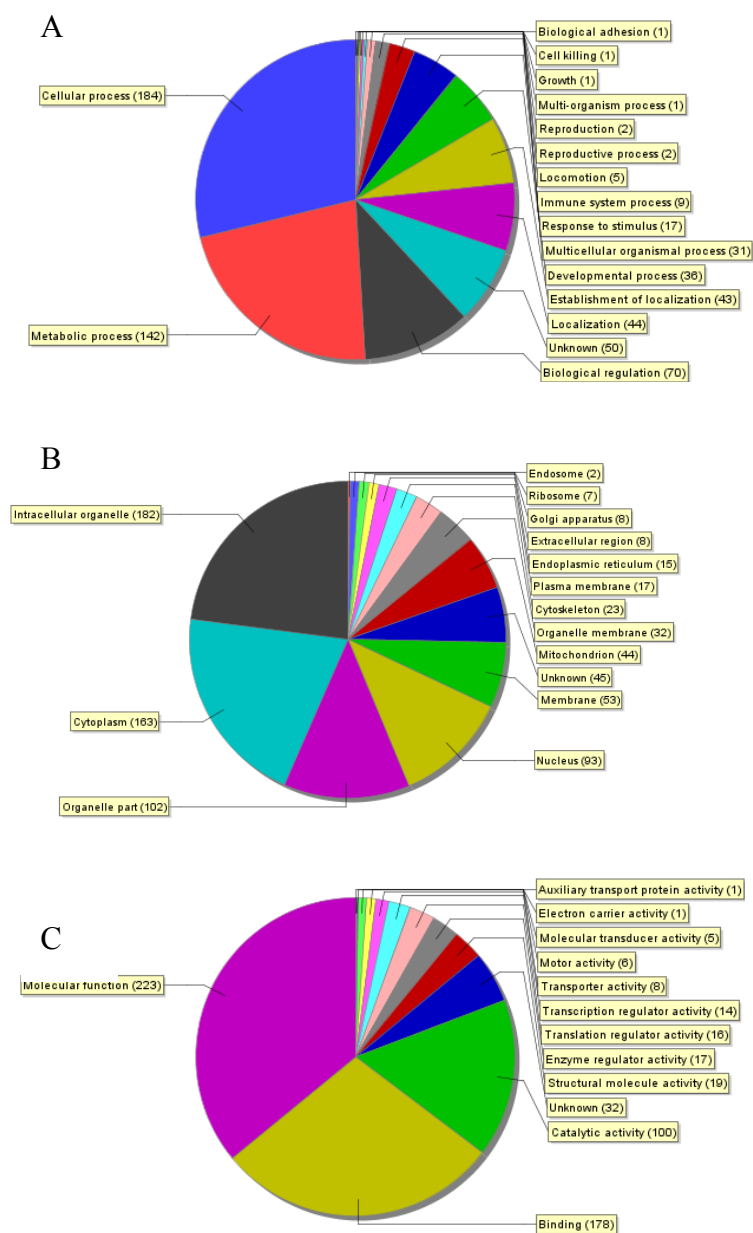


**Figure 12: Pie charts and bar charts illustrating GO terms of phospho-proteomics** (A) (D) Biological process; (B) (E) Cellular component; (C) Molecular function Grey indicates the whole dataset without consideration of any changes. Red represents Go terms significantly highlighted in SAG treated adipocytes and green in the Control sample (Ctr).

## 4.2. Quantitative proteomics of HH signaling in mature adipocytes

To gain information on lasting changes in protein expression we performed proteomics using the workflow illustrated in Figure 13. Differentiated 3T3-L1 cells were stimulated with SAG for 48 hours. The cytoplasmic fraction was purified by pushing cells through a needle and intact nuclei and insoluble material were removed by centrifugation. Metabolic labeling was performed to gain information on the cellular sites of synthetic processes by 2D-PAGE. Peptides were separated by nanoflow LC and identified by MSMS fragmentation analysis. The MSMS data were interpreted by Mascot and searched against the IPI db (International Protein Index database). Mass data were further processed with the Scaffold software tool to validate MSMS based peptide and protein identifications. Finally, the protein list was interpreted by Pathway Studio.

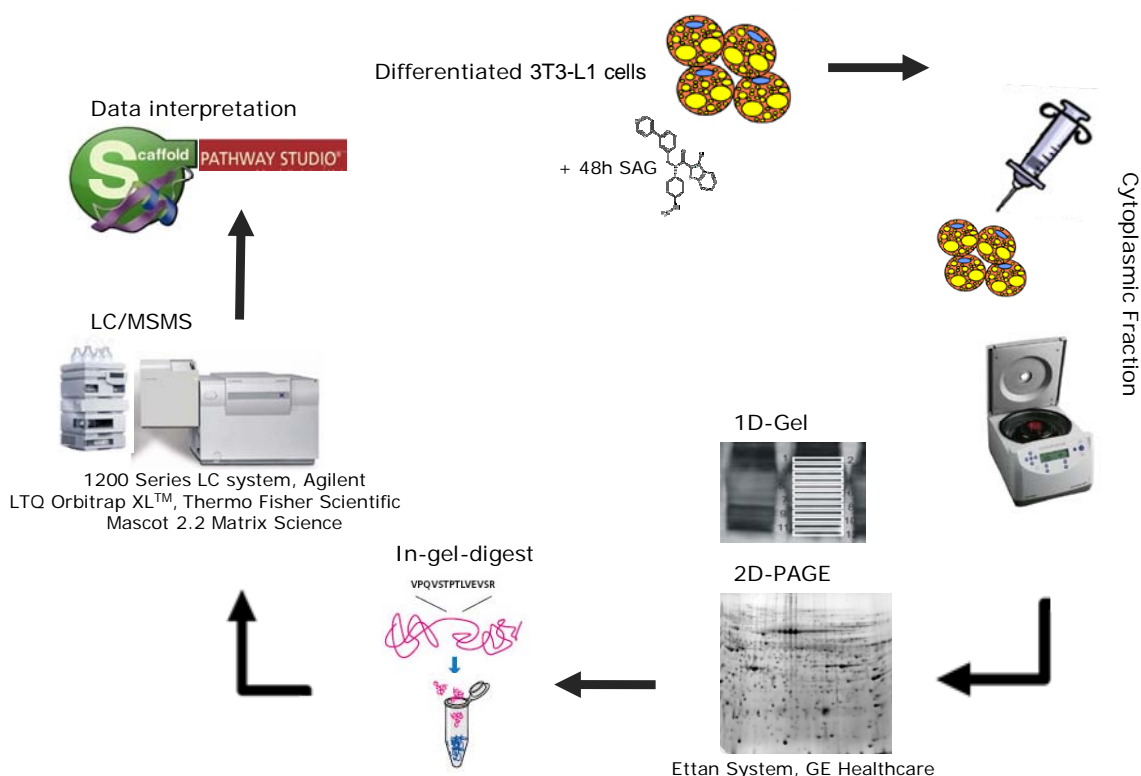


**Figure 13: Schematic workflow of expression proteomics**

Mature adipocytes were stimulated with SAG, a potent Hh agonist and 1D- and 2D-gels were performed with the cytoplasmic fraction. Spots of interest and bands were in-gel digested, analyzed by LC/MSMS and interpreted by Scaffold and Pathway Studio.

#### 4.2.1. Depth and coverage of the 3T3-L1 adipocyte proteome

Cytoplasmic fractions of adipocytes with and without HH activation were analyzed by 2D-PAGE and subsequent LC/MSMS analysis of isolated spots, as well as with 1D-GeLC/MSMS.

In four independent experiments of 2D-PAGE we detected in total 1146 spots (Figure 14). 50 proteins of interest were subjected to identification by MSMS. With a use of a 1.5 fold change as a cutoff to designate up- or down-regulated proteins, 23 proteins of them were up- and 7 down regulated in the HH treated sample d. Additional 5 increased proteins were identified only in the autoradiography image (Table 7).

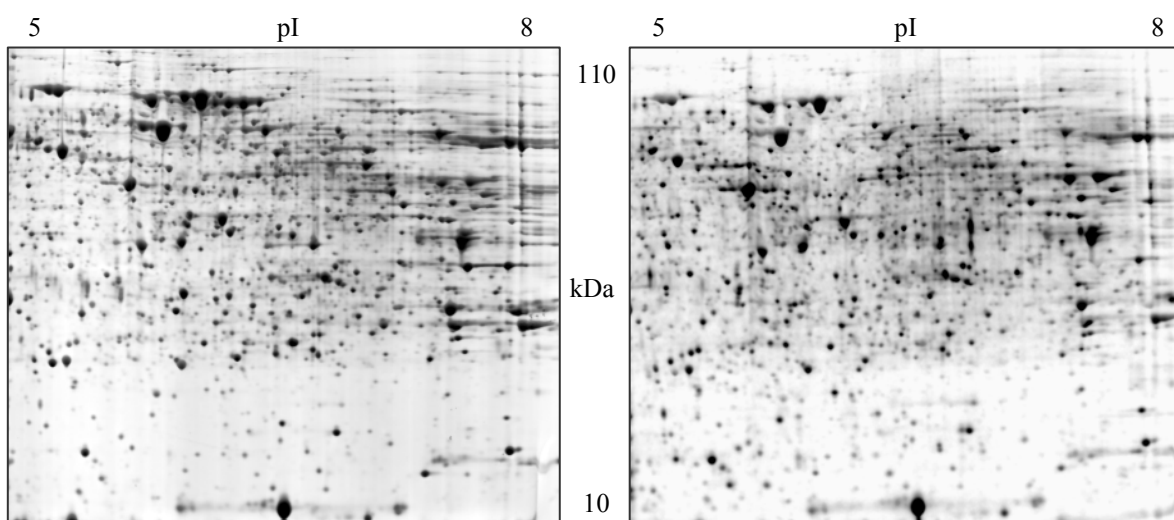


**Figure 14: 2D-gel of adipocytes**

Representative example of a fluorescence stain (left) and autoradiography (right) of cytoplasmic proteins of differentiated 3T3-L1 cells treated with SAG for 48 hours. 400  $\mu$ g were diluted in 7 M urea, 2 M thiourea, 2% CHAPS and 100 mM DTT and absorbed into 24 cm IPG strips pH 5-8.

For instance, both aconitate hydratase and FA synthase showed an up-regulation in the autoradiography, indicating a higher rate of synthesis of those proteins, but no alteration in the expression profile. Interestingly, several differentially expressed proteins are involved in the TCA cycle and oxidative phosphorylation (OXPHOS) further supporting a role of HH in cellular energy metabolism (Table 7).

Table 7: Proteins identified by 2D-PAGE

SwissProt	Proteinname	Gene Symbol		Fluorescence Stain		Autoradiography
Q99KI0	Aconitate hydratase	Aco2	=	1,16	+	1,88
Q9CR86	Calcium-regulated heat stable protein 1	Carhsp1	+	1,88	+	1,88
P18760	Cofilin-1	Cfl1	=	1,15	=	1,27
P45591	Cofilin-2	Cfl2	+	1,46	=	1,24
Q8VBV7	COP9 signalosome complex subunit 8	Cops8	+	3,32	+	1,51
Q61753	D-3-phosphoglycerate dehydrogenase	Phgdh	=	1,21	=	1,15
Q9R0P5	Destrin	Dstn	=	1,41	=	1,20
P57776	Elongation factor 1-delta	Eef1d	+	4,53	+	2,05
P34914	Epoxide hydrolase 2	Ephx2	=	0,92	=	1,03
Q3U0V1	Far upstream element-binding protein 2	Khsrp	-	0,64	+	1,70
P19096	Fatty acid synthase	Fasn	=	1,26	+	2,13
Q05816	Fatty acid-binding protein	Fabp5	+	1,52	+	1,57
Q9CQI3	Glia maturation factor beta	Gmfb	=	1,28	=	1,16
Q9CZD3	Glycyl-tRNA synthetase	Gars	=	0,94	+	1,82
Q61316	Heat shock 70 kDa protein 4	Hspa4	-	0,67	+	1,53
P63017	Heat shock cognate 71 kDa protein	Hspa8	+	2,49	=	1,20
Q9CQN1	Heat shock protein 75 kDa	Trap1	=	0,76	=	1,38
P61979	Heterogeneous nuclear ribonucleoprotein K	Hnrnpk	=	0,89	=	1,01
Q61025	Intraflagellar transport protein 20 homolog	Ift20	=	1,31	=	0,74
Q8CAQ8	Mitochondrial inner membrane protein	Immt	-	0,49	+	1,47
Q91VD9	NADH-ubiquinone oxidoreductase 75 kDa subunit	Ndufs1	-	0,59	=	0,89
Q9EQ80	NIF3-like protein 1	Nif3l1	-	0,65	=	1,00
P15532	Nucleoside diphosphate kinase A	Nme1	+	1,84	=	1,17
Q01768	Nucleoside diphosphate kinase B	Nme2	+	16,39	+	8,29
Q9CQ48	NudC domain-containing protein 2	Nudcd2	+	2,09	=	1,25
Q60597	Ogdh2-oxoglutarate dehydrogenase	Ogdh	+	1,61	+	2,10
Q8R2Y8	Peptidyl-tRNA hydrolase	Pthr2	+	3,56	+	1,64
Q9D0F9	Phosphoglucomutase-1	Pgm1	=	1,21	=	1,15
Q9WU28	Prefoldin subunit 5	Pfdn5	=	1,33	=	1,20
Q9R0E1	Procollagen-lysine,2-oxoglutarate 5-dioxygenase 3	Plod3	-	0,54	+	2,14
P56812	Programmed cell death protein 5	Pdcd5	+	2,23	=	1,17
Q9JKV1	Proteasomal ubiquitin receptor ADRM1	Adrm1	+	1,62	=	1,25
Q9CQT5	Proteasome maturation protein	Pomp	+	2,03	=	0,95
Q9QXT0	Protein canopy homolog 2	Cnpy2	+	3,43	+	2,58
P27773	Protein disulfide-isomerase A3	Pdia3	=	1,13	+	1,57
Q8K3C3	Protein LZIC	Lzic	=	1,25	=	1,00
Q05920	Pyruvate carboxylase	Pc	=	0,82	=	1,11
Q9Z1Z2	Serine-threonine kinase receptor-associated protein	Strap	+	1,71	=	1,19
P38647	Stress-70 protein	Hspa9	-	0,46	+	1,77

Q9Z2I8	Succinyl-CoA ligase [GDP-forming] subunit beta	Suclg2	+	2,49	=	1,20
P08228	Superoxide dismutase [Cu-Zn]	Sod1	+	1,76	=	1,36
P09671	Superoxide dismutase [Mn]	Sod2	+	3,56	+	1,64
P11983	T-complex protein 1 subunit alpha	Tcp1	=	0,95	=	1,12
Q91Z38	Tetratricopeptide repeat protein 1	Ttc1	=	1,06	+	1,55
Q9CQU0	Thioredoxin domain-containing protein 12	Txndc12	=	1,21	=	1,16
Q01853	Transitional endoplasmic reticulum ATPase	Vcp	=	1,25	=	1,37
Q9Z255	Ubiquitin-conjugating enzyme E2 A	Ube2a	+	1,63	+	2,37
P20152	Vimentin	Vim	+	2,92	=	1,24
Q64727	Vinculin	Vcl	+	1,85	+	1,94
Q9ERF3	WD repeat-containing protein 61	Wdr61	+	2,39	=	1,33

=...no regulation; +...  $\geq 1.5$ -fold up-regulated; -...  $\leq 1.5$ -fold down-regulated

1D-GeLC/MSMS experiments were done in duplicate and a total of 148057 spectra met our criteria for peptide validation (see 3.3.2.). More than 10000 unique peptides (FDR = 1.6%) corresponding to 2613 distinct proteins (FDR = 0.0%) were confidently identified. Quantitative evaluation of protein abundance using the number of MSMS spectra yielded 317 differentially expressed proteins. 202 proteins were 1.5 fold up-regulated and 115 were 1.5 fold down-regulated in the HH treated sample (Figure 15A, Table 8, 9). Comparative analysis revealed 45 proteins identified in both 1D- and 2D-gels, whereas 2568 proteins were only identified by 1D-GeLC/MSMS analysis and 5 proteins by 2D-PAGE (Figure 15B). Comparative analysis with the phospho-proteome discovered 236 proteins identified by both techniques. Interestingly, 11 out of 19 proteins identified only by the phospho-proteome approach belong to the nucleus (Figure 15C).

Many proteins we identified are consistent with prior 3T3-L1-studies. We compared our proteome dataset against the largest sets for 3T3-L1 adipocytes and human adipocytes to date, published by Adachi and Xie, respectively (Figure 15D) [2, 5]. The group of Matthias Mann, provided an in-depth analysis of the 3T3-L1 adipocyte proteome based on subcellular fractionation of nuclei, mitochondria, membrane and cytosol and identified a total of 3287 proteins [5]. Our cytoplasmic fraction, containing mitochondria and membranes, but no nuclear proteins, showed an overlap of 1622 proteins, corresponding to 62%. 1665 proteins were only identified by Mann's group, 30% of them belonging to the nucleus. Interestingly, our approach focused on cytoplasmic proteins identified 991 proteins specific for our dataset.

Comparative analysis with the human adipocytes proteome [2] revealed 1094 shared proteins. Hence our proteome of a murine adipocyte cell line showed an overlap of 73%

with a human adipocyte proteome, reflecting both the high homology of the approaches and the low differences in protein abundance in human and murine adipocytes.

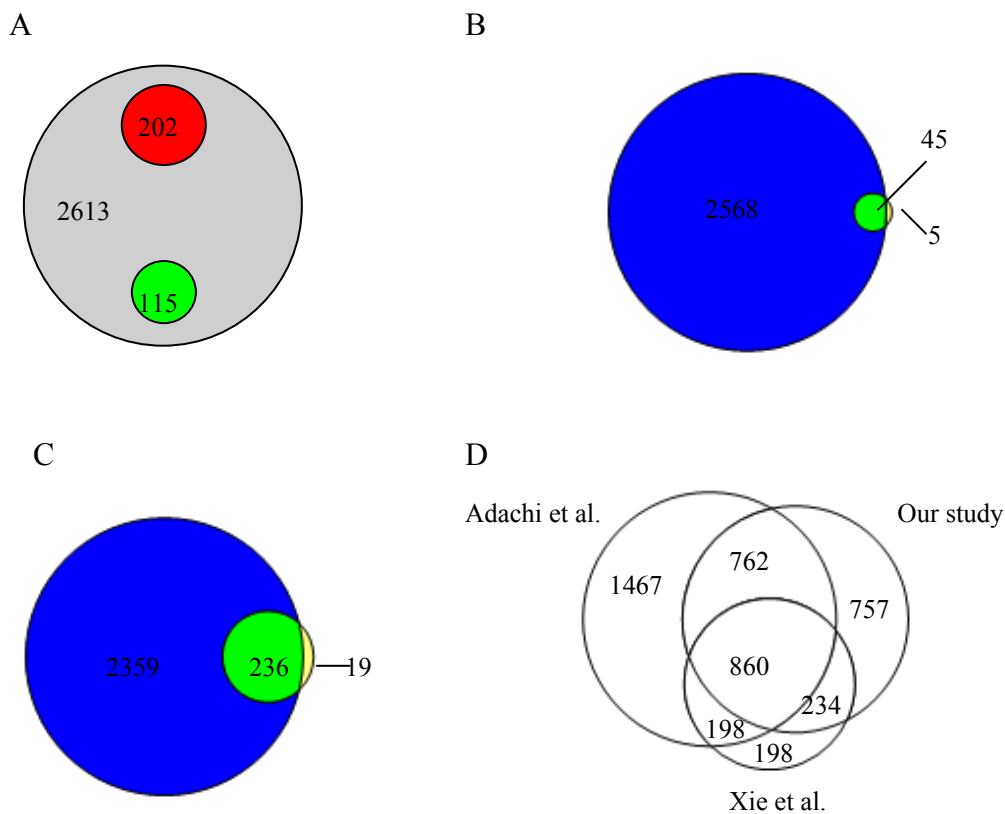


**Figure 15: Quantitative Venn diagrams visualize the outcome of the cytoplasmic-proteome approach**

(A) Venn diagram illustrating 2613 identified proteins by 1D-GeLC/MSMS, 202 up- and 115 down regulated proteins. (B) Comparative analysis revealed 45 proteins identified in both 1D- and 2D-gels, 2568 proteins were only identified by 1D-GeLC/MSMS analysis and 5 proteins by 2D-PAGE. (C) Comparative analysis with the phospho-proteome discovered 236 shared proteins, 19 proteins identified only by phospho-proteome and 2359 by cytoplasmic expression-proteome. (D) Comparative analysis against the human adipose tissue (Xie et al.) [2] and the whole 3T3-L1 cell proteome (Adachi et al.) [5].



**Table 8: Proteins up-regulated by the 1D-GeLC/MSMS approach**

IPI AccNr	Up-regulated proteins (202)	Gene Symbol	Fold-change		
			M	R1	R2
IPI00225796	Isoform 1 of UPF0554 protein C2orf43 homolog	-	2,22	2,00	2,50
IPI00136293	Transmembrane protein C9orf46 homolog	-	2,86	2,00	5,00
IPI00221782	Uncharacterized protein C18orf19 homolog	-	2,86	3,33	2,50
IPI00133737	Uncharacterized protein C19orf60 homolog	-	2,86	2,00	5,00
IPI00109632	Uncharacterized protein C7orf30 homolog	-	2,00	2,00	2,00
IPI00169840	ATP-binding cassette sub-family F member 3	ABCF3	4,00	5,00	3,33
IPI00129907	Golgi resident protein GCP60	ACBD3	4,00	3,33	5,00
IPI00930756	Peroxisomal acyl-coenzyme A oxidase 2	ACOX2	2,50	3,33	2,00
IPI00134135	Isoform 1 of Low molecular weight phosphotyrosine protein phosphatase	ACPI	1,82	2,00	1,67
IPI00409019	Acyl-CoA synthetase short-chain family member 2	ACSS2	2,00	2,00	1,67
IPI00170357	AFG3-like protein 2	AFG3L2	2,50	1,67	5,00
IPI00131231	N(4)-(beta-N-acetylglucosaminy)-L-asparaginase	AGA	2,22	2,50	2,00
IPI00662244	Amylo-1,6-glucosidase, 4-alpha-glucanotransferase	AGL	2,86	2,50	3,33
IPI00129350	Isoform Long of Delta-1-pyrroline-5-carboxylate synthase	ALDH18A1	2,00	2,00	2,00
IPI00118794	Isoform 3 of Ankyrin repeat domain-containing protein 17	ANKRD17	2,22	3,33	1,67
IPI00346041	Isoform 2 of Ankyrin repeat and SAM domain-containing protein 1A	ANKS1	3,33	3,33	3,33
IPI00346965	AP-1 complex subunit beta-1	AP1B1	1,82	1,67	2,00
IPI00119689	Isoform 1 of AP-2 complex subunit beta	AP2B1	2,00	1,67	2,50
IPI00224152	DNA-(apurinic or apyrimidinic site) lyase	APEX1	2,50	2,50	2,50
IPI00221615	ADP-ribosylation factor 5	ARF5	1,82	1,67	2,00
IPI00626688	Isoform 3 of Rho guanine nucleotide exchange factor 40	ARHGEF40	2,22	2,00	2,50
IPI00278498	ADP-ribosylation factor-like protein 1	ARL1	2,50	3,33	2,00
IPI00315504	ADP-ribosylation factor-like protein 2	ARL2	2,00	2,50	1,67
IPI00133218	ADP-ribosylation factor-like protein 8B	ARL8B	2,22	1,67	3,33
IPI00223420	Isoform 1 of Acid trehalase-like protein 1	ATHL1	3,33	3,33	3,33
IPI00130186	V-type proton ATPase subunit C 1	ATP6V1C1	2,50	1,67	5,00
IPI00458001	Isoform 2 of Ataxin-2-like protein	ATXN2L	2,00	2,00	1,67
IPI00409462	Spliceosome RNA helicase Bat1	BAT1A	3,33	2,50	5,00
IPI00130381	Large proline-rich protein BAT3	BAT3	1,67	1,67	1,67
IPI00677454	Chromobox homolog 3	C7	2,50	2,50	2,50
IPI00122450	Caldesmon 1	CALD1	2,22	2,50	2,00
IPI00626909	Calpain-1 catalytic subunit	CAPN1	3,33	2,50	5,00
IPI00229487	Isoform 2 of Core-binding factor subunit beta	CBFB	2,86	2,00	5,00
IPI00129466	Chromobox protein homolog 1	CBX1	2,22	2,50	2,00
IPI00331111	Kynurenine--oxoglutarate transaminase 1	CCBL1	2,00	2,00	2,00
IPI00153794	Coiled-coil domain-containing protein 58	CCDC58	2,22	2,50	2,00
IPI00224728	Putative uncharacterized protein	CD63	2,00	2,00	2,00
IPI00124389	Mitochondrial intermembrane space import and assembly protein 40	CHCHD4	1,82	2,00	1,67
IPI00117187	Charged multivesicular body protein 1b-1	CHMP1B	2,00	2,00	2,00
IPI00132350	CDGSH iron-sulfur domain-containing protein 2	CISD2	2,22	2,00	2,50
IPI00468223	COMM domain-containing protein 7	COMM7	2,50	3,33	2,00
IPI00112414	Exportin-2	CSE1L	1,82	1,67	2,00
IPI00123891	Cysteine and glycine-rich protein 1	CSRP1	2,22	2,00	2,50

IPI00338904	Isoform 1 of RNA polymerase II subunit A C-terminal domain phosphatase	CTDP1	2,22	2,00	2,50
IPI00316623	Isoform 3 of Catenin delta-1	CTNND1	2,50	2,00	3,33
IPI00329839	Isoform 1 of ATP-dependent RNA helicase DDX42	DDX42	2,00	2,00	2,00
IPI00221571	Dehydrogenase/reductase SDR family member 9	DHRS9	2,86	5,00	2,00
IPI00605842	Diablo homolog, mitochondrial precursor	DIABLO	2,22	2,50	2,00
IPI00272104	Diap1 protein	DIAP1	3,33	2,50	5,00
IPI00133713	Isoform 1 of D-tyrosyl-tRNA(Tyr) deacylase 1	DTD1	2,22	2,00	2,50
IPI00187434	Deoxyuridine triphosphatase isoform 1	DUT	2,50	2,00	3,33
IPI00115580	Eukaryotic translation initiation factor 3 subunit M	EIF3M	2,22	1,67	3,33
IPI00756424	Eukaryotic translation initiation factor 5B	EIF5B	2,86	2,00	5,00
IPI00108271	ELAV-like protein 1	ELAVL1	2,00	2,00	1,67
IPI00405986	Erythrocyte protein band 4.1-like 1	EPB4.1L1	2,00	3,33	1,43
IPI00309481	Band 4.1-like protein 2	EPB4.1L2	2,22	3,33	1,67
IPI00312468	Eukaryotic peptide chain release factor subunit 1	ETF1	1,67	1,67	1,67
IPI00322492	Ewing sarcoma breakpoint region 1	EWSR1	2,50	3,33	2,00
IPI00265386	Isoform 1 of FAS-associated factor 2	FAF2	4,00	3,33	5,00
IPI00109611	Protein FAM162A	FAM162A	2,50	3,33	2,00
IPI00122015	Protein FAM49B	FAM49B	2,50	3,33	2,00
IPI00830803	Fibulin-2 isoform b	FBLN2	3,33	5,00	2,50
IPI00228343	Ferrochelatase	FECH	2,50	3,33	2,00
IPI00338963	Peptidyl-prolyl cis-trans isomerase FKBP5	FKBP5	2,22	2,00	2,50
IPI00226787	Isoform 2 of FAD synthase	FLAD1	2,50	1,67	5,00
IPI00230145	Ferritin heavy chain	FTH1	2,00	2,00	1,67
IPI00221833	Alpha-(1,3)-fucosyltransferase 11	FUT11	2,00	2,00	2,00
IPI00122521	Isoform E of Fragile X mental retardation syndrome-related protein 1	FXR1	2,86	2,00	5,00
IPI00377455	GRIP and coiled-coil domain-containing protein 2	GCC2	1,67	1,67	1,67
IPI00406371	Isoform 1 of Glucosamine--fructose-6-phosphate aminotransferase [isomerizing] 1	GFPT1	2,00	1,67	2,50
IPI00416279	Golgi-associated plant pathogenesis-related protein 1	GLIPR2	2,00	2,00	2,00
IPI00110487	Protein C20orf11 homolog	GM5206	2,00	2,00	2,00
IPI00344567	Putative uncharacterized protein	GM561	2,00	2,00	2,00
IPI00621272	NHP2-like protein 1	GM6637	2,00	2,00	2,00
IPI00762316	Isoform 1 of Guanine nucleotide-binding protein-like 1	GNL1	2,00	2,00	2,00
IPI00223864	Isoform 1 of Putative glycerophosphocholine phosphodiesterase GPCPD1	GPCPD1	2,00	2,00	2,00
IPI00453582	G-rich sequence factor 1	GRSF1	2,50	3,33	2,00
IPI00264062	Glycogenin-1	GYG	1,82	1,67	2,00
IPI00230449	Hippocalcin-like protein 1	HPCAL1	2,22	2,00	2,50
IPI00453499	Isoleucyl-tRNA synthetase, mitochondrial	IARS2	1,67	1,67	1,67
IPI00380339	Isoform 1 of Peptidyl-tRNA hydrolase ICT1, mitochondrial	ICT1	2,86	3,33	2,50
IPI00116668	Integrin-linked protein kinase	ILK	5,00	3,33	10,00
IPI00396804	Isoform 1 of Integrin-linked kinase-associated serine/threonine phosphatase 2C	ILKAP	2,00	2,00	2,00
IPI00331027	Mitochondrial inner membrane protease subunit 2	IMMP2L	2,22	2,00	2,50
IPI00467447	Ras GTPase-activating-like protein IQGAP1	IQGAP1	2,00	2,00	2,00
IPI00857195	Integrin alpha-V precursor	ITGAV	3,33	3,33	3,33
IPI00132474	Integrin beta-1	ITGB1	2,22	2,00	2,50
IPI00129792	Importin subunit alpha-4	KPNA4	1,67	1,25	2,50
IPI00929786	Isoform 1 of La-related protein 1	LARP1	2,50	1,67	5,00

IPI00453819	Leucyl-tRNA synthetase, cytoplasmic	LARS	1,82	1,67	2,00
IPI00123138	Probable leucyl-tRNA synthetase, mitochondrial	LARS2	2,50	2,00	3,33
IPI00223987	Leucyl-cystinyl aminopeptidase	LNPEP	2,50	1,67	5,00
IPI00119063	Prolow-density lipoprotein receptor-related protein 1	LRP1	2,00	2,00	2,00
IPI00121579	U6 snRNA-associated Sm-like protein LSM1	LSM1	3,33	3,33	3,33
IPI00173156	Protein LZIC	LZIC	4,00	5,00	3,33
IPI00551412	Protein mago nashi homolog	MAGOH	2,00	2,00	2,00
IPI00169711	Amine oxidase [flavin-containing] A	MAOA	2,22	2,00	2,50
IPI00123875	Isoform Alpha-2 of Mitogen-activated protein kinase 9	MAPK9	2,22	2,00	2,50
IPI00626860	Isoform 2 of Malignant T cell-amplified sequence 1	MCTS1	2,00	2,00	2,00
IPI00331563	Mannose-P-dolichol utilization defect 1 protein	MPDU1	2,00	2,00	2,00
IPI00132412	39S ribosomal protein L10, mitochondrial	MRPL10	3,33	3,33	3,33
IPI00132470	39S ribosomal protein L11, mitochondrial	MRPL11	5,00	5,00	5,00
IPI00134011	39S ribosomal protein L13, mitochondrial	MRPL13	4,00	5,00	3,33
IPI00387389	39S ribosomal protein L18, mitochondrial	MRPL18	2,50	3,33	2,00
IPI00225318	39S ribosomal protein L22, mitochondrial	MRPL22	2,22	2,00	2,50
IPI00162942	39S ribosomal protein L37, mitochondrial	MRPL37	2,00	2,00	2,00
IPI00222753	mTERF domain-containing protein 3, mitochondrial	MTERFD3	2,00	1,67	2,50
IPI00112327	Metaxin-1 isoform 1	MTX1	4,00	3,33	5,00
IPI00400163	Isoform 4 of N-alpha-acetyltransferase 50, NatE catalytic subunit	NAA50	2,00	2,00	2,00
IPI00117839	Isoform 2 of Nuclear receptor coactivator 1	NCOA1	2,22	2,00	2,50
IPI00120212	NADH dehydrogenase [ubiquinone] 1 alpha subcomplex subunit 9, mitochondrial	NDUFA9	2,50	2,50	2,50
IPI00132531	NADH dehydrogenase [ubiquinone] 1 beta subcomplex subunit 5, mitochondrial	NDUFB5	2,22	2,00	2,50
IPI00229008	NADH dehydrogenase [ubiquinone] iron-sulfur protein 4, mitochondrial	NDUFS4	2,22	2,00	2,50
IPI00125448	Nucleoside diphosphate kinase, mitochondrial	NME4	2,00	2,00	2,00
IPI00132339	Nucleoside-triphosphatase C1orf57 homolog	NTPCR	1,82	1,67	2,00
IPI00461281	NudC domain-containing protein 2	NUDCD2	2,22	2,00	2,50
IPI00420870	Isoform 1 of UDP-N-acetylglucosamine--peptide N-acetylglucosaminyltransferase 110 kDa subunit	OGT	2,22	3,33	1,67
IPI00312507	Optic atrophy 3 protein homolog	OPA3	2,00	2,00	2,00
IPI00165817	55 kDa protein	ORF19	2,22	2,00	2,50
IPI00109253	UPF0480 protein C15orf24 homolog	ORF3	4,00	3,33	5,00
IPI00323064	Programmed cell death protein 4	PDCD4	2,86	3,33	2,50
IPI00336248	Isoform 2 of Myomegalin	PDE4DIP	2,22	2,00	2,50
IPI00123004	Pyruvate dehydrogenase [lipoamide] kinase isozyme 3, mitochondrial	PDK3	1,82	1,67	2,00
IPI00453792	Pyruvate dehydrogenase phosphatase regulatory subunit, mitochondrial	PDPR	4,00	3,33	5,00
IPI00315187	RhoA activator C11orf59 homolog	PDRO	3,33	10,00	2,00
IPI00136789	Isoform 2 of Peroxisome biogenesis factor 1	PEX1	3,33	5,00	2,50
IPI00378557	Prefoldin 4 isoform 1	PFDN4	2,50	3,33	2,00
IPI00653772	Isoform 2 of 6-phosphofructo-2-kinase/fructose-2,6-biphosphatase 1	PFKFB1	2,00	1,67	2,50
IPI00331541	6-phosphofructokinase, muscle type	PFKM	2,22	2,00	2,50
IPI00124444	Isoform 1 of 6-phosphofructokinase type C	PFKP	2,22	2,50	2,00
IPI00318898	Putative uncharacterized protein	PGM3	2,00	1,67	2,50
IPI00264501	Isoform 1 of Phosphatidylinositol-binding clathrin assembly protein	PICALM	2,00	1,67	2,50
IPI00132093	Peptidyl-prolyl cis-trans isomerase NIMA-interacting 1	PIN1L	4,00	5,00	3,33

IPI00129479	Phosphatidylinositol-5-phosphate 4-kinase type-2 gamma	PIP4K2C	2,00	2,00	2,00
IPI00405742	Plexin B2	PLXNB2	2,22	2,00	2,50
IPI00135686	Peptidyl-prolyl cis-trans isomerase B	PPIB	2,00	2,50	1,67
IPI00117072	Protein phosphatase 1G	PPM1G	2,22	2,00	2,50
IPI00119116	Protoporphyrinogen oxidase	PPOX	2,22	2,00	2,50
IPI00380331	Protein phosphatase 2A B56 delta subunit	PPP2R5D	2,50	1,67	5,00
IPI00338458	Putative uncharacterized protein	PTCD3	2,86	2,00	5,00
IPI00114410	Phosphatidylinositol-3,4,5-trisphosphate 3-phosphatase and dual-specificity protein phosphatase	PTEN	2,00	2,00	2,00
IPI00134918	Protein-tyrosine phosphatase mitochondrial 1	PTPMT1	2,86	5,00	2,00
IPI00345682	pyridine nucleotide-disulfide oxidoreductase domain-containing protein 2	PYROXD2	2,22	3,33	1,67
IPI00116729	Ras-related protein Rab-22A	RAB22A	2,50	3,33	2,00
IPI00116563	Rab5B	RAB5B	1,67	1,67	1,67
IPI00337844	E3 SUMO-protein ligase RanBP2	RANBP2	1,67	1,67	1,67
IPI00310972	RAP1, GTP-GDP dissociation stimulator 1 isoform b	RAP1GDS1	2,00	2,00	2,00
IPI00378430	81 kDa protein	RAPH1	2,00	2,00	2,00
IPI00323177	Probable arginyl-tRNA synthetase, mitochondrial	RARS2	1,82	1,67	2,00
IPI00474959	Putative uncharacterized protein	RCN2	3,33	5,00	2,50
IPI00315463	Receptor expression-enhancing protein 5	REEP5	1,82	1,67	2,00
IPI00116558	Rho-related GTP-binding protein RhoG	RHOG	2,86	2,00	5,00
IPI00127085	60S ribosomal protein L10a	RPL10A	2,22	2,50	2,00
IPI00132460	60S ribosomal protein L26	RPL26	2,86	2,00	5,00
IPI00230623	60S ribosomal protein L32	RPL32	2,50	3,33	2,00
IPI00115902	60S ribosomal protein L35a	RPL35A	3,33	10,00	2,00
IPI00137787	60S ribosomal protein L8	RPL8	2,00	1,67	2,50
IPI00309035	Dolichyl-diphosphooligosaccharide--protein glycosyltransferase subunit 1	RPN1	1,67	1,67	1,67
IPI00319231	40S ribosomal protein S15	RPS15	2,86	5,00	2,00
IPI00465880	40S ribosomal protein S17	RPS17	2,00	2,00	1,67
IPI00112948	Isoform 3 of Reticulon-3	RTN3	2,50	3,33	2,00
IPI00136213	Sarcosine dehydrogenase, mitochondrial	SARDH	2,00	2,00	1,67
IPI00224219	Isoform 1 of Sec1 family domain-containing protein 1	SCFD1	1,67	1,67	1,67
IPI00462855	N-terminal kinase-like protein	SCYL1	2,22	2,00	2,50
IPI00123349	Protein transport protein Sec23A	SEC23A	2,00	1,67	2,50
IPI00331016	Sec24 related gene family, member B	SEC24B	2,22	2,00	2,50
IPI00284595	SEC24 related gene family, member D	SEC24D	2,86	5,00	2,00
IPI00120433	SH2B adapter protein 2	SH2B2	2,50	3,33	2,00
IPI00454140	Superkiller viralicidic activity 2-like	SKIV2L	2,86	3,33	2,50
IPI00331163	S-phase kinase-associated protein 1	SKP1A	2,22	2,50	2,00
IPI00308162	Calcium-binding mitochondrial carrier protein Aralar1	SLC25A12	2,22	1,67	3,33
IPI00135651	Calcium-binding mitochondrial carrier protein Aralar2	SLC25A13	2,86	2,00	5,00
IPI00331076	Isoform 1 of STE20-like serine/threonine-protein kinase	SLK	1,82	1,67	2,00
IPI00170008	U2 small nuclear ribonucleoprotein A'	SNRPA1	2,00	2,00	2,00
IPI00876001	Sorting nexin-1	SNX1	1,82	1,67	2,00
IPI00122346	Translocon-associated protein subunit delta	SSR4	2,50	2,50	2,50
IPI00453975	Isoform 2 of Transcription elongation factor SPT5	SUPT5H	2,50	2,00	3,33
IPI00226515	Transgelin	TAGLN	2,00	2,00	1,67

IPI00468688	Threonyl-tRNA synthetase, cytoplasmic	TARS	1,82	1,67	2,00
IPI00229485	Isoform 2 of Transcription elongation regulator 1	TCERG1	2,00	1,67	2,50
IPI00112822	Isoform Mitochondrial of Transcription factor A, mitochondrial	TFAM	2,22	2,00	2,50
IPI00114862	THUMP domain-containing protein 1	THUMPD1	2,22	2,00	2,50
IPI00129504	Mitochondrial import inner membrane translocase subunit Tim17-B	TIMM17B	2,86	5,00	2,00
IPI00135971	Tight junction protein ZO-1	TJP1	1,82	2,00	1,67
IPI00127983	Transmembrane emp24 domain-containing protein 2	TMED2	2,50	2,50	2,50
IPI00466640	Transmembrane emp24 domain-containing protein 5	TMED5	2,50	3,33	2,00
IPI00153101	Transmembrane protein 109	TMEM109	2,86	2,00	5,00
IPI00222447	Transmembrane protein 11	TMEM11	2,00	2,00	2,00
IPI00112227	Transmembrane protein 126A	TMEM126A	4,00	2,50	10,00
IPI00378438	Tensin 1	TNS1	2,00	1,43	3,33
IPI00120715	Mitochondrial import receptor subunit TOM20 homolog	TOMM20	2,50	3,33	2,00
IPI00315135	Mitochondrial import receptor subunit TOM22 homolog	TOMM22	2,00	2,00	2,00
IPI00761429	Hypothetical protein LOC75964 isoform 1	TRAPPC8	2,00	2,00	2,00
IPI00321005	E3 ubiquitin-protein ligase TRIM32	TRIM32	3,33	3,33	3,33
IPI00420483	Isoform 1 of Ubiquitin carboxyl-terminal hydrolase 19	USP19	4,00	3,33	5,00
IPI00420143	Isoform 2 of Ubiquitin carboxyl-terminal hydrolase 47	USP47	1,82	1,67	2,00
IPI00132276	Vesicle-associated membrane protein 3	VAMP3	4,00	3,33	5,00
IPI00222180	Valyl-tRNA synthetase, mitochondrial	VAR2	2,00	2,00	2,00
IPI00377609	Isoform 1 of Deubiquitinating protein VCIP135	VCPIP1	2,00	2,00	1,67
IPI00111181	Vacuolar protein sorting-associated protein 35	VPS35	2,50	1,67	5,00
IPI00468996	Neural Wiskott-Aldrich syndrome protein	WASL	2,86	3,33	2,50
IPI00655217	Xanthine dehydrogenase/oxidase	XDH	2,00	1,67	2,50

IPI...International Protein Index; AccNr...Accession Number; M...mean; R1...replicate 1; R2...replicate 2

**Table 9: Proteins up-regulated by the 1D-GeLC/MSMS approach**

IPI AccNr	Down-regulated proteins (115)	Gene Symbol	Fold-change		
			M	R1	R2
IPI00126172	Ester hydrolase C11orf54 homolog	-	0,63	0,67	0,59
IPI00121834	Hcp beta-lactamase-like protein C1orf163 homolog	-	0,44	0,50	0,40
IPI00111946	Putative uncharacterized protein	-	0,34	0,33	0,36
IPI00331251	Putative uncharacterized protein	ACADS	0,63	0,59	0,67
IPI00420440	Acylphosphatase-1	ACYP1	0,33	0,43	0,27
IPI00272401	Acylphosphatase-2	ACYP2	0,26	0,25	0,27
IPI00111149	Protein ADP-ribosylarginine hydrolase	ADPRH	0,63	0,67	0,59
IPI00135969	Adenylosuccinate synthetase isozyme 2	ADSS	0,61	0,56	0,67
IPI00122620	UPF0696 protein C11orf68 homolog	AI837181	0,35	0,50	0,27
IPI00115506	Isoform 3 of A-kinase anchor protein 1, mitochondrial	AKAP1	0,53	0,56	0,50
IPI00323465	Putative N-acetylglucosamine-6-phosphate deacetylase	AMDHD2	0,50	0,40	0,67
IPI00624501	ATPase Asna1	ASNA1	0,48	0,50	0,45
IPI00223875	L-asparaginase	ASRGL1	0,36	0,67	0,25
IPI00230241	ATP synthase subunit epsilon, mitochondrial	ATP5E	0,49	0,45	0,53
IPI00127598	ATPase inhibitor, mitochondrial	ATPIF1	0,51	0,50	0,53

IPI00109131	Uncharacterized protein C1orf50 homolog	AU022252	0,51	0,50	0,53
IPI00109966	Beta-2-microglobulin	B2M	0,33	0,25	0,50
IPI00111953	BolA-like protein 1	BOLA1	0,32	0,67	0,21
IPI00310474	Brain protein 16	BRP16	0,42	0,50	0,36
IPI00130439	Calcium/calmodulin-dependent protein kinase type 1	CAMK1	0,50	0,40	0,67
IPI00124616	Isoform 1 of COBW domain-containing protein 1	CBWD1	0,57	0,67	0,50
IPI00153742	Coiled-coil domain-containing protein 25	CCDC25	0,39	0,31	0,53
IPI00381495	Uncharacterized protein	CCDC6	0,42	0,50	0,36
IPI00461969	Isoform 1 of Cell division cycle protein 123 homolog	CDC123	0,53	0,43	0,67
IPI00133562	Coiled-coil-helix-coiled-coil-helix domain-containing protein 3, mitochondrial	CHCHD3	0,65	0,67	0,63
IPI00124248	Putative uncharacterized protein	CLNS1A	0,47	0,67	0,36
IPI00112668	COMM domain-containing protein 8	COMMD8	0,59	0,67	0,53
IPI00114377	Cytochrome c oxidase subunit 7A2, mitochondrial	COX7A2	0,34	0,33	0,36
IPI00113362	Crk-like protein	CRKL	0,34	0,25	0,53
IPI00125931	Cystatin-B	CSTB	0,30	0,50	0,21
IPI00111013	Cathepsin D	CTSD	0,65	0,67	0,63
IPI00230113	Cytochrome b5	CYB5	0,56	0,50	0,63
IPI00330057	Density-regulated protein	DENR	0,34	0,33	0,36
IPI00223482	DnaJ homolog subfamily B member 10 isoform 3	DNAJB2	0,44	0,33	0,67
IPI00315225	Dynein light chain roadblock-type 1	DYNLRB1	0,42	0,50	0,36
IPI00928532	Eukaryotic translation initiation factor 3 subunit F	EIF3F	0,61	0,67	0,56
IPI00330477	Isoform 2 of Epsin-1	EPN1	0,42	0,50	0,36
IPI00336840	F-box only protein 4	FBXO4	0,54	0,59	0,50
IPI00135939	Adrenodoxin, mitochondrial	FDX1	0,30	0,50	0,21
IPI00406794	GRB2-associated-binding protein 1	GAB1	0,54	0,50	0,59
IPI00473475	GTP cyclohydrolase 1 feedback regulatory protein	GCHFR	0,41	0,33	0,53
IPI00331528	Glutaredoxin-1	GLRX	0,36	0,67	0,25
IPI00121419	Uncharacterized protein	GM5457	0,44	0,67	0,33
IPI00119853	Isoform Gnas-1 of Guanine nucleotide-binding protein G(s) subunit alpha isoforms short	GNAS	0,45	0,40	0,53
IPI00127501	Protein C10	GRCC10	0,38	0,40	0,36
IPI00267855	GRIP1-associated protein 1	GRIPAP1	0,31	0,25	0,40
IPI00323911	Glutathione S-transferase A4	GSTA4	0,57	0,56	0,59
IPI00138238	Prefoldin subunit 6	H2-KE2	0,57	0,50	0,67
IPI00137694	HD domain-containing protein 2	HDCC2	0,44	0,40	0,50
IPI00221463	Histone H2A type 3	HIST3H2A	0,40	0,50	0,33
IPI00409148	Haptoglobin	HP	0,24	0,17	0,40
IPI00130640	Ribonuclease UK114	HRSP12	0,34	0,67	0,23
IPI00261188	Interferon-induced 35 kDa protein homolog	IFI35	0,61	0,56	0,67
IPI00381357	RIKEN cDNA 2310044H10	INM02	0,57	0,50	0,67
IPI00828610	La-related protein 4 isoform 2	LARP4	0,54	0,59	0,50
IPI00122307	Lipoyltransferase 1, mitochondrial	LIPT1	0,34	0,25	0,53
IPI00129873	U6 snRNA-associated Sm-like protein LSM6	LSM6	0,42	0,50	0,36
IPI00471097	LYR motif-containing protein 5	LYRM5	0,51	0,50	0,53
IPI00229534	Myristoylated alanine-rich C-kinase substrate	MARCKS	0,33	0,23	0,56
IPI00469123	Isoform 1 of Cell surface glycoprotein MUC18	MCAM	0,45	0,50	0,42
IPI00881197	NADP-dependent malic enzyme	ME1	0,61	0,63	0,59
IPI00165711	BRCA1-A complex subunit MERIT40	MERIT40	0,51	0,50	0,53
IPI00153664	Alpha N-terminal protein methyltransferase 1A	METTL11A	0,42	0,50	0,36
IPI00406624	Isoform 3 of Bifunctional protein NCOAT	MGEA5	0,51	0,50	0,53
IPI00229662	Methylated-DNA--protein-cysteine methyltransferase	MGMT	0,34	0,33	0,36

IPI00137706	55 kDa erythrocyte membrane protein	MPP1	0,51	0,50	0,53
IPI00885509	Methylthioribose-1-phosphate isomerase	MRI1	0,54	0,67	0,45
IPI00321858	28S ribosomal protein S15, mitochondrial	MRPS15	0,41	0,33	0,53
IPI00756996	Mevalonate kinase	MVK	0,54	0,56	0,53
IPI00758413	N-alpha-acetyltransferase 10, NatA catalytic subunit isoform 2	NAA10	0,49	0,45	0,53
IPI00136107	Protein NDRG3	NDRG3	0,38	0,40	0,36
IPI00331332	NADH dehydrogenase [ubiquinone] 1 alpha subcomplex subunit 5	NDUFA5	0,28	0,67	0,18
IPI00128285	NADH dehydrogenase (Ubiquinone) flavoprotein 3	NDUFV3	0,24	0,50	0,15
IPI00132005	Neudesin	NENF	0,44	0,33	0,67
IPI00169979	Isoform 1 of NmrA-like family domain-containing protein 1	NMRAL1	0,29	0,19	0,67
IPI00128904	Poly(rC)-binding protein 1	PCBP1	0,63	0,67	0,59
IPI00331596	Peroxisomal trans-2-enoyl-CoA reductase	PECR	0,33	0,23	0,59
IPI00307963	Peflin	PEF1	0,45	0,36	0,63
IPI00132485	Prefoldin subunit 1	PFDN1	0,67	0,67	0,67
IPI00380195	Phosphoglycolate phosphatase	PGP	0,67	0,67	0,67
IPI00919293	Protein	PHLDB1	0,40	0,45	0,36
IPI00453516	Phytanoyl-CoA dioxygenase domain-containing protein 1	PHYHD1	0,51	0,50	0,53
IPI00109437	Pirin	PIR	0,34	0,25	0,53
IPI00885519	Protein	PLEKHG1	0,54	0,45	0,67
IPI00131228	Phosphomannomutase 2	PMM2	0,56	0,67	0,48
IPI00331644	Proteasome subunit alpha type-3	PSMA3	0,65	0,63	0,67
IPI00119239	Proteasome subunit beta type-6	PSMB6	0,56	0,63	0,50
IPI00761650	26S proteasome non-ATPase regulatory subunit 9	PSMD9	0,59	0,59	0,59
IPI00471441	Ptms protein	PTMS	0,67	0,67	0,67
IPI00119807	Mitogen-activated protein-binding protein-interacting protein	ROBLD3	0,19	0,67	0,11
IPI00331092	40S ribosomal protein S4, X isoform	RPS4X	0,65	0,63	0,67
IPI00126175	Protein S100-A1	S100A1	0,20	0,67	0,12
IPI00222555	Protein S100-A10	S100A10	0,38	0,67	0,27
IPI00119202	Protein S100-A11	S100A11	0,17	0,43	0,11
IPI00124115	Protein S100-A13	S100A13	0,54	0,56	0,53
IPI00830189	Isoform 1 of Selenocysteine lyase	SCLY	0,63	0,59	0,67
IPI00761959	Protein SCO1 homolog, mitochondrial	SCO1	0,51	0,50	0,53
IPI00134131	Isoform SCPx of Non-specific lipid-transfer protein	SCP2	0,57	0,67	0,50
IPI00515330	Isoform 3 of Septin-9	Sep 09	0,56	0,56	0,56
IPI00221759	Selenide, water dikinase 1	SEPHS1	0,54	0,56	0,53
IPI00110852	Translocon-associated protein alpha, muscle specific isoform	SSR1	0,44	0,33	0,67
IPI00121514	Stress-induced-phosphoprotein 1	STIP1	0,67	0,67	0,67
IPI00119524	Isoform 1 of Striatin-4	STRN4	0,63	0,67	0,59
IPI00315948	Tubulin-folding cofactor B	TBCB	0,59	0,67	0,53
IPI00121887	Isoform 2 of Transcription elongation factor A protein 1	TCEA1	0,44	0,50	0,40
IPI00323130	Transcription elongation factor B polypeptide 1	TCEB1	0,30	0,50	0,21
IPI00125776	Mitochondrial import inner membrane translocase subunit Tim8 A	TIMM8A1	0,26	0,33	0,21
IPI00132169	Mitochondrial import inner membrane translocase subunit Tim8 B	TIMM8B	0,59	0,67	0,53
IPI00125513	Mitochondrial import inner membrane translocase subunit Tim9	TIMM9	0,34	0,33	0,36

IPI00132768	Transmembrane protein 14C	TMEM14C	0,50	0,50	0,50
IPI00469251	Isoform 2 of Thioredoxin reductase 1, cytoplasmic	TXNRD1	0,34	0,25	0,53
IPI00453622	NEDD8-activating enzyme E1 catalytic subunit isoform 1	UBA3	0,51	0,50	0,53
IPI00123589	UBX domain-containing protein 1	UBXN1	0,42	0,67	0,30
IPI00111958	Uroporphyrinogen decarboxylase	UROD	0,50	0,43	0,59
IPI00133024	Vacuolar protein sorting-associated protein VTA1 homolog	VTA1	0,35	0,50	0,27
IPI00114819	Methylosome protein 50	WDR77	0,54	0,50	0,59

IPI...International Protein Index; AccNr...Accession Number; M...mean; R1...replicate 1; R2...replicate 2

#### 4.2.2. **In-depth analysis of the 1D-adipocyte-proteome identified major changes in glycolysis and mitochondrial function**

To obtain the same information as in the phospho-proteome screen pathway analysis and protein functional categorizations were performed by Pathway Studio and/or Scaffold using the same conditions. Again, we found pathways as notch signaling and adipocytokine signaling highly present. In almost the same manner we identified proteins involved in glucose metabolism, respiratory chain, OXPHOS and insulin signaling (Table 10, 11), consistent with prior studies [5, 52] and our phospho-proteome dataset.

Phospho-proteomics revealed a highly reproducible phosphorylation of PDHA1, which blocks the conversion of pyruvate to acetyl-CoA and therefore the link of glycolysis with the TCA cycle.

Notable, the PDHA1 phosphorylating enzyme pyruvate dehydrogenase kinase (PDK) was increased in HH treated adipocytes (Figure 7). Interestingly, close inspection of mass spectrometry data of cytoplasmic fractions revealed a stable phosphorylation of PDHA1 even after 48 hours (Figure 16). Furthermore respiratory chain and OXPHOS (Atp5e, NDUFV3, NDUFA5, COX7A2) were significantly down-regulated ( $p = 0.0031$ ).

The GO-term Insulin signaling was significantly up-regulated ( $p = 1.44E-05$ ). Insulin is a hormone regulating carbohydrate and fat metabolism. It activates glucose uptake by muscle and fat tissue and stores it as glycogen in liver and muscle. In line with the up-regulation of Insulin signaling glycogen metabolism ( $p = 0.0214$ ) and the most important regulatory enzyme of glycolysis, phosphofructokinase-1 (PFK1) showed an up-regulation, too. PFK1 catalyzes the conversion of fructose 6-phosphate and ATP to fructose 1,6-bisphosphate (FBP) and ADP and is the rate-limiting step in glycolysis.



Taken together we observed an increased glucose turnover, demonstrated by higher insulin action and an up-regulation of PFK1. Further, we found evidence for decreased mitochondrial function.

Table 10 and 11 show metabolic and signaling pathways significantly present (all p-values  $\leq 0.05$ ) in the dataset. Pie charts illustrate related tables (Figure 17, 18). The map of cellular energy metabolism shows the coverage of major enzymes and their regulation (Figure 19) and differentially expressed proteins are listed in Table 8, 9.

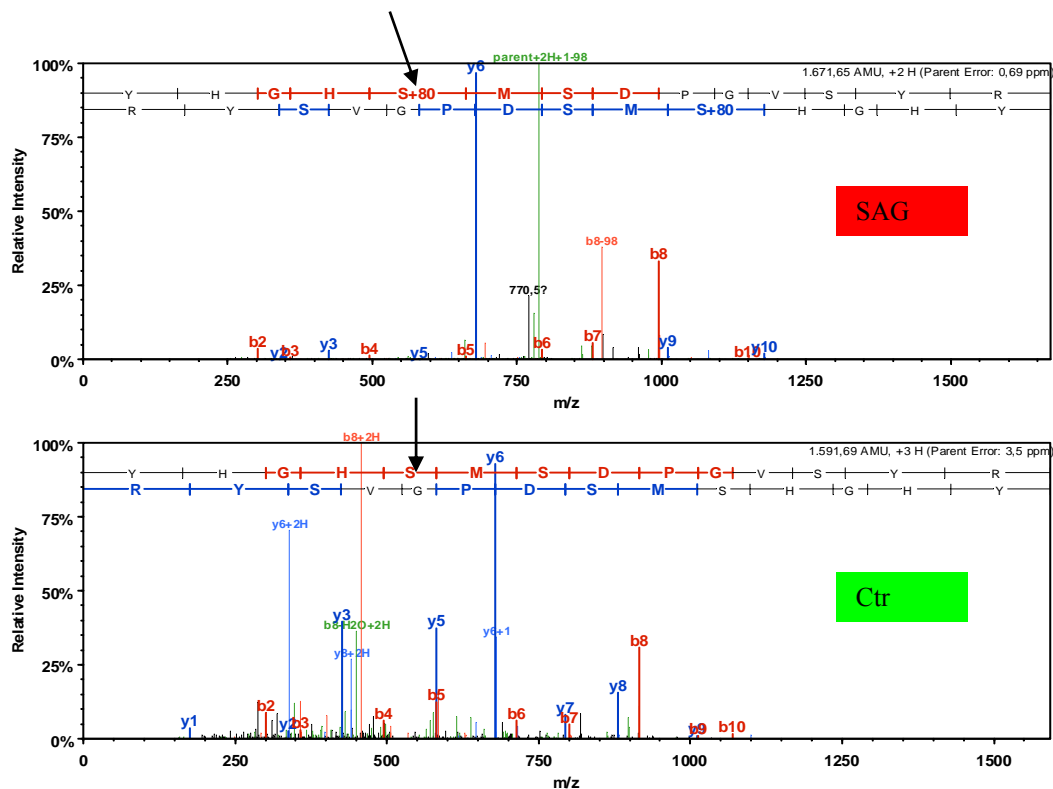


**Figure 16: Spectrum of (non)-phosphorylated PDHA1**

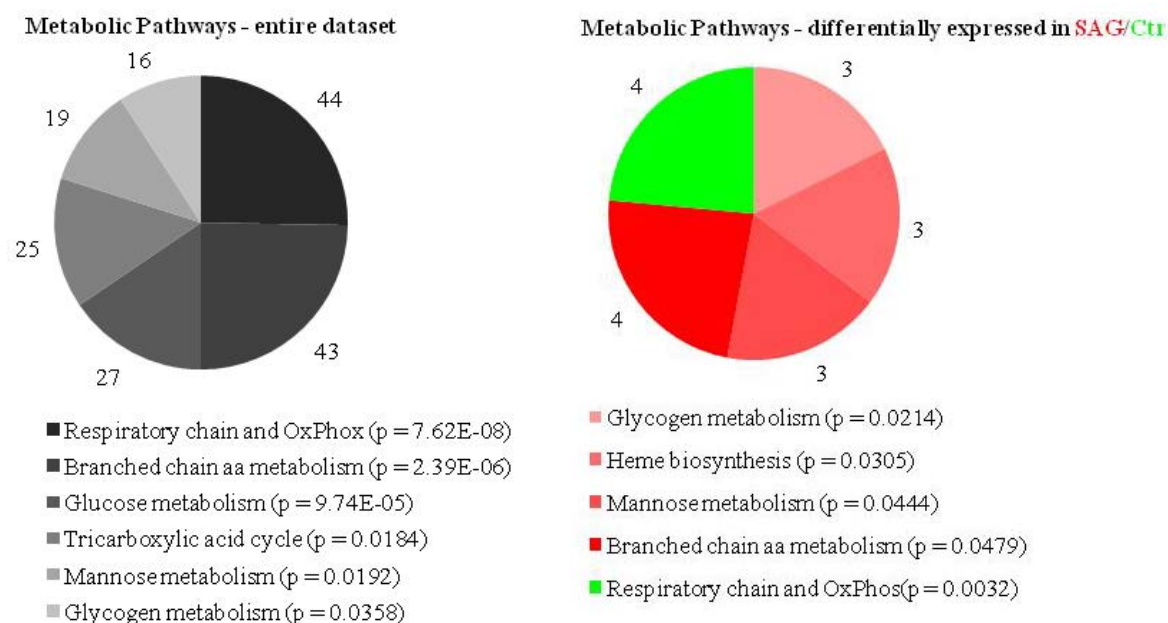
Spectrum of SAG treated samples with a phosphorylation at Serine<sup>293</sup> (S+80) and control (Ctr) sample without any phosphorylation at Serine<sup>293</sup> (S). 80 Da presents the mass of a phosphate group.

**Table 10: Metabolic Pathway analysis of cytoplasmic fraction**

Metabolic Pathway - entire dataset	p-value	Entities	Gene Symbol
Respiratory chain and OXPHOS	7.62E-08	44	NDUFA4,NDUFA8,NDUFA10,NDUFS6,NDUFS2,UQCRC2,ATP6V1G1,PPA2,ATP6V1D,Atp5e,ATP6V1E1,ATP6V1C1,SDHB,PRUNE,UQCRFS1,NDUFS1,COX5B,ATP6V1A,NDUFV2,COX2,PPA1,SDHA,NDUFS7,COX5A,COX4I1,NDUFB6,ATP6V1B2,NDUFB7,UQCRB,NDUFV3,NDUFV1,NDUFA5,UQCRC1,NDUFS3,COX7A2,ATP5B,COX6C,NDUFB5,NDUFS8,ATP6V1H,ATP6V0D1,COX6B1,ATP6V1F,UQCRQ
Branched chain aa metabolism	2.39E-06	43	HIBCH,IARS2,VARS2,Aldh1a7,Acaa1b,GPT,ACAT1,ACAT2,ALDH2,HSD17B4,DLD,OXCT1,ACADM,HADH,MUT,AOX1,HSD17B10,DBT,ACADS,GPT2,BCAT2,AUH,MCCC2,HIBADH,HADHA,ALDH9A1,ACADL,HMGCL,MCEE,ALDH6A1,VARS,LARS2,HMGCS1,ECHS1,PCCA,HADHB,IVD,ACAA2,LARS,MCCC1,BCKDHA,BCKDHB,ACADSB
Glucose metabolism	9.74E-05	27	IDH3G,DHTKD1,FASN,ACO1,ACO2,IDH1,OGDH,DLD,IDH3A,PCK2,FK,ACLY,SDHB,CS,SDHA,PCK1,IDH2,SUCLG1,DLST,SUCLG2,MDH2,MDH1,OXSM,SUCLA2,IDH3B
TCA cycle	0.0184	25	Gapdh,HK2,PGK1,GPI,DLD,LDHA,TPI1,PCK2,DLAT,HK1,PKM2,PGM1,ALDOA,PCK1,PFKL,PFKM,MPI,LDHB,ENO3,PGAM1,PFKP,ACYP2,PDHA1,PGM3,PDHB,GALM,ACYP1
Mannose metabolism	0.0192	19	PPA2,HK2,GPI,HK1,PRUNE,PGM1,GYS1,PPA1,AGL,GYG1,GBE1,MPI,PYGB,UGP2,PGM3,GALM
Glycogen metabolism	0.0358	16	GMPPB,LOC441282,HK2,AKR1B1,GPI,TPI1,HK1,PFKFB1,GMDS,ALDOA,PMM2,PFKL,PFKM,SORD,MPI,PFKP,C12orf5,GMPPA,TSTA3

Metabolic Pathway - enriched in SAG	p-value	Entities	Gene Symbol
Glycogen metabolism	0.0214	3	AGL,GYG1,PGM3
Heme biosynthesis	0.0305	3	FECH,FTH1,PPOX
Mannose metabolism	0.0444	3	PFKFB1,PFKM,PFKP
Branched chain aa metabolism	0.0479	4	IARS2,VARS2,LARS2,LARS

Metabolic Pathway - depleted in SAG	p-value	Entities	Gene Symbol
Respiratory chain and OXPHOS	0.0031	4	Atp5e,NDUFV3,NDUFA5,COX7A2

**Figure 17: Pie charts illustrating metabolic pathways of expression proteomics**

Grey indicates the whole dataset without consideration of any changes. Red represents pathways differentially expressed in SAG treated adipocytes and green in the Control sample (Ctr).

**Table 11: Signaling Pathway analysis of cytoplasmic fraction**

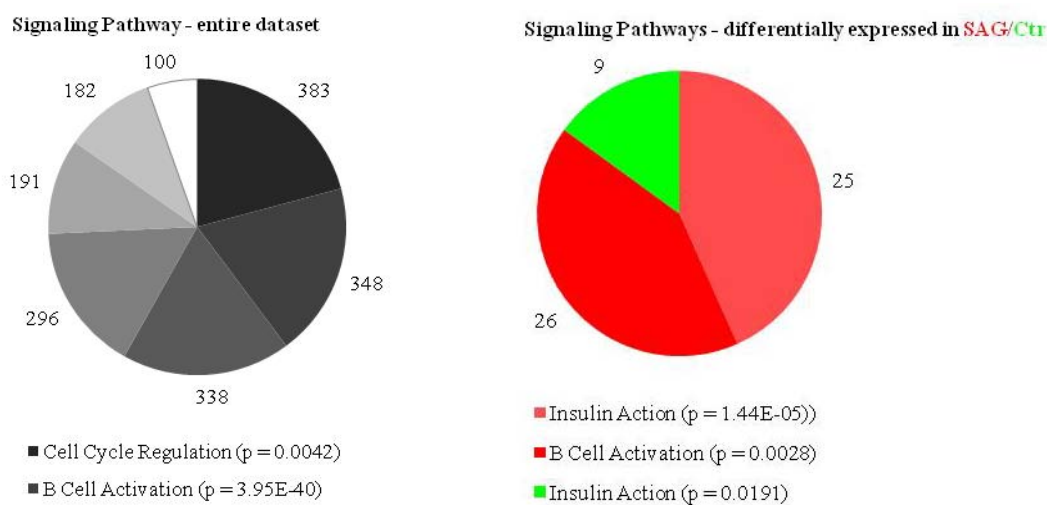
Signaling Pathway - entire dataset	p-value	Entities	Gene Symbol
Cell Cycle Regulation	0.0042	383	MRPL49,AGFG2,MRPL23,RPS11,RPS23,RPS29,...
B Cell Activation	3.95E-40	348	EIF2B4,MRPL19,FARSB,MRPS30,DHRS4,...
Insulin Action	1.26E-66	338	IDH3A,RPL10,LDHA,RPS19,EP515,NRAS,...
Notch Pathway	2.01E-06	296	H2AFZ,PGM1,FBXW8,CAPZA2,SIRT4,MAOA,...
Adipocytokine Signaling	2.99E-11	191	IDH3G,OSBPL1A,ADHFE1,CLYBL,Nudt8,...
Other	< 0.05	~100	RELA,COL3A1,IKBKG,IKBKAP,COL5A2,...

Signaling Pathway - enriched in SAG	p-value	Entities	Gene Symbol
Insulin Action	1.44E-05	26	MRPL18,MRPL22,IARS2,PTEN,ETF1,PICALM,RPL35A,PFKFB1,OGT,AP2B1,RPL26,EIF5B,AGL,GYG1,PFKM,PDK3,TARS,RPL32,RAB5B,TCERG1,GRSF1,PFKP,MRPL11,LARS,PGM3,MRPL13
B Cell Activation	0.0028	25	MRPL18,MRPL22,IARS2,PTEN,TAGLN,EPB41L2,PIN1,ETF1,PIIB,WASL,SH2B2,FKBP5,RPL35A,PFDN4,AP2B1,RHOG,RPL26,EIF5B,TARS,RPL32,TCERG1,GRSF1,MRPL11,LARS,MRPL13

Signaling Pathway - depleted in SAG	p-value	Entities	Gene Symbol
Insulin Action	0.0191	9	MRPS15,ME1,SCP2,EPN1,PMM2,ACADS,RPS4X,ACY2,ACY1

**Figure 18: Pie charts illustrating signaling pathways of expression proteomics**

Grey indicates the whole dataset without consideration of any changes. Red represents pathways differentially expressed in SAG treated adipocytes and green in the Control sample

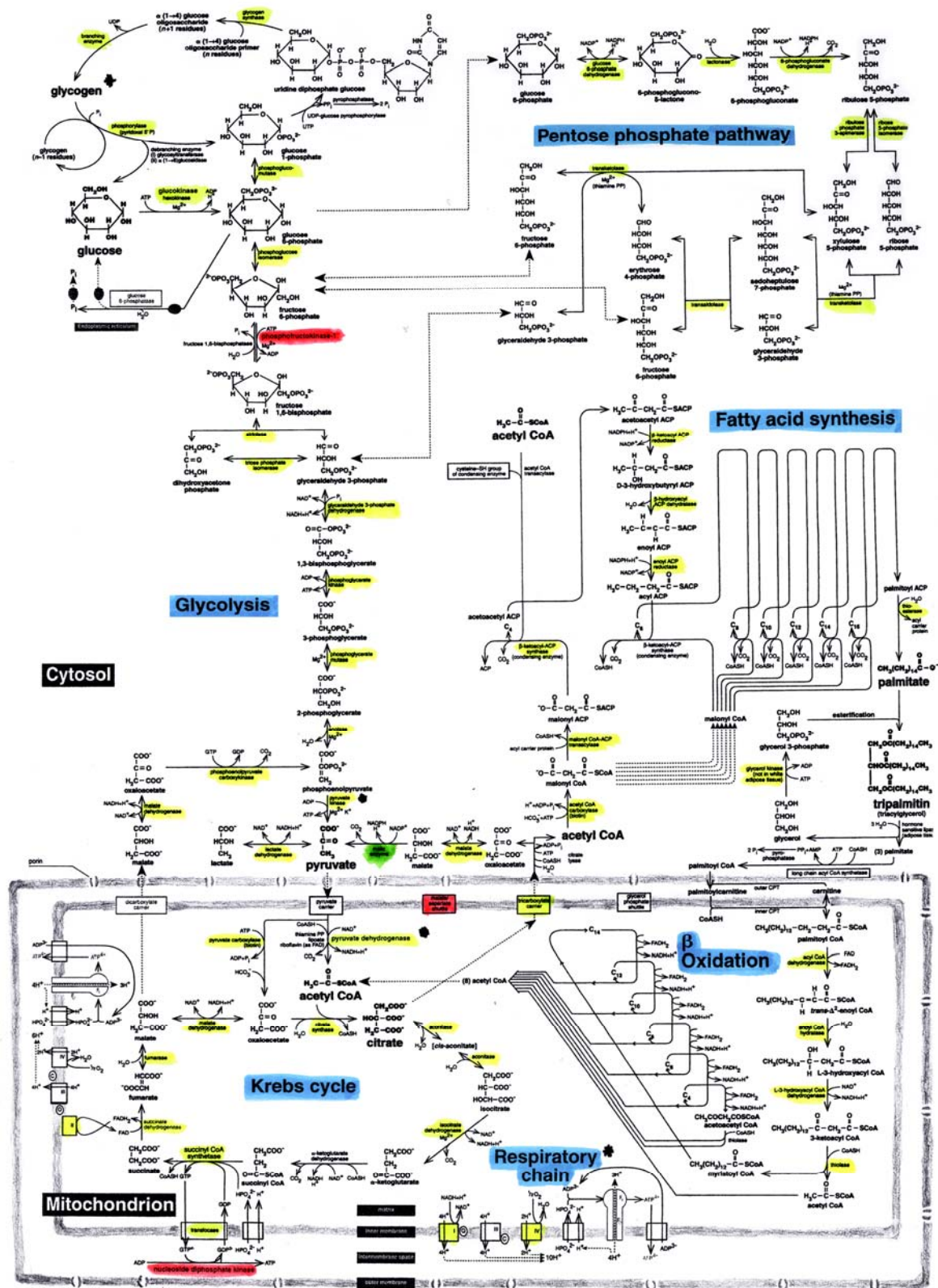
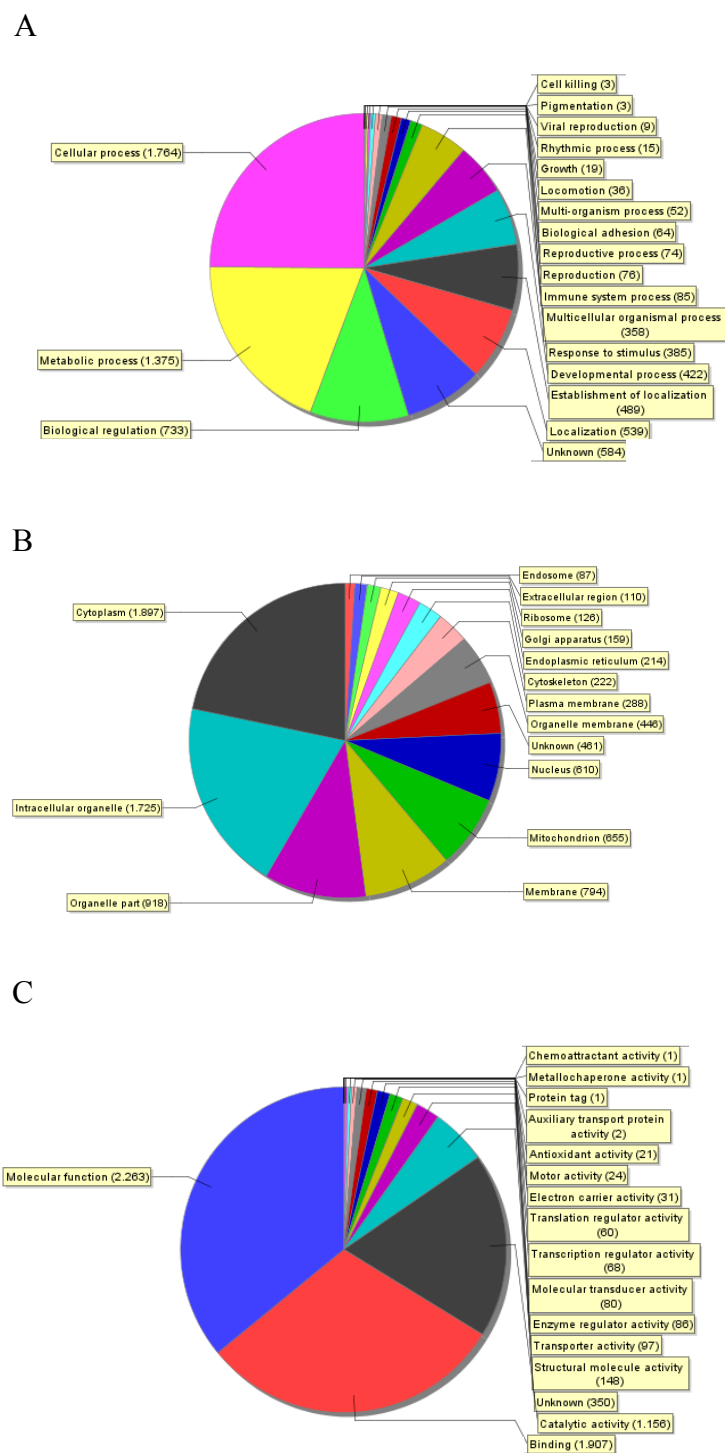


Figure 19: Map of cellular energy metabolism and its main reactions (Salway, Metabolism at a Glance) Highlighted proteins were identified by mass spectrometry. Yellow represents unregulated, red up- and green down-regulated proteins

In agreement with the enriched pathways described before, assigned GO terms confirmed the notion of HH relevant changes on glycolysis and mitochondrial function in adipocytes. Proteins categorized by the term “Biological process” were mainly related to cellular process (1764) and metabolic process (1375) (Figure 20A). Transport ( $p = 7.6E-44$ ) in general and (intracellular)-protein transport as well as vesicle-mediated transport in particular, showed the most significant enrichment for the entire dataset. They were also highly significantly up-regulated in the HH treated sample. As aforementioned, one of the important features of adipocytes is insulin-regulated glucose uptake, which mainly results from translocation of the glucose transporter 4 (GLUT4) to the cell surface membrane. Some of the identified vesicle-mediated transport proteins are known to be involved in insulin signaling and GLUT4 translocation. For example RAB-2, RAB-4, RAB-10, RAB-14, and vesicle-associated membrane protein (VAMP) 8 were identified. Interestingly VAMP3 showed a 4-fold up-regulation that might contribute to increased glucose uptake in HH treated adipocytes. In contrast the most significantly decreased processes in HH treated adipocytes were protein import into mitochondrial inner membrane ( $p = 1.86E-06$ ) and electron transport chain ( $p = 4.35E-05$ )

Importantly proteins assigned to “Cellular component” were highly related to intracellular organelles, mainly to mitochondria (Figure 20B, Table 10, 11). 548 mitochondrial proteins were identified with a p-value of  $1.1E-230$ , 43 were up-regulated ( $p = 1.7E-16$ ) and 21 down-regulated ( $p = 9.3E-09$ ). Especially mitochondrial matrix displayed a significantly increase in treated samples.



**Figure 20: Pie charts illustrating GO terms of expression proteomics (A) Biological process, (B) Cellular component, (C) Molecular function.**

**Table 12: Mitochondrial proteins revealed by GO analysis**

Cellular Component	Entities	p-value	Entities	p-value	Entities	p-value
	Entire dataset		SAG down		SAG up	
mitochondrion	548	1.1E-230	21	9.3E-09	43	1.7E-16
mitochondrial envelope	9	0.0026	-	-	1	0.2184
mitochondrial matrix	96	4.2E-51	2	0.1420	8	6.8E-05
mitochondrial membrane	17	0.0008	1	0.2498	-	-
mitochondrial inner membrane	155	3.6E-63	8	6.5E-05	15	1.4E-07
mitochondrial inner membrane presequence translocase complex	9	1.6E-07	-	-	-	-
mitochondrial intermembrane space	17	2.3E-09	-	-	4	0.0001
mitochondrial intermembrane space protein transporter complex	6	6.4E-05	-	-	-	-
mitochondrial outer membrane	45	4.1E-18	2	0.0647	4	0.0104
mitochondrial outer membrane translocase complex	5	0.0016	-	-	-	-
mitochondrial nucleoid	18	2.5E-11	-	-	1	0.2122
mitochondrial ribosome	11	1.3E-06	-	-	2	0.0118
mitochondrial large ribosomal subunit	14	1.5E-08	-	-	3	0.0010
mitochondrial small ribosomal subunit	12	4.5E-07	1	0.0854	-	-
mitochondrial proton-transporting ATP synthase complex	5	0.0064	1	0.0492	-	-
mitochondrial proton-transporting ATP synthase complex, catalytic core F(1)	4	0.0083	-	-	-	-
mitochondrial proton-transporting ATP synthase complex, coupling factor F(o)	5	0.0350	-	-	-	-
mitochondrial respiratory chain	3	0.3225	1	0.0747	-	-
mitochondrial respiratory chain complex I	27	3.4E-19	2	0.0095	3	0.0034
mitochondrial respiratory chain complex II	1	0.0999	-	-	-	-
mitochondrial respiratory chain complex III	5	5.5E-05	-	-	-	-
respiratory chain	9	0.0020	2	0.0060	-	-
respiratory chain complex I	1	0.1898	-	-	1	0.0158
respiratory chain complex III	1	0.1898	-	-	-	-



**Table 13: Regulation of mitochondrial proteins revealed by GO analysis**

SAG - significantly down-regulated	Gene Symbol
mitochondrion	TIMM8B,TMEM14C,CHCHD3,MRPS15,CTSD,MGEA5,SCP2,AKAP1,S100A10,HRSP12,FDX1,ACADS,TIMM8A,TIMM9,PECR,SCO1,ATPIF1,NDUFV3,LIPT1,NDUFA5,COX7A2
mitochondrial matrix	FDX1,ACADS
mitochondrial membrane	TMEM14C
mitochondrial inner membrane	TIMM8B,CHCHD3,TIMM8A,TIMM9,SCO1,NDUFV3,NDUFA5,COX7A2
mitochondrial outer membrane	AKAP1,TIMM8A
mitochondrial small ribosomal subunit	MRPS15
mitochondrial proton-transporting ATP synthase complex	ATPIF1
mitochondrial respiratory chain	COX7A2
mitochondrial respiratory chain complex I	NDUFV3,NDUFA5
respiratory chain	NDUFV3,NDUFA5
SAG - significantly up-regulated	Gene Symbol
mitochondrion	MRPL18,MRPL22,PTCD3,IARS2,C9orf46,C15orf24,VAR2,IMMP2L,TMEM126A,MRPL10,PTEN,MAPK9,DIABLO,TFAM,FECH,DUT,NDUFS4,MAOA,NME4,TOMM20,CHCHD4,SLC25A13,PKD3,ALDH18A1,TOMM22,SLC25A12,PTPMT1,LARS2,MTX1,PPOX,MRPL11,MRPL37,OPA3,AFG3L2,MTERFD3,ACBD3,NDUFA9,MRPL13,NDUFB5,RARS2,SARDH,TIMM17B,4930402E16Rik
mitochondrial envelope	TOMM20
mitochondrial matrix	IARS2,FECH,PKD3,LARS2,NDUFA9,RARS2,SARDH,4930402E16Rik
mitochondrial inner membrane	IMMP2L,FECH,NDUFS4,NME4,SLC25A13,ALDH18A1,TOMM22,SLC25A12,PTPMT1,MTX1,PPOX,AFG3L2,NDUFA9,NDUFB5,TIMM17B
mitochondrial intermembrane space	DIABLO,NME4,CHCHD4,PPOX
mitochondrial outer membrane	MAOA,TOMM20,TOMM22,MTX1
mitochondrial ribosome	MRPL18,MRPL37
mitochondrial large ribosomal subunit	MRPL10,MRPL11,MRPL13
mitochondrial nucleoid	TFAM
mitochondrial respiratory chain complex I	NDUFS4,NDUFA9,NDUFB5
respiratory chain complex I	NDUFS4



### 4.3. Kinexus – antibody microarray

To gain additional insight microarrays were performed using Kinexus antibody microarrays, containing ~500 pan-specific antibodies and ~300 phospho-site-specific antibodies.

Crosstalk between mitogen-activated protein kinase (MAPK) and HH has been reported in several cancer types [55]. Similar results by Kinexus reflected the high confidence of our dataset. Among others significant changes in phosphorylation pattern of insulin receptor substrate 1 (IRS1) and protein-serine kinase B alpha (AKT1) were observed (Table 14).

**Table 14: Examples of phospho-proteins identified by Kinexus, the Systems Proteomic Company**

Gene Symbol	Protein Name	10 min	30 min	48 h	Phospho Site
IRS1	Insulin receptor substrate 1	1.72	1.85	5.48	Y612
IRS1	Insulin receptor substrate 1	0.95	1.25	0.52	S312
IRS1	Insulin receptor substrate 1	0.76	1.10	0.63	S639
AKT1	Protein-serine kinase B alpha	1.66	1.72	1.15	T308
AKT1	Protein-serine kinase B alpha	1.13	1.40	1.35	S473

Insulin activates the insulin receptor tyrosine kinase (IR), which phosphorylates and subsequently activates IRS1 (Figure 21). Tyrosine phosphorylated IRS1 then activates phosphatidylinositol 3-kinase (PI3K), which has a major role in insulin function, mainly via the activation of the AKT cascade by phosphorylation. Activated AKT induces glycogen synthesis, through inhibition of glycogen synthase kinase 3 (GSK3). A negative feedback signal emanating from AKT results in serine phosphorylation and inactivation of IRS signaling [3].

Furthermore, insulin stimulates glucose uptake in muscle and adipocytes via translocation of glucose transporter type 4 (GLUT4) vesicles to the plasma membrane. GLUT4 translocation involves the PI3K/AKT pathway.

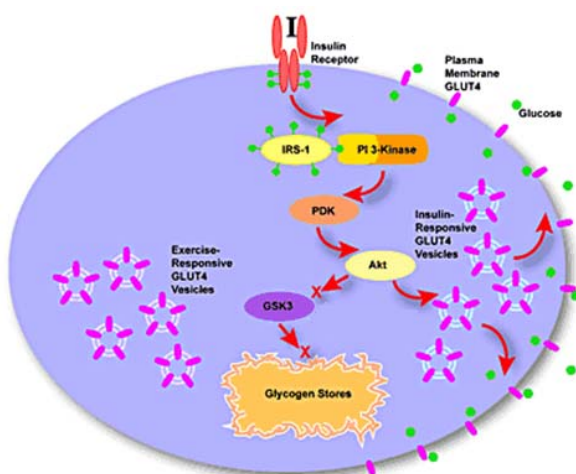


**Figure 21: Schematic cartoon of insulin signaling** Insulin (I) binds to its receptor and activates by phosphorylation (green dots) insulin receptor substrate 1 (IRS-1). Activation of phosphatidylinositol 3-kinase (PI3-Kinase) and AKT induces glycogen synthesis by inhibiting glycogen synthase kinase 3 (GSK3). Insulin binding stimulates glucose uptake via translocation of glucose transporter type 4 (GLUT4) vesicles to the plasma membrane [3].

#### 4.4. Validation of HH triggered reprogramming of cellular energy metabolism

To confirm our observations, Western blots (WB) and enzyme-linked immunosorbent assays (ELISA) were performed. First, real time PCR data showed similar GLI1 mRNA expression levels for SAG and the recombinant HH protein (Figure 22A). Furthermore we could verify (i) the rapid and long lasting phosphorylation of PDHA1 (PDHE1 $\alpha$ ) and (ii) the increased expression levels of its kinase, PDK1 (Figure 22B). AKT showed an up-regulation of the phosphorylated form, highest after 5- and 30 minutes. In line with this time course, GSK-3 $\beta$  showed a prolonged phosphorylation with peaks after 5- and 30 minutes and 48 hours.

Elevated levels of PDK and phosphorylation of its substrate PDHA1 are key regulators of the so called Warburg-effect. A phenomenon were proliferating cells (tumor cells) metabolize most of the glucose to lactate to trigger anabolism. Notable, the enzyme pyruvate kinase (PK), which catalyses the production of phosphoenolpyruvate (PEP) and ADP to pyruvate and ATP, is a rate-limiting enzyme and the last step within glycolysis. Four mammalian isozymes are known, L (liver), R (red blood cells), M1 (adult) and M2 (fetal tissues and tumor cells), which exist in either active tetramers or inactive dimers [56-58]. Actually, in tumor cells PKM2 occurs in dimers with low enzymatic activity, shifting glycolysis towards lactate production instead of entering TCA cycle. Formation of the dimer is supposed to be controlled by the phosphorylation of tyrosine<sup>105</sup> (Y<sup>105</sup>). Interestingly, the ratio of PKM1 versus PKM2 showed a slight increase of PKM2 detected by 1D-GeLC/MSMS in our dataset. Furthermore WB showed an increase of total PKM2 after 10 minutes and a similar abundance after 48 hours. Elevated phosphorylation of PKM Y<sup>105</sup> was already detectable after 2 minutes and lasted for at least 48 hours (Figure 22B).

A

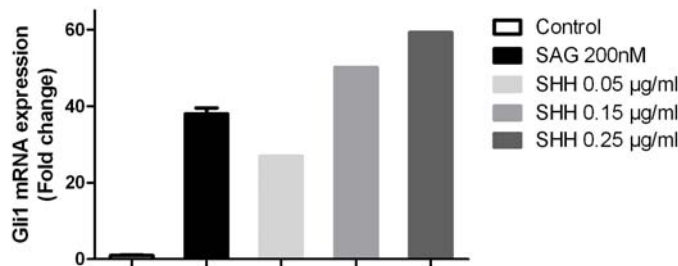
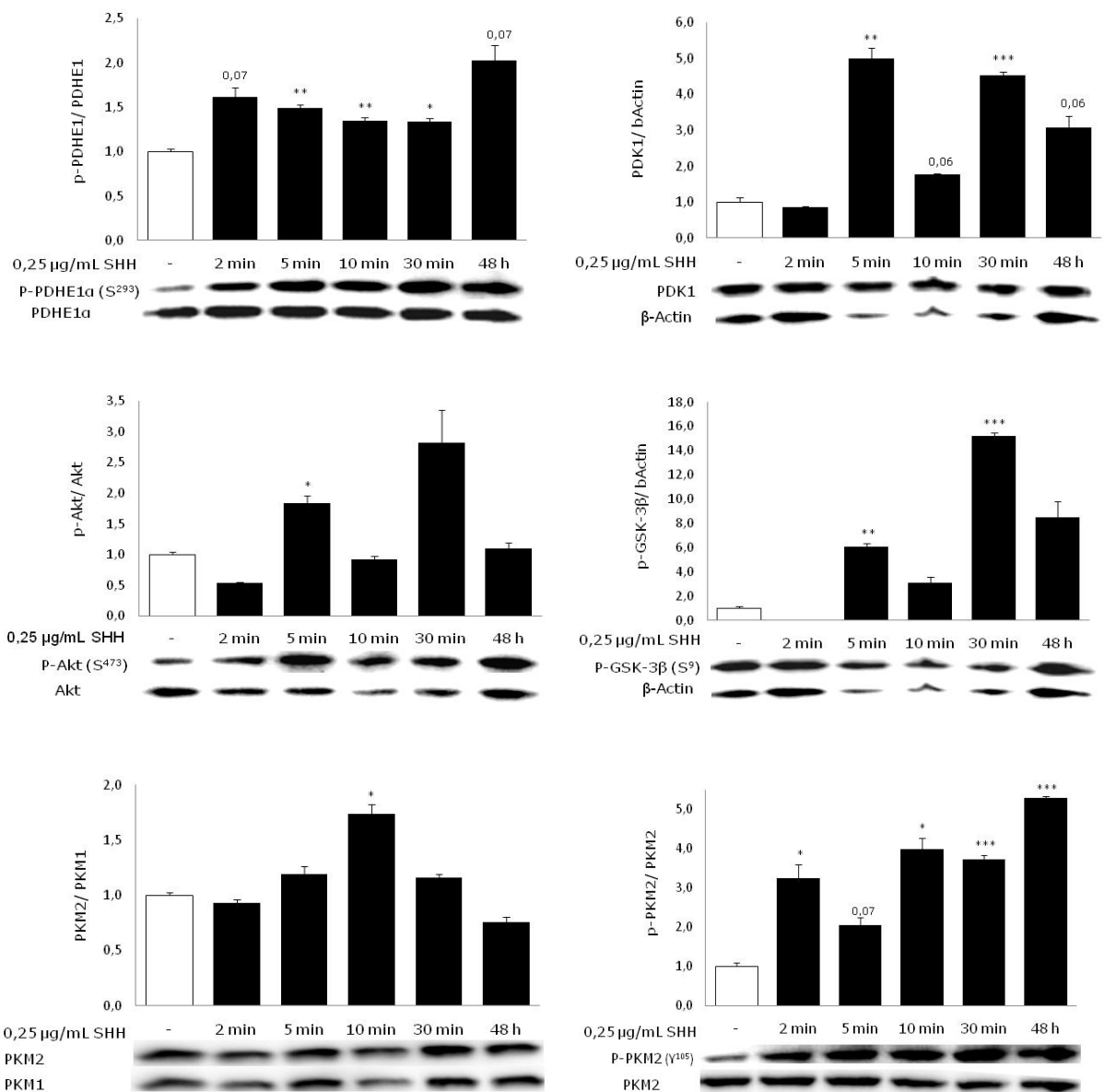


**Figure 22: Validation of HH triggered reprogramming of cellular energy metabolism**

(A) mRNA level of GLI1 were measured by quantitative RT-PCR analysis and normalized to Rplp0. (B) Representative Western blot of whole-cell lysates. Data are presented as mean  $\pm$  SEM, n = 3. \* $p$  < 0.05, \*\*  $p$  < 0.01, \*\*\* $p$  < 0.001.

(P)-PDHE1 $\alpha$ , (phospho) pyruvate dehydrogenase E1 $\alpha$ ; PDK1, pyruvate dehydrogenase kinase 1; (P)-AKT, (phospho)-protein-serine kinase B alpha; p-GSK3 $\beta$ , phospho-glycogen synthase kinase 3 $\beta$ ; (P)-PKM2, (phospho) pyruvate kinase M2; PKM1, pyruvate kinase M1;  $\beta$ -Actin as loading control; SHH, Sonic hedgehog

B



Measurements of glucose uptake and lactate production validated our findings (with the aid of Raffaele Teperino). HH activation in adipocytes resulted in a 5-fold increase in glucose uptake and an 10-fold increased in lactate production (Figure 23A, B). Determination of  $\text{NAD}^+/\text{NADH}$  ratios exhibited higher  $\text{NAD}^+$  levels, confirming the shift from pyruvate to lactate (Figure 23C). Increased  $\text{NADP}^+$  levels might reflect lower FA synthesis (Figure 23D).

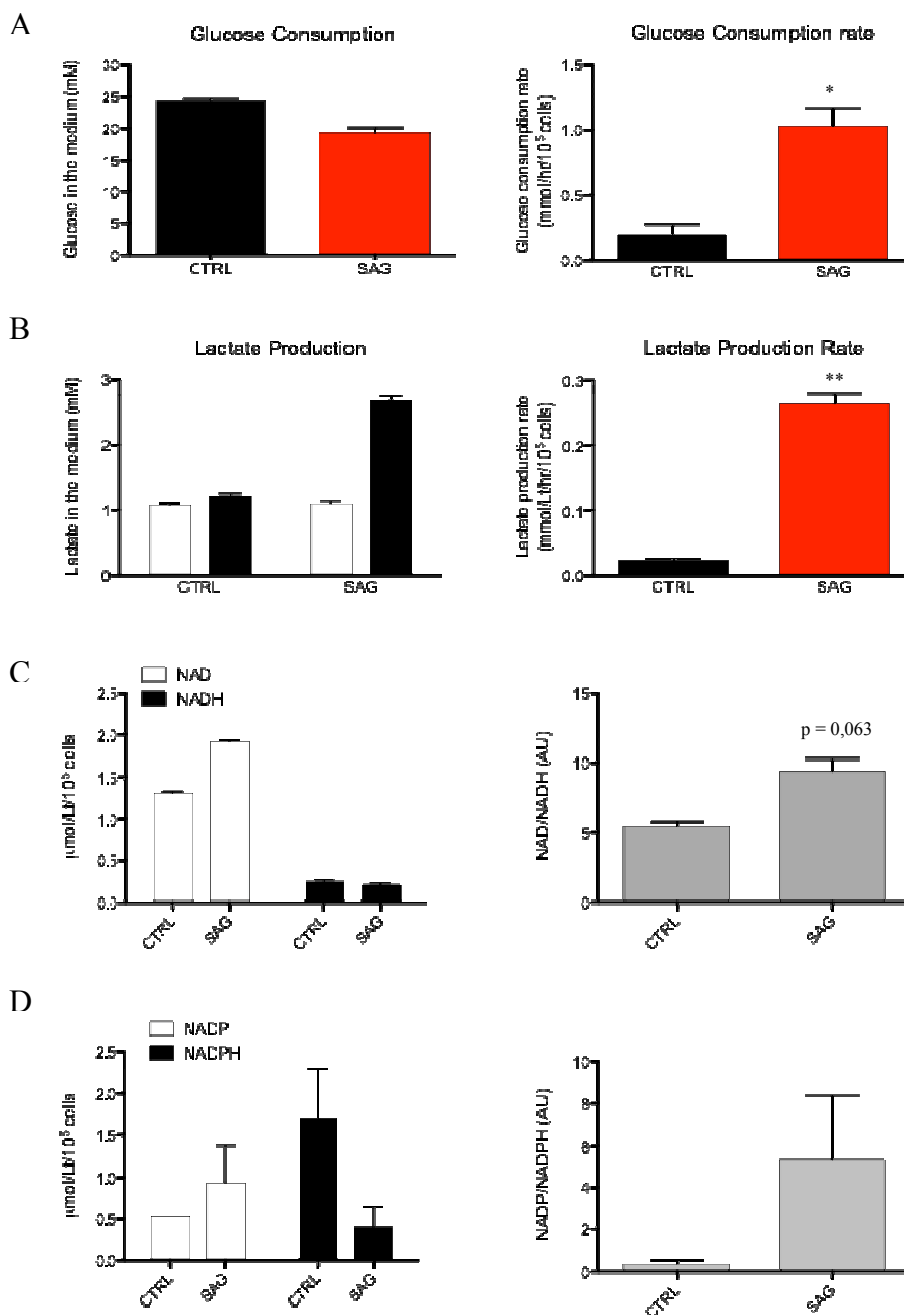


**Figure 23: Cellular metabolites in SAG treated 3T3-L1 adipocytes**

(A) Glucose consumption and (B) lactate production rate measured by ELISA.

(C) Colorimetric determination of  $\text{NAD}^+/\text{NADH}$  and (D)  $\text{NADP}^+/\text{NADPH}$  ratios.

Data are presented as mean  $\pm$  SEM, n = 3; \* $p < 0.05$ , \*\* $p < 0.01$ .

## 5. DISCUSSION AND CONCLUSION

Hedgehog signaling is a fundamental developmental pathway directing embryonic differentiation and adult tissue homeostasis through stem cell regulation and guidance of complex differentiation programs [59]. We and others have demonstrated that HH is important in adipose tissue differentiation in vitro and in vivo and that expression of HH target genes is significantly decreased in adipose tissue of genetic and diet-induced obese mouse models [13, 14]. In detail we identified the HH pathway as a master regulator of white and brown adipose tissue development in a genome-wide RNAi screen in drosophila [13]. Mice with a fat-specific HH-activation showed almost complete loss of white adipose tissue, whereas development of brown adipose tissue was not affected. Despite the WAT-specific lipotrophy these mice exhibited normal glucose tolerance and insulin sensitivity. Interestingly, they revealed enhanced glucose uptake in the remaining white adipose tissue. Obesity is related to a chronic low-grade inflammation leading to metabolic dysfunction, including insulin resistance. Furthermore, in addition to macrophages, the number of T cells and its secreted cytokine IFN- $\gamma$  is elevated in adipose tissue in obesity. Based on our latest findings and the notion of a persistent inhibition of the pathway in obesity, we further investigated the role of HH in adipogenesis in combination with the pro-inflammatory cytokine IFN- $\gamma$  [43]. We could demonstrate for the first time a novel antagonistic cross-talk between IFN- $\gamma$  and HH by directly inhibiting HH in (pre)-adipocytes in vitro and in AT in vivo through the activated T cell cytokine IFN- $\gamma$ .

However, no studies have so far addressed the impact of HH on mature adipocytes. A few groups focused on HH in adipocyte maturation of human mesenchymal stem cells [60, 61]. Most of the HH research to date focused on human cancer and therapies [10, 11], the role in neural cell-fate specification or differentiation elsewhere in the nervous system [62, 63], or on signal transduction involving the primary cilium [23, 64]. To the best of our knowledge there are no data available on HH in mature adipocytes and no study ever profiled the pathway using quantitative (phospho)-proteomic approaches. Therefore we set out to address both aspects and made use of quantitative proteomic approaches to elucidate new HH targets and mechanisms in mature adipocytes.

In this study, we used high resolution quantitative proteomics technologies to discover both phospho-protein and lasting expression changes. 2D-PAGE has often been used to compare protein expression patterns between different samples. This method is also useful to compare phospho-protein enriched samples, but it is labor-intensive and time-consuming and therefore not often used. However, exactly this method provided us with the identification of PDHA1, a key enzyme in cellular energy metabolism with different phosphorylation sites and states. This data demonstrate the power of phospho-protein specific 2D-PAGE as this information was lost in our mass spectrometry based approach. Screening by 1D-GeLC/MSMS not only proofed the high impact on metabolism, it also revealed deeper insights and provided new working points. Though, phospho-proteomics alone does not generate information on lasting alterations. Therefore expression proteomics critically expanded our dataset and insights into HH induced changes on the adipocyte proteome. Taken together our results emphasize the importance of profiling post translational modifications (PTM) in unveiling complex metabolic issues, whereas expression proteomics provided critical information on lasting protein alterations. Therefore, the combined measurements of the phospho- and cytoplasmic-proteome performed by 2D-PAGE and 1D-GeLC/MSMS show the power of the integrating approach. Overall, this combination strategy yielded more reliable information, which might otherwise be missed if only one of the approaches would have been used.

We could identify about 250 phospho-proteins by both 2D-PAGE and 1D-GeLC/MSMS and 2600 proteins by expression proteomics with an overlap of 93% between these two settings (Figure 6B-C; 15A-C). Comparative analysis of our cytoplasmic-expression proteome against the largest set for 3T3-L1 adipocytes published to date by Adachi et al. [5] revealed an overlap of 62% (Figure 15D). However about 1000 unique proteins were observed by our technique whereas 1500 were unique to Adachi et al. The difference in cell fractions and used mass spectrometers, may explain unique proteins identified by both techniques. Interestingly, comparison against a human adipocyte proteome published by Xie et al. [2] showed an 73% overlap (Figure 15D), illustrating the high homology of our murine model system with human adipocytes.

Otto Warburg and co-workers showed already in the 1920s that under aerobic conditions tumor tissue metabolize approximately 10-fold more glucose to lactate than normal tissue [4]. A phenomenon now termed “Warburg effect”. A lot has happened since this seminal

discovery and it is nowadays accepted that this strongly induced aerobic glycolytic state is only one aspect that results from a complex metabolic rearrangement. It is not only glycolysis, but also the TCA cycle, and anabolic metabolism in general that are reprogrammed [65]. The primary function of the Warburg effect and aerobic glycolysis is to provide fast growing cells (e.g. cancer cells) with enough building blocks and reducing equivalents to support cell growth and division. Therefore macromolecular precursors such as acetyl-CoA for FA, glycolytic intermediates for amino acids and ribose for nucleotides are more essential than a high production of ATP in mitochondria (Figure 24).

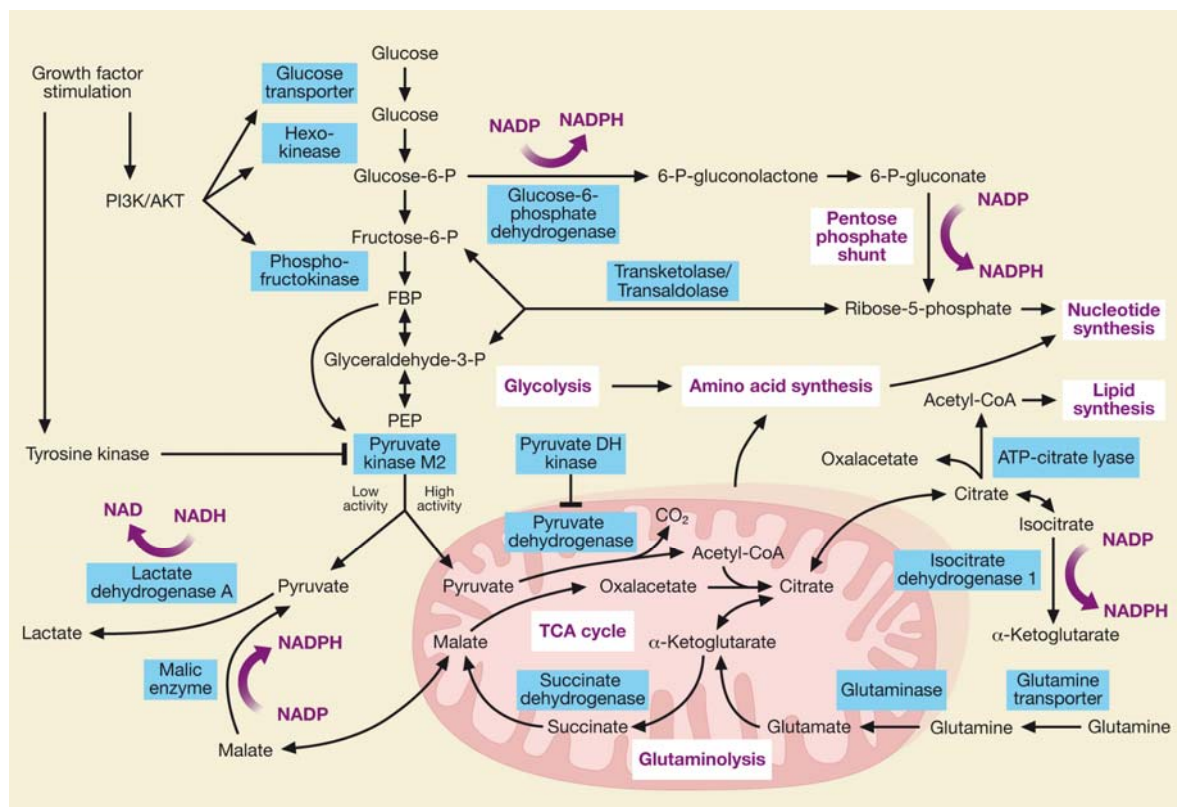


**Figure 24:** Schematic illustration of aerobic glycolysis (Warburg effect), Vander Heiden 2009, modified [4].

Our results obtained in HH stimulated adipocyte showed a Warburg-like effect. Elevated glucose turnover, indicated by higher insulin-like action, increased PFK, higher levels of lactate production, and inhibitory phosphorylation of PKM2 are all in line with a classical Warburg effect. Furthermore higher levels of PDK1 and increased phosphorylation of its substrate PDHA1 by HH, represents another hallmark of aerobic glycolysis. However, our data also suggest a down-regulation of FA synthesis, an up-regulation of  $\beta$ -oxidation and an increased glycogen metabolism build-up which is not in agreement with the anabolic



metabolism of the Warburg effect. Of note, our data also suggest a decrease in mitochondrial function and hence respiratory chain and OXPHOS. These major impacts of HH on adipocyte energy metabolism are shown in our current working model (Figure 25). Individual steps, future aspects and a possible clinical relevance for obesity and its related disorders like insulin resistance are discussed below.

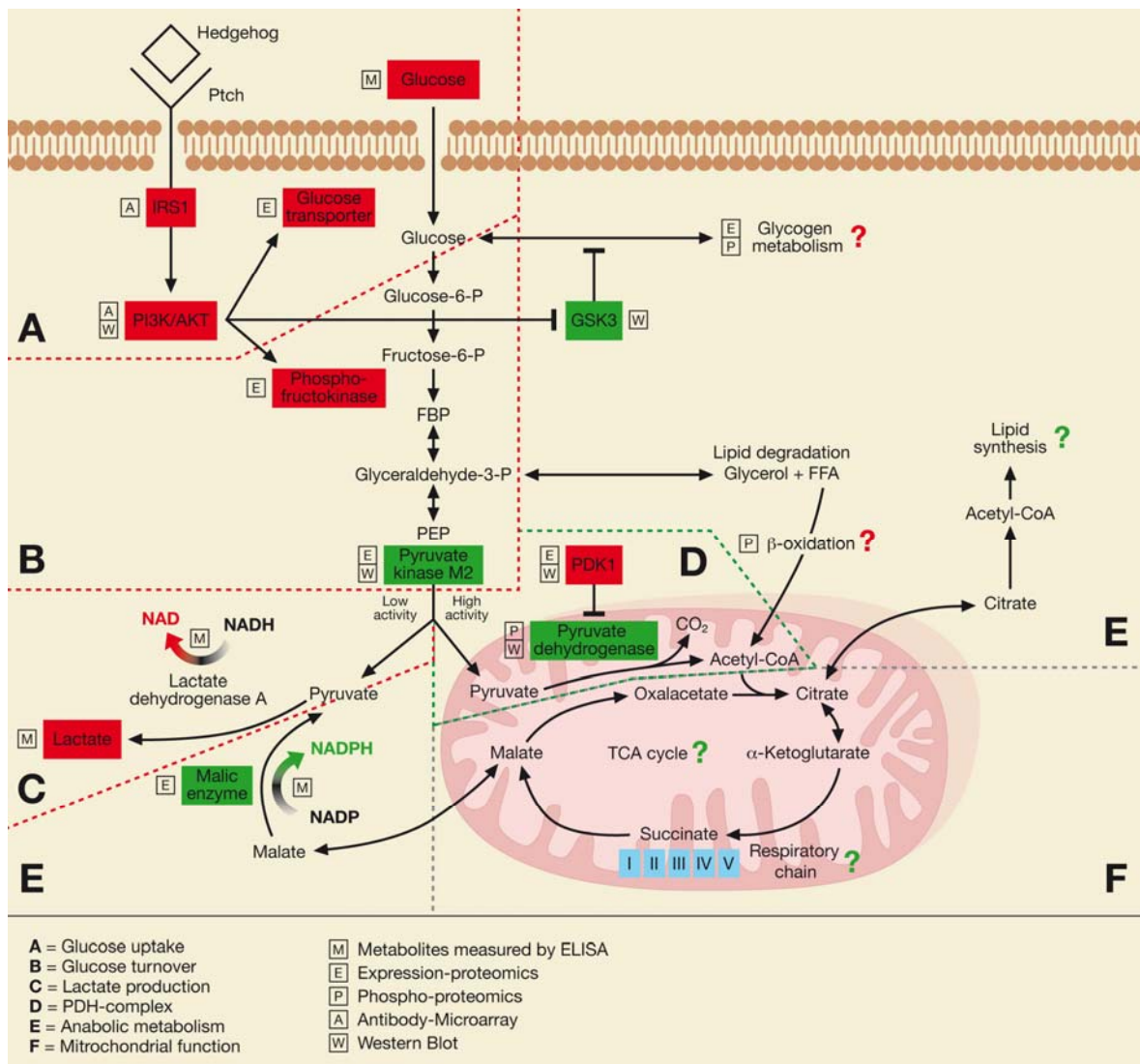


**Figure 25: Current working model of Hh stimulated adipocytes**

Red represents up-regulations and green down-regulations by Hh. Figure is based on Vander Heiden, 2009

First, we observed elevated insulin-like action and glucose uptake in HH stimulated adipocytes (Glucose uptake, Figure 25A). Upon stimulation of insulin receptor, the glucose transporter GLUT4 translocates from intracellular compartments to the adipocyte plasma membrane to increase uptake of glucose. Vesicle-associated membrane proteins (VAMPs) are known to be involved in this process [66]. Interestingly, VAMP3 showed a 4-fold up-



regulation in the expression proteome. However VAMP3 expression data do not necessarily imply a role of HH on GLUT4 translocation. Thus, direct testing of GLUT4 translocation by immunocytochemistry or similar methods will be necessary to proof our hypothesis of increased GLUT4 shuttling [67]. Interestingly, further in depth analysis of our dataset revealed a highly significant enrichment of insulin action ( $p = 1.44E-05$ ). Insulin action activates IRS1 and the PI3/AKT pathway. Antibody microarray data and WB confirmed tyrosine phosphorylation, and therefore activation of IRS-1. Next, measurements of cellular glucose consumption rates by ELISA showed increased glucose turnover in HH treated adipocytes. Of note, our findings were insulin-independent. Thus, we were able to identify by four different techniques (proteomics, antibody microarrays, WB and ELISA) an insulin-like action and glucose uptake by HH.

Beside higher glucose uptake, adipocyte glucose turnover in general was increased (Glucose turnover, Figure 25B). Expression proteomics identified the glycolytic key enzyme PFK to be 2-fold up-regulated in HH treated samples. PFK catalyzes the reaction of fructose-6-phosphate (F6P) to fructose-1,6-bisphosphate (FBP) and is the rate limiting step in glycolysis. Next the final step in glycolysis, the conversion of phosphoenolpyruvate (PEP) to pyruvate by pyruvate kinase (PKM) showed an interesting alteration. Of note, in adipocytes the PKM isozyme M2, typical assumed to be found in fetal tissue and fast growing tumor cells [68], showed similar abundance as the isozyme M1. This is in contrast to most other adult tissues that are typically expressing only the PKM1 variant [69]. WB verified this long-term observation and even revealed a significant up-regulation of PKM2 compared to PKM1 after 10 minutes. Furthermore, PKM showed a phosphorylation at S<sup>105</sup> starting from 2 minutes and lasting over 48 hours. This phosphorylation site has primarily been attributed to cancer metabolism and the Warburg effect, as it seems to cause the switch of an active tetrameric PKM to a less active dimeric PKM form. Several onco-proteomic studies consistently reported PKM2 alterations in a variety of tumor types and linked their findings to the Warburg effect [56, 57, 68]. Furthermore, FBP, the product of PFK, allosterically activates PKM2 but not PKM1 [70]. This is an important feed forward mechanism, linking two rate-limiting steps in glycolysis and thereby enabling coordinated glycolytic flux in tumor cells. Ultimately, as a result of PKM phosphorylation glycolysis is shifted towards aerobic lactate production [58, 71]. We also observed increased lactate and NAD<sup>+</sup> levels in adipocytes (Figure 25C). Thus, our HH activated adipocyte dataset closely mimics a classical cancer metabolism signature, consisting of (i) higher glucose turnover,

indicated by up-regulation of PFK and serine phosphorylation of PKM2, and (ii) a shift of glycolysis towards aerobic lactate production.

Furthermore not only PKM2 was inhibited by phosphorylation. The critical interface between glycolysis and the TCA cycle was also inhibited by phosphorylation. We detected by 2D-PAGE and 1D-GeLC/MSMS a highly reproducible phosphorylation of PDHA1 in HH treated samples (PDH-complex, Figure 25D). Phosphorylated PDHA1 decreases glucose oxidation by blocking the conversion of pyruvate to acetyl-CoA [72]. In line with this data we observed a significant up-regulation of its kinase (PDK1). This regulation of PDC activity provides another convenient way for cells to divert pyruvate into anabolic pathways and is beside PKM2 another hallmark of aerobic glycolysis [72]. Furthermore PDK1 is a hypoxia-inducible factor-1 $\alpha$  (HIF-1 $\alpha$ ) regulated gene [68, 72]. HIF-1 $\alpha$  is a transcription factor (TF) and plays an essential role in cellular and systemic responses to hypoxia. Interestingly, it has been shown, that HIF-1 $\alpha$  speeds up tumorigenesis by activating glycolysis through PDK1, as well as by decreasing mitochondrial action. Therefore, more detailed examination on the expression of HIF-1 $\alpha$  will be necessary to obtain deeper insights on signaling pathways involved in a HH mediated Warburg effect in adipocytes.

Of note, pathway analysis and functional categorizations of our proteomics data indicated a significant impact on mitochondrial function and hence on TCA cycle and OXPHOS, but different to the classical Warburg effect (Mitochondrial function, Figure 25F). First, due to the insufficient supply of acetyl-CoA observed in our and several cancer related studies, TCA cycle function could be decreased. Enzymes like isocitrate dehydrogenase (IDH), succinate dehydrogenase (SDH) and fumarate hydratase (FH) function as tumor suppressors in cancer cell metabolism [73]. IDH, which converts isocitrate to  $\alpha$ -ketoglutarate, provide NADPH for FA synthesis and is up-regulated in tumors. In contrast SDH and FH are down-regulated as accumulation of their substrates succinate and fumarate leads to inhibition of antioncogenic enzymes [73]. Interestingly, we identified the aforementioned enzymes including several isoforms and subunits, but we did not observe any alterations. Furthermore we found an increase of aconitate hydratase in the autoradiography 2D-gel, indicating a higher rate of synthesis. This enzyme catalyzes the isomerization of citrate to isocitrate. However, we could not observe any alterations at the expression level. This missing regulation at the expression level could be based on the

lacking acetyl-CoA, whereas the increase of synthesis suggests a setup of the cell itself for a possible nutrient future resupply. Such an observation might be unusual for cancer cells as they are supposed to increase glutaminolysis to replenish substrates of the TCA cycle to supply enough building blocks for amino acid and nucleotide synthesis [69]. Therefore, high levels of glutamine are an essential bioenergetic and anabolic substrate for many cancer cell types. In contrast, our dataset did not show an increase in glutaminolysis and/or amino acid and nucleotide synthesis. Hence, our observations suggest a decrease in TCA cycle dependent building blocks in adipocytes, which is in contrast to the classical Warburg effect. Further investigations on oncometabolites such as succinate and fumarate and on glutamine/glutamate flux, will be necessary to exactly elucidate HH mediated TCA cycle alterations in compared to classical cancer cell alterations. Second, mitochondrial respiratory chain has been shown to be decreased in cancer metabolism [68]. More precisely, inhibition of SDH, alterations in the cytochrome c oxidase subunit levels and the down-regulation of the catalytic subunit of the mitochondrial H<sup>+</sup>-ATP synthase ( $\beta$ -F1-ATPase), suppress respiratory chain complexes II, IV and V [68]. In fact, our data showed that mitochondrial proteins and function were significantly altered. Pathway analysis showed a significant decrease in respiratory chain and OXPHOS. Interestingly, functional categorization revealed (i) protein import into mitochondrial inner membrane and (ii) electron transport chain in HH treated adipocytes as most significant decreased biological processes. However, in depth investigations revealed a more complex situation. Several proteins involved in complex I to V showed opposite regulations, especially in complex I. Based on these findings we are at the moment not able to give any reliable information on the regulation of mitochondrial action of HH treated adipocytes. Of note, the hallmarks of cancer metabolism  $\beta$ -F1-ATPase and cytochrome c oxidase were not altered. To discover the explicit role of HH on mitochondrial function in adipocytes further investigation will be needed. Quantification of mitochondrial DNA, determination of mitochondrial mass and coupling as well as mitochondria-enriched proteomics should help us to elucidate the exact role of HH on mitochondrial function.

Finally, analysis of the phospho- and expression-proteome suggests a negative impact of HH on anabolic metabolism that is in contrast to a classic Warburg effect (Anabolic metabolism, Figure 25E). Our proteomics data suggest that glycogen synthesis might be up-regulated, which would be in line with inactivation of GSK3 $\beta$  by AKT. Glycogen functions as important energy storage and is primarily made by the liver and the muscles.

Thus, further investigation on glycogen metabolism *in vitro* and *in vivo* will be necessary, to elucidate the exact mechanism and function of glycogen storage by quiescent adipocyte. Lipid metabolism showed a diverse phenomenon compared to the Warburg effect. Our data provide some initial hints of a decreased FA synthesis. First, the main resources for lipid formation acetyl-CoA and NADPH are both down in HH treated adipocytes. Acetyl-CoA is expected to be lacking through the prolonged inhibition of PKM2 and PDHA1, and the missing evidence of higher rates of glutaminolysis. ELISA tests confirmed decreased amounts of NADPH, a cofactor that provides reducing equivalents in many anabolic reactions. This is unexpected since the PKM2/PDHA1 promoted switch of glycolysis, should increase the pentose phosphate pathway (PPP) and its products ribose and NADPH. However, our proteomic analysis also identified a down-regulation of malic enzyme, which converts malate to pyruvate by reducing  $\text{NADP}^+$  to NADPH, a finding that might explain the overall net decrease in NADPH. Second, FA synthase catalyzes the formation of long-chain fatty acids and 2D-PAGE revealed an increase in *de-novo* synthesis, but no regulation at the expression profile. In cancer metabolism FA synthesis was shown to be increased [69]. Thus, as already indicated by converse alterations in the TCA cycle, lipid formation seemed to be suppressed. In contrast, several enzymes involved in lipid degradation, more precisely  $\beta$ -oxidation displayed an up-regulation. Although not tested yet, the breakdown of FA may provide the acetyl-CoA needed to replenish the TCA cycle. Despite the fact, that all our proteomics data clearly support the hypothesis that FA synthesis is decreased and FA oxidation increased in HH treated adipocytes further studies will be necessary to proof this concept. Metabolic flux studies by the Seahorse Extracellular Flux Analyzer will provide the detailed information, since it profiles the metabolic activity of cells by determining real time oxygen consumption and proton production.

Taken together, we observed that upon HH stimulation non-proliferating, mature adipocytes mimic several aspects of the classical Warburg effect, by boosting (i) glucose uptake and (ii) turnover and (iii) lactate production. However these observations did not result in the switch to anabolic metabolism that is typically found in cancer cells relying on the Warburg effect. Actually, our results are consistent with human and mouse data showing a release of lactate from AT after glucose ingestion, which in a healthy state is taken up by the liver and converted to glycogen and triglycerides [74]. During obesity it has been suggested that high levels of circulating lactate contribute to insulin resistance by

decreasing glucose utilization by skeletal muscle and enhancing hepatic gluconeogenesis [74]. Interestingly, Munoz et al. described a transgenic mouse model displaying not only increased glucose uptake but also glycolytic flux by over-expressing the enzyme glucokinase [74]. They found higher lactate production but improved insulin sensitivity, rather than fat accumulation and obesity. We presume that HH activated adipocytes mimic a similar effect, i.e. increased glucose turnover, lactate production, but decreased lipid synthesis. Therefore, this novel aspect of non-canonical HH signaling may represent an exciting therapeutic target for treating obesity and type 2 diabetes. In addition future studies will have to address whether blocking of non-canonical HH signaling in cancer cells inhibits the Warburg effect and thus might be exploited to treat cancer.

In summary, our unbiased (phospho)-proteomic screen identified HH as a hitherto unknown regulator of cellular energy metabolism, leading to increased glucose turnover and lactate production.

## 6. REFERENCES

1. Deng, W.J., et al., *Proteome, phosphoproteome, and hydroxyproteome of liver mitochondria in diabetic rats at early pathogenic stages*. Mol Cell Proteomics, 2009. **9**(1): p. 100-16.
2. Xie, X., et al., *Characterization of the Human Adipocyte Proteome and Reproducibility of Protein Abundance by One-Dimensional Gel Electrophoresis and HPLC-ESI-MS/MS*. J Proteome Res, 2010. **9**(9): p. 4521-34.
3. Taniguchi, C.M., B. Emanuelli, and C.R. Kahn, *Critical nodes in signalling pathways: insights into insulin action*. Nat Rev Mol Cell Biol, 2006. **7**(2): p. 85-96.
4. Vander Heiden, M.G., L.C. Cantley, and C.B. Thompson, *Understanding the Warburg effect: the metabolic requirements of cell proliferation*. Science, 2009. **324**(5930): p. 1029-33.
5. Adachi, J., et al., *In-depth analysis of the adipocyte proteome by mass spectrometry and bioinformatics*. Mol Cell Proteomics, 2007. **6**(7): p. 1257-73.
6. Ingham, P.W. and A.P. McMahon, *Hedgehog signaling in animal development: paradigms and principles*. Genes Dev, 2001. **15**(23): p. 3059-87.
7. Varjosalo, M. and J. Taipale, *Hedgehog signaling*. J Cell Sci, 2007. **120**(Pt 1): p. 3-6.
8. Varjosalo, M. and J. Taipale, *Hedgehog: functions and mechanisms*. Genes Dev, 2008. **22**(18): p. 2454-72.
9. King, P.J., L. Guasti, and E. Laufer, *Hedgehog signalling in endocrine development and disease*. J Endocrinol, 2008. **198**(3): p. 439-50.
10. Mimeault, M. and S.K. Batra, *Frequent deregulations in the hedgehog signaling network and cross-talks with the epidermal growth factor receptor pathway involved in cancer progression and targeted therapies*. Pharmacol Rev, 2010. **62**(3): p. 497-524.
11. Yang, L., et al., *Activation of the hedgehog-signaling pathway in human cancer and the clinical implications*. Oncogene, 2009. **29**(4): p. 469-81.
12. Cousin, W., et al., *Hedgehog and adipogenesis: fat and fiction*. Biochimie, 2007. **89**(12): p. 1447-53.
13. Pospisilik, J.A., et al., *Drosophila genome-wide obesity screen reveals hedgehog as a determinant of brown versus white adipose cell fate*. Cell, 2010. **140**(1): p. 148-60.
14. Suh, J.M., et al., *Hedgehog signaling plays a conserved role in inhibiting fat formation*. Cell Metab, 2006. **3**(1): p. 25-34.
15. Wang, Y., A.P. McMahon, and B.L. Allen, *Shifting paradigms in Hedgehog signaling*. Curr Opin Cell Biol, 2007. **19**(2): p. 159-65.
16. Sharghi-Namini, S., et al., *The structural and functional integrity of peripheral nerves depends on the glial-derived signal desert hedgehog*. J Neurosci, 2006. **26**(23): p. 6364-76.
17. Ma, Y., et al., *Hedgehog-mediated patterning of the mammalian embryo requires transporter-like function of dispatched*. Cell, 2002. **111**(1): p. 63-75.
18. Riobo, N.A. and D.R. Manning, *Pathways of signal transduction employed by vertebrate Hedgehogs*. Biochem J, 2007. **403**(3): p. 369-79.

19. Lum, L., et al., *Hedgehog signal transduction via Smoothed association with a cytoplasmic complex scaffolded by the atypical kinesin, Costal-2*. Mol Cell, 2003. **12**(5): p. 1261-74.
20. Ingham, P.W., *Hedgehog signalling*. Curr Biol, 2008. **18**(6): p. R238-41.
21. Rohatgi, R. and M.P. Scott, *Patching the gaps in Hedgehog signalling*. Nat Cell Biol, 2007. **9**(9): p. 1005-9.
22. Ingham, P.W. and A.P. McMahon, *Hedgehog signalling: Kif7 is not that fishy after all*. Curr Biol, 2009. **19**(17): p. R729-31.
23. Tukachinsky, H., L.V. Lopez, and A. Salic, *A mechanism for vertebrate Hedgehog signaling: recruitment to cilia and dissociation of SuFu-Gli protein complexes*. J Cell Biol, 2010. **191**(2): p. 415-28.
24. Aikin, R.A., K.L. Ayers, and P.P. Therond, *The role of kinases in the Hedgehog signalling pathway*. EMBO Rep, 2008. **9**(4): p. 330-6.
25. Stanton, B.Z., et al., *A small molecule that binds Hedgehog and blocks its signaling in human cells*. Nat Chem Biol, 2009. **5**(3): p. 154-6.
26. Chen, T., et al., *Identification of small-molecule inhibitors of the JIP-JNK interaction*. Biochem J, 2009. **420**(2): p. 283-94.
27. Zehentner, B.K., U. Leser, and H. Burtscher, *BMP-2 and sonic hedgehog have contrary effects on adipocyte-like differentiation of C3H10T1/2 cells*. DNA Cell Biol, 2000. **19**(5): p. 275-81.
28. Tocci, A. and L. Forte, *Mesenchymal stem cell: use and perspectives*. Hematol J, 2003. **4**(2): p. 92-6.
29. Rodriguez, A.M., et al., *Adipocyte differentiation of multipotent cells established from human adipose tissue*. Biochem Biophys Res Commun, 2004. **315**(2): p. 255-63.
30. Gregor, M.F. and G.S. Hotamisligil, *Inflammatory Mechanisms in Obesity*. Annu Rev Immunol, 2011.
31. Kopelman, P.G., *Obesity as a medical problem*. Nature, 2000. **404**(6778): p. 635-43.
32. Balistreri, C.R., C. Caruso, and G. Candore, *The role of adipose tissue and adipokines in obesity-related inflammatory diseases*. Mediators Inflamm, 2010. **2010**: p. 802078.
33. Rosen, E.D. and B.M. Spiegelman, *Adipocytes as regulators of energy balance and glucose homeostasis*. Nature, 2006. **444**(7121): p. 847-53.
34. Calabro, P. and E.T. Yeh, *Obesity, inflammation, and vascular disease: the role of the adipose tissue as an endocrine organ*. Subcell Biochem, 2007. **42**: p. 63-91.
35. Farmer, S.R., *Obesity: Be cool, lose weight*. Nature, 2009. **458**(7240): p. 839-40.
36. Hotamisligil, G.S., N.S. Shargill, and B.M. Spiegelman, *Adipose expression of tumor necrosis factor-alpha: direct role in obesity-linked insulin resistance*. Science, 1993. **259**(5091): p. 87-91.
37. Guilherme, A., et al., *Adipocyte dysfunctions linking obesity to insulin resistance and type 2 diabetes*. Nat Rev Mol Cell Biol, 2008. **9**(5): p. 367-77.
38. Rosen, E.D. and O.A. MacDougald, *Adipocyte differentiation from the inside out*. Nat Rev Mol Cell Biol, 2006. **7**(12): p. 885-96.
39. Farmer, S.R., *Transcriptional control of adipocyte formation*. Cell Metab, 2006. **4**(4): p. 263-73.

40. Lefterova, M.I. and M.A. Lazar, *New developments in adipogenesis*. Trends Endocrinol Metab, 2009. **20**(3): p. 107-14.
41. Wang, Y.X., *PPARs: diverse regulators in energy metabolism and metabolic diseases*. Cell Res, 2010. **20**(2): p. 124-37.
42. Green, H. and O. Kehinde, *An established preadipose cell line and its differentiation in culture. II. Factors affecting the adipose conversion*. Cell, 1975. **5**(1): p. 19-27.
43. Todoric, J., et al., *Cross-Talk Between Interferon- $\gamma$  and Hedgehog Signaling Regulates Adipogenesis*. Diabetes, 2011.
44. Haudek, V.J., et al., *Proteome maps of the main human peripheral blood constituents*. J Proteome Res, 2009. **8**(8): p. 3834-43.
45. Wessel, D. and U.I. Flugge, *A method for the quantitative recovery of protein in dilute solution in the presence of detergents and lipids*. Anal Biochem, 1984. **138**(1): p. 141-3.
46. Rabilloud, T., et al., *A comparison between Sypro Ruby and ruthenium II tris (bathophenanthroline disulfonate) as fluorescent stains for protein detection in gels*. Proteomics, 2001. **1**(5): p. 699-704.
47. Haudek, V.J., et al., *Consequences of Acute and Chronic Oxidative Stress upon the Expression Pattern of Proteins in Peripheral Blood Mononuclear Cells*. J Proteome Res, 2008.
48. Mortz, E., et al., *Improved silver staining protocols for high sensitivity protein identification using matrix-assisted laser desorption/ionization-time of flight analysis*. Proteomics, 2001. **1**(11): p. 1359-63.
49. Mortensen, P., et al., *MSQuant, an open source platform for mass spectrometry-based quantitative proteomics*. J Proteome Res, 2010. **9**(1): p. 393-403.
50. MacLaine, N.J. and T.R. Hupp, *How phosphorylation controls p53*. Cell Cycle, 2011. **10**(6): p. 916-21.
51. Kowluru, A., S. Klumpp, and J. Krieglstein, *Protein histidine [de]phosphorylation in insulin secretion: abnormalities in models of impaired insulin secretion*. Naunyn Schmiedebergs Arch Pharmacol, 2011.
52. Choi, S., et al., *Comparative proteome analysis using amine-reactive isobaric tagging reagents coupled with 2D LC/MS/MS in 3T3-L1 adipocytes following hypoxia or normoxia*. Biochem Biophys Res Commun, 2009. **383**(1): p. 135-40.
53. Dave, R.K., et al., *Sonic hedgehog and notch signaling can cooperate to regulate neurogenic divisions of neocortical progenitors*. PLoS One, 2011. **6**(2): p. e14680.
54. Schreck, K.C., et al., *The Notch target Hes1 directly modulates Gli1 expression and Hedgehog signaling: a potential mechanism of therapeutic resistance*. Clin Cancer Res, 2010. **16**(24): p. 6060-70.
55. Wei, L. and Z. Xu, *Cross-signaling among phosphoinositide-3 kinase, mitogen-activated protein kinase and sonic hedgehog pathways exists in esophageal cancer*. Int J Cancer, 2010.
56. Christofk, H.R., et al., *The M2 splice isoform of pyruvate kinase is important for cancer metabolism and tumour growth*. Nature, 2008. **452**(7184): p. 230-3.
57. Christofk, H.R., et al., *Pyruvate kinase M2 is a phosphotyrosine-binding protein*. Nature, 2008. **452**(7184): p. 181-6.



58. Hitosugi, T., et al., *Tyrosine phosphorylation inhibits PKM2 to promote the Warburg effect and tumor growth*. *Sci Signal*, 2009. **2**(97): p. ra73.
59. Hooper, J.E. and M.P. Scott, *Communicating with Hedgehogs*. *Nat Rev Mol Cell Biol*, 2005. **6**(4): p. 306-17.
60. Fontaine, C., et al., *Hedgehog signaling alters adipocyte maturation of human mesenchymal stem cells*. *Stem Cells*, 2008. **26**(4): p. 1037-46.
61. Plaisant, M., et al., *Inhibition of hedgehog signaling decreases proliferation and clonogenicity of human mesenchymal stem cells*. *PLoS One*, 2011. **6**(2): p. e16798.
62. Mainwaring, L.A. and A.M. Kenney, *Divergent functions for eIF4E and S6 kinase by sonic hedgehog mitogenic signaling in the developing cerebellum*. *Oncogene*, 2010.
63. Parathath, S.R., et al., *Insulin receptor substrate 1 is an effector of sonic hedgehog mitogenic signaling in cerebellar neural precursors*. *Development*, 2008. **135**(19): p. 3291-300.
64. Chen, Y., et al., *Dual Phosphorylation of Suppressor of Fused (Sufu) by PKA and GSK3{beta} Regulates Its Stability and Localization in the Primary Cilium*. *J Biol Chem*, 2011. **286**(15): p. 13502-11.
65. Koppenol, W.H., P.L. Bounds, and C.V. Dang, *Otto Warburg's contributions to current concepts of cancer metabolism*. *Nat Rev Cancer*, 2011. **11**(5): p. 325-37.
66. Zhao, P., et al., *Variations in the requirement for v-SNAREs in GLUT4 trafficking in adipocytes*. *J Cell Sci*, 2009. **122**(Pt 19): p. 3472-80.
67. Koshy, S., et al., *Quantitative measurement of GLUT4 translocation to the plasma membrane by flow cytometry*. *J Vis Exp*, 2010(45).
68. Scatena, R., et al., *Revisiting the Warburg effect in cancer cells with proteomics. The emergence of new approaches to diagnosis, prognosis and therapy*. *Proteomics Clin Appl*, 2010. **4**(2): p. 143-58.
69. Cairns, R.A., I.S. Harris, and T.W. Mak, *Regulation of cancer cell metabolism*. *Nat Rev Cancer*, 2011. **11**(2): p. 85-95.
70. Tennant, D.A., R.V. Duran, and E. Gottlieb, *Targeting metabolic transformation for cancer therapy*. *Nat Rev Cancer*, 2010. **10**(4): p. 267-77.
71. Dang, C.V., *PKM2 tyrosine phosphorylation and glutamine metabolism signal a different view of the Warburg effect*. *Sci Signal*, 2009. **2**(97): p. pe75.
72. McFate, T., et al., *Pyruvate dehydrogenase complex activity controls metabolic and malignant phenotype in cancer cells*. *J Biol Chem*, 2008. **283**(33): p. 22700-8.
73. Frezza, C., P.J. Pollard, and E. Gottlieb, *Inborn and acquired metabolic defects in cancer*. *J Mol Med*, 2011. **89**(3): p. 213-20.
74. Munoz, S., et al., *Chronically increased glucose uptake by adipose tissue leads to lactate production and improved insulin sensitivity rather than obesity in the mouse*. *Diabetologia*, 2010. **53**(11): p. 2417-30.

## 7. SUPPLEMENT

### 7.1. Curriculum Vitae

#### Martina Bayer

E-mail: [martina\\_bayer@gmx.at](mailto:martina_bayer@gmx.at)

Mobile phone: +43 650/ 890 77 85

Date of birth: 10/ 02 /1984

Nationality: Austria

#### Work Experience

- 04/ 2008 – present      Medical University of Vienna/ Austria  
 Department of Laboratory Medicine  
 Thesis: “*Quantitative (phospho)-Proteomics identifies a Novel Role for Hedgehog in Reprogramming Adipocyte Energy Metabolism*”
- 09/ 2006 – 08/ 2007      HBLVA für chemische Industrie  
 Rosensteingasse Vienna/ Austria  
 Assistant Professor for Analytic Laboratory
- 02/ 2006 – 07/ 2006      Medical University of Vienna/ Austria  
 Department of Laboratory Medicine  
 Diploma thesis “*Spezifische Effekte der Komplementfaktoren C1 und C3 auf das Zellproteom und Sekretom von primären vaskulären Zellen und deren Relevanz in der Atherogenese*“  
 (Final grade 1.0)
- 10/ 2004 – 02/ 2005      University of Veterinary Medicine Vienna/ Austria  
 Institute for Medical Chemistry  
 Trainee-period    „*Untersuchung von Expressionsmustern immunologisch relevanter Proteine beim Schwein*“  
 (Final grade 1.0)
- Summer 2003 – 2005      Internships:  
 Kwizda Pharma GmbH, Vienna/ Austria – Quality control  
 VetMed Uni Vienna/ Austria – Institute for Medical Chemistry  
 TU Vienna/ Austria – Group Gene Technology

**Education**

04/ 2008 – 07/ 2011	Doctor of Natural Sciences University of Technology, Vienna/ Austria
10/ 2006 – 03/ 2008	Postgraduate studies for Chemical Engineering University of Technology, Vienna/ Austria
03/ 2008	Diploma (Final grade 1.2)
10/ 2004 –07/ 2006	University of Applied Sciences of chemistry and biology Fresenius Idstein/ Germany
07/ 2006	Diploma (Final grade 1.5)
09/ 2002 – 09/ 2004	College of chemistry Rosensteingasse Vienna/ Austria
09/ 2004	Diploma (Final grade 1.5)
09/ 1994 – 06/ 2002	Gymnasium with focus on natural sciences and mathematics Franklinstraße 26, Vienna/ Austria
06/ 2002	Matura (A-level equivalent)

**Computer Skills**

Excellent skills in MS-Office (Word, Excel, PowerPoint, Outlook and EndNote)

Very good skills in Progenesis Same Spot and PG 200, Scaffold, Pathway Studio, ImageJ and TotalLab)

Basic skills in GraphPad Prism and MS Access

**Scientific skills and lab techniques:**

Cell- and molecular biological methods  
RNA/DNA isolation, PCRs, quantitative real-time PCR

Protein biochemical methods  
Protein isolation and isolation of subcellular fractions,  
Western blotting, ELISA

Bioanalytical methods  
2D-PAGE, 1D-GeLC/MSMS, different label strategies  
(label-free, iTRAQ, SILAC, S35)

Cell culture  
Cultivation- and harvest of primary cells and common cell lines

**Language**

German – native

English – fluent

Vienna, June 2011

# *Drosophila* Genome-wide Obesity Screen Reveals Hedgehog as a Determinant of Brown versus White Adipose Cell Fate

J. Andrew Pospisilik,<sup>1,12,13</sup> Daniel Schramek,<sup>1,12</sup> Harald Schnidar,<sup>2</sup> Shane J.F. Cronin,<sup>1</sup> Nadine T. Nehme,<sup>3</sup> Xiaoyun Zhang,<sup>4</sup> Claude Knauf,<sup>5</sup> Patrice D. Cani,<sup>6</sup> Karin Aumayr,<sup>1</sup> Jelena Todoric,<sup>9</sup> Martina Bayer,<sup>9</sup> Arvand Haschemi,<sup>9</sup> Vijitha Puvindran,<sup>4</sup> Krisztina Tar,<sup>9</sup> Michael Orthofer,<sup>1</sup> G. Gregory Neely,<sup>1</sup> Georg Dietzl,<sup>7</sup> Armen Manoukian,<sup>8</sup> Martin Funovics,<sup>10</sup> Gerhard Prager,<sup>11</sup> Oswald Wagner,<sup>9</sup> Dominique Ferrandon,<sup>3</sup> Fritz Aberger,<sup>2</sup> Chi-chung Hui,<sup>4</sup> Harald Esterbauer,<sup>9,\*</sup> and Josef M. Penninger<sup>1,\*</sup>

<sup>1</sup>Institute of Molecular Biotechnology of the Austrian Academy of Science, Dr. Bohrgasse 3, A 1030 Vienna, Austria

<sup>2</sup>Department of Molecular Biology, University of Salzburg, Hellbrunnerstrasse 34, A-5020 Salzburg, Austria

<sup>3</sup>Equipe Fondation Recherche Médicale, UPR 9022 du CNRS, Université de Strasbourg, Institut de Biologie Moléculaire et Cellulaire du CNRS, 15 rue René Descartes F67084 Strasbourg, France

<sup>4</sup>Program in Developmental & Stem Cell Biology, The Hospital for Sick Children, and Department of Molecular Genetics, University of Toronto, Toronto, Ontario M5S 1A8, Canada

<sup>5</sup>INSERM U858, Team 3, Institut de Médecine Moléculaire de Rangueil, Paul Sabatier University, Bat. L4, IFR150, CHU Rangueil, BP 84225, 31432 Toulouse Cedex 4, France

<sup>6</sup>Université catholique de Louvain, LDRI, Unit PMNT-73/69, Av. E. Mounier, 73/69 B-1200 Brussels, Belgium

<sup>7</sup>Howard Hughes Medical Institute, Stanford University, 318 Campus Drive, Stanford, CA 94305, USA

<sup>8</sup>Ontario Cancer Institute/Princess Margaret Hospital, 610 University Avenue, Toronto, Ontario M5G 2M9, Canada

<sup>9</sup>Department of Medical and Chemical Laboratory Diagnostics

<sup>10</sup>Department of Radiology

<sup>11</sup>Department of Surgery

Medical University Vienna, Waehringer Guertel 18-20, A-1090 Vienna, Austria

<sup>12</sup>These authors contributed equally to this work

<sup>13</sup>Present address: Max Planck Institute of Immunobiology, Stübeweg 51, D-79108 Freiburg, Germany

\*Correspondence: harald.esterbauer@meduniwien.ac.at (H.E.), josef.penninger@imba.oeaw.ac.at (J.M.P.)

DOI 10.1016/j.cell.2009.12.027

## SUMMARY

Over 1 billion people are estimated to be overweight, placing them at risk for diabetes, cardiovascular disease, and cancer. We performed a systems-level genetic dissection of adiposity regulation using genome-wide RNAi screening in adult *Drosophila*. As a follow-up, the resulting ~500 candidate obesity genes were functionally classified using muscle-, oenocyte-, fat-body-, and neuronal-specific knock-down in vivo and revealed hedgehog signaling as the top-scoring fat-body-specific pathway. To extrapolate these findings into mammals, we generated fat-specific hedgehog-activation mutant mice. Intriguingly, these mice displayed near total loss of white, but not brown, fat compartments. Mechanistically, activation of hedgehog signaling irreversibly blocked differentiation of white adipocytes through direct, coordinate modulation of early adipogenic factors. These findings identify a role for hedgehog signaling in white/brown adipocyte determination and link in vivo RNAi-based scanning of the *Drosophila* genome to regulation of adipocyte cell fate in mammals.

## INTRODUCTION

The world health organization (WHO) currently estimates that over 1 billion individuals worldwide are overweight. Almost one-third of these individuals are clinically obese, markedly raising their chances of cardiovascular disease, type 2 diabetes, cancer, and stroke (WHO, 2009). The regulation of body fat content in animals results from the integration of multiple nutrient, sensory, and hormonal inputs primarily at the level of the brain and adipose tissues (Farooqi and O'Rahilly, 2007). This integrative network is influenced not only by genetics but also by circadian rhythm and physical and social environments. Obesity is thus a complex, systems-level disease.

Spurred by the discovery of leptin (Zhang et al., 1994), tremendous progress has been made in identifying the molecular players and pathways regulating adiposity. The impressive bounds made through the study of gene-targeted mice (Speakman et al., 2008) and the tracking of monogenic obesity disorders in humans (Farooqi and O'Rahilly, 2007) have been complemented by studies in lower organisms (Gronke et al., 2005; Leopold and Perrimon, 2007; Schlegel and Stainier, 2007). Virtually all key metabolic regulators examined to date display conserved functions across phyla, including, for instance, insulin signaling, mTOR, and key lipases such as ATGL (Baker and Thummel, 2007; Gronke et al., 2005; Oldham and Hafen, 2003). Similar to mammals, model organisms such as

*Drosophila melanogaster*, *Danio rerio*, and *Caenorhabditis elegans* employ multiple molecular and tissue-based regulatory networks to balance energy needs, nutritional state, and aging and thus represent potent genomics tools for the study of metabolism. For instance, an RNAi feeding model was used to identify potential regulators of fat storage in the *C. elegans* genome (Ashrafi et al., 2003). More recent developments in functional genomics have now harnessed the potential of transgenic RNAi in *Drosophila* to allow both temporal and spatial control of RNAi knockdown at the whole-genome level (Dietzl et al., 2007).

## RESULTS

### An In Vivo High-Throughput Screen for Obesity Genes in *Drosophila*

To identify candidate obesity genes, we performed a genome-wide transgenic RNAi screen for fat content in adult *Drosophila* using a heat shock-inducible Hsp70-GAL4 system (Figure 1A). Triglycerides, the major lipid storage form in animals, were chosen as a direct measure of fly adiposity. Total fly triglyceride levels were measured by colorimetric determination and normalized to protein (Figure 1A). Using this experimental set-up, we were able to track triglyceride changes throughout development as well as to clearly distinguish sex-specific differences in fat content (Figure 1B; Figures S1A and S1B available online) and those induced by varying nutrient availability (Figure 1C). After the first round of screening, double-blinded analysis of RNAi lines targeting genes previously reported to regulate fat content revealed lipid alterations consistent with expected lean (Figure 1D) and obese (Figure 1E) phenotypes. Included were the LSD (lipid storage droplet) and LPD (lipid depleted) genes as well as the *Drosophila* insulin-like peptides (*IIP*'s), the glucagon homolog *akh* and its receptor *akhr*, as well as *adipose* (*adp*), *bubblegum* (*bbg*), and the *Drosophila* SREBP homolog, *HLH106* (Gronke et al., 2007; Hader et al., 2003; Min and Benzer, 1999).

### A Genome-wide Obesity Screen in Adult *Drosophila*

We tested the fat regulatory potential of 11,594 different UAS-RNAi transgenic lines corresponding to 10,812 transgene constructs and 10,489 distinct open reading frames (ORFs) in the adult fly (Table S1). Primary screening involved three rounds of testing where candidates with a Z score greater than 1.65 were selected for retesting (Figures 1A and 1F). After three rounds of selection 516 RNAi-transgenic lines remained, 462 of which had only single primary target predictions (S19 score  $\geq 0.8$  and  $\leq 6$  CAN repeats as described by Dietzl et al., 2007) (Table S2). Important for the translation of these findings into the mammalian context, 319 of 516 (62%) have human orthologs according to InParanoid, OrthoMCL, and Ensembl databases (Table S2).

Gene ontology (GO) based pathway analysis for *biological process* revealed enrichment of gene sets involved in cell fate determination, cellular protein metabolic processes, signal transduction, intracellular transport, and regulation of smoothed signaling (Figure 1G; Table S3). Pathways most depleted during the screen, i.e., those not relevant to fat regulation, included genes regulating behavior, cell cycle, organelle organi-

zation and biogenesis, locomotory behavior, and chromosome organization (Figure S1D). A network interaction assembly based on yeast-two-hybrid, text-mining, and pathway database information on the *Drosophila* hits and their mammalian orthologs revealed an interaction network map (Figure S2) highlighting genes of development, nutrient transport, cell-cycle regulation, the proteasome, protein translation, and chromatin remodeling. Of particular interest, the candidate gene list included a number of potential regulators of feeding control. For instance, six odorant and two gustatory receptor genes were targeted (odorant receptors 10a, 56a, 65a, 67a, 83cd, and CG10407; gustatory receptors 98b and 36b). Also, the dopamine receptor *DopR2*, two octopamine receptors (*TyrR* and *oa2*), and the Nmda receptor-associated protein *Nmda1* all showed reduced body fat content following RNAi induction. In addition, altered fat deposition was observed in response to RNAi knockdown of known mediators of glucose/lipid mobilization including fructose-1,6-bisphosphatase (*fbp*), the two members of the glycerol phosphate shuttle (CG31169 and *Gpo-1*), mitochondrial acyl-carrier protein 1 (*mtacp1*), ADP/ATP translocase 2 (*Ant2*), pyruvate carboxykinase (CG1516), and fatty-acid synthetase (*fasn*). Also identified were the *Drosophila* orthologs of glucagon (*akh*), the insulin receptor (*dInR*), the downstream kinases PI3-kinase (*dPI3K*) and ribosomal-S6-kinase (*dRSK*), as well as the CREB-coactivator *dTORC*, and the critical TOR-signaling constituent *dTSC-1*. Of similar interest, *Drosophila* homologs of the critical early adipogenic regulators NCOR1/2, Jag1/2, and TAK1 (Ross et al., 2004; Suzawa et al., 2003; Yu et al., 2005) and the metabolic regulators CRT1/2 and pyruvate carboxylase (PC) all showed marked alteration of the whole-body triglycerides (Altarjos et al., 2008; Koo et al., 2005; Zhang et al., 1995). We also hit the *Drosophila* lipoprotein *rfabg* (retinol fatty-acid binding glycoprotein) previously shown to transport key developmental morphogens such as *hedgehog* (Panakova et al., 2005). Indeed, "regulation of smoothed [hedgehog] signaling" was the most highly enriched signal transduction pathway in our GO analysis (Figure 1G; Table S3). Thus, our genome-wide approach identified multiple known molecular players previously associated with adipocyte development and function. Most importantly, the screen revealed a large number of candidate genes not previously associated with obesity.

### Tissue-Specific Mapping of Candidate Obesity Genes

Considering the complexity of metabolism and the recognized diversity of tissue-specific processes that govern lipid storage (Leopold and Perrimon, 2007; Speakman et al., 2008), we set out to functionally categorize the candidate lipid regulators according to tissue specificity. RNAi lines of the 462 primary screen candidate genes were crossed to four independent GAL4 drivers with pan-neuronal (*nsyb-GAL4*), muscle (*C57-GAL4*), oenocyte (*oe-GAL4*), and fat-body (*ppl-GAL4*) specificity, and their respective triglyceride levels determined (Figure 2A; Table S4). Interestingly, RNAi lines most strongly regulating fat content after pan-neuronal (*nsyb-GAL4*) knockdown elicited little or no change in fly triglyceride levels when induced in the muscle, oenocyte, or fat body (Figure 2B). Muscle-specific gene silencing (*C57-GAL4*), by contrast, enriched for genes that also elicited significant changes in triglycerides when targeted in oenocytes

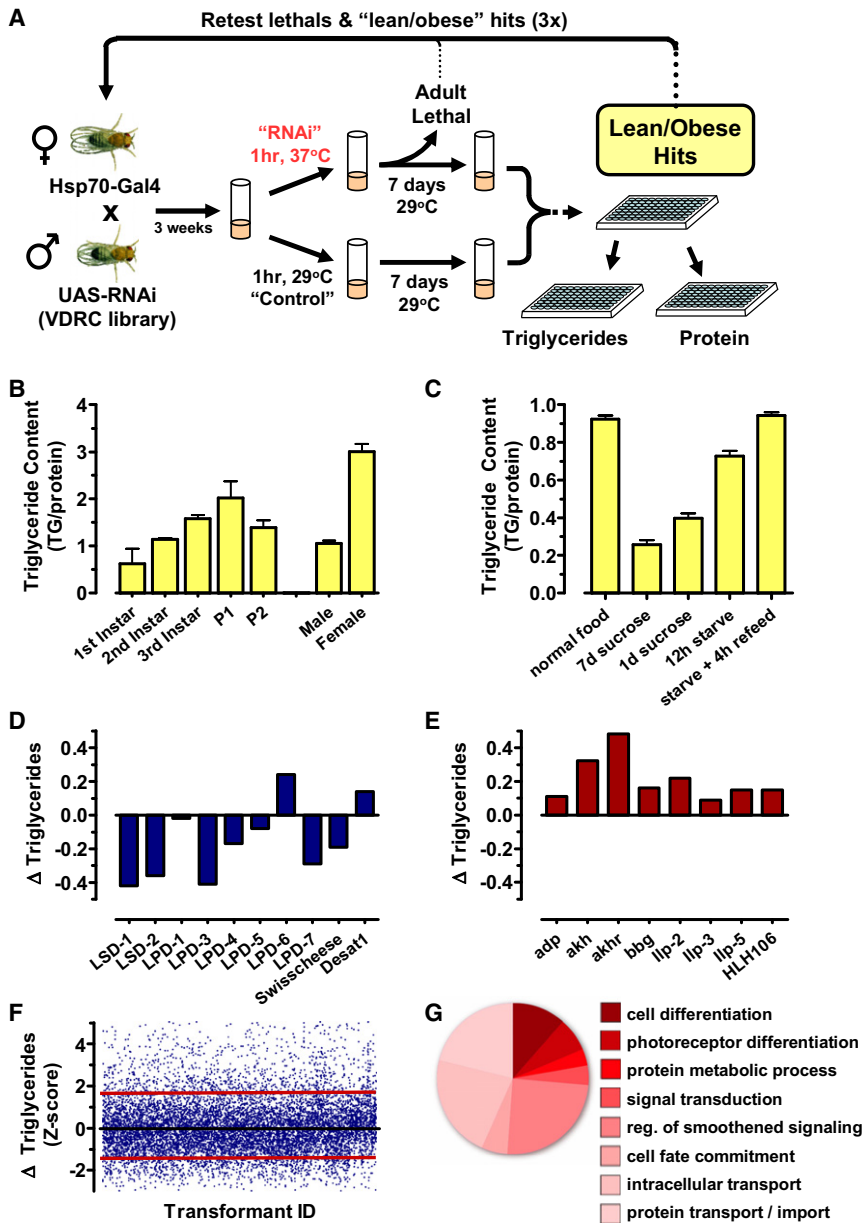


**Figure 1. Genome-wide RNAi Screen for Obesity Factors in Adult *Drosophila* In Vivo**

(A) Schematic of the screen design: virgin heat-shock-inducible (*Hsp70-GAL4; Tub-GAL80<sup>ts</sup>*) females were crossed to UAS-RNAi transgenic males. RNAi was induced 2 days post-eclosure and again after 4 days. One week after RNAi induction, triglyceride and protein levels were determined in a 96-well format and compared to internal controls: noninduced progeny of the same cross. (B) The system was capable of detecting developmental and sex-specific fat storage patterns and (C) a variety of feeding conditions. Data are shown as mean triglyceride content  $\pm$  SEM,  $n = 8$ . (D and E) Double-blinded retrieval of primary screen results for positive control lines predicted to (D) reduce or (E) increase triglyceride levels. (F) Z score distribution of the primary screen results. Red lines indicate Z scores of +1.65 above and -1.65 below baseline levels. (G) Gene ontology analysis with a level 5 cut-off for biological processes for all annotated genes with Z scores above or below  $\pm 1.65$  after three rounds of testing. See also Figures S1 and S2.

**Neuronal Hits**

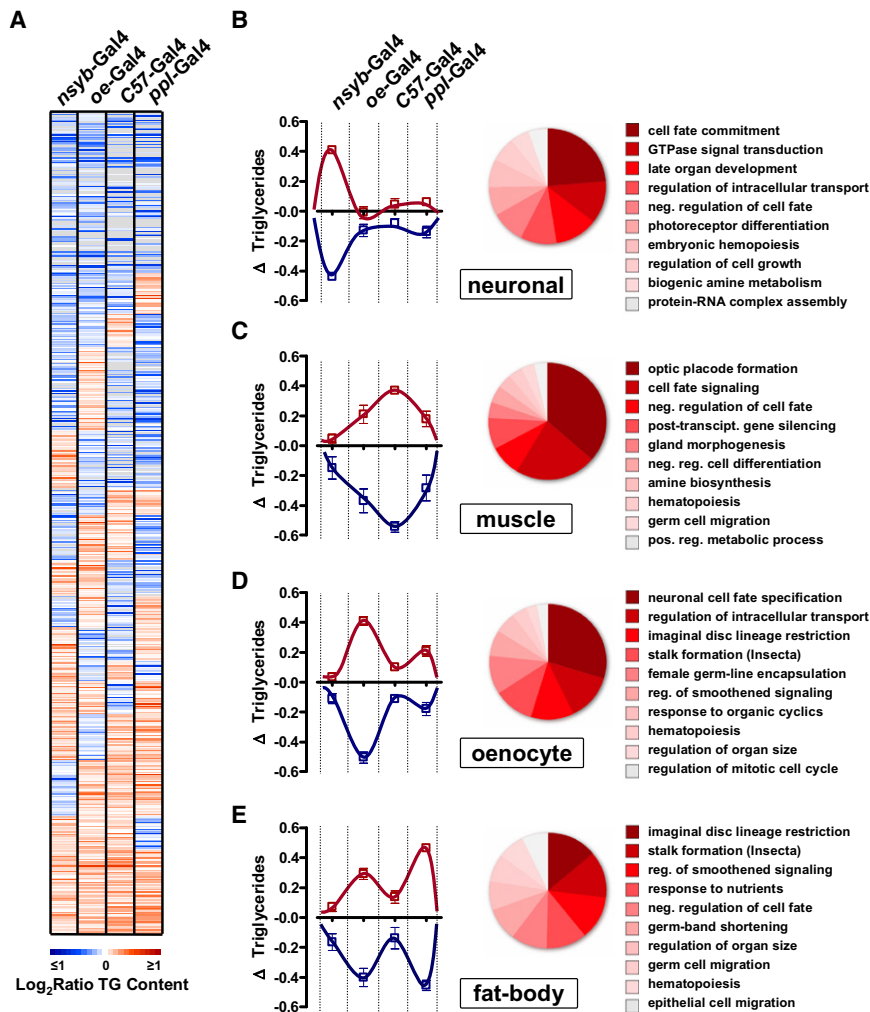
In mammals, the leptin/AgRP/POMC axis exemplifies the profound neuronal dependency of feeding behavior, metabolic rate, insulin resistance, and, thus, obesity risk (Farooqi and O’Rahilly, 2007). Flies do not possess known homologs to this axis, but their feeding behavior is also neuronally anchored (Melcher et al., 2007). Approximately one-third of the primary screen hit list elicited triglyceride changes >25% when crossed with the neuronal *nsyb-GAL4* driver (Table S5). A select number exhibited tight neuronal restriction in their response (Figure 3A). Included was the *Drosophila* homolog for SLC5A8 (CG8451; Figure 3A), a neuronal fatty-acid and lactate transporter (Martin et al., 2006). In rodents, fatty acids are

sensed by neuronal processing of lactate generated by adjacent glial cells. Similarly, lines targeting homologs of glucagon (*akh*, neuronally secreted in *Drosophila*) and the neuronal Zn-transporter SLC39A10 both displayed tight neuronal responses. Also, TSC1 (*dTSC1*), a critical regulator of the amino acid-responsive TOR-signaling pathway, showed marked neuronal and fat-body-specific responsiveness (Figure 3D). It is an attractive hypothesis that aside from peripheral regulation of nutrient storage, TOR signaling in the central nervous system (CNS) might relay amino acid status to feeding behavior. Additional neuronal responsive targets likely to play a direct role in nutrient sensing included the odorant/gustatory receptors *Obp56a* and *TyR*. Thus, similar to mammals, fat storage in *Drosophila* appears regulated by a complex network of neuronal genes.

and the fat body (Figure 2C). RNAi lines responding most substantially to oenocyte and fat-body-specific knockdown displayed a coordinate and reciprocal pattern of adiposity regulation (Figures 2D and 2E); these findings are in keeping with the tight regulatory interplay reported for these correlates of the mammalian adipose and liver (Gutierrez et al., 2007). GO analysis of the combined fat-enhancing and fat-diminishing gene sets for each of the four tissues tested are summarized in Figures 2B–2E and Tables S5, S6, S7, and S8. In support of the inducible design of the current screen, cell fate, cell differentiation, and organ development pathways showed strong enrichment in the analysis (Figures 2B–2E, right panels; Tables S5, S6, S7, and S8). Thus, we provide functional annotation of ~500 candidate obesity genes in four key metabolic tissues in *Drosophila*.

sensed by neuronal processing of lactate generated by adjacent glial cells. Similarly, lines targeting homologs of glucagon (*akh*, neuronally secreted in *Drosophila*) and the neuronal Zn-transporter SLC39A10 both displayed tight neuronal responses. Also, TSC1 (*dTSC1*), a critical regulator of the amino acid-responsive TOR-signaling pathway, showed marked neuronal and fat-body-specific responsiveness (Figure 3D). It is an attractive hypothesis that aside from peripheral regulation of nutrient storage, TOR signaling in the central nervous system (CNS) might relay amino acid status to feeding behavior. Additional neuronal responsive targets likely to play a direct role in nutrient sensing included the odorant/gustatory receptors *Obp56a* and *TyR*. Thus, similar to mammals, fat storage in *Drosophila* appears regulated by a complex network of neuronal genes.





### Muscle Hits

Several genes showed tight muscle specificity (Figure 3B and Table S6), including homologs of the proline biosynthetic PYCR1 (*P5cr*), the glycogen debranching enzyme AGL (*CG9485*), and the *fbp* (fructose-1,6-bisphosphatase), a key regulator of glycolysis. Mevalonate decarboxylase (*CG8239*), which supports cholesterol biosynthesis and is currently being tested therapeutically to reduce cholesterol levels, showed similar muscle specificity as did the sterol-regulating enzyme ARV1 (*CG32442*). Mutants of ARV1 have previously been shown to exhibit altered lipid metabolism. Interestingly, genes involved in TLR signaling (*IM10*), the ribosome and protein translation (*CG3213*), proteolysis (*Fur1*), transcriptional regulation (*CG5591*), and microRNA-mediated silencing (*Smg5*) (Figure 3B) were also found to regulate triglyceride levels specifically in muscle cells.

### Fat and Oenocyte Candidate Genes

The largest number of primary screen hits showed oenocyte- (*oe-GAL4*) and fat-body (*ppl-GAL4*) responses (Figures 3C and 3D; Tables S7 and S8). Interesting targets included homologs of inflammation-related genes: ARID2 (regulates interferon-responsive genes; Yan et al., 2005), *dTraf* (fly Traf-like protein), the

### Figure 2. Tissue-Specific Regulation of Fat Storage

(A) Heat map of changes in triglyceride for primary screen hits crossed to *nsyb-GAL4* (pan-neuronal), *oe-GAL4* (oenocyte), *C57-GAL4* (muscle), and *ppl-GAL4* (fat-body) drivers. Changes are relative to control RNAi lines and isogenic *w<sup>1118</sup>* flies crossed to the respective GAL4 drivers.

(B–E) Left panels show the mean changes in triglycerides after tissue-specific knockdown for the top-scoring fat-enhancing (red lines) and fat-depleting (blue lines) genes in each tissue category. Note the marked neuronal specificity, an overlap in fat-body and oenocyte responses, and a relative lack of specificity for top-scoring muscle-responsive genes. Right panels summarize gene-ontology analysis for each category (level 5 cut-off for biological processes). Intensity of the red reflects increased significance of the GO term.

pattern recognition receptor PGLYRP2, the interleukin enhancer-binding factor ILF2, the extracellular matrix protein tenascin (TNC), the ubiquitin-conjugating enzyme UBE2N (critical for TNF- and Toll-like-receptor signaling), or the deubiquitinating enzyme USP7. Additional components of the ubiquitin-ligase machinery were also revealed, namely UBR2, HERC4, and FBWX5 (also controls TSC1 and thus TOR signaling). Together these data support roles for immune regulatory networks and ubiquitination in fat storage regulation in *Drosophila*.

Oenocyte- and fat-body-specific knock-down analyses also identified genes involved in glycerol and lipid metabolism (Figures 3C and 3D; Tables S7 and S8). For instance, genes related to insulin signaling include the homologs of PP1 (inhibitory subunit 15b), S6KII, EIF2B, PI3K, and the insulin receptor (IR) itself. Also, direct mediators of lipid and glucose metabolism were identified, such as homologs of the ADP/ATP symporter ANT, NDUFAB1, GPD, and GPD2. The latter, part of the glycerol-phosphate shuttle, regulates glycolytic rate and ROS production. Of interest, mice lacking GPD2 exhibit a 40% reduction in white adipose mass (Brown et al., 2002) and share a number of phenotypic features with deficiencies of glycerol kinase (GK), another enzyme found using the oenocyte-specific driver. In addition, we found *T3dh* (an iron-dependent regulator of fatty acid and ketone body metabolism), *Cyp6a2* (cytochrome P450 proteins catalyze numerous steps of cholesterol, steroids, and lipids synthesis), and the *Drosophila* homolog of the fatty-acid elongase ELOVL6 (which was particularly robust in both the oenocyte- and fat-body analyses). *Elov6<sup>-/-</sup>* mice develop marked obesity and hepatosteatosis and show protection from hyperinsulinemia, hyperglycemia, and hyperleptinemia (Matsuzaka et al., 2007). Using fat-body-specific knockdown we also hit the *Drosophila* homolog of ELOVL7. Perhaps most importantly, we found multiple

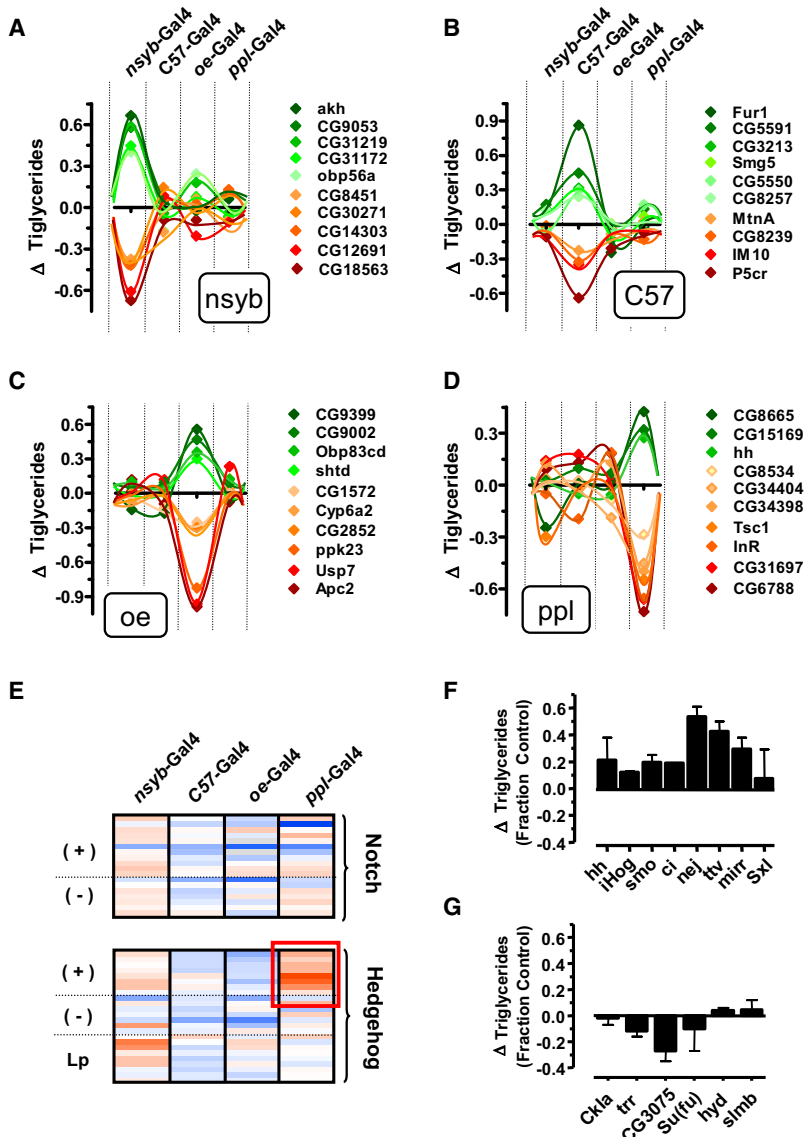


**Figure 3. Analysis of Tissue Specificity Reveals Hedgehog Signaling as a Fat-Body-Specific Regulator of Triglyceride Levels**

Triglyceride responses of candidate genes. Changes in adiposity in RNAi lines with the most tissue-restricted responses in the (A) pan-neuronal, (B) muscle, (C) oenocyte, and (D) fat-body compartments. (E) Heat map of adiposity observed in UAS-RNAi transgenic fly lines targeting available annotated hedgehog and notch pathways. Changes are relative to averages of control RNAi lines and *w<sup>1118</sup>* flies crossed to the respective GAL4 drivers. Genes are grouped according to their role as either positive (+) or negative (–) effectors, or as mediators of ligand processing and release (Lp). Red indicates increased triglycerides; blue indicates reduced triglycerides. (F) Representative triglyceride changes in response to *ppl*-GAL4-driven knockdown of effectors of hedgehog signaling and (G) repressors of the pathway. Data are presented as mean ± SEM, n = 4. \*p < 0.05. See also Figure S3.

sive pathways while not scoring at all in muscle or neuronal datasets (Figure 3E; Figure S3A).

Intriguingly, activators of the smoothed signaling pathway including the hedgehog ligand (*hh*), the binding protein *iHog*, the coreceptor *smoothened* (*smo*), the *nejire* coactivator (*nej*), the downstream transcription factors *cubits interruptus* (*ci*) and *mirror* (*mirr*), as well as *toutvelu* (*ttv*) and the hedgehog target *Sxl* all yielded increased triglycerides after *ppl*-GAL4 specified knockdown (Figure 3F). Conversely, decreased triglycerides levels were observed after knockdown of the known hedgehog repressors *trithorax-related* (*trr*), CG3075, and *Suppressor of Fused* (*Sufu*) (Figure 3G). Interestingly, whereas fat-body-specific knockdown of genes involved in processing or release of the hh ligand itself showed no coordinate effect on triglyceride levels (Figure 3E and Figure S3B), *nsyb*-GAL4-driven knockdown elicited mild elevation in triglycerides, suggesting that the hedgehog

previously uncharacterized genes that regulate fat content in an oenocyte- and/or fat-body-dependent manner (Figures 3C and 3D). Thus, our screen has revealed a large number of general and tissue-specific candidate fly genes and multiple pathways that control triglyceride storage levels.

**Hedgehog Is a Fat-Specific Obesity Pathway in *Drosophila***

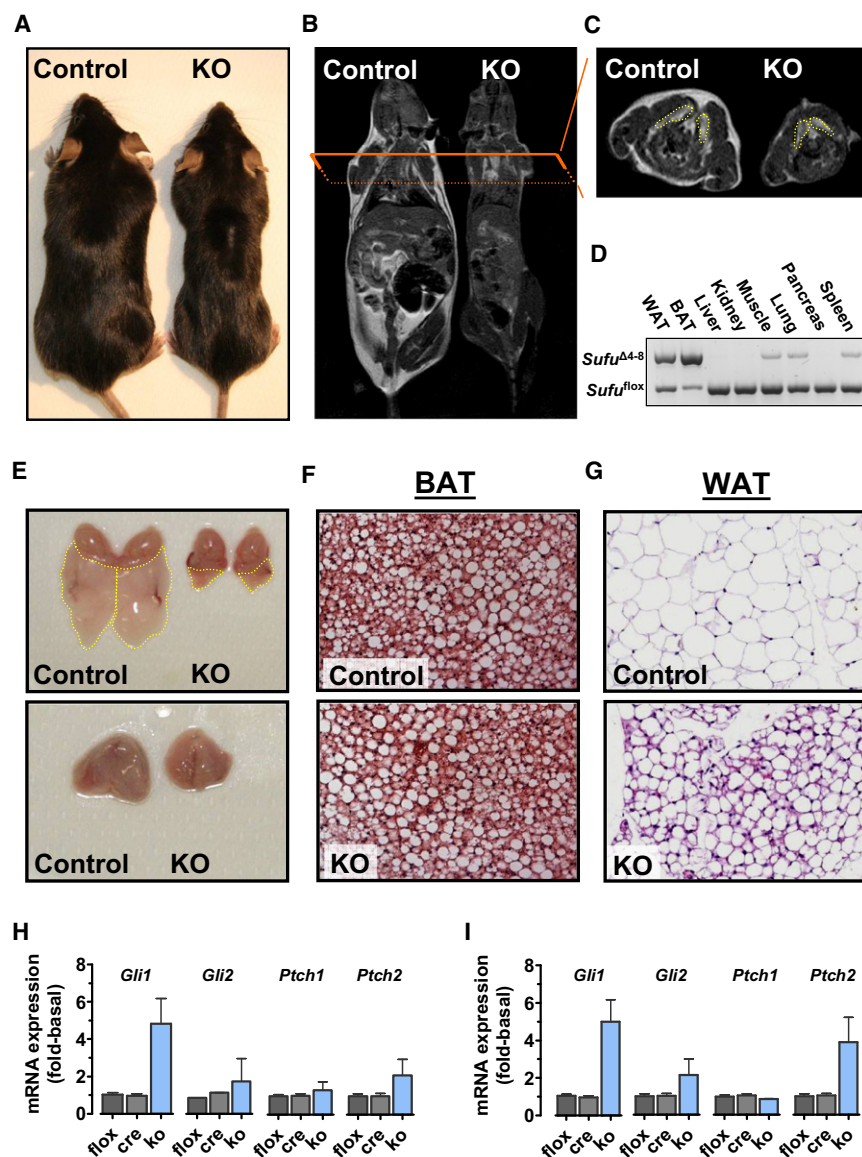
The biological process “regulation of smoothed [hedgehog] signaling” was the top-scoring signal transduction pathway of all annotated pathways in the primary screen (Tables S3). An additional eight potential hedgehog signaling members recently identified in a *Drosophila* S2 cell screen for modulators of hedgehog signaling (Nybakken et al., 2005) were also hit in our primary obesity screen (Figure S2). Together these represent a >20-fold enrichment for the hedgehog signaling pathway. Importantly, hedgehog signaling scored third in fat-body-respon-

ligand may originate from a neuronal cell population (Figure 3E). As controls, knockdown of neither the effectors nor repressors of notch signaling showed any coordinate triglyceride response whereas knockdown of OXPHOS genes revealed coordinate fat-body and neuronal-specific reductions in triglyceride content (Figure 3E and Figures S3C and S3D), consistent with the fundamental role of the process in lipid flux. These data show that modulation of the hedgehog pathway in the fat body results in marked alterations in triglyceride levels.

**cAMP, Glucocorticoid, and Hedgehog Crosstalk in White Adipogenesis**

Our data show that the hedgehog pathway regulates triglyceride levels in adult *Drosophila*. A role for the hedgehog pathway has also been postulated in mammalian adipocyte biology both through systemic manipulation (Buhman et al., 2004) and in vitro (Suh et al., 2006). Cyclic AMP (cAMP) and dexamethasone





blocked induction of hedgehog activation, rendering SAG treatment ineffective (Figure S4B). Thus, hedgehog activation blocks white adipocyte differentiation solely in the absence of cAMP and glucocorticoid signaling.

#### Defective White but Normal Brown Adipose Tissue in Fat-Specific *Sufu* Mutant Mice

To assess the in vivo relevance of hedgehog signaling in mammalian adipogenesis, we generated fat-specific *Sufu* knockout animals (*aP2-Sufu*KO) (Figure S4C). *Sufu* is a potent endogenous inhibitor of hedgehog signaling in mammals (Jiang and Hui, 2008). *Sufu*<sup>flox/flox</sup> mice were crossed to the adipose tissue deleting *aP2-Cre* transgenic line (Figure S4C), and the resulting *aP2-Sufu*KO animals were born healthy and at Mendelian ratios. PCR amplification revealed target deletion in both white adipose tissue (WAT) and brown adipose tissue (BAT) (Figures 4A and 4D). *aP2-Sufu*KO mice displayed an immediate and obvious lean phenotype. MRI analysis revealed a significant and global reduction in white adipose tissue mass, including subcutaneous, perigonadal, and mesenteric depots (Figure 4B). Intriguingly, though, in contrast to the gross loss of WAT, cross-sectional examination of the interscapular region revealed fully developed BAT depots of both normal size and lipid content (Figures 4B and 4C). Direct measurement of WAT and BAT depot weights corroborated the divergent WAT/BAT phenotype, with an ~85%

(Dex), key inducers of differentiation in adipocyte cultures, have been shown to block hedgehog activation in several systems (Fan et al., 1995; Heine and Rowitch, 2009; Jiang and Struhl, 1995). Therefore, to establish a model system to investigate hedgehog signaling and adipogenesis, we subjected 3T3-L1 pre-adipocytes to two differentiation cocktails: a minimal induction medium containing insulin and troglitazone and the standard Dex and IBMX (increases cAMP) containing cocktail. We observed complete differentiation of 3T3-L1 cells under both culture conditions (Figure S4A). Importantly, in the presence of IBMX/Dex 3T3-L1 cells underwent complete differentiation whether in the presence or absence of the hedgehog activator Smoothed AGonist (SAG). Cells cultured in minimal induction medium, however, displayed a total block of differentiation upon addition of SAG (Figure S4A), suggesting that IBMX/Dex interferes with hedgehog stimulation. Expression of the hedgehog target genes *Gli1* and *Ptch1* showed that IBMX and Dex completely

blocked induction of hedgehog activation, rendering SAG treatment ineffective (Figure S4B). Thus, hedgehog activation blocks white adipocyte differentiation solely in the absence of cAMP and glucocorticoid signaling.

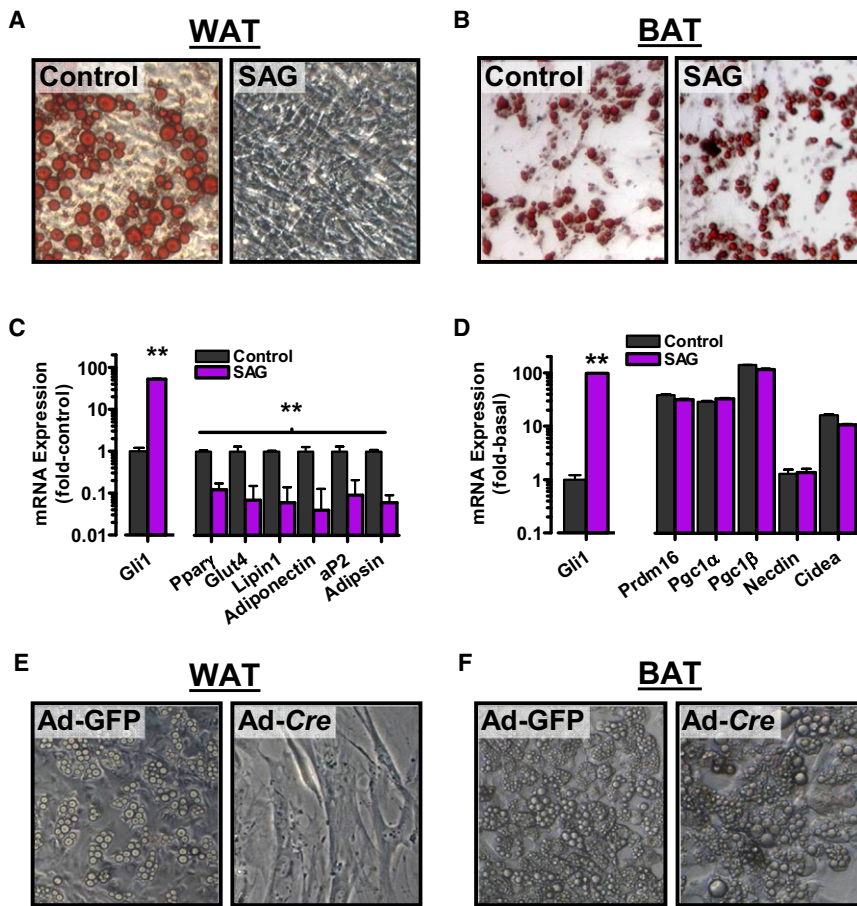


**Figure 5. Hedgehog Signaling Specifically Blocks White Adipogenesis**

(A and B) Microscopic view of Oil Red O-stained cell cultures reveals that activation of hedgehog signaling using SAG blocks differentiation of (A) white (WAT) but not (B) brown (BAT) primary murine adipocyte progenitors (stromal vascular cell, SVC, preparations). Data are from 12 days after induction using minimal induction medium (see [Experimental Procedures](#)).

(C) Quantitative RT-PCR 96 hr after induction of WAT-derived precursors reveals activation of hedgehog signaling (Gli1 expression) and reduction in WAT differentiation markers.

(D) BAT-derived precursors show no indication of altered differentiation after 96 hr of hedgehog activation. Data are mean  $\pm$  SEM,  $n = 3$ –5 mice per group. \*\* $p < 0.01$ .

(E) Phase-contrast images of primary WAT SVCs from *Sufu*<sup>fl/fl</sup> animals induced to differentiate using minimal induction medium after infection with Adeno-Cre or the Adeno-GFP control vector.

(F) Same as (E) but using primary brown adipose SVCs.

See also [Figure S5](#).

reduction in perigonadal fat pad mass in *aP2-Sufu*KO mice concomitant with unaltered BAT mass ([Figure 4E](#); [Figure S4D](#)). Tissue weight and histological analyses confirmed lack of any remarkable phenotype in multiple other tissues including pancreas and liver (no indication of steatosis), and muscle mass was unaffected ([Figure S4D](#)). Cutaneous adipose was also markedly diminished ([Figure S4E](#)). Whereas the morphology of *Sufu*-deficient BAT depots was largely indistinguishable from that of control animals ([Figures 4E and 4F](#)), examination of multiple WAT pads revealed marked and significant reductions in both adipocyte size ([Figures 4E and 4G](#); [Figure S4F](#)) and total numbers ([Figure S4G](#)) in mutant animals. Of note, qPCR showed elevated Gli1, Gli2, and Ptch2 expression in both WAT ([Figure 4H](#)) and BAT ([Figure 4I](#)), verifying the intended pathway activation in both tissues. Thus, deletion of *Sufu* in fat tissue results in a markedly decreased white fat cell number and, remarkably, in normal brown adipose tissue.

#### Hedgehog Activation Blocks White but Not Brown Adipocyte Differentiation

Since the phenotype of *aP2-Sufu*KO mice suggested a defect in white adipocyte differentiation, we next stimulated 3T3-L1 “white” and HIB-1B “brown” adipocyte cell lines with SAG to induce hedgehog activation. Intriguingly, while robust block of 3T3-L1 differentiation was again observed ([Figures S4A and](#)

[S4B](#)), HIB-1B cells showed no such response and underwent complete differentiation (not shown). These data were also confirmed using recombinant Sonic hedgehog (shh). Next, stromal vascular cell (SVC) fractions from both white and brown adipose depots were isolated from mice and stimulated with minimal induction cocktail in either the presence or absence of SAG. Activation of hedgehog signaling completely blocked adipogenesis in WAT-derived SVCs while showing no effect on BAT-derived SVCs ([Figures 5A and 5B](#)). qPCR analysis confirmed activation of hedgehog signaling in both the WAT- and BAT-derived SVC fractions and recapitulated on a transcriptional level the WAT-specific block in adipogenesis ([Figures 5C and 5D](#) and [Figure S5A](#)). To validate these findings, and to rule out differential kinetics of aP2-Cre expression between WAT and BAT in vivo, we isolated and tested SVC fractions from WAT and BAT of *Sufu*<sup>fl/fl</sup> activating the hedgehog pathway genetically, through administration of a Cre-recombinase containing adenovirus ([Figures 5E and 5F](#); [Figures S5B and S5C](#)). Control (Adeno-GFP) and *Sufu*-deletion-induced (Adeno-Cre) SVCs derived from BAT showed equivalent and complete differentiation ([Figure 5F](#); [Figure S5C](#)). Once again, WAT-derived SVCs differentiated only under control conditions, even after 12 days of induction ([Figure 5E](#); [Figure S5C](#)). Thus, activation of hedgehog signaling in vivo and in vitro blocks white but not brown adipocyte differentiation.

#### Hedgehog Activation Dysregulates Early Adipogenic Factors

When we cross-referenced with literature focusing on adipogenesis, we found that an impressive 18 of 65 key regulators of

adipogenesis (Farmer, 2006; Gesta et al., 2007; Lefterova and Lazar, 2009; Rosen and MacDougald, 2006) had been described as Gli targets in other systems (Table S9). Intriguingly, when examined in 3T3-L1 preadipocytes, hedgehog activation induced a coordinated downregulation of the proadipogenic targets *Bmp2*, *Bmp4*, *Egr2/Krox20*, *Sfrp1*, and *Sfrp2* by an average of ~50% after only 24 hr (Figure 6A). In contrast, quantification of the antiadipogenic target set showed upregulation of the multiple critical repressors (*Nr2f2*, *Gilz*, *Hes1*, and *Ncor2*); the negative regulators *Jag1* and *Pref1* remained unchanged at this time point (Figure 6B). Analysis of the master regulatory machinery downstream of these effectors revealed critical reductions in *Ppar $\gamma$* , *Cebpb*, and *Cebp $\delta$*  and increases in the antiadipogenic factors *Cebp $\gamma$*  and *Ddit3* (Figure 6C). Outside of this dramatic antiadipogenic profile, elevated levels of *Cebp $\alpha$*  were observed (Figure 6C). Importantly, a similar coordinate downregulation of *Ppar $\gamma$* , *Cebpb*, *Cebp $\delta$* , as well as *Cebp $\alpha$*  was observed in WAT-derived SVCs following genetic activation of hedgehog signaling (Figure 6D).

To establish a direct link between hedgehog activation and adipogenic block in white adipose, *in silico* predictions were used to identify clusters of probable Gli-binding sites in the highly SAG-responsive genes *Ncor2*, *Nr2f2*, *Sfrp2*, and *Hes1* (Figure S6A). To assess the functionality of these putative binding sites, we cloned the relevant promoter fragments and performed luciferase reporter assays (Figure 6E; Figure S6A; Tables S11 and S12). *Gli1* and *Gli2* induced activation of all *Ncor2* and *Nr2f2* reporter constructs, with the binding site clusters *Ncor2\_B*, *Nr2f2\_A*, and *Nr2f2\_B* showing responses comparable to the hallmark target *Ptch* (Figure 6E). Further, chromatin immunoprecipitations on 3T3-L1 preadipocytes using *Gli2*- and *Gli3*-specific antibodies revealed increases in *Gli2* and *Gli3* binding within the endogenous *Ncor2*, *Hes1*, *Nr2f2*, and *Sfrp2* regulatory regions following SAG treatment. Together, these findings demonstrate endogenous *Gli2*/*Gli3* binding to multiple adipogenic loci and implicate direct modulation of *Ncor2* and *Nr2f2* in the dysregulation of adipogenesis (Figure S6B).

### Normal Glucose Tolerance and Insulin Sensitivity in *aP2-Sufu*KO Mice

To relate metabolic consequences of the unique WAT-specific lipotrophy observed in our *aP2-Sufu*KO mice to previous models, we assessed glucose, insulin, and lipid tolerance, insulin sensitivity, and energy expenditure. Surprisingly, *aP2-Sufu*KO mice displayed normal glucose tolerance and glucose-induced insulin secretion during an oral glucose tolerance test (Figure 7A), and insulin tolerance testing was unremarkable (Figure S7A). In keeping with lack of apparent insulin resistance, *aP2-Sufu*KO showed no evidence of enhanced ectopic lipid accumulation. Further, euglycemic hyperinsulinemic clamps confirmed the lack of detectable insulin resistance, and interestingly, addition of tracers identified a tripling in glucose utilization within the residual white adipose tissue depot (Figures 7B and 7C). Measurement of serum leptin levels and, unexpectedly, an increase in adiponectin levels (Figure 7D). Direct culture of freshly isolated BAT and WAT fragments from control and *aP2-Sufu*KO animals recapitulated this pattern with significantly

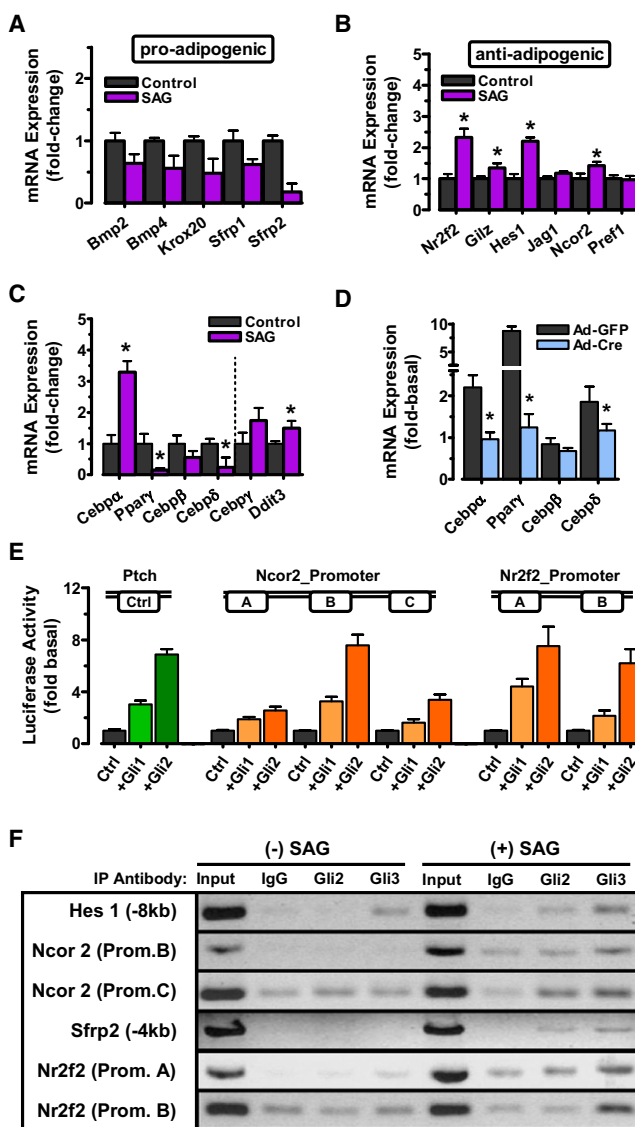


**Figure 6. Hedgehog Signaling Blocks White Adipogenesis through Coordinate Repression of the Adipogenic Program**

(A and B) Quantitative RT-PCR for known (A) proadipogenic and (B) antiadipogenic transcriptional hedgehog targets in 3T3-L1 cells 24–48 hr after induction in the absence (control) and presence of SAG (200 nM).

(C) Quantitative RT-PCR of the *Ppar $\gamma$* -*Cebp $\alpha$*  adipogenic regulatory system in 3T3-L1 cells 96 hr after induction, in the presence or absence of SAG.

(D) Same as (C), but performed in primary WAT SVCs derived from *Sufu*<sup>fl/fl</sup> animals and induced to differentiate after infection with Adeno-Cre or an Adeno-GFP control vector.

(E) Luciferase reporter assays showing activation of *Ncor2* and *Nr2f2* promoter constructs in response to *Gli1* or *Gli2*. The *Gli* target gene *PTCH* was used as positive control. Data are the mean of two experiments in triplicate.

(F) PCR analysis of chromatin immunoprecipitations of 3T3-L1 cells grown in the presence or absence of 200 nM SAG for 72 hr.

Data in (A)–(D) are presented as mean  $\pm$  SEM,  $n = 3$ –5. \* $p < 0.05$ . See also Figure S6.



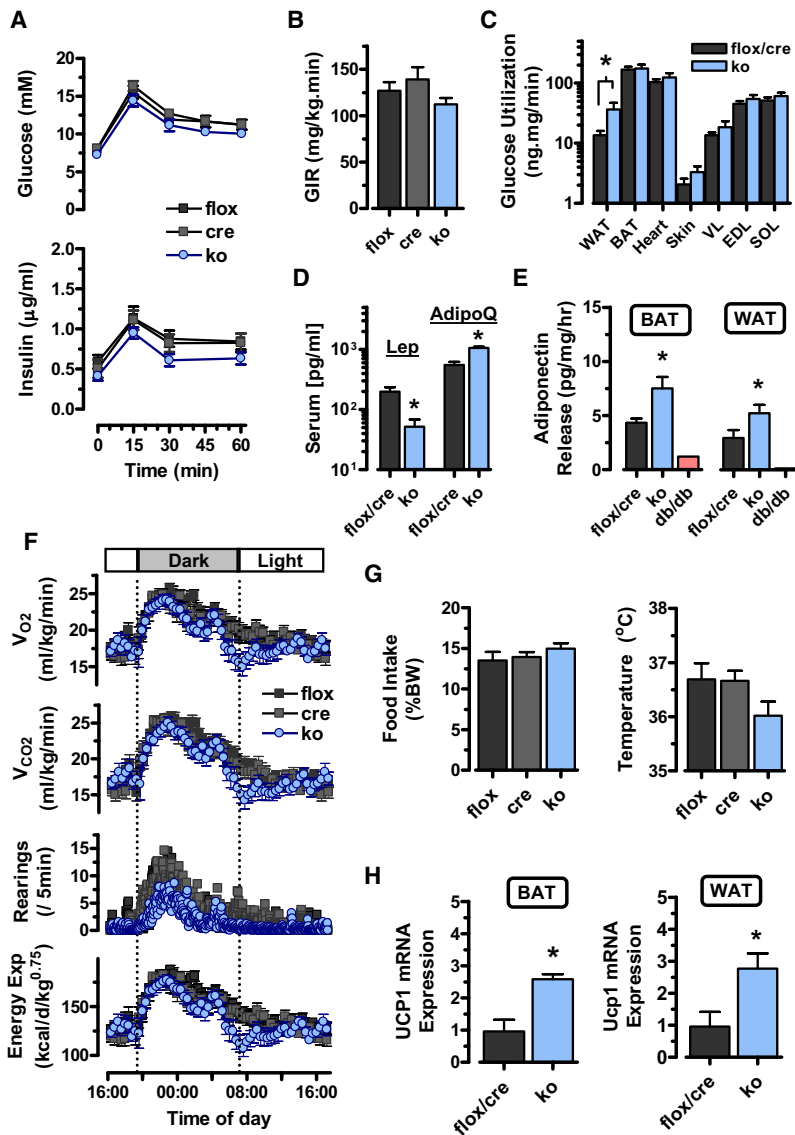


**Figure 7. *aP2-Sufu*KO Mice Exhibit Normal Glucose and Energy Handling**

(A) *aP2-Sufu*KO mice exhibit unaltered glucose handling during an oral glucose tolerance test (1 g/kg). (B) Whole-body glucose infusion rate (GIR) was normal during euglycemic hyperinsulinemic clamp. (C) Glucose tracing revealed enhanced glucose uptake in WAT of mutant mice but no differences in BAT, skin, cardiac, or skeletal muscles. (D) Circulating serum leptin and adiponectin levels. (E) In vitro culture of BAT and WAT fragments revealed increased adiponectin secretion in adipose of *aP2-Sufu*-KO mice. (F) Indirect calorimetry in 10- to 12-week-old control and *aP2-Sufu*KO mice including O<sub>2</sub>-consumption (VO<sub>2</sub>), CO<sub>2</sub>-production (VCO<sub>2</sub>), and activity, as well as subsequent calculation of energy expenditure. Activity was measured as number of infrared beams broken with time. (G) Food intake and body temperature measured at 12 weeks of age. (H) *Ucp1* expression in WAT determined by qPCR. Data are mean ± SEM (n = 6–12). \*p < 0.05. See also Figure S7.

reduced leptin (Figures S7C and S7D) and elevated adiponectin secretion (Figure 7E and Figure S7E). Thus, despite significant lipotrophy, *aP2-Sufu*KO mice exhibit largely normal glucose homeostasis.

When tested using indirect calorimetry, little evidence was found of altered O<sub>2</sub>-consumption or CO<sub>2</sub>-production rates in the *aP2-Sufu*KO mice with exception of a short period of reduced gas exchange at the end of the dark cycle (Figure 7F; equivalent to a ~5% decrease in daily energy expenditure). Despite the marked differences in WAT and body weight (Figure S7F), *aP2-Sufu*KO mice showed no evidence of altered food intake relative to littermate controls (Figure 7G), respiratory quotient estimation suggested normal macronutrient partitioning (Figure S7G), and intestinal uptake and disposal of lipids were also normal (Figure S7H). What we did observe was markedly reduced activity in the *aP2-Sufu*KO animals during the dark cycle (Figure 7F). In the context of unaltered caloric intake and essentially normal energy expen-

diture, reduced activity suggests a significant shift in energy toward basal metabolic rate (BMR) or thermogenesis. O<sub>2</sub>/CO<sub>2</sub> flux during periods of inactivity showed no evidence of increased BMR (Figure 7F). Direct measurement of body temperature showed a mild, albeit not significant, reduction in body temperature in the *aP2-Sufu*KO mice (Figure 7G, right panel), a somewhat paradoxical finding. Body temperature, however, only reflects thermogenesis in subjects of equivalent thermal state. *aP2-Sufu*KO mice exhibit little or no cutaneous (Figure S4E) and subcutaneous adipose stores (Figures 4B and 4C) and, therefore, at 22°C are under relative cold stress. Indeed, performing metabolic measurements at ambient temperature (22°C) can mask phenotypes as profound as obesity (Feldmann et al., 2009). *Ucp1* mRNA

levels measured in brown and white adipose tissue of our *aP2-Sufu*KO mice housed at 22°C were markedly elevated (Figure 7H), suggesting exaggerated thermal stress. We therefore analyzed body temperature, food intake, and body weight in littermate control and *aP2-Sufu*KO mice kept at 30°C (thermoneutrality) for a period of 1 month. Within 1 day at thermoneutrality, body temperature in *aP2-Sufu*KO mice normalized and even elevated slightly above controls (Figure S7I). Food intake also decreased in parallel with control littermates. Both food intake and body temperature shifts were maintained into a steady state (Figure S7I and not shown). Of note, oral glucose tolerance showed no deviation over this time period. Together these findings suggest that at ambient temperature *aP2-Sufu*KO mice divert bulk energy toward thermogenesis explaining at least in part the observed reduction in activity. Thus, *aP2-Sufu*KO mice exhibit WAT-specific lipotrophy, normal glucose tolerance, and largely normal regulation of energy expenditure.

## DISCUSSION

The power of *D. melanogaster* RNAi transgenics to probe gene function on a genome-wide scale has allowed us to screen ~78% coverage of the *Drosophila* genome. One significant advantage of our inducible approach employed here is the ability to interrogate the fat regulatory potential of the ~30% of the *Drosophila* genome that is developmentally lethal under classic mutation conditions. Indeed, the result that cell differentiation genes scored as the most enriched ontology subcategory substantiates the inducible strategy employed and identifies a large number of developmentally lethal genes with strong lipid storage regulatory potential. Consistent with a previous feeding-induced RNAi *C. elegans* screen, the fraction of candidate genes resulting in decreased fat content upon knockdown (360 of 516; 70%) exceeded that of obesity-causing candidates (216 of 516; 30%), which is consistent with the hypothesis that the major evolutionary pressures for animals have been to favor nutrient storage. Our screen identified a large number of genes already known to play a key role in mammalian fat or lipid metabolism, including enzymes of membrane lipid biosynthesis, fatty acid and glucose metabolism, and sterol metabolism. Further, our whole-genome screen has uncovered a plethora of additional candidate genes of adiposity regulation, a large proportion of which had no previous annotated biological function. Moreover, we identified multiple genes that either positively or negatively regulate whole fly triglyceride levels when targeted specifically in neurons, the fly liver (oenocyte), the fat body, or muscle cells. Analyses of the hits allowed us to define either gene sets that function globally in all these tissues or others that display coordinate regulation of adiposity when targeted in metabolically linked organs such as the fat and the liver. Since >60% of the candidate genes are conserved across phyla to humans, our data set is a unique starting point for the elucidation of novel regulatory modalities in mammals.

The top-scoring signal transduction pathway in our GO-based enrichment analysis was the hedgehog pathway. Tissue-specificity assessment revealed further that this enrichment was primarily derived from a pronounced fat-body restriction in function. Hedgehog signaling has been previously implicated in adipose tissue biology (Suh et al., 2006; Wu et al., 2002; Zehentner et al., 2000). In *Drosophila* larvae, hedgehog activation reduces lipid content consistent with what we found in adult flies and our fat-specific fly knockdown lines (Suh et al., 2006). Similarly, knockdown of the *C. elegans* equivalent of the inhibitory hedgehog receptor *Ptch* results in a prominent adiposity reducing phenotype in a feeding-based RNAi screen (Ashrafi et al., 2003). We therefore homed into the hedgehog pathway to provide proof of principle for the fly screen and to translate our *Drosophila* results directly into the mammalian context.

Several reports exist describing systemic manipulation of hedgehog signaling, either by injection of ligand-depleting antibody or through examination of a systemic hypomorphic mutant, the *Ptch*<sup>mes/mes</sup> mouse (Buhman et al., 2004; Makino et al., 2001). Indeed *Ptch*<sup>mes/mes</sup> mice display largely normal white adipose tissue depots albeit reduced in size (Li et al., 2008). Hedgehog signaling plays a crucial role in multiple organs systems including at least one intimately involved in nutrient

storage and the etiologies of obesity and insulin resistance, namely, the pancreatic islet (Hebrok et al., 2000; Thomas et al., 2000). Our in vitro and in vivo data using the adipose-specific *Sufu* mutant mice clearly show that hedgehog activation results in a complete and cell-autonomous inhibition of white adipocyte differentiation. The residual white adipose tissue observed in our *aP2-Sufu*KO mice is most likely due to late inefficient deletion and/or is due to developmental timing effects. Indeed, *aP2* (and thus *aP2-Cre*) are expressed relatively late during adipocyte differentiation (Gesta et al., 2007). The remarkable finding was that genetic activation of hedgehog signaling in vivo and in vitro blocks only white but not brown adipocyte differentiation.

Fat is mainly stored in two cell types: WAT, which is the major storage site for triglycerides, and BAT, which, through the burning of lipids to heat (through uncoupling of mitochondrial oxidative phosphorylation), serves to regulate body temperature (Farmer, 2009). Recent PET-CT data have revealed that adult humans contain functional BAT and that the amount of BAT is inversely correlated with body mass index (Cypess et al., 2009; van Marken Lichtenbelt et al., 2009; Virtanen et al., 2009; Zingaretti et al., 2009). These new data in humans rekindle the notion that a functional BAT depot in humans could represent a potent therapeutic target in the context of obesity control. Lineage tracking and genetic studies have shown that WAT and interscapular BAT cells derive from two different but related progenitor pools (Seale et al., 2009; Tseng et al., 2008). Our genetic data now demonstrate both in vitro and in vivo that hedgehog activation results in a virtually complete block of WAT development but leaves the differentiation process of brown adipocytes wholly intact. These data further support the concept that white and brown adipocytes are derived from distinct precursor cells.

To the best of our knowledge *aP2-Sufu*KO mice are the first white adipose-specific lipoatrophic mice with a fully functional BAT depot over the long-term and normal glucose tolerance and insulin sensitivity. The capacity of an intact BAT depot to burn energy in *aP2-Sufu*KO mice likely underlies, at least in part, their lack of ectopic lipid accumulation and insulin resistance. This largely normal metabolic picture highlights the potent regulatory capacity of brown adipose tissue and should prove invaluable in understanding the distinct roles of brown and white adipose tissues.

## EXPERIMENTAL PROCEDURES

### Fly Screening

For detailed experimental procedures, please see the [Extended Experimental Procedures](#). Male UAS-RNAi transgenic flies were obtained from the Vienna *Drosophila* RNAi Centre (VDRC) and crossed with *Hsp70-GAL4;Tub-GAL80<sup>ts</sup>* virgins and the progeny transferred to new vials after 3 weeks. Flies were heat-shocked immediately and after 4 days. On day 7, flies were manually crushed, sonicated, heat-inactivated, and centrifuged and the supernatant used for 96-well based colorimetric determination of triglycerides (GPO Trinder, Sigma) and protein (BCA, Pierce). Tissue-specific secondary screen followed a parallel procedure without heat-shock and controlled against *w<sup>1118</sup>* wild-types and a random set of RNAi lines shown to exhibit no phenotype.

### Data Analysis and Ortholog Retrieval

Orthologs were retrieved from InParanoid, OrthoMCL, and Ensembl. Gene Ontology analysis used GoStat with a Benjamini and Hochberg correction

using the online GOToolbox application. Network maps were generated using cytoscape and based on online protein interaction databases.

#### Generation of *Sufu* Mutant Mice

Conditional *Sufu* mice were generated by the laboratory of C.-c.H. (unpublished data). Adipose-specific *Sufu* knockout mice were generated by crossing conditional *Sufu*<sup>fl/fl</sup> mice with *aP2*-Cre transgenic mice (R. Evans; JAX). Cre recombinase-positive wild-type and Cre recombinase-negative *Sufu*<sup>fl/fl</sup> littermates served as controls.

#### Euglycemic Hyperinsulinemic Clamp, Tissue Glucose Utilization, and Indirect Calorimetry

Indirect calorimetry was performed for 72 hr using an open-circuit, indirect calorimetry system including spontaneous activity by beam breaking (Oxylet, Panlab-Bioseb). Euglycemic hyperinsulinemic clamp studies were performed on conscious mice 5 days insertion of a femoral catheter and after a 6 hr fast. D-[3-<sup>3</sup>H]-glucose and <sup>3</sup>H-2-deoxyglucose (tissue-specific utilization) were used as tracers and insulin was infused at 18 mU/kg/min. Euglycemia was maintained by variable infusion of 15% glucose. Calculations were based on blood sampled at steady state (T = 120–180 min). Total radioactivity was determined by scintillation counting, and glucose concentrations by the glucose oxidase method (BioMerieux).

#### Histology, Adipocyte Size, and Number

For staining of neutral lipids, cells were fixed and stained with Oil Red O (OrO) according to standard procedures. Adipocyte number and size analyses were performed using H&E-stained paraffin sections of perigonadal WAT pads by semi-automated morphometry. Definiens software suite was used for the automated determination of adipocyte size and number from multiple intervalled histological sections.

#### Isolation of Mouse Primary Brown and White Preadipocytes

Primary preadipocytes were obtained by collagenase digestion from perigonadal white and interscapular brown adipose tissue depots in mice. Isolated cells were plated in DMEM/F12 containing 10% FBS. On the next day, and to remove most of the contaminating macrophages, adherent cells were trypsinized and transferred to experimental dishes at a density of 15,000 cells/cm<sup>2</sup>. Sca-1<sup>+</sup>CD31<sup>-</sup> Lin<sup>-</sup> primary white and brown preadipocytes were facs sorted from adipose stromal cell preparations immediately after collagenase digestion.

#### Cell Culture and Adipocyte Differentiation

Murine 3T3-L1 preadipocytes (ATCC) and HIB-1B cells, kindly provided by Bruce Spiegelman, were propagated in DMEM containing 10% calf and fetal bovine serum, respectively. Mouse primary cells were expanded in DMEM/F12 supplemented with 10% FBS. For adipocyte differentiation experiments, cells were differentiated and maintained in an IBMX/dexamethasone-free minimal induction medium including insulin, T3, biotin, pantothenic acid, and troglitazone, with the exception of those exploring the effects of IBMX and Dex (Figure S4). Recombinant sonic hedgehog (Shh; 300 ng/ml; R&D Systems) or SAG (200 nM; Alexis) were added to the cells as indicated. All chemicals for cell culture were obtained from Sigma unless otherwise indicated.

#### Excision of *Sufu*<sup>fl/fl</sup> in Primary Adipocyte Progenitors

For adenoviral infection of primary white and brown fat precursors, near confluent cultures of SVC fractions of perigonadal white and interscapular brown adipose tissue depots were infected overnight with either Ad5-eGFP or Ad5-Cre-IRES-GFP. One day after infection, the medium was replaced and cells were maintained in complete growth medium for an additional 24 hr before inducing differentiation.

#### Quantitative RT-PCR

For quantitative PCR (qRT-PCR), analysis of total RNA was performed on an AbiPRISM 7900HT real-time cyler (Applied Biosystems) using iQ SYBR Green Supermix (Bio-Rad). Threshold cycles (C<sub>T</sub>-values) of all replicate analyses were normalized to acidic ribosomal phosphoprotein P0 (Rplp0/36B4). To compare

the effect of various treatments with untreated controls, 2<sup>-ΔΔC<sub>T</sub></sup> values were calculated to obtain fold expression levels. Primers are listed in Table S8.

#### Western Blot

Proteins were extracted by homogenizing in RIPA buffer containing protease inhibitors (Complete Mini, Roche). Adipose tissue homogenates were resolved by SDS-PAGE, transferred to PVDF membranes (GE Healthcare), and probed with anti-*Sufu* and anti-Hsc70 antibodies (Santa Cruz Biotechnology).

#### In Silico Gli Target Analysis, Luciferase Assays, and ChIP Analysis

Genomic sequences including 10 kb upstream of mouse *Ncor2*, *Nr2f2*, *Hes1*, and *Sfrp2* were analyzed for putative Gli-binding sites using ScanAce. Luciferase reporter plasmids were assembled from Gli-binding site clusters of *Ncor2* and *Nr2f2* cloned into pGL3-basic vector (Promega). Restriction sites and primer sequences are given in Table S12. 3T3-L1 cells were cotransfected with Gli effector plasmids or empty vector control and luciferase activity measured 48 hr post-transfection. For chromatin immunoprecipitation, chromatin was isolated from 3T3-L1 cells treated for 72 hr with or without SAG (200 nM) using the SimpleChIP Enzymatic ChIP kit (Cell Signaling Technology). ChIP assays were performed using the ChIP-IT (Active Motif) and IgG (Active Motif) used as a negative control. Anti-Gli2 (Abcam) and anti-Gli3 (Santa Cruz) rabbit polyclonal antibodies were used to immunoprecipitate the DNA/protein complex. Crosslink reversed samples were treated with Proteinase K and the DNA purified and analyzed using PCR. A primer list and promoter maps are included in Table S13 and Figure S6.

#### Statistical Analyses

All data unless otherwise indicated are shown as mean values ± standard error of the mean (SEM) and tested statistically using two-tailed Student's *t* test or ANOVA. All figures and statistical analyses were generated using GraphPad Prism 4. *p* < 0.05 was considered to indicate statistical significance.

#### SUPPLEMENTAL INFORMATION

Supplemental Information includes Extended Experimental Procedures, seven figures, and thirteen tables and can be found with this article online at doi:10.1016/j.cell.2009.12.027.

#### ACKNOWLEDGMENTS

The authors are indebted to the IMBA and MUW service departments, all members of the VDRC Drosophila library, and Barry Dickson, Pawel Pasierbek, Maria Novatchkova, Patricia Schittenhelm, Helen Damhofer, and Maria Ozsvar-Kozma for excellent technical help. J.A.P. was supported by fellowships from the JDRF and the Marie-Curie Foundation. This project, J.A.P., and H.E. are supported by the WWTF. C.-c.H. was supported by CIHR and CCSRI. J.M.P. is supported by the Austrian Academy of Sciences, GEN-AU (Genome Austria), the Austrian Ministry of Science and Education, and a European Union Advanced ERC grant. P.D.C. is a research associate from the FRS-FNRS Belgium. D.F. is supported by the CNRS and a Drosophila grant from the Programme MIME, and the D.F. laboratory is an "Equipe FRM" (Fondation pour la Recherche Médicale).

Received: May 22, 2009

Revised: September 30, 2009

Accepted: December 4, 2009

Published: January 7, 2010

#### REFERENCES

- Altarejos, J.Y., Goebel, N., Conkright, M.D., Inoue, H., Xie, J., Arias, C.M., Sawchenko, P.E., and Montminy, M. (2008). The *Creb1* coactivator *Crtc1* is required for energy balance and fertility. *Nat. Med.* 14, 1112–1117.
- Ashrafi, K., Chang, F.Y., Watts, J.L., Fraser, A.G., Kamath, R.S., Ahringer, J., and Ruvkun, G. (2003). Genome-wide RNAi analysis of *Caenorhabditis elegans* fat regulatory genes. *Nature* 421, 268–272.

- Baker, K.D., and Thummel, C.S. (2007). Diabetic larvae and obese flies—emerging studies of metabolism in *Drosophila*. *Cell Metab.* **6**, 257–266.
- Brown, L.J., Koza, R.A., Marshall, L., Kozak, L.P., and MacDonald, M.J. (2002). Lethal hypoglycemic ketosis and glyceroluria in mice lacking both the mitochondrial and the cytosolic glycerol phosphate dehydrogenases. *J. Biol. Chem.* **277**, 32899–32904.
- Buhman, K.K., Wang, L.C., Tang, Y., Swietlicki, E.A., Kennedy, S., Xie, Y., Liu, Z.Y., Burkly, L.C., Levin, M.S., Rubin, D.C., et al. (2004). Inhibition of Hedgehog signaling protects adult mice from diet-induced weight gain. *J. Nutr.* **134**, 2979–2984.
- Cypess, A.M., Lehman, S., Williams, G., Tal, I., Rodman, D., Goldfine, A.B., Kuo, F.C., Palmer, E.L., Tseng, Y.H., Doria, A., et al. (2009). Identification and importance of brown adipose tissue in adult humans. *N. Engl. J. Med.* **360**, 1509–1517.
- Dietzl, G., Chen, D., Schnorrer, F., Su, K.C., Barinova, Y., Fellner, M., Gasser, B., Kinsey, K., Oettel, S., Scheiblauer, S., et al. (2007). A genome-wide transgenic RNAi library for conditional gene inactivation in *Drosophila*. *Nature* **448**, 151–156.
- Fan, C.M., Porter, J.A., Chiang, C., Chang, D.T., Beachy, P.A., and Tessier-Lavigne, M. (1995). Long-range sclerotome induction by sonic hedgehog: direct role of the amino-terminal cleavage product and modulation by the cyclic AMP signaling pathway. *Cell* **81**, 457–465.
- Farmer, S.R. (2006). Transcriptional control of adipocyte formation. *Cell Metab.* **4**, 263–273.
- Farmer, S.R. (2009). Obesity: Be cool, lose weight. *Nature* **458**, 839–840.
- Farooqi, I.S., and O’Rahilly, S. (2007). Genetic factors in human obesity. *Obes. Rev.* **8** (Suppl 1), 37–40.
- Feldmann, H.M., Golozoubova, V., Cannon, B., and Nedergaard, J. (2009). UCP1 ablation induces obesity and abolishes diet-induced thermogenesis in mice exempt from thermal stress by living at thermoneutrality. *Cell Metab.* **9**, 203–209.
- Gesta, S., Tseng, Y.H., and Kahn, C.R. (2007). Developmental origin of fat: tracking obesity to its source. *Cell* **131**, 242–256.
- Gronke, S., Mildner, A., Fellert, S., Tennagels, N., Petry, S., Muller, G., Jackle, H., and Kuhnlein, R.P. (2005). Brummer lipase is an evolutionary conserved fat storage regulator in *Drosophila*. *Cell Metab.* **1**, 323–330.
- Gronke, S., Muller, G., Hirsch, J., Fellert, S., Andreou, A., Haase, T., Jackle, H., and Kuhnlein, R.P. (2007). Dual lipolytic control of body fat storage and mobilization in *Drosophila*. *PLoS Biol.* **5**, e137.
- Gutierrez, E., Wiggins, D., Fielding, B., and Gould, A.P. (2007). Specialized hepatocyte-like cells regulate *Drosophila* lipid metabolism. *Nature* **445**, 275–280.
- Hader, T., Muller, S., Aguilera, M., Eulenberg, K.G., Steuernagel, A., Ciossek, T., Kuhnlein, R.P., Lemaire, L., Fritsch, R., Dohrmann, C., et al. (2003). Control of triglyceride storage by a WD40/TPR-domain protein. *EMBO Rep.* **4**, 511–516.
- Hebrok, M., Kim, S.K., St Jacques, B., McMahon, A.P., and Melton, D.A. (2000). Regulation of pancreas development by hedgehog signaling. *Development* **127**, 4905–4913.
- Heine, V.M., and Rowitch, D.H. (2009). Hedgehog signaling has a protective effect in glucocorticoid-induced mouse neonatal brain injury through an 11betaHSD2-dependent mechanism. *J. Clin. Invest.* **119**, 267–277.
- Jiang, J., and Hui, C.C. (2008). Hedgehog signaling in development and cancer. *Dev. Cell* **15**, 801–812.
- Jiang, J., and Struhl, G. (1995). Protein kinase A and hedgehog signaling in *Drosophila* limb development. *Cell* **80**, 563–572.
- Koo, S.H., Flechner, L., Qi, L., Zhang, X., Srean, R.A., Jeffries, S., Hedrick, S., Xu, W., Boussouar, F., Brindle, P., et al. (2005). The CREB coactivator TORC2 is a key regulator of fasting glucose metabolism. *Nature* **437**, 1109–1111.
- Lefterova, M.I., and Lazar, M.A. (2009). New developments in adipogenesis. *Trends Endocrinol. Metab.* **20**, 107–114.
- Leopold, P., and Perrimon, N. (2007). *Drosophila* and the genetics of the internal milieu. *Nature* **450**, 186–188.
- Li, Z., Zhang, H., Denhard, L.A., Liu, L.H., Zhou, H., and Lan, Z.J. (2008). Reduced white fat mass in adult mice bearing a truncated Patched 1. *Int. J. Biol. Sci.* **4**, 29–36.
- Makino, S., Masuya, H., Ishijima, J., Yada, Y., and Shiroishi, T. (2001). A spontaneous mouse mutation, mesenchymal dysplasia (mes), is caused by a deletion of the most C-terminal cytoplasmic domain of patched (ptc). *Dev. Biol.* **239**, 95–106.
- Martin, P.M., Gopal, E., Ananth, S., Zhuang, L., Itagaki, S., Prasad, B.M., Smith, S.B., Prasad, P.D., and Ganapathy, V. (2006). Identity of SMCT1 (SLC5A8) as a neuron-specific Na<sup>+</sup>-coupled transporter for active uptake of L-lactate and ketone bodies in the brain. *J. Neurochem.* **98**, 279–288.
- Matsuzaka, T., Shimano, H., Yahagi, N., Kato, T., Atsumi, A., Yamamoto, T., Inoue, N., Ishikawa, M., Okada, S., Ishigaki, N., et al. (2007). Crucial role of a long-chain fatty acid elongase, Elovl6, in obesity-induced insulin resistance. *Nat. Med.* **13**, 1193–1202.
- Melcher, C., Bader, R., and Pankratz, M.J. (2007). Amino acids, taste circuits, and feeding behavior in *Drosophila*: towards understanding the psychology of feeding in flies and man. *J. Endocrinol.* **192**, 467–472.
- Min, K.T., and Benzer, S. (1999). Preventing neurodegeneration in the *Drosophila* mutant bubblegum. *Science* **284**, 1985–1988.
- Nybakken, K., Vokes, S.A., Lin, T.Y., McMahon, A.P., and Perrimon, N. (2005). A genome-wide RNA interference screen in *Drosophila melanogaster* cells for new components of the Hh signaling pathway. *Nat. Genet.* **37**, 1323–1332.
- Oldham, S., and Hafen, E. (2003). Insulin/IGF and target of rapamycin signaling: a TOR de force in growth control. *Trends Cell Biol.* **13**, 79–85.
- Panakova, D., Sprong, H., Marois, E., Thiele, C., and Eaton, S. (2005). Lipoprotein particles are required for Hedgehog and Wingless signalling. *Nature* **435**, 58–65.
- Rosen, E.D., and MacDougald, O.A. (2006). Adipocyte differentiation from the inside out. *Nat. Rev.* **7**, 885–896.
- Ross, D.A., Rao, P.K., and Kadesch, T. (2004). Dual roles for the Notch target gene *Hes-1* in the differentiation of 3T3-L1 preadipocytes. *Mol. Cell Biol.* **24**, 3505–3513.
- Schlegel, A., and Stainier, D.Y. (2007). Lessons from “lower” organisms: what worms, flies, and zebrafish can teach us about human energy metabolism. *PLoS Genet.* **3**, e199.
- Seale, P., Kajimura, S., and Spiegelman, B.M. (2009). Transcriptional control of brown adipocyte development and physiological function—of mice and men. *Genes Dev.* **23**, 788–797.
- Speakman, J., Hambly, C., Mitchell, S., and Krol, E. (2008). The contribution of animal models to the study of obesity. *Lab. Anim.* **42**, 413–432.
- Suh, J.M., Gao, X., McKay, J., McKay, R., Salo, Z., and Graff, J.M. (2006). Hedgehog signaling plays a conserved role in inhibiting fat formation. *Cell Metab.* **3**, 25–34.
- Suzawa, M., Takada, I., Yanagisawa, J., Ohtake, F., Ogawa, S., Yamauchi, T., Kadowaki, T., Takeuchi, Y., Shibuya, H., Gotoh, Y., et al. (2003). Cytokines suppress adipogenesis and PPAR-gamma function through the TAK1/TAB1/NIK cascade. *Nat. Cell Biol.* **5**, 224–230.
- Thomas, M.K., Rastalsky, N., Lee, J.H., and Habener, J.F. (2000). Hedgehog signaling regulation of insulin production by pancreatic beta-cells. *Diabetes* **49**, 2039–2047.
- Tseng, Y.H., Kokkotou, E., Schulz, T.J., Huang, T.L., Winnay, J.N., Taniguchi, C.M., Tran, T.T., Suzuki, R., Espinoza, D.O., Yamamoto, Y., et al. (2008). New role of bone morphogenetic protein 7 in brown adipogenesis and energy expenditure. *Nature* **454**, 1000–1004.
- van Marken Lichtenbelt, W.D., Vanhomerig, J.W., Smulders, N.M., Dros-saerts, J.M., Kemerink, G.J., Bouvy, N.D., Schrauwen, P., and Teule, G.J. (2009). Cold-activated brown adipose tissue in healthy men. *N. Engl. J. Med.* **360**, 1500–1508.

- Virtanen, K.A., Lidell, M.E., Orava, J., Heglind, M., Westergren, R., Niemi, T., Taittonen, M., Laine, J., Savisto, N.J., Enerback, S., et al. (2009). Functional brown adipose tissue in healthy adults. *N. Engl. J. Med.* *360*, 1518–1525.
- WHO (2009). Global Strategy on Diet (Physical Activity and Health).
- Wu, X., Ding, S., Ding, Q., Gray, N.S., and Schultz, P.G. (2002). A small molecule with osteogenesis-inducing activity in multipotent mesenchymal progenitor cells. *J. Am. Chem. Soc.* *124*, 14520–14521.
- Yan, Z., Cui, K., Murray, D.M., Ling, C., Xue, Y., Gerstein, A., Parsons, R., Zhao, K., and Wang, W. (2005). PBAF chromatin-remodeling complex requires a novel specificity subunit, BAF200, to regulate expression of selective interferon-responsive genes. *Genes Dev.* *19*, 1662–1667.
- Yu, C., Markan, K., Temple, K.A., Deplewski, D., Brady, M.J., and Cohen, R.N. (2005). The nuclear receptor corepressors NCoR and SMRT decrease peroxisome proliferator-activated receptor gamma transcriptional activity and repress 3T3-L1 adipogenesis. *J. Biol. Chem.* *280*, 13600–13605.
- Zehentner, B.K., Leser, U., and Burtscher, H. (2000). BMP-2 and sonic hedgehog have contrary effects on adipocyte-like differentiation of C3H10T1/2 cells. *DNA Cell Biol.* *19*, 275–281.
- Zhang, J., Xia, W.L., and Ahmad, F. (1995). Regulation of pyruvate carboxylase in 3T3-L1 cells. *Biochem. J.* *306*, 205–210.
- Zhang, Y., Proenca, R., Maffei, M., Barone, M., Leopold, L., and Friedman, J.M. (1994). Positional cloning of the mouse obese gene and its human homologue. *Nature* *372*, 425–432.
- Zingaretti, M.C., Crosta, F., Vitali, A., Guerrieri, M., Frontini, A., Cannon, B., Nedergaard, J., and Cinti, S. (2009). The presence of UCP1 demonstrates that metabolically active adipose tissue in the neck of adult humans truly represents brown adipose tissue. *FASEB J.* *23*, 3113–3120.



## EXTENDED EXPERIMENTAL PROCEDURES

### Fly Strains

Stocks were raised on standard cornmeal-agar medium at 25°C. The *Hsp70-GAL4;Tub-GAL80<sup>ts</sup>* (McGuire et al., 2004), *ppl-GAL4* (Colombani et al., 2003), *oe-GAL4* (line C; (Ferveur et al., 1997)), and *C57-GAL4* (Koh et al., 1999) lines have all been previously described. The *nsyb-GAL4* line (*synaptobrevin-GAL4*), was generated and kindly provided by Julie Simpson (Janelia Farm) and enhanced in its potency for driving the short hairpin RNAi lines by co-expression of *UAS-dicer2* (a kind gift of Barry Dickson). For tissue-specific secondary RNAi experiments a random set of RNAi lines plus RNAi directed against CG12333, which had been shown to behave as the isogenic *w<sup>1118</sup>* wild-type fly strain were used as control lines.

### Screening Procedure

In order to ensure tight temporal control and limit premature RNAi expression during development, we generated an *Hsp70-GAL4; Tub-GAL80<sup>ts</sup>* driver line where a *GAL80<sup>ts</sup>* element prevented potential leaky *GAL4* expression through development. This inducible RNAi expression system represented a means to bypass the developmental lethality associated with 30% of fly genes, and thus interrogate several thousand previously untested genes. Male flies containing the *UAS-RNAi* transgene against gene “X” were provided by the Vienna *Drosophila* RNAi Centre (VDRC) and crossed with 5 virgin *Hsp70-GAL4;Tub-GAL80<sup>ts</sup>* female flies at 18°C. One week later, parent flies were removed. Two weeks after crossing, vials were moved to 25°C for an additional week after which progeny were transferred to new vials and kept at 29°C for 2 days. Twice 20 adult male flies were sorted and placed into separate vials, one of which was subsequently heat shocked. Each RNAi line was determined in parallel with non-heat-shocked control flies of the same cross to control exactly for age, genetics and environment. Based on pilot experiments (not shown) the most effective heat-shock protocol was as follows: 30 min at 37°C; 30 min at 18°C; 30 min at 37°C. Flies were then returned to 29°C for 1 additional week. An additional 60 min heat shock in a dry incubator was performed after 2 days to increase the RNAi response. For the *ppl-GAL4*, *nsyb-GAL4*, *oe-GAL4*, and *C57-GAL4* drivers, crosses were set up at 25°C for 2 weeks and the progeny monitored for fat accumulation. At the end of the experiment eight male flies from heat-shock and control vials were manually crushed into 150  $\mu$ l of H<sub>2</sub>O in 96-well nonskirted PCR plates on ice. Plates were sonicated to homogeneity (Diagenode, 2 min, high intensity). Sonicates were heat-inactivated at 95°C for 10 min, centrifuged 30 min at 300 g and 4°C and frozen until analysis. On the day of analysis plates were thawed, vortexed, re-centrifuged, and 20  $\mu$ l of cold supernatant used for 96-well based colorimetric determination of triglycerides (GPO Trinder, Sigma) and protein (BCA, Pierce). Reproducibility of the system based on assaying 80 replicates of 8 *w<sup>1118</sup>* wild-type flies (isogenic background line of the RNAi library) 2 to 4 days post-eclosure was  $0.45 \pm 0.06$  mg/ml for triglycerides and  $0.45 \pm 0.04$  mg/ml for protein content (Suppl. Figure S1c).

### Data Analysis and Ortholog Retrieval

Mouse and human orthologs were retrieved from the orthology resources InParanoid, OrthoMCL or Ensembl. Gene Ontology enrichment was performed using GoStat with a Benjamini and Hochberg correction through the online GOToolbox application (Martin et al., 2004). For each Gene Ontology term of the class “biological process” a Fisher exact test was performed where the number of genes assigned to a term in the candidate set and in all other genes from the screen is compared.

### Generation of *Sufu* Mutant Mice

Conditional *Sufu* mice were generated by the laboratory of C.-c.H. (unpublished data). Briefly, the genomic fragment including exons 4–8 of the *Sufu* gene was inserted between two *loxP* (fl) sites of a Neomycin resistance selectable targeting construct. After electroporation into embryonic stem cells, neomycin resistant clones were picked and screened by PCR and Southern blot for homologous recombination into the appropriate genomic locus. Correctly targeted ES cells were injected into blastocysts and transferred to pseudo-pregnant mice. The resulting chimeric mice were mated to obtain germline transmission and generate a mouse line harbouring a conditional *Sufu* allele. Mice were maintained on a standard rodent chow diet with 12 hr light and dark cycles. Adipose-specific *Sufu* knockout mice were generated by crossing conditional *Sufu<sup>fl/fl</sup>* mice with *aP2-Cre* transgenic mice generated by the Evans laboratory and obtained from JAX (B6.Cg-Tg[Fabp4-cre]1Rev/J; Strain:005069) (He et al., 2003). Both, *Cre* recombinase positive wild-type and *Cre* recombinase negative *Sufu<sup>fl/fl</sup>* littermate served as controls. All experimental procedures in the current study were performed on mice backcrossed at least 6 generations onto C57BL/6J. All animal experiments were carried out according to an ethical animal license protocol and contract approved by the Medical University Vienna (MUW), IMBA and the Austrian Ministry of Sciences (BMWF-66.009/0104-C/GT/2007).

### Indirect Calorimetry

Mice were placed for 72 hr in metabolic cages connected to an open-circuit, indirect calorimetry system combined with the determination of spontaneous activity by beam breaking (Oxylet, Panlab-Bioseb). The animals were accustomed to the apparatus during the first 24 hr, followed by measurement for a further 48 hr. Oxygen consumption and carbon dioxide production were recorded at 5 min intervals using a computer-assisted data acquisition program (Chart 5.2, AD Instruments Sydney, Australia).

### Euglycemic Hyperinsulinemic Clamps and Tissue Glucose Utilization

An indwelling catheter was placed into the left femoral vein and externalised in the interscapular region. The animals were allowed to recover for 5 days and fasted for 6 hr on the day of the experiment. For 3 hr D-[3-<sup>3</sup>H]-glucose was infused at a rate of 30  $\mu$ Ci/kg/min and insulin at a rate of 18 mU/kg/min. Euglycemia was maintained by variable infusion of 15% glucose. Whole blood was sampled from the tail every 10 min during the last hour. Total radioactivity in the supernatant was determined by scintillation counting. Total glucose concentrations were determined by the glucose oxidase method (BioMerieux). Released glucose was determined by a glucose oxidase method (BioMerieux). In order to determine glucose utilization of individual tissues, mice were injected with <sup>3</sup>H-2-deoxyglucose (Perkin Elmer) through the intrafemoral catheter one hour before completion of the infusion procedure (Knauf et al., 2005). Tail blood was sampled at 5, 10, 15, 20, 30, 45, and 60 min after the injection to determine the time course of <sup>3</sup>H-2-deoxyglucose disappearance. The <sup>3</sup>H-2 deoxyglucose-6-phosphate content was determined from NaOH hydrolysed tissues by the Somogyi procedure.

### DNA Isolation, Genotyping, and Detection of Recombined *Sufu*<sup>fl</sup> Alleles

Genomic DNA was isolated from various tissues using the QIAamp DNA mini kit (QIAGEN). Mice were genotyped on tail DNA. For the detection of the Cre transgene, genomic PCR was performed using Cre-forward (5'-TCGCGATTATCTTCTATATCTTCAG-3') and Cre-reverse (5'-GCTCGACCAGTTTAGTTACCC-3') primers, respectively. Genotyping and detection of different *Sufu* alleles was done using the following primer combinations: *Sufu* wild-type allele: P1 (5'-GCTGAATTCTTGACTCACTG-3') and P2 (5'-CCTACCCTTTCCAGTGAAG-3'); *Sufu*<sup>fl</sup> allele: P1 (5'-GCTGAATTCTTGACTCACTG-3') and P3 (5'-CTGAAGGCTCTTTACTATTGCT-3'); *Sufu* recombined allele: P4 (5'-GTGTCAGTTTCATAGCCTG-3') and P5 (5'-GCTGTTGTACTCATGGTC-3').

### Histology

For tissue sections, hematoxylin and eosin (H&E) staining was performed on 5  $\mu$ m paraffin sections of tissues fixed for 16 hr in 4% phosphate-buffered formalin at 4°C. Adipocyte number analysis was performed according to method of (Cinti et al.). The morphometric technique measures adipocyte number and area relative to total tissue area. All cells on 3 sections (0.5 mm intervals) per animal were quantified; in excess of 10,000 adipocytes per knockout fat pad and >35,000 for controls. Perigonadal WAT pads from 4 animals per group were analyzed. Definiens software suite was used to define and quantify tissue compartments based on shape, size and presence of a lipid droplet. Calculations of total number per fat pad were then made based on adipose tissue mass measured upon tissue harvesting.

### Isolation of Mouse Primary Brown and White Preadipocytes

Primary pre-adipocytes were obtained by collagenase digestion from perigonadal white and interscapular brown adipose tissue depots in mice. In brief, minced white and brown adipose tissue depots from 6-8 week old mice were digested at 37°C for 45-60 min in a shaking water bath with a cocktail consisting of 1 mg/ml collagenase II (Worthington) in DMEM containing 3% fatty acid free BSA (Sigma) and DNase I (100 Units/ml, Sigma). For brown adipose tissue digestions, Dispase 1 (1.2 U/ml, Worthington) was added to the cocktail to increase digestion efficiency. After digestion, the slurry was passed through a 100  $\mu$ m cell strainer (Becton Dickinson). Cells were then pelleted by centrifugation at 250 g for 5 min, washed with DMEM/F12 containing 10% FBS, and red blood cells were lysed using RBC lysis buffer (Sigma). After a final washing step cells were passed through a 30  $\mu$ m cell strainer (Partec) to remove clumps and most of the endothelial cell aggregates. On the next day, and to remove most of the contaminating macrophages, adherent cells were trypsinized and transferred to experimental dishes at a density of 15,000 cells/cm<sup>2</sup>.

### Isolation of Sca-1<sup>+</sup>CD31<sup>-</sup>Lin<sup>-</sup> Primary Adult Brown and White Preadipocytes

Primary white and brown preadipocytes from adipose stromal cells were isolated as described (Scime et al., 2005). In brief, stromal vascular cell (SVCs) fractions of white and brown adipose tissue depots from 6-week-old C57B/6J mice were digested. Isolated SVCs were re-suspended and incubated on ice for 20 min with conjugated antibodies (Becton Dickinson) recognizing Stem Cell Antigen-1 (Sca-1) conjugated to APC (Caltag), CD31 conjugated to FITC (Becton Dickinson), and Lineage antibodies (Becton Dickinson) including the blood markers Mac-1, Gr-1, Ter119, CD45R/B220, and CD3 $\epsilon$  conjugated to biotin (Lin-biotin). Detection of Lin-biotin was done by avidin conjugated to PE (Becton Dickinson). Labeled cells were sorted on an automated cell sorter (FACSARIA, Becton Dickinson). The Sca-1<sup>+</sup> CD31<sup>-</sup>Lin<sup>-</sup> cell sorted fraction was plated at a density of 15,000 cells/cm<sup>2</sup>.

### Cell Culture and Adipocyte Differentiation

Murine 3T3-L1 pre-adipocytes (ATCC) and HIB-1B cells, kindly provided by Bruce Spiegelman, were propagated in DMEM containing 10% calf and fetal bovine serum, respectively. Mouse primary cells were expanded in DMEM/F12 supplemented with 10% FBS. Cells were never allowed to become confluent, strictly split before reaching 70%–80% confluence, and were kept at 37°C and 5% CO<sub>2</sub>. For adipocyte differentiation experiments, cells were allowed to become confluent and post-confluent cells were then differentiated and maintained until analyses in an IBMX/dexamethasone-free minimal induction medium. This cocktail consisted of the respective growth media supplemented with 850 nM insulin, 1 nM T3, 33  $\mu$ M biotin, 17  $\mu$ M pantothenic acid, 5  $\mu$ M troglitazone, and was changed every 2-3 days. All differentiation experiments, BAT and WAT, cell line and primary cell based, were performed using the minimal induction media with exception of those exploring the effects of IBMX and Dex (Figure S4). For the classical

IBMX/dexamethasone protocol, adipocyte differentiation was induced by treating post confluent cells for 48 hr by adding 0.5 mM IBMX, 1 mM dexamethasone, 850 nM insulin, 1 nM T3, and 5  $\mu$ M troglitazone. When using this regimen, cells were switched back after 48 hr to growth medium supplemented with 850 nM insulin, 33  $\mu$ M biotin and 17  $\mu$ M pantothenic acid, which was changed every other day. Recombinant sonic hedgehog (Shh; 300 ng/ml; R&D Systems) or SAG (200 nM; Alexis) were added to the cells as indicated in the text or figure legends. All chemicals for cell culture were obtained from Sigma unless otherwise indicated.

### Excision of *Sufu* from *Sufu<sup>fl/fl</sup>* Adult Primary Adipocyte Progenitors

For adenoviral infection of primary white and brown fat precursors, near confluent cultures of SVC fractions of perigonadal white and interscapular brown adipose tissue depots were isolated from homozygous *Sufu<sup>fl/fl</sup>* mice and plated as outlined above. Isolated cells were infected overnight with adenoviruses expressing GFP (Ad5-eGFP) and adenoviruses expressing Cre and GFP (Ad5-Cre-IRES-GFP) (The multiplicity of infection = 100; in DMEM/F12 containing 10% FBS). Both adenoviruses were obtained from the Developmental Studies Hybridoma Bank, Iowa. One day after infection, the medium was replaced and cells were maintained in complete growth medium for an additional 24 hr before inducing adipogenic differentiation using our IBMX/dexamethasone-free protocol described above.

### Oil Red O Staining

For staining of neutral lipids, cells were fixed and stained with Oil Red O (OrO) according to standard procedures. In brief, cells were washed with PBS and fixed with 2% PFA in PBS at room temperature for 10 min. Fixed cells were washed again with PBS and stained with OrO (1% w/v isopropanol, diluted 3:2 in PBS) for 1 hr at room temperature. Stained cells were washed and selected wells photographed using either a digital camera or a microscope to obtain pictures at higher magnifications.

### Quantitative RT-PCR

For qRT-PCR analysis total RNA was extracted from respective tissues and cells using the RNeasy Mini and Micro Isolation Kits (QIAGEN) according to the manufacturer's instructions. Isolated total RNA was reverse-transcribed into cDNA using commercially available kits (Applied Biosystems). All subsequent qRT-PCR reactions were performed on an AbiPRISM 7900HT real-time cyclor (Applied Biosystems) using the iQ SYBR Green Supermix (Bio-Rad). Post-amplification melting curve analysis was performed to check for unspecific products and primer-only controls were included to ensure the absence of primer dimers. For normalization threshold cycles ( $C_t$ -values) of all replicate analyses were normalized to acidic ribosomal phosphoprotein P0 (Rplp0/36B4) within each sample to obtain sample-specific  $\Delta C_t$  values (=  $C_t$  gene of interest -  $C_t$  Rplp0). To compare the effect of various treatments with untreated controls,  $2^{-\Delta\Delta C_t}$  values were calculated to obtain fold expression levels, where  $\Delta\Delta C_t = (\Delta C_t \text{ treatment} - \Delta C_t \text{ control})$ . Primers used are listed in Table S10.

### Western Blot Analysis

Proteins were extracted from tissues by homogenizing in RIPA buffer (0.5% NP-40, 0.1% sodium deoxycholate, 150 mM NaCl, 50 mM Tris-HCl, pH 7.5) containing protease inhibitors (Complete Mini, Roche). The homogenate was cleared by centrifugation at 4°C for 30 min at 15,000 g and the supernatant portion containing the protein fraction recovered. 20  $\mu$ g of white and 10  $\mu$ g of brown adipose tissue homogenate were resolved by SDS-PAGE, transferred to PVDF membranes (GE Healthcare) and probed with anti-Sufu and anti-Hsc70 antibodies (sc-10934; dilution 1:500 and sc-7298; dilution 1:20,000, Santa Cruz Biotechnology). Antigen-specific binding of antibodies was visualized using a commercial chemiluminescence detection system (ECL plus, GE Healthcare).

### In Silico Gli Target Gene Analysis, Luciferase Reporter Assays and ChIP Analysis

Genomic sequences including the 10kb upstream regions of mouse nuclear receptor co-repressor 2 (Ncor2, RefSeq NM\_011424), nuclear receptor subfamily 2, group F, member 2 (Nr2f2, RefSeq NM\_183261), hairy and enhancer of split 1 (Hes1, RefSeq NM\_008235), and secreted frizzled-related protein 2 (Sfrp2, RefSeq NM\_009144), were retrieved from <http://genome.ucsc.edu> and analyzed for putative Gli binding sites using the ScanAce motif search algorithm (Roth et al., 1998). Potential Gli responsive elements selected for chromatin immunoprecipitation and reporter analysis had to fulfill the following criteria: i) a maximum of 2 mismatches to the consensus Gli-binding site GACCACCCA (Kinzler and Vogelstein, 1990), ii) no mismatch at essential positions 4C and 6C, and iii) clustering of two or more high-scoring sites fulfilling the first two criteria within a maximum distance of 1 kb. For the construction of luciferase reporter plasmids, fragments containing clustered Gli-binding sites in the 5' cis-regulatory or intron regions of Ncor2 and Nr2f2 were PCR-amplified from mouse genomic DNA and cloned into a pGL3-basic vector (Promega). Respective restriction sites and primer sequences are given in Table S12. For luciferase reporter assays, 3T3-L1 cells were cotransfected with Gli effector plasmids or empty vector as control, the respective reporter construct and a lacZ expression vector for normalization. Luciferase activity was measured 48 hr post-transfection on a Luci-II luminometer (Anthos) using Luciferase Assay Substrate (Promega) according to the manufacturer's instructions. For chromatin immunoprecipitation, 3T3-L1 cells were grown in DMEM (high glucose) supplemented with 10% fetal calf serum and either treated for 72 hr with 200 nM SAG (Alexis Biochemicals) or left untreated. Preparation of chromatin was done with the SimpleChIP Enzymatic ChIP kit (Cell Signaling Technology) according to the manufacturer's instructions. ChIP assays were performed using the ChIP-IT kit (Active Motif) according to the manufacturer's protocol. Negative control IgG (Active Motif), anti-Gli2 rabbit polyclonal antibodies (Abcam), and anti-Gli3 rabbit polyclonal

antibodies (Santa Cruz) were used to immunoprecipitate the DNA/protein complex. Following immunoprecipitation, crosslinking was reversed, the proteins were removed by treatment with Proteinase K, and the DNA was purified and analyzed using PCR. A primer list and promoter map are included in [Table S13](#) and [Figure S6](#).

### Statistical Analyses

All data unless otherwise indicated are shown as mean values  $\pm$  SEM. Data sets were compared for statistical significance using the two-tailed Students t test or ANOVA where appropriate. All figures and statistical analyses were generated using GraphPad Prism 4.  $p < 0.05$  was considered to indicate statistical significance.

### SUPPLEMENTAL REFERENCES

- Cinti, S., Zingaretti, M., Cancellato, R., Ceresi, E., and Ferrara, P. (2001). Morphologic techniques for the study of brown adipose tissue and white adipose tissue. In *Adipose Tissue Protocols*, G. Ailhaud, ed. (Totowa, New Jersey: Humana Press), pp. 21–51.
- Colombani, J., Raisin, S., Pantalacci, S., Radimerski, T., Montagne, J., and Leopold, P. (2003). A nutrient sensor mechanism controls *Drosophila* growth. *Cell* *114*, 739–749.
- Ferveur, J.F., Savarit, F., O’Kane, C.J., Sureau, G., Greenspan, R.J., and Jallon, J.M. (1997). Genetic feminization of pheromones and its behavioral consequences in *Drosophila* males. *Science* *276*, 1555–1558.
- He, W., Barak, Y., Hevener, A., Olson, P., Liao, D., Le, J., Nelson, M., Ong, E., Olefsky, J.M., and Evans, R.M. (2003). Adipose-specific peroxisome proliferator-activated receptor gamma knockout causes insulin resistance in fat and liver but not in muscle. *Proc. Natl. Acad. Sci. USA* *100*, 15712–15717.
- Kinzler, K.W., and Vogelstein, B. (1990). The *GLI* gene encodes a nuclear protein which binds specific sequences in the human genome. *Mol. Cell. Biol.* *10*, 634–642.
- Knauf, C., Cani, P.D., Perrin, C., Iglesias, M.A., Maury, J.F., Bernard, E., Benhamed, F., Gremeaux, T., Drucker, D.J., Kahn, C.R., et al. (2005). Brain glucagon-like peptide-1 increases insulin secretion and muscle insulin resistance to favor hepatic glycogen storage. *J. Clin. Invest.* *115*, 3554–3563.
- Koh, Y.H., Popova, E., Thomas, U., Griffith, L.C., and Budnik, V. (1999). Regulation of DLG localization at synapses by CaMKII-dependent phosphorylation. *Cell* *98*, 353–363.
- Martin, D., Brun, C., Remy, E., Mouren, P., Thieffry, D., and Jacq, B. (2004). GOToolBox: functional analysis of gene datasets based on Gene Ontology. *Genome Biol.* *5*, R101.
- McGuire, S.E., Mao, Z., and Davis, R.L. (2004). Spatiotemporal gene expression targeting with the TARGET and gene-switch systems in *Drosophila*. *Sci. STKE* *2004*, pl6.
- Roth, F.P., Hughes, J.D., Estep, P.W., and Church, G.M. (1998). Finding DNA regulatory motifs within unaligned noncoding sequences clustered by whole-genome mRNA quantitation. *Nat. Biotechnol.* *16*, 939–945.
- Scime, A., Grenier, G., Huh, M.S., Gillespie, M.A., Bevilacqua, L., Harper, M.E., and Rudnicki, M.A. (2005). Rb and p107 regulate preadipocyte differentiation into white versus brown fat through repression of PGC-1alpha. *Cell Metab.* *2*, 283–295.

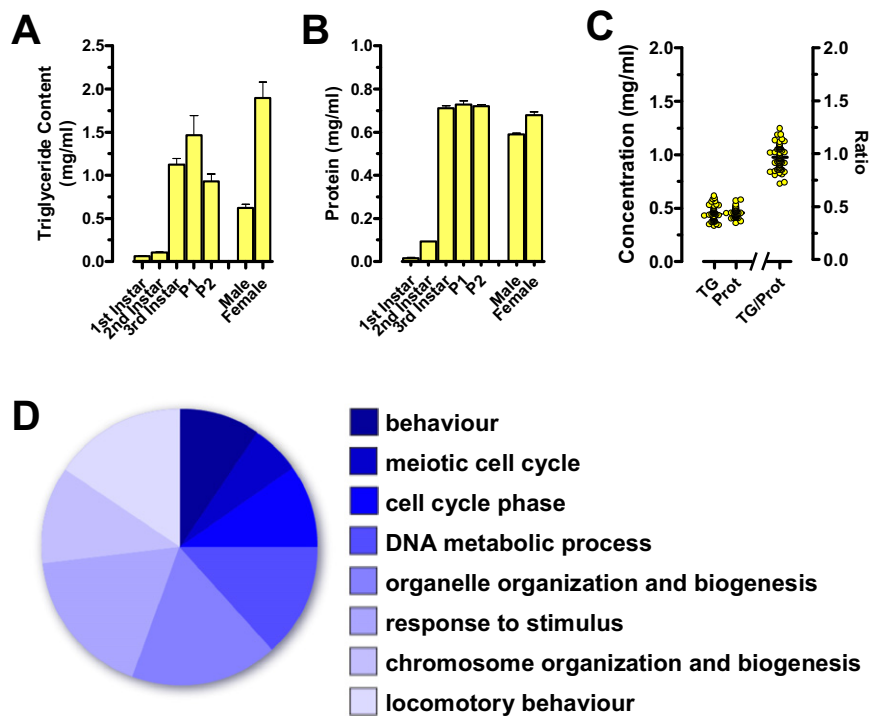


**Figure S1. Basal Triglyceride and Protein Contents in *Drosophila*, Relates to Figure 1**

(A) Triglyceride content of *w<sup>1118</sup>* *Drosophila* strain measured throughout development using a medium-throughput 96-well plate based system with a colorimetric determination endpoint.

(B) Protein content of *w<sup>1118</sup>* *Drosophila* measured with the same experimental set-up. Data in a and b are shown as mean triglyceride content  $\pm$  SEM.  $n = 5-8$ .

(C) Individual triglyceride and protein content in 80 different sets of 8 male flies each measured 2 to 4 days after eclosion. Measurement was made to validate the medium throughput experimental system designed for the genome-wide screen.

(D) Pie chart summarizing the most depleted functional classifications using gene ontology for biological processes for all annotated genes with Z-scores in excess of  $\pm 1.65$  through three rounds of testing.

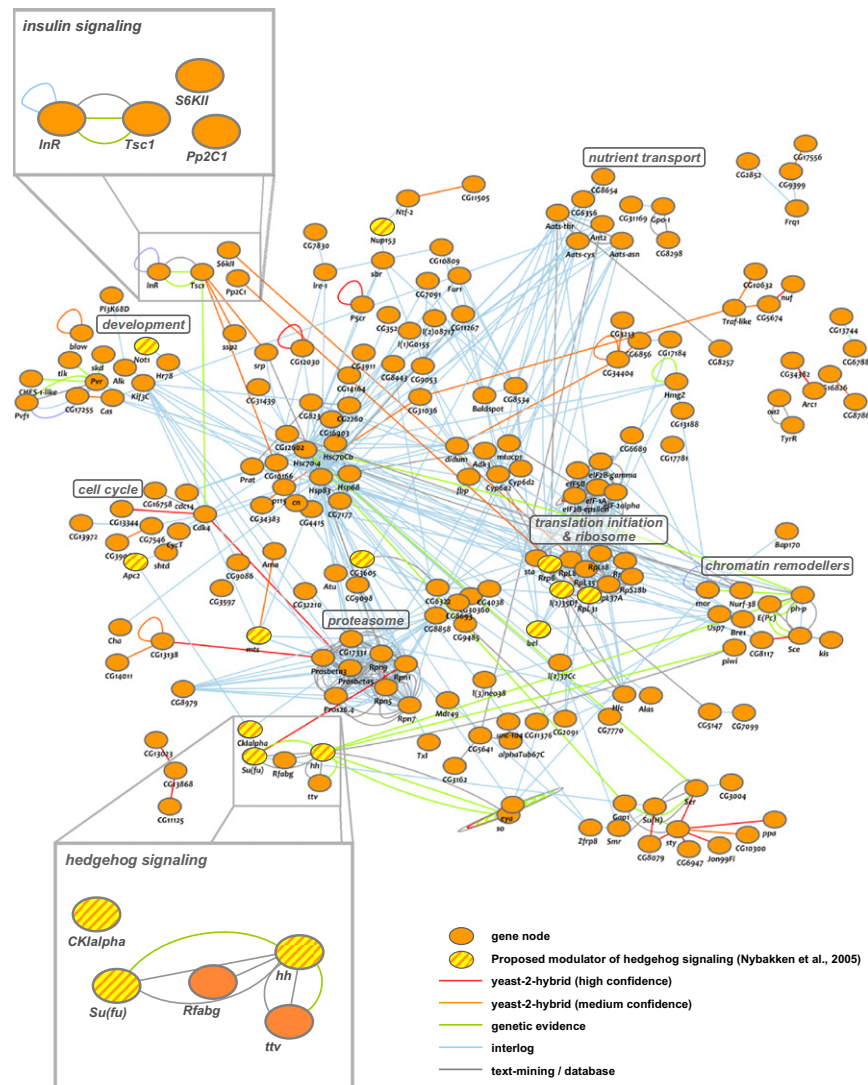


**Figure S2. Interaction Network for Candidate Obesity Genes, Relates to Figure 1**

The interaction network was assembled using Cytoscape 2.6.2 based on interactions retrieved from STRING, DROIDB, and BIOGRID. Datasets consisted of yeast-two-hybrid, text-mining, and database annotations (e.g., KEGG). Assembly of the visual layout was performed using manual modification of an automated force-directed layout. Insets highlight the location of both the hedgehog and insulin signaling pathways.



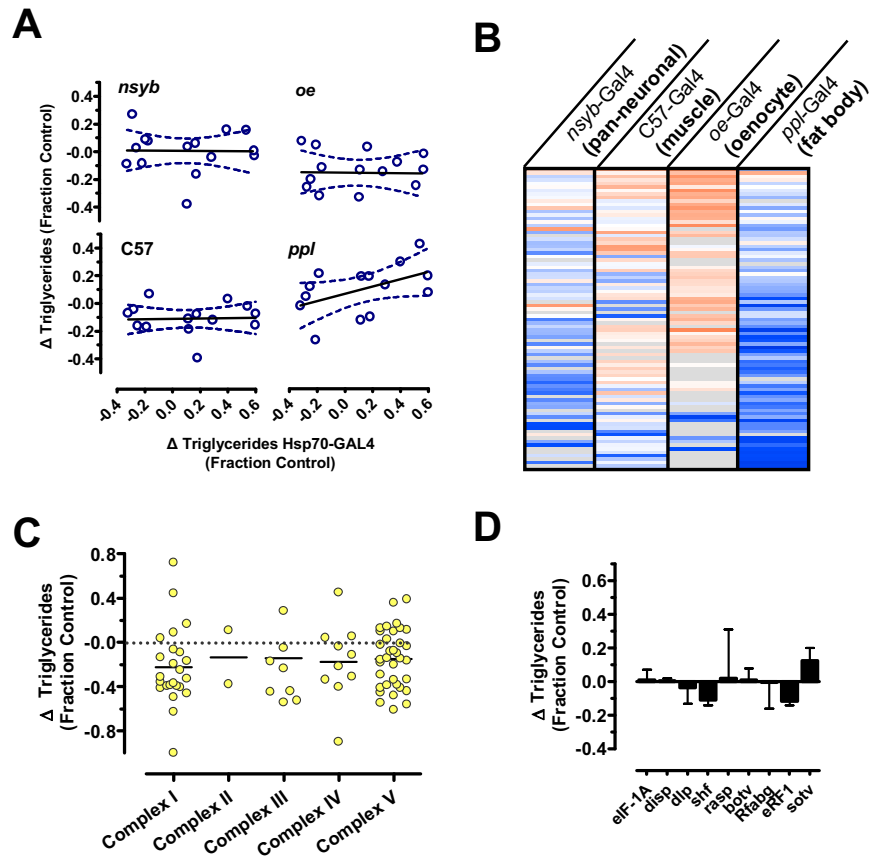


**Figure S3. Tissue Specificity of Hedgehog and OxPhos Pathway Triglyceride Changes, Relates to Figure 3**

(A) Correlation analysis of triglyceride levels in RNAi lines targeting hedgehog signaling crossed to the tissue-specific drivers *nsyb*-GAL4 (pan-neuronal), *oe*-GAL4 (oocyte), *C57*-GAL4 (muscle), and *ppl*-GAL4 (fat-body). Tissue-specific triglyceride changes (y-axes) are correlated with those observed using the inducible ubiquitous *Hsp70*-GAL4;*Tub*-GAL80<sup>ts</sup> (x axis).

(B) Triglyceride changes in *ppl*-GAL4 driven UAS-RNAi transgenic lines targeting hedgehog specific ligand processing and release genes.

(C) Heat-map of the adiposity of UAS-RNAi transgenic fly lines targeting the members of the gene ontology category *oxidative phosphorylation*. Changes in adiposity were in response to tissue-specific silencing using the drivers *nsyb*-GAL4 (pan-neuronal), *oe*-GAL4 (oocyte), *C57*-GAL4 (muscle), and *ppl*-GAL4 (fat-body). Changes are relative to averages of control RNAi-lines and *w<sup>1118</sup>* flies crossed to the respective GAL4 lines.

(D) Triglyceride responses of the same *oxidative phosphorylation* targeting RNAi-transgenic lines to heat-shock induced ubiquitous knockdown. Data are presented as mean  $\pm$  SEM, n = 4.

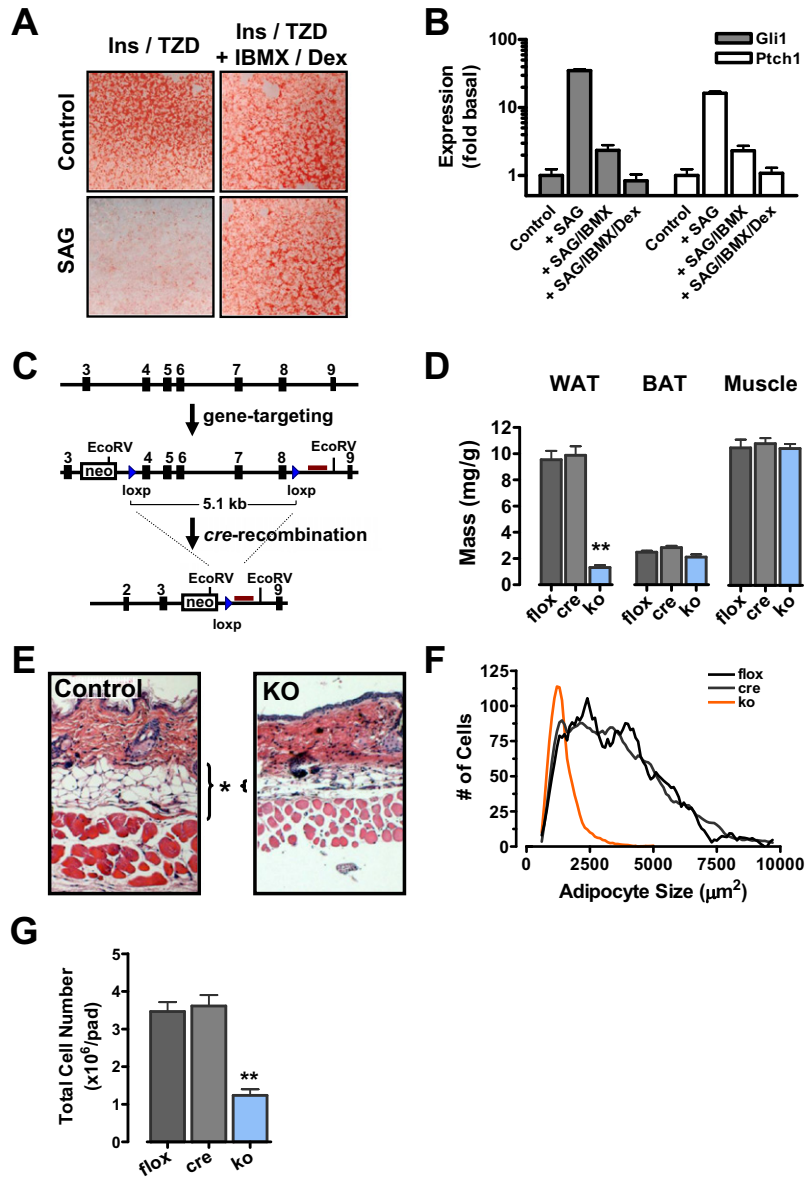


**Figure S4. IBMX and Dexamethasone Dependence of Hedgehog Signaling in Adipocytes and Generation of Lipotrophic *Sufu* Mutant Mice, Relates to Figure 4**

(A) Oil Red O staining of 3T3-L1 cells induced with minimal (Insulin/Troglitazone) or complete (Insulin/Troglitazone/IBMX/Dex) differentiation cocktails in the absence (control) or presence (SAG) of the hedgehog agonist SAG (200nM). One experiment representative of 5 repeats is shown.

(B) Quantitative RT-PCR monitoring of hedgehog pathway activation with the target genes *Gli1* and *Ptch1* confirmed activation by SAG and abrogation of hedgehog induction in the presence IBMX and Dex.

(C) To establish an in vivo model to assess hedgehog effects on adipose biology, a targeting strategy was used to generate mice with a conditional *Sufu* allele. The conditional allele incorporates two *Cre*-sensitive loxP sites flanking exons 4-8 of the *Sufu* open reading frame. Numbered boxes indicate exons.

(D) White (perigonadal) adipose tissue, interscapular brown adipose tissue and muscle (soleus and gastrocnemius) masses were determined in *aP2-Sufu*KO mice at 8 weeks of age. Data from littermates that carry the floxed allele (flox) or *aP2-Cre* (cre) are shown as controls. Data are presented as mean  $\pm$  SEM, n = 6 mice per group. \*\*p < 0.01.

(E) H&E stained sections of skin highlight a clear reduction in cutaneous adipose tissue.

(F) White adipocyte size distributions in perigonadal fat pads taken from 4 week old male *aP2-Sufu*KO mice and littermate floxed (flox) and *aP2-Cre* (cre) controls. Measurements were made by morphometry on > 10,000 (KO) and > 35,000 (controls) cells per animal using a combination of scanning of H&E stained interval sectioned adipose tissue (3 per mouse) and subsequent software assisted morphometric analysis (G)

(G) Total white adipocyte cell numbers in 4- to 8-week-old male *aP2-Sufu*KO mice and littermate floxed (flox) and *aP2-Cre* (cre) controls. Data are presented as mean  $\pm$  SEM, n = 5.



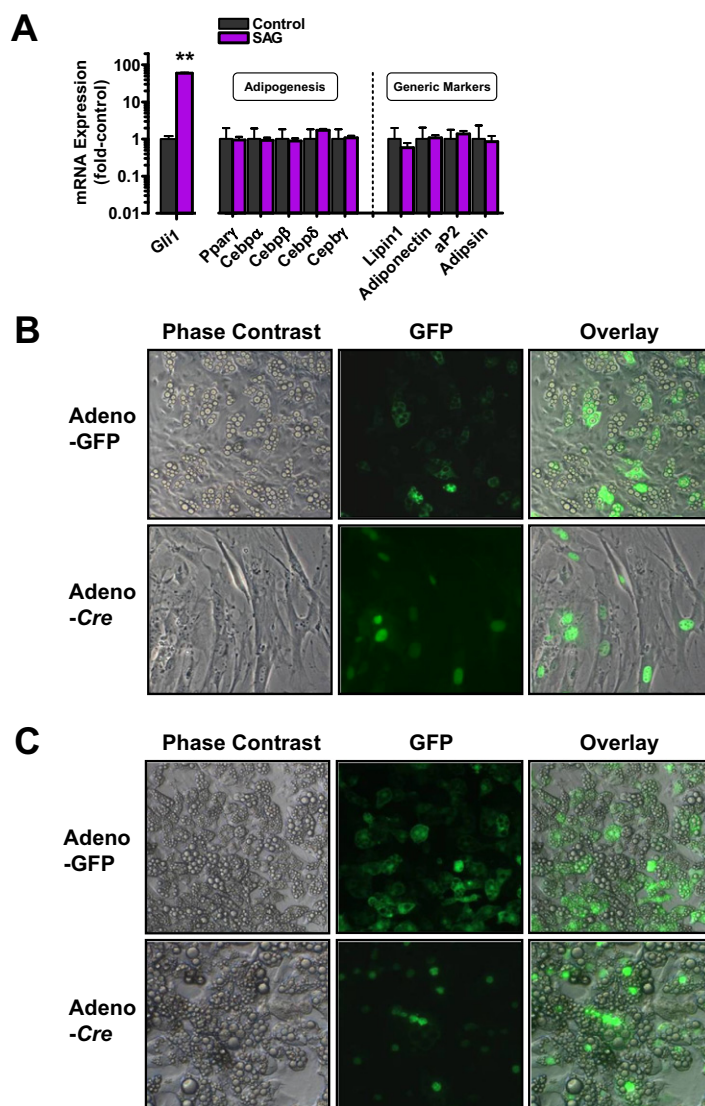


**Figure S5. Hedgehog Activation Blocks White Adipogenesis in Primary White but Not Brown Progenitor Cells, Relates to Figure 5**

(A) BAT-derived SVC precursors show no indication of altered generic adipocyte markers despite marked hedgehog activation. Quantitative RT-PCR analysis for *Gli1* and the indicated markers are shown for 96 hr after induced differentiation using minimal induction medium. Data are presented as mean  $\pm$  s.e.m.,  $n = 3-5$  mice per group. \*\* $p < 0.01$ .

(B) Phase-contrast and immunofluorescence images of primary white adipose SVC's from *Sufu<sup>fl/fl</sup>* animals induced to differentiate after infection with Adeno-Cre or and the Adeno-GFP control vector. Adeno-Cre contained an IRES-GFP with a nuclear localization sequence. Infected cells therefore display fluorescent green nuclei. The Adeno-GFP control produces cytoplasmic GFP. Right panels show an overlay of the phase contrast and GFP images.

(C) Phase-contrast and immunofluorescence images of primary brown adipose SVC's from *Sufu<sup>fl/fl</sup>* animals induced to differentiate after infection with Adeno-Cre or and the Adeno-GFP control vector. Representative experiments are shown that for both WAT and BAT differentiation were repeated multiple times. Note that the same experiments as in Figure 5E and 5F are shown.

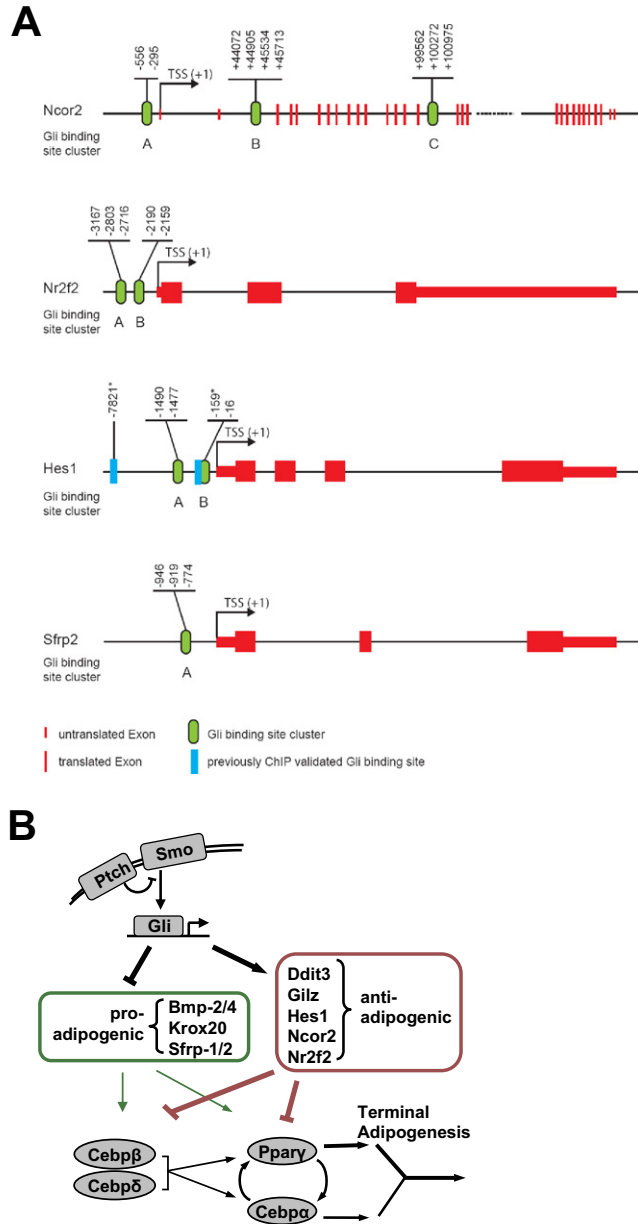


**Figure S6. Proposed Role of Hedgehog Signaling in White Adipogenesis, Relates to Figure 6**

(A) The relative positions of *in silico* predicted Gli binding sites in the 5' upstream regulatory or intron regions of the respective genomic loci (not drawn to scale) are shown. Numbers indicate the position of each predicted binding site relative to the transcriptional start site (TSS), which was set to +1. Blue rectangles in the Hes1 promoter region highlight previously ChIP validated Gli binding sites.

(B) Schematic summarizing the postulated mechanism of hedgehog induced blockade of white adipocyte differentiation.

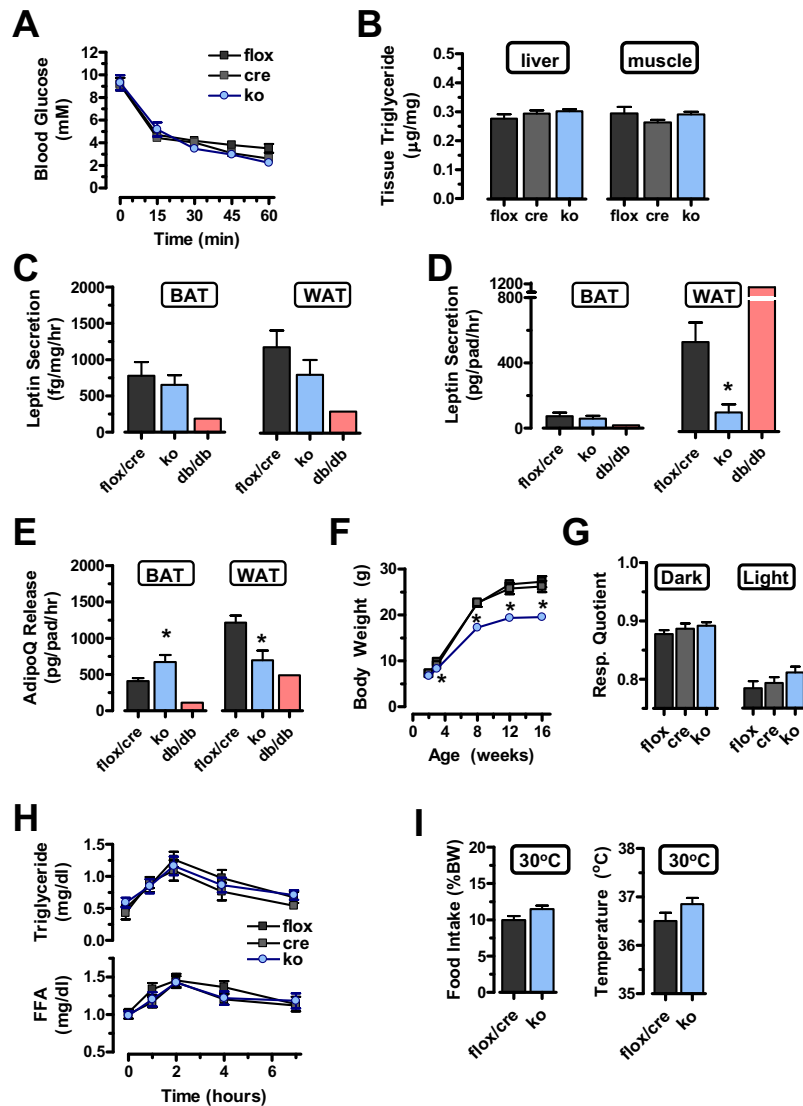


**Figure S7. Glucose and Energy Handling in *aP2-Sufu*KO Mice Is Largely Normal, Relates to Figure 7**

(A) Insulin tolerance testing showed no evidence of insulin resistance (i.p. 1 U/kg) consistent with (B) unaltered intra-hepatic and intra-muscular triglyceride levels. Lipids were measured after lipid extraction from biopsies taken in the fed state.

(C–E) Adiponectin and leptin secretion in vitro from BAT and WAT fragment cultures from *aP2-Sufu*KO animals. Secretion is calculated both (C) per mg tissue, as well as (D and E) per adipose tissue pad to highlight the relative contribution of WAT versus BAT and to directly relate knockout to control tissues.

(F) Body weight measurements of *aP2-Sufu*KO mice and littermate controls.

(G) Respiratory quotient calculated from gas exchange values measured by indirect calorimetry.

(H) Lipid tolerance testing (2 g/kg olive oil) in *aP2-Sufu*KO mice after a 6 hr fast highlight normal uptake and disposal of a lipid load.

(I) Food intake and body temperature in mice moved from 22°C to 30°C. Data are mean  $\pm$  SEM (n = 6–12). \*p < 0.05.

# Cross-Talk Between Interferon- $\gamma$ and Hedgehog Signaling Regulates Adipogenesis

Jelena Todoric,<sup>1</sup> Birgit Strobl,<sup>2</sup> Alexander Jais,<sup>1</sup> Nicole Boucheron,<sup>3</sup> Martina Bayer,<sup>1</sup> Sabine Amann,<sup>1</sup> Josefine Lindroos,<sup>1</sup> Raffaele Teperino,<sup>4</sup> Gerhard Prager,<sup>5</sup> Martin Bilban,<sup>1</sup> Wilfried Ellmeier,<sup>3</sup> Franz Krempler,<sup>6</sup> Mathias Müller,<sup>2</sup> Oswald Wagner,<sup>1</sup> Wolfgang Patsch,<sup>7</sup> J. Andrew Pospisilik,<sup>4</sup> and Harald Esterbauer<sup>1</sup>

**OBJECTIVE**—T cells and level of the cytokine interferon- $\gamma$  (IFN- $\gamma$ ) are increased in adipose tissue in obesity. Hedgehog (Hh) signaling has been shown to potently inhibit white adipocyte differentiation. In light of recent findings in neurons that IFN- $\gamma$  and Hh signaling cross-talk, we examined their potential interaction in the context of adipogenesis.

**RESEARCH DESIGN AND METHODS**—We used Hh reporter cells, cell lines, and primary adipocyte differentiation models to explore costimulation of IFN- $\gamma$  and Hh signaling. Genetic dissection using *Ifngr1*<sup>-/-</sup> and *Stat1*<sup>-/-</sup> mouse embryonic fibroblasts, and ultimately, anti-IFN- $\gamma$  neutralization and expression profiling in obese mice and humans, respectively, were used to place the findings into the in vivo context.

**RESULTS**—T-cell supernatants directly inhibited hedgehog signaling in reporter and 3T3-L1 cells. Intriguingly, using blocking antibodies, *Ifngr1*<sup>-/-</sup> and *Stat1*<sup>-/-</sup> cells, and simultaneous activation of Hh and IFN- $\gamma$  signaling, we showed that IFN- $\gamma$  directly suppresses Hh stimulation, thus rescuing adipogenesis. We confirmed our findings using primary mouse and primary human (pre)adipocytes. Importantly, robust opposing signals for Hh and T-cell pathways in obese human adipose expression profiles and IFN- $\gamma$  depletion in mice identify the system as intact in adipose tissue in vivo.

**CONCLUSIONS**—These results identify a novel antagonistic cross-talk between IFN- $\gamma$  and Hh signaling in white adipose tissue and demonstrate IFN- $\gamma$  as a potent inhibitor of Hh signaling.

**T**he World Health Organization (WHO) currently estimates that more than 1 billion individuals worldwide are overweight. Almost one-third of these individuals are clinically obese, markedly raising their chances of cardiovascular disease, type 2 diabetes, cancer, and stroke (1).

Interestingly, not all obesity results in metabolic disease, and thus, it is not adiposity alone that contributes to adipose tissue abnormalities (2–9). For instance, large, lipid-loaded fat cells appear to be particularly important for the development of obesity-related cardiovascular and metabolic disorders. Increases in adipocyte size correlate with higher production of inflammatory adipokines, and increased circulating inflammatory markers are clinically observed in patients with hypertrophic adipocytes compared with fat mass-matched control subjects with smaller fat cells. Exactly why this is the case remains to be proven; one suggestion has been that the impaired function of large adipocytes results from the relative hypoxia of the micro-environment (2,3).

Poor expandability of the adipocyte pool, combined with chronic low-grade inflammation, is thought to initiate a vicious cycle that ultimately culminates in obesity with full metabolic dysfunction, including insulin resistance (10–13). Several studies have shown that in addition to macrophages, the number of CD3<sup>+</sup> T cells is increased in adipose tissue in obesity (14,15). Furthermore, genetic or diet-induced obese (DIO) mouse models exhibit a prominent and early influx of cytotoxic CD8<sup>+</sup> T cells (16–19). Local mRNA levels of the activated T-cell cytokine interferon- $\gamma$  (IFN- $\gamma$ ) are increased in adipose tissue of DIO mice compared with lean controls, and IFN- $\gamma$ -deficient animals show significantly decreased proinflammatory gene expression and macrophage accumulation in adipose tissue in obesity (20). In addition, IFN- $\gamma$  decreases insulin sensitivity and suppresses differentiation in human adipocytes (21,22). However, whether T-cell activation and associated increases in IFN- $\gamma$  per se cause insulin resistance in adipose tissue has been questioned (23). Indeed, macrophage infiltration is the most robust discriminant between insulin-sensitive (IS) and insulin-resistant (IR) individuals with morbid obesity (24).

Hedgehog (Hh) signaling is an ancestral developmental process directing embryonic differentiation and adult tissue homeostasis through stem cell regulation and orchestration of complex differentiation programs (25–28). Activation of the Hh pathway is initiated by the Hh ligands, which release inhibition of the Smoothed (Smo)-Patched (Ptch) dual-receptor system at the cell surface, ultimately culminating in translocation of the Gli transcription factors to the nucleus and modulation of their target genes. Activation reinforces the signaling system as promoters of a number of the signaling constituents themselves represent Gli-targets, including Gli1 and Ptch1. We and others have demonstrated that Hh signaling is important in adipose tissue differentiation in vivo (29,30), specifically blocking white but not brown adipocyte differentiation at an early stage (30). Of

From the <sup>1</sup>Department of Laboratory Medicine, Medical University Vienna, Vienna, Austria; the <sup>2</sup>Institute of Animal Breeding and Genetics, University of Veterinary Medicine, Vienna, Austria; the <sup>3</sup>Institute of Immunology, Medical University Vienna, Vienna, Austria; <sup>4</sup>Epigenetic Focus, Max Planck Institute for Immunobiology and Epigenetics, Freiburg, Germany; the <sup>5</sup>Department of Surgery, Medical University Vienna, Vienna, Austria; the <sup>6</sup>Department of Internal Medicine, Krankenhaus Hallein, Salzburg, Austria; and the <sup>7</sup>Department of Laboratory Medicine, Paracelsus Medical University, Salzburg, Austria.

Corresponding author: Harald Esterbauer, harald.esterbauer@meduniwien.ac.at; or J. Andrew Pospisilik, pospisilik@immunbio.mpg.de.

Received 24 November 2010 and accepted 12 March 2011.

DOI: 10.2337/db10-1628

This article contains Supplementary Data online at <http://diabetes.diabetesjournals.org/lookup/suppl/doi:10.2337/db10-1628/-/DC1>.

© 2011 by the American Diabetes Association. Readers may use this article as long as the work is properly cited, the use is educational and not for profit, and the work is not altered. See <http://creativecommons.org/licenses/by-nc-nd/3.0/> for details.

note, expression of Hh target genes is significantly decreased in adipose tissue of genetic and DIO mouse models, suggesting persistent inhibition of the pathway in obesity (29).

Cross-talk between Hh and IFN- $\gamma$  signaling has been described in some cells of the central nervous system (31–33). Canonical Hh signaling has been shown to mediate neuronal and oligodendroglial differentiation (34–37). Interestingly, IFN- $\gamma$  induces sonic Hh (Shh) mRNA expression in astroglia and neuronal stem cells (32) and has been shown to contribute to medulloblastoma development by reactivating Hh signaling via induction of Shh (38). IFN- $\gamma$  stimulation induces *Shh* gene expression in cultured primary granular neuronal precursor cells, with subsequent induction of the Hh target gene *Gli1* (33). However, IFN- $\gamma$  might also be capable of inhibiting canonical Hh-signaling and *Gli1* expression in neuronal stem cells in multiple sclerosis and associated animal models (32).

Considering that CD8<sup>+</sup> T cells that produce IFN- $\gamma$  are among the first invaders of adipose tissue in obesity and that Hh blocks white fat expansion in vivo (30), we hypothesized that IFN- $\gamma$  might interfere with ongoing Hh signaling and support increased adipocyte turnover. Using a combination of in vitro and in vivo models we show that IFN- $\gamma$ - and Hh-signaling pathways independently impair white adipocyte differentiation. Surprisingly, costimulation of both signaling cascades resulted in reciprocal cosuppression, relieving their individual antiadipogenic actions and permitting adipogenesis. Our data demonstrate for the first time inhibition of Hh signaling via the IFN- $\gamma$ /Janus kinase (Jak)/signal transducer and activator of transcription (Stat1) axis in adipose tissue and suggest a novel antagonistic regulatory module to optimize white adipocyte turnover according to the metabolic state.

## RESEARCH DESIGN AND METHODS

**Screening of Hh pathway activities using Shh-LIGHT2 and *Ptch*<sup>-/-</sup> cells.** Shh-LIGHT2 cells, a NIH-3T3-derived cell line generated to screen for Hh pathway activities (39) were obtained from the American Type Culture Collection (cat. CRL-2795, Manassas, VA) and cultured according to recommended protocols (39). After reaching confluence, cells were starved in Dulbecco's modified Eagle's medium containing 0.5% FCS. Starved cells were stimulated for 48 h with the synthetic Smoothed AGONIST (SAG; ALEXIS Biochemicals, San Diego, CA) or recombinant sonic Hh (Shh) protein (R&D Systems, Minneapolis, MN) and/or IFN- $\gamma$  (BD Pharmingen, San Diego, CA), or were left untreated. Jak proteins were inhibited by Jak Inhibitor I (Calbiochem, San Diego, CA). Primary fibroblasts lacking functional *Ptch* (*Ptch*<sup>-/-</sup>) were derived from *Ptch*<sup>-/-</sup> mouse embryos (strain 003081, The Jackson Laboratory, Bar Harbor, ME). After the cells had reached confluence, they were maintained in low-serum medium (0.5% FCS) and treated with IFN- $\gamma$  or left untreated for 2 days. Hh signaling activities in Shh-LIGHT2 and *Ptch*<sup>-/-</sup> cells were measured using the Dual-Luciferase Reporter Assay System (Promega, Madison, WI) or the Tropix galacto-light plus assay system (Tropix, Bedford, MA), respectively. Signal intensities were normalized to Renilla luciferase (Shh-LIGHT2 cells) or total protein content (*Ptch*<sup>-/-</sup> cells), as described (39).

**Preparation and activation of T cells.** CD8<sup>+</sup> lymphocytes were purified from spleens from C57BL/6J mice using negative selection with IMag Streptavidin Particles Plus-DM (BD Biosciences, Bedford, MA) according to the manufacturer's protocol. T cells were added to 48-well plates coated with 1 mg/mL anti-Cd3e and 3 mg/mL anti-Cd28 (both BD Pharmingen). Supernatants of stimulated T cells were harvested after 48 h.

**Cell culture and adipocyte differentiation.** Mouse 3T3-L1 preadipocytes, primary mouse, and human cells were isolated, propagated, and differentiated as described ([30] and Supplementary Methods). Recombinant Shh (R&D Systems), SAG (ALEXIS Biochemicals), and/or recombinant IFN- $\gamma$  (BD Pharmingen) were added to the cells, as indicated in the text or Figure legends.

**Oil Red O staining.** For staining of neutral lipids, cells were fixed and stained with Oil Red O (OrO; Sigma-Aldrich, St. Louis, MO) according to standard procedures. In brief, cells were washed with PBS and fixed with 2% paraformaldehyde in PBS at room temperature for 10 min. Fixed cells were washed

again with PBS and stained with OrO (1% w/v isopropanol, diluted 3:2 in PBS) for 1 h at room temperature. Nuclei were counterstained with bromophenol blue. Stained cells were washed and photographed.

**Quantitative RT-PCR.** Transcript levels were quantified as described in the Supplementary Appendix.

**Western blot analysis.** Antibodies and detailed methods are described in the Supplementary Appendix.

**Isolation of primary mouse embryonic fibroblasts.** Primary mouse embryonic fibroblasts (MEFs) were derived from day 13.5 embryos obtained from wild-type, *Stat1*<sup>-/-</sup> (40) and *Ifngr1*<sup>-/-</sup> (41) mice. MEFs were prepared as described (42). All mice were of C57BL/6 background. The animal experiments were discussed and approved by the ethics committee at the Institute of Animal Breeding and Genetics, University of Veterinary Medicine Vienna and the Austrian laws (GZ 68.205/0204-C/GT/2007 and GZ 68.205/0233-II/10b/2009).

**Animal handling and treatment of mice with anti-IFN- $\gamma$  monoclonal antibody.** C57BL/6J mice were purchased from The Jackson Laboratory. At age 6 weeks, male littermates were placed for 24 weeks on a high-fat (HF) diet (HF group,  $n = 15$ , 60 kcal% fat, D12492) to induce obesity and on a low-fat (LF) diet (LF group,  $n = 10$ , 10 kcal% fat, D12450B) to serve as lean controls (both diets from Research Diets, New Brunswick, NJ). For the last 2 weeks of diets, mice fed the HF diet were randomly split into two groups: HF and HF treated with antibodies (HF+Ab,  $n = 5$ ). HF+Ab mice were injected with 0.5 mg i.p. anti-IFN- $\gamma$  monoclonal antibodies (BD Pharmingen) three times within the last 2 weeks of the diet. Control LF and HF animals received the same amount of rat IgG (Sigma-Aldrich). All experimental protocols were approved by the Institutional Animal Care and Use Committee at Medical University Vienna (protocol no. BMWF-66.009/0066-II/106/2009), and all studies were performed according to the methods approved in the protocol.

**IFN- $\gamma$  and adiponectin ELISA.** IFN- $\gamma$  and adiponectin levels in mouse serum were determined by ELISA (R&D Systems). For details see Supplementary Methods.

**Adipose tissue fractionation.** Digestion of perigonadal white fat pads was performed as described previously (30). Adipose tissue macrophages were isolated from stromal vascular fraction (SVF) cells using an antibody directed against the panmacrophage marker F4/80 (eBiosciences, San Diego, CA) coupled to magnetic beads (Miltenyi Biotec, Auburn, CA) according to the manufacturer's protocol.

**Human samples and clinical parameters.** The study included 25 obese patients and 21 nonobese control subjects who underwent weight-reducing surgery or elective surgical procedures such as cholecystectomy. Participants were included if they had fasting plasma glucose levels <7.0 mmol/L, no history of diabetes or use of blood glucose-lowering medications, no weight changes >3% during the previous 2 months, and C-reactive protein levels <20 mg/L. To reduce confounding by insulin resistance, obese subjects with a homeostasis model assessment (HOMA) index >2.5 were excluded. All study subjects provided informed consent, and the local ethics committee approved the study protocols. Tissue biopsy specimens from visceral adipose tissue, obtained during surgery, were collected in RNA-later (Ambion, Austin, TX) and stored at -80°C until further processing. Plasma glucose, insulin, C-reactive protein concentrations, and the HOMA index were determined as described (43).

**Gene set enrichment analysis.** Gene set enrichment analysis methods were done as described in the Supplementary Appendix.

**Statistical analyses.** All data are shown as mean  $\pm$  SEM, unless otherwise indicated. The significance of differences between means was assessed by two-tailed Student *t* test or ANOVA with the Tukey honestly significance difference test post hoc, where appropriate. Differences between human study groups were ascertained by ANOVA. We used multiple regression to adjust all measurements for concomitant effects of sex and age. Adjustments for *CD68* and *CD144* were performed as indicated. Categorical data were summarized by frequencies and analyzed by the  $\chi^2$  test. All reported *P* values are two-tailed.

## RESULTS

**T-cell activation blocks Hh signaling in an IFN- $\gamma$ -dependent manner.** Previous studies have shown that Hh signaling activity is diminished in the adipose tissue of obese mice (29) and that CD8<sup>+</sup> T-cell infiltration is an early hallmark of obese adipose tissue in both mice and humans (17). To test whether the two phenomena are causally related, we examined the effects of activated T-cell supernatants on the Hh-responsive luciferase reporter cell line Shh-LIGHT2 (39). Addition of the Hh-activator SAG to Shh-LIGHT2 cells robustly induces luciferase activity (Fig. 1A). Intriguingly, cotreatment with supernatants from CD8<sup>+</sup> T cells activated in vitro with anti-CD3 and anti-CD28

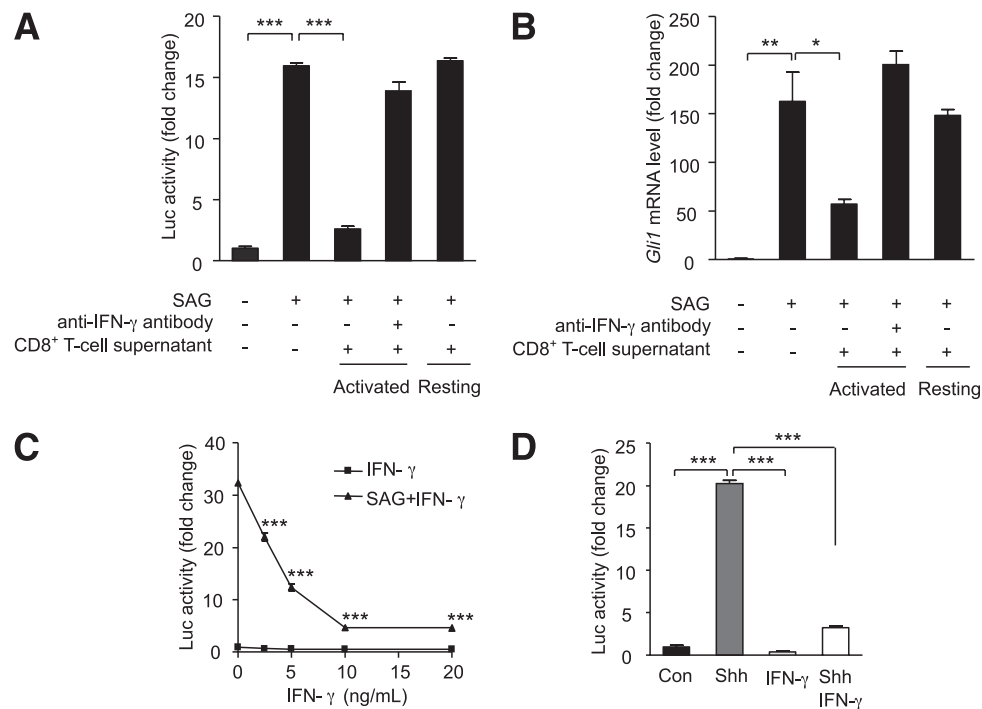


**FIG. 1. Suppression of Shh signaling by activated T cells is IFN- $\gamma$  dependent.** **A:** Shh-LIGHT2 cells were cultured for 48 h with no stimulus, SAG (200 nmol/L), SAG in presence or absence of supernatant from resting or activated CD8<sup>+</sup> T cells, with or without anti-IFN- $\gamma$  monoclonal antibody (25 ng/ $\mu$ L) and assayed for luciferase activity. **B:** 3T3-L1 preadipocytes were treated in the same way as described for the Shh-LIGHT2 cells above (SAG 20 nmol/L). *Gli1* mRNA was measured by quantitative RT-PCR and normalized for ribosomal protein, large, P0, (*Rplp0*). **C:** Shh-LIGHT2 cells were cultured for 48 h in the absence or presence of SAG plus the indicated concentrations of IFN- $\gamma$  and assayed for luciferase activity. **D:** Confluent Shh-LIGHT2 reporter cells were left untreated (Con), or treated with recombinant Shh (200 ng/mL), IFN- $\gamma$  (10 ng/mL), or both, for 48 h. Data represent means  $\pm$  SEM of triplicate samples. \* $P$  < 0.05; \*\* $P$  < 0.01; \*\*\* $P$  < 0.001.

antibodies markedly diminished the SAG-induced luciferase response. Importantly, the supernatant from resting T cells showed no inhibitory effect (Fig. 1A). To test whether the observed effect was unique to Shh-LIGHT2 cells, we exposed 3T3-L1 preadipocytes to parallel treatment conditions. In direct corroboration of the Shh-LIGHT2 findings, the activated CD8<sup>+</sup> T-cell supernatant substantially reduced SAG-induced *Gli1* mRNA expression in 3T3-L1 cells (Fig. 1B). Once again, the addition of supernatant from resting, rather than activated cells, showed no effect. Importantly, the addition of anti-IFN- $\gamma$ -blocking antibodies abolished the marked inhibitory effect of the T-cell supernatant on Hh activation in both experimental systems (Fig. 1A and B), directly implicating IFN- $\gamma$  in the inhibition of Hh signaling in Shh-LIGHT2 cells and in preadipocytes. Characterization of the potency of IFN- $\gamma$ -mediated Hh inhibition revealed significant effects at the low nmol/L level in Shh-LIGHT2 cells (Fig. 1C). Indeed, IFN- $\gamma$  alone was sufficient to affect a nearly total block of SAG-induced Hh activity. Importantly, these findings were confirmed pharmacologically using the endogenous Shh ligand as well as genetically using fibroblasts derived from *Ptch* knockout mouse embryos (39) harboring constitutive activation of Hh signaling and downstream target genes (Fig. 1D and Supplementary Fig. 1). Thus, activated CD8<sup>+</sup> T cells inhibit Hh signaling in an IFN- $\gamma$ -dependent manner.

**IFN- $\gamma$  rescues adipogenesis in vitro by over-riding the strong inhibitory effect of Hh signaling.** To functionally assess the inhibitory role of IFN- $\gamma$  on Hh signaling in adipocytes, we induced 3T3-L1 cells to undergo adipogenesis in the presence or absence of SAG, IFN- $\gamma$ , or vehicle for

10 days. In line with our previous data (30), SAG treatment of 3T3-L1 cells completely blocked adipogenesis. These effects were observed macroscopically with OrO staining for lipid droplets (Fig. 2A and B), by quantitative PCR-based expression profiling of the hallmark Hh target genes *Gli1*, *Hhip*, and *Ptch1* (Fig. 2C), and on corresponding protein levels of *Gli1* and *Hhip* (Fig. 2D and Supplementary Fig. 2).

In keeping with the macroscopic findings, we observed substantially reduced mRNA expression levels of the key adipogenic markers *Fabp4* and *Adipoq* as well as the master regulators of adipogenesis, *Cebpa* and *Ppar $\gamma$*  (Fig. 2E). In line with published data, IFN- $\gamma$  also partially blocked differentiation of 3T3-L1 cells with a reduction of OrO-positive adipocytes and a decrease of key adipose-specific markers ([20–22]; Fig. 2A, B, and E). Intriguingly, whereas treatment of 3T3-L1 cells with IFN- $\gamma$  alone induced a partial inhibitory effect on adipogenesis, simultaneous activation of Hh and IFN- $\gamma$  signaling pathways in 3T3-L1 preadipocytes rescued any observable Hh-induced block and restored nearly complete adipogenesis (Fig. 2A–E). Restoration of differentiation capacity by coaddition of IFN- $\gamma$  and SAG was associated with substantial reductions in Hh target gene expression relative to SAG alone on both the protein and the mRNA levels (*Gli1* and *Hhip*; Fig. 2C and D and Supplementary Fig. 2) as well as recovery of mRNA expression for all key differentiation markers (*Fabp4*, *Adipoq*, *Cebpa*, and *Ppar $\gamma$* ; Fig. 2E). Further, IFN- $\gamma$  treatment blunted the SAG-induced increase of chicken ovalbumin upstream promoter-transcription factor 2 (Coup-TF2) and *Gata2* (Supplementary Fig. 3), direct downstream mediators of Hh-induced adipogenic block (30,44). Thus, IFN- $\gamma$  rescues Hh-induced adipogenic block.



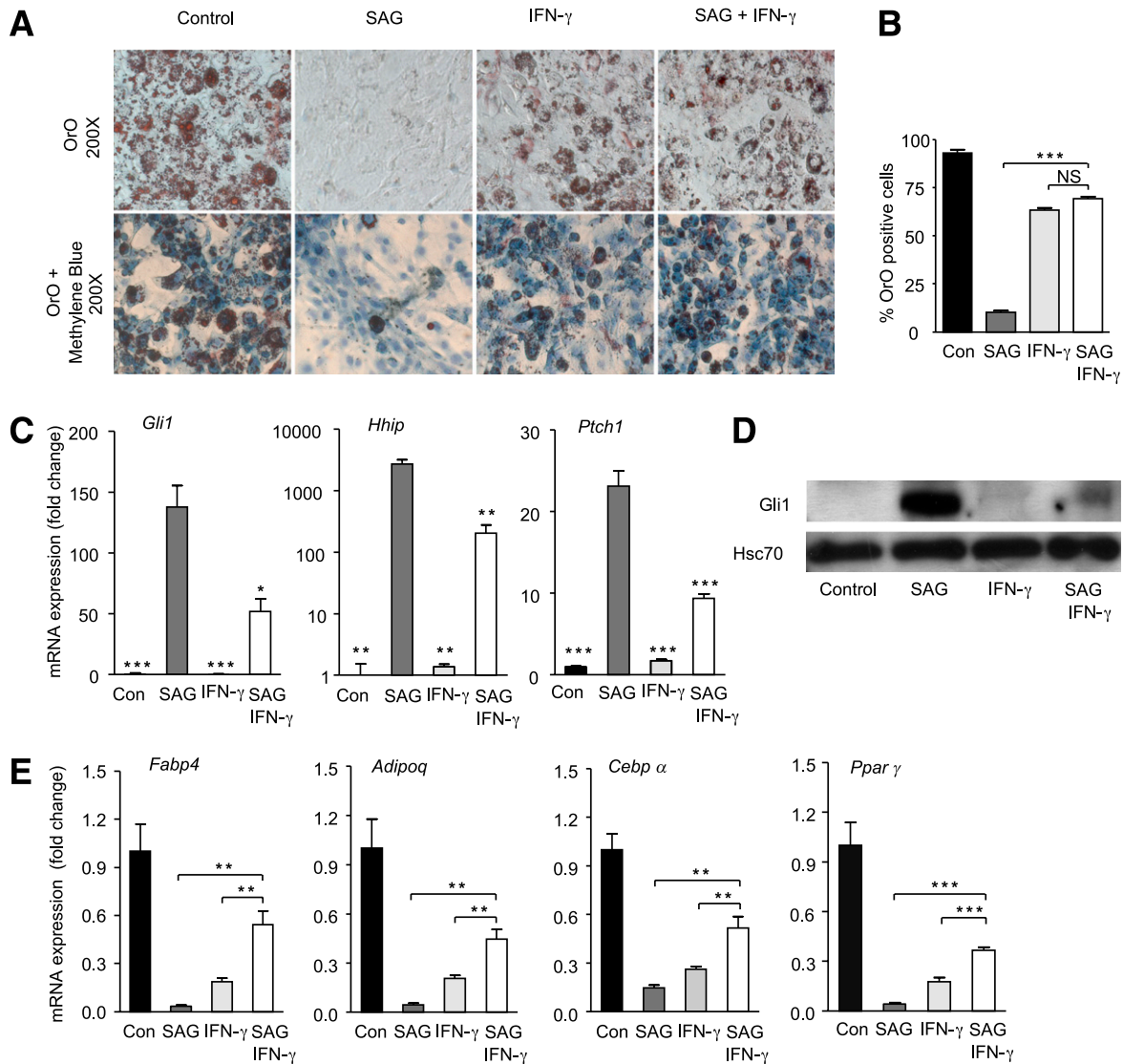


**FIG. 2.** IFN- $\gamma$  prevents SAG-induced inhibition of adipocyte differentiation. **A:** 3T3-L1 cells were induced to differentiate into adipocytes in the presence of 20 nmol/L SAG and/or 50 ng/mL IFN- $\gamma$  or were left untreated (Con) for 10 days. OrO staining was performed 10 days after induction. **B:** Adipocytes were counted under a bright-field microscope and presented as the percentage of the total number of methylene blue-stained nuclei. **C:** mRNA levels of Hh target genes (*Gli1*, *Hhip*, and *Ptch1*) were measured by quantitative RT-PCR analysis and normalized to *Rplp0*. **D:** *Gli1* Western blot of whole-cell lysates. Heat shock protein 70 was used as the loading control. **E:** mRNA levels of marker genes of adipocyte differentiation (*Fabp4*, *Adipoq*, *Cebp $\alpha$* , and *Ppar $\gamma$* ) were measured by quantitative RT-PCR analysis. Data represent means  $\pm$  SEM of triplicate samples. \* $P < 0.05$ ; \*\* $P < 0.01$ ; \*\*\* $P < 0.001$ ; NS, not significant. (A high-quality color representation of this figure is available in the online issue.)

**IFN- $\gamma$ -mediated inhibition of Hh responses requires activation of Jak-Stat signaling.** Among others, IFN- $\gamma$  activates the Jak-Stat pathway (45). To test whether activated Jak-Stat signaling was responsible for inhibition of SAG responses, we treated Shh-LIGHT2 cells with SAG and/or IFN- $\gamma$  in the presence or absence of a pan-Jak inhibitor (JakInh) (46). As expected, of the single-compound control wells, only SAG elicited a substantial luciferase response (Fig. 3A). IFN- $\gamma$  and JakInh alone or combined showed no significant induction of Hh signaling. Surprisingly, simultaneous treatment of cells with SAG (200 nmol/L) and JakInh (2  $\mu$ mol/L) resulted in a marked potentiation of the Gli-induced luciferase activity compared with SAG treatment alone (Fig. 3A). Critically, the addition of JakInh to IFN- $\gamma$ /SAG costimulated wells also resulted in a potentiated response compared with SAG alone, indicating that IFN- $\gamma$  requires downstream Jak activity to inhibit

Hh signaling (Fig. 3A). Of note, there is evidence that IFN- $\gamma$  can regulate the expression of select downstream genes even in the absence of Stat1 (47). To address this issue, we tested whether IFN- $\gamma$  suppression of *Gli1* expression was maintained in MEFs isolated from IFN- $\gamma$  receptor 1-deficient (*Ifngr1*<sup>-/-</sup>) and Stat1-deficient (*Stat1*<sup>-/-</sup>) mice. Importantly, we observed that the inhibitory effect of IFN- $\gamma$  on Hh signaling was abolished in MEFs isolated from both strains, direct genetic evidence implicating *Ifngr1* and *Stat1* in Hh signaling control (Fig. 3B–D). Thus, IFN- $\gamma$  inhibits Hh signaling via *Ifngr1*-induced activation of Stat1.

To corroborate the 3T3-L1 studies, we attempted to test IFN- $\gamma$ -Hh cross-talk in human and mouse primary white preadipocytes. Because the key differentiation factors 3-isobutyl-1-methylxanthin (IBMX) and dexamethasone (Dex) block Hh activation (30), 3T3-L1 and primary preadipocytes were induced using a minimal induction medium containing

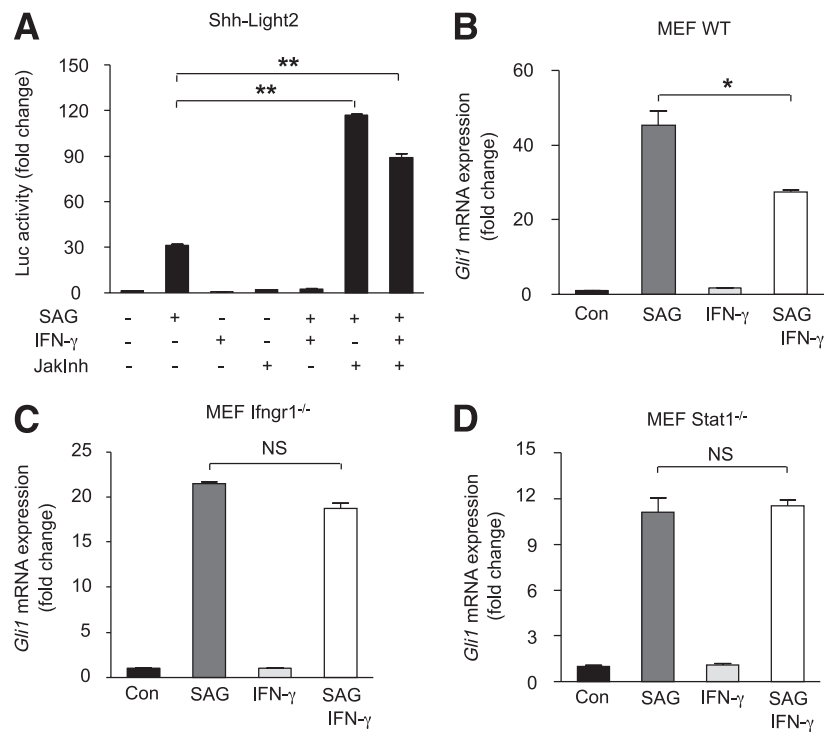


**FIG. 3.** IFN- $\gamma$  prevents SAG-induced inhibition of adipocyte differentiation via Jak-Stat signaling. **A:** Shh-LIGHT2 cells were treated with 200 nmol/L SAG and/or 25 ng/ $\mu$ L IFN- $\gamma$  in the absence or presence of JakInh. Simultaneous treatment of cells with SAG and JakInh resulted in an additional increase in relative Gli1 luciferase activity compared with SAG-only treated cells. **B–D:** We also tested whether effects of IFN- $\gamma$  on Gli1 expression could persist in MEFs from Ifngr1<sup>-/-</sup> and Stat1<sup>-/-</sup> mice. The inhibitory effect of IFN- $\gamma$  on Shh signaling was cancelled in Ifngr1<sup>-/-</sup> and Stat1<sup>-/-</sup> MEFs. These experiments demonstrate that IFN- $\gamma$  acts by means of the Jak-Stat pathway to abrogate the effects of Shh signaling. Data represent means  $\pm$  SEM of triplicate samples. \* $P$  < 0.01; \*\* $P$  < 0.001; NS, not significant.

insulin and troglitazone only. We previously used this differentiation cocktail to successfully explore Hh signaling effects of adipogenesis in 3T3-L1 cells (30). In contrast to 3T3-L1 cells, induction of primary mouse and human preadipocytes by the minimal induction medium was insufficient to induce substantial differentiation, even after 10 days.

Primary cells cultured in parallel under classical conditions differentiated efficiently (Supplementary Fig. 4A and B). IBMX/Dex completely blocked Hh activation by SAG (Supplementary Fig. 4D). These findings were supported by OrO staining of the same cells (Supplementary Fig. 4E and F). We confirmed this IBMX/Dex Hh-neutralizing effect by qPCR of the Hh target gene *Gli1* and the early adipogenic marker peroxisome proliferator-activated receptor- $\gamma$  (*Ppar- $\gamma$* ) 48 h after induction (Supplementary Fig. 4G and H). Looking instead at preadipocytes, IFN- $\gamma$  efficiently inhibited SAG-induced *Gli1* mRNA expression in both human and mouse primary cultures (Fig. 4A and Supplementary Fig. 4J), providing strong evidence that the appropriate signaling framework exists and is functional in the human and mouse progenitor pool. Importantly, in direct agreement with the findings in 3T3-L1 cells above, addition of IFN- $\gamma$  attenuated SAG-induced Hh activation and relieved Hh suppression of *Ppar $\gamma$*  expression (Fig. 4B and Supplementary Fig. 4J).

**IFN- $\gamma$  depletion restores Hh signaling in adipose tissue stromal vascular cells in vivo.** Genetic-induced and diet-induced obesity both decrease expression levels of Hh target genes in perigonadal white fat pads of mice (29). This is in accordance with antiadipogenic properties of Hh signaling and the substantial generation of new

adipocytes during weight gain. However, the underlying cause of this deregulation of Hh targets is not understood. We examined the effects of IFN- $\gamma$  depletion on the expression of Hh target genes in obese adipose tissue using an in vivo neutralizing antibody strategy. Male C57BL/6J mice exposed to a HF diet for 22 weeks were randomly assigned to a control group (HF;  $n$  = 10) or a group that received intraperitoneal anti-IFN- $\gamma$ -neutralizing antibody (HF+IFN- $\gamma$ -Ab;  $n$  = 5). Control animals were injected in parallel with a control IgG antibody. Consistent with previous findings (20) IFN- $\gamma$  serum levels in the HF group were significantly higher than in animals fed normal chow (Supplementary Fig. 5). Immunoneutralization in the treated animals was similarly confirmed by ELISA.

As expected, body weight, fasted blood glucose levels, perigonadal fat mass, adipose tissue infiltration with Mac2<sup>+</sup> macrophages, and adipocyte size were significantly higher in HF fed mice relative to LF fed controls (Supplementary Table 1 and Supplementary Fig. 6A–K). Anti-IFN- $\gamma$ -neutralizing antibody treatment for 2 weeks did not significantly affect any of these gross metabolic parameters (Supplementary Table 1 and Supplementary Fig. 6A–K). To characterize the system, we compared Hh signaling activity in adipose tissue fractionated into mature adipocytes, macrophages, and macrophage-depleted stromal vascular cells. In line with the role of Hh signaling in inhibiting fat formation, the Hh target *Gli1* showed low expression in mature adipocytes compared with macrophage- and macrophage-depleted stromal vascular fractions (dSVF). Indeed, the highest *Gli1* mRNA expression levels were found in the macrophage fraction (Fig. 5A). Further, *Gli1* expression in all three adipose tissue compartments was



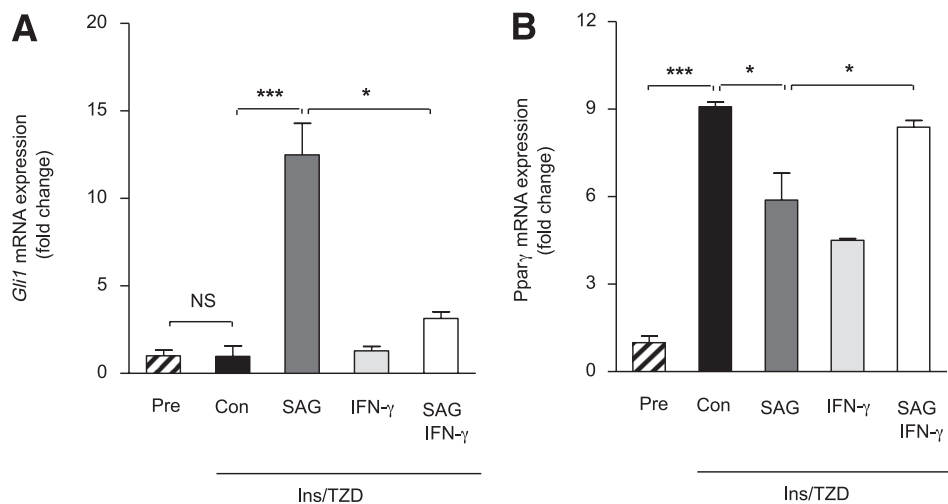


**FIG. 4.** IFN- $\gamma$  inhibits Hh signaling in mouse primary preadipocytes. Mouse primary preadipocytes were cultured in medium containing insulin and troglitazone for induction of adipogenic markers or in medium without any adipogenic inducers (Pre). Induced cells were stimulated with the Hh agonist SAG (200 nmol/L) and/or 50 ng/mL IFN- $\gamma$  or left untreated (Con) for 48 h. **A–B:** Quantitative RT-PCR monitoring of Hh target gene *Gli1* and adipogenic marker *Pparg*. mRNA levels of the genes of interest were normalized to *Rplp0*. Data represent means  $\pm$  SEM of triplicate samples. \* $P$  < 0.05; \*\*\* $P$  < 0.001; NS, not significant.

significantly lower in HF-treated mice relative to the LF-treated control animals, suggesting that the HF diet imposed a broad suppressive effect on Hh activity in adipose tissue (Fig. 5B).

Intriguingly, examination of expression profiles from IFN- $\gamma$ -depleted animals suggested that IFN- $\gamma$  mediates Hh-suppression in adipose tissue in vivo. Immunoneutralization substantially reversed HF-induced suppression of the downstream Hh target *Gli1* (greater than twofold), and impressively, completely restored expression of the target *Hhip* to normal chow levels ( $\sim$ 20-fold increase; Fig. 5C and D). Critically, the Hh target *Nr2f2/Coup-Tf2* also showed restoration of expression (Supplementary Fig. 7), as did the key insulin-sensitizing adipokine adiponectin (*Adipoq*; Fig. 5E). This latter finding correlated directly with increased serum adiponectin levels in immunoneutralized animals (Supplementary Fig. 8).

Together, these data identify Hh signaling as a target of IFN- $\gamma$  in adipose tissue in vivo and support a functional role for their cross-talk in balancing adipose tissue function. Thus, IFN- $\gamma$  mediates functional suppression of Hh signaling by a HF diet in vivo.

**Hh signaling is downregulated in human obesity.** Next, we determined *GLI1* transcript levels in human intra-abdominal adipose tissue of lean and insulin sensitive (IS) obese subjects. This design allowed us to detect potential associations of Hh signaling activity with intra-abdominal adipose tissue expandability in humans without confounding interference of insulin resistance. Despite a slight age and sex variation in this unique patient set, no differences were observed in plasma glucose and insulin levels or in the HOMA index (Supplementary Table 2). *GLUT4* expression values were similar in both groups, reflecting the equal presence of glucose transporters (Table 1). In line with current knowledge, IS obese subjects did not show increased *CD68* expression levels or alterations in the endothelial marker *VE-cadherin* (*CD144*). However, and in line with our hypothesis that increased Hh activity inhibits adipose tissue expansion, *GLI1* expression was significantly decreased in adipose tissue samples of IS obese subjects ( $P = 0.0237$ ). Importantly, adjusting for age, sex, *CD68*, and

*CD144* did not affect any of the statistical results, suggesting that decreased *GLI1* levels in IS obese subjects are not due to changes in vascularization or macrophage infiltration (Table 1). These findings highlight reduced Hh activity in patients with a likely intact expandable progenitor pool and no evidence of immune cell infiltration.

Next, we sought additional, more generalized evidence where inflammation is present. We used gene set enrichment to analyze publicly available adipose tissue expression arrays from two of the best genetically controlled human obesity cohorts, Pima Indians (GEO Reference Series GSE2508) and a set of 13 pairs of monozygotic twins discordant for adiposity (EBI-EMBL Reference Series E-MEXP-1425). Not without surprise, pathway enrichment for Th1/Th2 T-cell differentiation markers, a surrogate for T-cell infiltration, exhibited robust enrichment in obese Pima Indian and obese MZ-twin adipose tissues (FDR 0.08 and 0.16, respectively; nom.  $P = 0.006$  and  $P = 0.01$ , respectively; Supplementary Fig. 9). Intriguingly, and with equally robust signal intensity to that of the Th1/Th2 pathway, Hh signaling exhibited an enrichment signal in the control subjects of both genetically distinct cohorts, indicating consistent downregulation of the pathway in both obesity cohorts (FDR 0.08 and 0.12, respectively; nom.  $P = 0.08$  and  $P = 0.12$ , respectively).

These findings indicate that in the absence of inflammation, low Hh signaling is associated with insulin sensitivity and, presumably, a highly plastic progenitor pool, and that T-cell infiltration correlates highly with suppressed Hh signaling in human adipose tissue.

## DISCUSSION

Understanding the molecular mechanisms involved in adipocyte differentiation is of great importance because it may lead to new ways of treating obesity and, in particular, its associated metabolic complications. Hh signaling and IFN- $\gamma$  already have an established role in inhibiting adipogenesis (21,22,29,30).

Here we demonstrate for the first time that inhibition of adipocyte differentiation by Hh signaling can be balanced

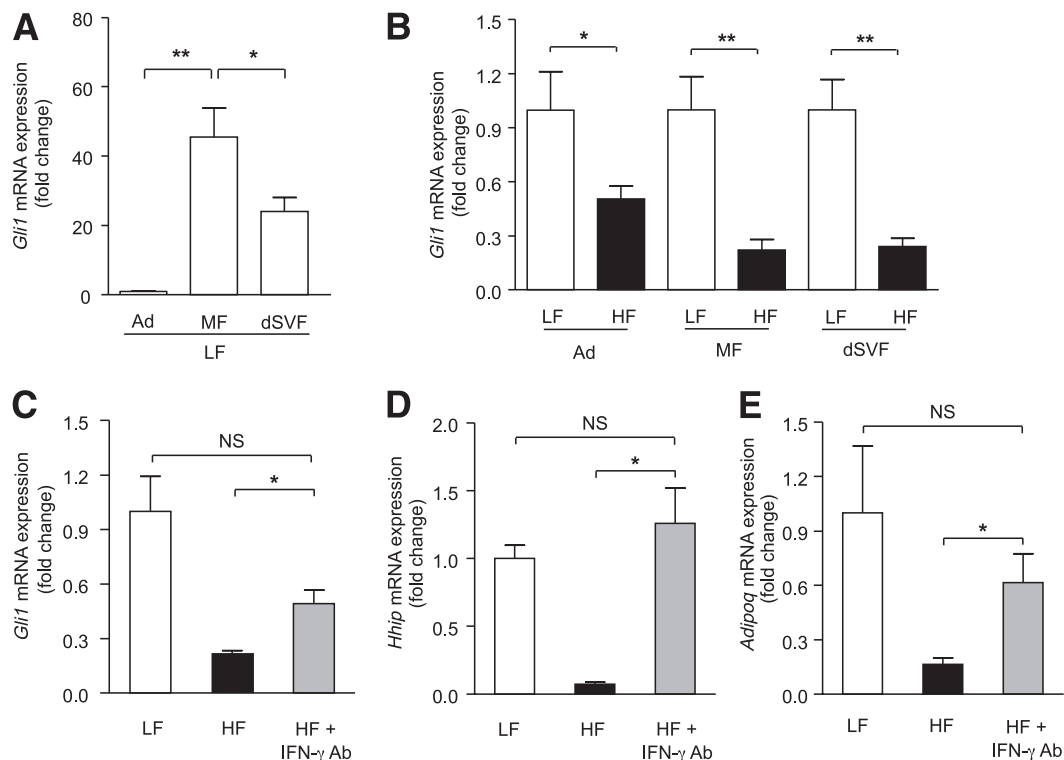


**FIG. 5. IFN- $\gamma$  inhibits Hh signaling in obesity in vivo. A–B:** C57BL/6J mice were fed a LF or HF diet for 24 weeks ( $n = 10$  or  $15$  mice per group, respectively). For the last 2 weeks of diets, mice fed the HF diet were randomly split into HF and HF+Ab groups. The HF+Ab ( $n = 5$ ) group was treated with monoclonal antibodies against IFN- $\gamma$ . Adipose tissue was separated into adipocytes (Ad), macrophage fraction (MF), and macrophage-dSVF using magnetic immunoaffinity isolation. Cell fractions from mice fed LF and HF diets were analyzed for *Gli1* mRNA expression. **C–E:** dSVF from mice fed LF and HF diets was analyzed for *Gli1*, *Hhip*, and *Adipoq*. \* $P < 0.05$ ; \*\* $P < 0.01$ .

by the antagonistic actions of IFN- $\gamma$ . The effect was observed in 3T3-L1 adipocytes (Fig. 2A–E) as well as in three different primary culture systems—mouse embryonic fibroblasts (Fig. 3B–D), primary mouse preadipocytes (Fig. 4A and B), and primary human preadipocytes (Supplementary Fig. 4I and J). These data, as well as recapitulation of the phenotype using the endogenous *Shh* ligand, rule out cell-line or chemical artifacts. The difficulty associated with recapitulating these studies in mature primary adipocytes is caused by the direct inhibition of Hh signaling by both IBMX and Dex, required constituents of primary adipocyte differentiation cocktails.

Cross-talk between the Hh signaling pathway and IFN- $\gamma$  has already been shown to influence cell differentiation

and proliferation in specific neuronal settings (31–33). IFN- $\gamma$  indirectly regulates proliferation of neuronal precursor cells through mechanisms involving elevated expression of *Shh* and its major target genes, *Gli1* and *Ptch* (31). Discordant upregulation of *Shh* by IFN- $\gamma$ , while suppressing its target *Gli1*, was observed in studies on the differentiation of neuronal stem cells (32). Interestingly, our studies demonstrate that IFN- $\gamma$ -mediated inhibition of Hh target genes (*Gli1*, *Ptch*, *Hhip*, and *Nr2f2/Coup-Tf2*) in 3T3-L1 cells promotes adipocyte differentiation. IFN- $\gamma$  not only rescued adipocyte differentiation but also decreased Coup-Tf2 and *Gata2* levels, further supporting an antiadipogenic role of both genes (32). Thus, it appears that IFN- $\gamma$  signaling can have very context-dependent effects on Hh signaling.

After binding of IFN- $\gamma$  to its receptor, Jak1 and Jak2 are activated and regulate downstream phosphorylation of Stat1 (46). Although Stat1 is required for many IFN- $\gamma$ -dependent actions, evidence shows that in the absence of Stat1, IFN- $\gamma$  can still regulate the expression of some genes (46,47). Because IFN- $\gamma$ -mediated inhibition of Hh signaling did not occur in Stat1<sup>-/-</sup> MEFs, we conclude that this cross-talk depends on Stat1. Interestingly, blocking constitutive Jak-Stat activation by a pan-Jak inhibitor resulted in greatly increased Gli1 luciferase activities in SAG-treated Shh-LIGHT2 cells, even in the absence of IFN- $\gamma$ . This suggests that basal Jak activity exerts an inhibitory tone on Hh pathway activation.

Because the concentration of IFN- $\gamma$  is elevated in obesity and the Hh signaling pathway was less active in obese compared with lean mice, we hypothesized that IFN- $\gamma$  might inhibit Hh signaling in vivo. Interestingly, when examining

**TABLE 1**  
Comparison of intraperitoneal adipose mRNA expression levels in lean vs. obese study subjects ( $n = 46$ )

Gene	Lean ( $n = 21$ )	Obese ( $n = 25$ )	Adjusted for	$P^*$
<i>GLUT4</i>	5.77 (0.70)	4.78 (0.43)	Sex, age	NS
<i>CD68</i>	3.38 (0.39)	3.03 (0.29)	Sex, age	NS
<i>CD144</i>	8.18 (0.81)	10.16 (0.77)	Sex, age	NS
<i>GLI1</i>	7.46 (0.79)	5.17 (0.39)	Sex, age	0.0237
<i>GLI1</i>	7.54 (0.79)	5.32 (0.39)	Sex, age, CD68	0.0224
<i>GLI1</i>	7.80 (0.79)	5.06 (0.39)	Sex, age, CD144	0.0049
<i>GLI1</i>	7.85 (0.79)	5.27 (0.39)	Sex, age, CD68, CD144	0.0065

Data are arbitrary units and presented as mean  $\pm$  SEM. \* $P$  values obtained from ANOVA. NS, not significant.

adipose tissue fractions for differences in *Gli1* expression in the lean and obese state, we found low *Gli1* expression in mature adipocytes. Levels of mRNA in dSVF were >20-fold and in macrophages >40-fold higher than in the adipocyte fraction. This is in accordance with previous data that show decreased expression of positively acting Hh components (Smo and the Glis) during adipogenesis (29,30). To determine whether reduced expression of Hh target genes in white fat of obese animals depends on higher IFN- $\gamma$  concentrations in obesity, we treated obese mice with a neutralizing antibody against IFN- $\gamma$ . Our results demonstrate that obesity-associated repression of Hh-target genes like *Gli1* and *Hhip* in the dSVF was partially or completely relieved by inhibiting IFN- $\gamma$  elicited Jak/Stat signaling. This suggests that IFN- $\gamma$  opposes inhibition of Hh signaling in obese adipose tissue in vivo.

Increases in fat mass can involve both hypertrophy and hyperplasia of adipocytes. Obesity in adults is typically associated with adipocyte hypertrophy, and an additional adipocyte hyperplasia occurs in morbidly obese humans and rodents (48–50). Adiposity-induced cellular and tissue hypoxia is an important contributor to adipose tissue immunopathies and adipocyte and adipose tissue dysfunction (2,8,9,16). Data suggest that the initial hypertrophic response of adipocytes promotes necrotic-like death, after which the lipid storage capacity of adipose tissue can be efficiently maintained or increased only by adipocyte hyperplasia. Interestingly, current concepts support that early adipose tissue expandability prevents metabolic consequences like insulin resistance, even in morbid obesity (9).

Some have proposed that the generation of new adipocytes may be balanced by adipocyte death, with the constant and tightly regulated total number set by early adulthood (50). Our findings suggest a model where the inhibition of Hh signaling by IFN- $\gamma$  in obesity contributes to the development of new adipocytes (Fig. 6). At steady-state in lean individuals, basal Hh-pathway activity prevents the formation of new adipocytes. T-cell infiltration, as an early event in obesity development, leads to elevated IFN- $\gamma$

production in adipose tissue and inhibition of Hh-signaling, a scenario that is permissive for the recruitment and development of new adipocyte populations. Such an early inhibition of Hh signaling may be a prerequisite for compensatory increases in total adipocyte numbers, although that is speculation.

Our observation that the main Hh target gene *GLI1* is downregulated in intraperitoneal adipose tissue from metabolically healthy IS obese subjects supports the concept that early inactivation of Hh signaling and subsequent release of the intracellular progenitor pool to expansion might alleviate obesity associated insulin resistance. Clearly though, the system is more complex. Indeed, robust opposing signals for T-cell infiltration (upregulated) and Hh signaling (downregulated) in the adipose tissue of MZ twins as well as in Pima Indian cohorts support the idea that inhibition of Hh signaling alone is insufficient to block pathologies associated with obesity and chronic inflammation (Supplementary Fig. 9). It is almost certain that additional positive expansion signals are required for proper expansion. A deeper understanding of these concepts will be aided by long-term genetic dissections in vivo, using for instance inducible adipose tissue specific IFN- $\gamma$  receptor-deficient mice.

In conclusion, we have established for the first time that IFN- $\gamma$  directly inhibits Hh signaling in (pre)adipocytes in vitro and in adipose tissue in vivo. Our results suggest that the cross-talk between IFN- $\gamma$  and the Hh-signaling pathway is essential in the maintenance of optimal adipocyte differentiation. The ability to control the plasticity of adipocyte turnover would be a powerful tool in alleviating many complications associated with obesity. That Hh antagonists will one day be used for such purposes in the clinic is perhaps a stretch. However, understanding the regulatory architecture that controls the progenitor cell decision “To differentiate, or not to differentiate?” will be critical to the development of any such therapies. We believe we have added one of the first pieces with which to construct this complex puzzle.

#### ACKNOWLEDGMENTS

This work was supported by research grants to J.A.P. and H.E. from the Vienna Science and Technology Fund (project LS07-058) and to J.T. from the Austrian Society for Laboratory Medicine. B.S. and M.M. were supported by the FWF-funded SFB F28 and by BM.W<sub>1</sub><sup>a</sup> GEN-AU III (Austromouse). F.K. and W.P. were supported by the Bundesland Salzburg (grant 2005-20089).

No potential conflicts of interest relevant to this article were reported.

J.T. researched data, contributed to discussion, and drafted the manuscript. B.S. researched data and contributed to discussion. A.J. researched data. N.B. researched data and contributed to discussion. M.Ba., S.A., J.L., R.T., G.P., and M.Bi. researched data. W.E. contributed to discussion and edited the manuscript. F.K. researched data and contributed to discussion. M.M. and O.W. contributed to discussion and edited the manuscript. W.P. researched data and contributed to discussion. J.A.P. and H.E. researched data, contributed to discussion, and wrote and edited the manuscript. The contribution by M.Ba. constitutes part of her PhD work.

The authors are indebted to the service departments and Maria Ozsvar of the Medical University of Vienna for excellent technical help.

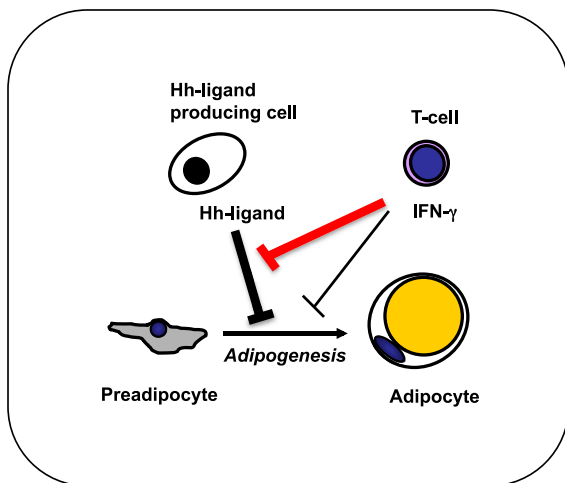


**FIG. 6.** Model shows a novel cross-talk mechanism between IFN- $\gamma$  and Hh signaling maintains adipogenesis in adipose tissue. Activation of Hh signaling blocks white adipocyte differentiation. T cells infiltrating white adipose tissue early during the development of obesity secrete IFN- $\gamma$ , and thus inhibit ongoing Hh signaling. Decreased Hh signaling activity in (pre)adipocytes rescues adipogenesis.

## REFERENCES

- World Health Organization. *Global Strategy on Diet, Physical Activity and Health*. Geneva, Switzerland, World Health Organization, 2009
- Blüher M. Adipose tissue dysfunction in obesity. *Exp Clin Endocrinol Diabetes* 2009;117:241–250
- Karelis AD, St-Pierre DH, Conus F, Rabasa-Lhoret R, Poehlman ET. Metabolic and body composition factors in subgroups of obesity: what do we know? *J Clin Endocrinol Metab* 2004;89:2569–2575
- Allende-Vigo MZ. Pathophysiologic mechanisms linking adipose tissue and cardiometabolic risk. *Endocr Pract* 2010;16:692–698
- Ballantyne CM. T cells, macrophages, chemokines, and adiposopathy in diet-induced obesity [Internet], 2010. NIH Report. Lambertville, NJ. Available from <http://www.labome.org>. Accessed 1 February 2011
- Heilbronn L, Smith SR, Ravussin E. Failure of fat cell proliferation, mitochondrial function and fat oxidation results in ectopic fat storage, insulin resistance and type II diabetes mellitus. *Int J Obes Relat Metab Disord* 2004;28(Suppl. 4):S12–S21
- Ravussin E, Smith SR. Increased fat intake, impaired fat oxidation, and failure of fat cell proliferation result in ectopic fat storage, insulin resistance, and type 2 diabetes mellitus. *Ann N Y Acad Sci* 2002;967:363–378
- Bays HE, González-Campoy JM, Bray GA, et al. Pathogenic potential of adipose tissue and metabolic consequences of adipocyte hypertrophy and increased visceral adiposity. *Expert Rev Cardiovasc Ther* 2008;6:343–368
- Ouchi N, Parker JL, Lugus JJ, Walsh K. Adipokines in inflammation and metabolic disease. *Nat Rev Immunol* 2011;11:85–97
- Wellen KE, Hotamisligil GS. Inflammation, stress, and diabetes. *J Clin Invest* 2005;115:1111–1119
- Schenk S, Saberi M, Olefsky JM. Insulin sensitivity: modulation by nutrients and inflammation. *J Clin Invest* 2008;118:2992–3002
- Shoelson SE, Lee J, Goldfine AB. Inflammation and insulin resistance. *J Clin Invest* 2006;116:1793–1801
- Olefsky JM, Glass CK. Macrophages, inflammation, and insulin resistance. *Annu Rev Phys* 2010;72:219–246
- Wu H, Ghosh S, Perrard XD, et al. T-cell accumulation and regulated on activation, normal T cell expressed and secreted upregulation in adipose tissue in obesity. *Circulation* 2007;115:1029–1038
- Kintscher U, Hartge M, Hess K, et al. T-lymphocyte infiltration in visceral adipose tissue: a primary event in adipose tissue inflammation and the development of obesity-mediated insulin resistance. *Arterioscler Thromb Vasc Biol* 2008;28:1304–1310
- Rausch ME, Weisberg S, Vardhana P, Tortorello DV. Obesity in C57BL/6J mice is characterized by adipose tissue hypoxia and cytotoxic T-cell infiltration. *Int J Obes (Lond)* 2008;32:451–463
- Nishimura S, Manabe I, Nagasaki M, et al. CD8+ effector T cells contribute to macrophage recruitment and adipose tissue inflammation in obesity. *Nat Med* 2009;15:914–920
- Winer S, Chan Y, Paltser G, et al. Normalization of obesity-associated insulin resistance through immunotherapy. *Nat Med* 2009;15:921–929
- Lumeng CN, Maillard I, Saltiel AR. T-ing up inflammation in fat. *Nat Med* 2009;15:846–847
- Rocha VZ, Folco EJ, Sukhova G, et al. Interferon-gamma, a Th1 cytokine, regulates fat inflammation: a role for adaptive immunity in obesity. *Circ Res* 2008;103:467–476
- McGillicuddy FC, Chiquoine EH, Hinkle CC, et al. Interferon gamma attenuates insulin signaling, lipid storage, and differentiation in human adipocytes via activation of the JAK/STAT pathway. *J Biol Chem* 2009;284:31936–31944
- Duffaut C, Zakaroff-Girard A, Bourlier V, et al. Interplay between human adipocytes and T lymphocytes in obesity: CCL20 as an adipochemokine and T lymphocytes as lipogenic modulators. *Arterioscler Thromb Vasc Biol* 2009;29:1608–1614
- Sultan A, Strodthoff D, Robertson AK, et al. T cell-mediated inflammation in adipose tissue does not cause insulin resistance in hyperlipidemic mice. *Circ Res* 2009;104:961–968
- Klötting N, Fasshauer M, Dietrich A, et al. Insulin-sensitive obesity. *Am J Physiol Endocrinol Metab* 2010;299:E506–E515
- Ingham PW, McMahon AP. Hedgehog signaling in animal development: paradigms and principles. *Genes Dev* 2001;15:3059–3087
- Varjosalo M, Taipale J. Hedgehog: functions and mechanisms. *Genes Dev* 2008;22:2454–2472
- Beachy PA, Karhadkar SS, Berman DM. Tissue repair and stem cell renewal in carcinogenesis. *Nature* 2004;432:324–331
- Hooper JE, Scott MP. Communicating with Hedgehogs. *Nat Rev Mol Cell Biol* 2005;6:306–317
- Suh JM, Gao X, McKay J, McKay R, Salo Z, Graff JM. Hedgehog signaling plays a conserved role in inhibiting fat formation. *Cell Metab* 2006;3:25–34
- Pospisilik JA, Schramek D, Schnidar H, et al. Drosophila genome-wide obesity screen reveals hedgehog as a determinant of brown versus white adipose cell fate. *Cell* 2010;140:148–160
- Wang J, Lin W, Popko B, Campbell IL. Inducible production of interferon-gamma in the developing brain causes cerebellar dysplasia with activation of the Sonic hedgehog pathway. *Mol Cell Neurosci* 2004;27:489–496
- Wang Y, Imitola J, Rasmussen S, O'Connor KC, Khoury SJ. Paradoxical dysregulation of the neural stem cell pathway sonic hedgehog-Gli1 in autoimmune encephalomyelitis and multiple sclerosis. *Ann Neurol* 2008;64:417–427
- Sun L, Tian Z, Wang J. A direct cross-talk between interferon-gamma and sonic hedgehog signaling that leads to the proliferation of neuronal precursor cells. *Brain Behav Immun* 2010;24:220–228
- Tekki-Kessarri N, Woodruff R, Hall AC, et al. Hedgehog-dependent oligodendrocyte lineage specification in the telencephalon. *Development* 2001;128:2545–2554
- Lai K, Kaspar BK, Gage FH, Schaffer DV. Sonic hedgehog regulates adult neural progenitor proliferation in vitro and in vivo. *Nat Neurosci* 2003;6:21–27
- Ahn S, Joyner AL. In vivo analysis of quiescent adult neural stem cells responding to Sonic hedgehog. *Nature* 2005;437:894–897
- Gao L, Miller RH. Specification of optic nerve oligodendrocyte precursors by retinal ganglion cell axons. *J Neurosci* 2006;26:7619–7628
- Lin W, Kemper A, McCarthy KD, et al. Interferon-gamma induced medulloblastoma in the developing cerebellum. *J Neurosci* 2004;24:10074–10083
- Taipale J, Chen JK, Cooper MK, et al. Effects of oncogenic mutations in Smoothened and Patched can be reversed by cyclopamine. *Nature* 2000;406:1005–1009
- Durbin JE, Hackenmüller R, Simon MC, Levy DE. Targeted disruption of the mouse Stat1 gene results in compromised innate immunity to viral disease. *Cell* 1996;84:443–450
- Huang S, Hendriks W, Althage A, et al. Immune response in mice that lack the interferon-gamma receptor. *Science* 1993;259:1742–1745
- Todaró GJ, Green H. Quantitative studies of the growth of mouse embryo cells in culture and their development into established lines. *J Cell Biol* 1963;17:299–313
- Oberkofler H, Linnemayr V, Weitgasser R, et al. Complex haplotypes of the PGC-1alpha gene are associated with carbohydrate metabolism and type 2 diabetes. *Diabetes* 2004;53:1385–1393
- Xu Z, Yu S, Hsu CH, Eguchi J, Rosen ED. The orphan nuclear receptor chicken ovalbumin upstream promoter-transcription factor II is a critical regulator of adipogenesis. *Proc Natl Acad Sci USA* 2008;105:2421–2426
- Platanias LC. Mechanisms of type-I- and type-II-interferon-mediated signalling. *Nat Rev Immunol* 2005;5:375–386
- Aaronson DS, Horvath CM. A road map for those who don't know JAK-STAT. *Science* 2002;296:1653–1655
- Ramana CV, Gil MP, Schreiber RD, Stark GR. Stat1-dependent and -independent pathways in IFN-gamma-dependent signaling. *Trends Immunol* 2002;23:96–101
- Maumus M, Sengenès C, Decaunes P, et al. Evidence of in situ proliferation of adult adipose tissue-derived progenitor cells: influence of fat mass microenvironment and growth. *J Clin Endocrinol Metab* 2008;93:4098–4106
- Arner P, Spalding KL. Fat cell turnover in humans. *Biochem Biophys Res Commun* 2010;396:101–104
- Spalding KL, Arner E, Westermark PO, et al. Dynamics of fat cell turnover in humans. *Nature* 2008;453:783–787